Université de Montréal

Opérateurs monopôles dans les transitions hors d'un liquide de spin de Dirac

par

Éric Dupuis

Département de physique
Faculté des arts et des sciences

Thèse présentée en vue de l'obtention du grade de
Philosophiæ Doctor (Ph.D.)
en Sciences

Août 2021

Université de Montréal

Faculté des arts et des sciences

Cette thèse intitulée

Opérateurs monopôles dans les transitions hors d'un liquide de spin de Dirac

présentée par

Éric Dupuis

a été évaluée par un jury composé des personnes suivantes :

Richard MacKenzie
(président-rapporteur)

William Witczak-Krempa
(directeur de recherche)

Manu B. Paranjape
(codirecteur)

Andrea Bianchi
(membre du jury)

Silviu Pufu
(examinateur externe)

Pierre Chaurand
(représentant du doyen de la FESP)

Résumé

Dans la description à basse énergie de systèmes fortement corrélés, les champs de jauge peuvent émerger comme excitations collectives couplées à des quasiparticules fractionalisées. En particulier, certains aimants bidimensionnels dits frustrés sont décrits par un liquide de spin de Dirac comportant une symétrie de jauge U(1) compacte. La description infrarouge est donnée par une théorie conforme des champs, soit l'électrodynamique quantique en $2+1$ dimensions avec $2N$ saveurs de fermions sans masse. Dans les aimants typiques, $N = 2$ ou 4. L'aspect compact du champ de jauge implique également l'existence d'excitations topologiques, soit des instantons créés, dans ce contexte, par des opérateurs monopôles.

Cette thèse porte sur les transitions de phase quantiques à partir d'un liquide de spin de Dirac et les propriétés des monopôles aux points critiques correspondants. Ces transitions sont induites en activant diverses interactions de type Gross-Neveu. Dans tous les cas à l'étude, la dimension d'échelle des monopôles est obtenue grâce à la correspondance état-opérateur et à un développement en $1/N$. L'accent est d'abord mis sur une transition de confinement-déconfinement vers une phase antiferromagnétique décrite par la condensation d'un monopôle. Une levée de dégénérescence est observée au point critique alors que certaines dimensions d'échelle de monopôles sont réduites par rapport à leur valeur dans le liquide de spin de Dirac. Cette hiérarchie est caractérisée quantitativement en comparant les dimensions d'échelle dans des secteurs distincts du spin magnétique à l'ordre dominant en $1/N$, puis qualitativement par une analyse en théorie des représentations. Des exposants critiques pour d'autres observables dans la théorie non compacte sont également obtenus. Enfin, deux transitions vers des liquides de spin topologiques, soit le liquide de spin chiral et le liquide de spin Z_2, sont considérées. Les dimensions anormales des monopôles sont obtenues à l'ordre sous-dominant en $1/N$. Ces résultats permettent de vérifier une dualité conjecturée avec un modèle bosonique et la valeur d'un coefficient universel pour les théories de jauge U(1).

Mots-clés

- Opérateurs de désordre topologique
- Théorie de jauge et dualités
- Transitions de phase quantiques
- Liquides de spin quantiques
- Théorie conforme des champs

Abstract

In strongly correlated systems, gauge fields can emerge as collective excitations coupled to fractionalized quasiparticles. In particular, certain frustrated two-dimensional quantum magnets are described by a Dirac spin liquid which has a U(1) gauge symmetry. The infrared description is given by a conformal field theory, namely quantum electrodynamics in $2+1$ dimensions with $2N$ flavours of massless fermions. In typical magnets, $N = 2$ or 4. The compact aspect of the gauge field also implies the existence of topological excitations corresponding to instantons, which are created by monopole operators in this context.

This thesis focuses on quantum phase transitions out of a Dirac spin liquid and the properties of monopoles at the corresponding critical points. These transitions are driven by activating various types of Gross-Neveu interactions. In all the cases studied, the scaling dimension of monopoles are obtained using the state-operator correspondence and a $1/N$ expansion. The confinement-deconfinement transition to an antiferromagnetic order produced by a monopole condensate is first studied. A degeneracy lifting is observed at the critical point, as certain monopoles have their scaling dimension reduced in comparison with the value in the Dirac spin liquid. This hierarchy is charactized quantitatively by comparing monopole scaling dimensions in distinct magnetic spin sector at leading-order in $1/N$, and qualitatively by an analysis in representation theory. Critical exponents of various other operators are obtained in the non-compact model. Transitions to two topological spin liquids, namely a chiral spin liquid and a Z_2 spin liquid, are also considered. Anomalous dimensions of monopoles are obtained at sub-leading order in $1/N$. These results allow the verification of a conjectured duality with a bosonic model and the value of a universal coefficient in U(1) gauge theories.

Keywords

- Topological disorder operators
- Gauge theories and dualities
- Quantum phase transitions
- Quantum spin liquids
- Conformal field theory

Table des matières

Liste des tableaux

Table des figures

Liste des sigles et des abréviations

AFM	antiferroaimant
CFT	théorie conforme des champs
cHGN	chiral-Heisenberg Gross-Neveu
cHGNY	chiral-Heisenberg Gross-Neveu-Yukawa
CSL	liquide de spin chiral
DMRG	groupe de renormalisation par la matrice densité
dQCP	point critique quantique déconfiné
DSL	liquide de spin de Dirac
GN	Gross-Neveu
irrep	représentation irréductible
KHAFM	antiferroaimant de Heisenberg sur réseau kagome
QCP	point critique quantique
QED_3	électrodynamique quantique en $2+1$ dimensions
QFT	théorie quantique des champs
QSL	liquide de spin quantique
RG	groupe de renormalisation
RVB	solide de liens de valence résonant
VBS	solide de liens de valence
VMC	Monte Carlo variationnel
Z_2 GN	Gross-Neveu de type supraconducteur «s-wave»
Z_2 QSL	liquide de spin Z_2

Remerciements

J'aimerais d'abord remercier mon superviseur William Witczak-Krempa. Merci de m'avoir transmis ta rigueur pour les calculs et la rédaction d'articles, et d'avoir partagé ton intuition et ta passion pour les phases quantiques de la matière, c'était palpitant ! Merci aussi de m'avoir fait confiance pour la supervision, tant en recherche qu'en enseignement. J'aimerais aussi remercier mon cosuperviseur Manu Paranjape. Ton support et ta patience au début de mon doctorat ont été importants, et ton enthousiasme (« whatever's fun ! ») pour les instantons a été contagieux. Merci aussi à Richard MacKenzie, mon premier guide en physique théorique.

L'expérience du doctorat n'aurait pas été la même sans les gens du A et du V. J'ai été chanceux d'avoir un groupe de recherche dynamique et agréable à côtoyer. Merci à Rufus pour nos échanges sur la physique et bien d'autres choses, travailler avec toi a été un vrai plaisir. Merci à Simon pour les questions intéressantes sur la théorie des champs. Merci aussi à Sergueï, Alex et Lena pour votre bonne humeur, votre compagnie au bureau. Merci à Mirjam et Marie-Maude pour votre support et toutes les discussions.

L'apport de mon entourage a aussi été important. Merci à mes colocs et ami.es pour votre présence réconfortante qui m'a changé les idées. Merci à ma collègue de bureau pandémique pour ton support indéfectible et ta précieuse compagnie. Merci à ma famille d'avoir été là pour moi.

Introduction

Il y a un autre monde mais il est dans celui-ci.

Paul Éluard

Un thème important en physique de la matière condensée concerne la classification des phases de la matière et l'étude des transitions entre celles-ci. Dans la théorie de Landau, les phases de la matière sont distinguées par un paramètre d'ordre local qui rend compte des symétries brisées. Une transition continue se produit par la condensation d'un ordre qui brise la symétrie G d'une première phase en un sous-groupe H décrivant une deuxième phase

$$G \to H\,, \quad H \subset G\,. \tag{0.0.1}$$

Depuis la découverte de l'effet Hall quantique [1–4], plusieurs systèmes échappant à cette description ont été trouvés. Notamment, les paramètres d'ordre de Landau sont insuffisants pour décrire les phases topologiques de la matière. La fonction d'onde de l'état fondamental de ces phases possède des propriétés globales dont la description nécessite l'introduction d'un ordre topologique. Dans une limite de basse énergie, ces phases sont décrites par des théories de champs topologiques. Il existe également des contre-exemples au mécanisme de transition entre phases conventionnelles. À un point critique quantique déconfiné (dQCP), une symétrie émergente G permet la transition entre des phases voisines dont les symétries H_1 et H_2 ne sont pas contenues l'une dans l'autre. Le cas d'étude prototype est le dQCP qui sépare des phases antiferroaimant (AFM) et solide de liens de valence (VBS) [5–7]. Du côté AFM, la polarisation du spin magnétique brise la symétrie de rotation interne SU(2), alors que du côté VBS, un pavage de singulets de spins brise certaines symétries discrètes du réseau.

Les phases fractionalisées de la matière montrent également les limites des paradigmes de Landau. Les quasiparticules y portent seulement une fraction des nombres quantiques des éléments constituants du système et forment des excitations non locales qui ne peuvent être exprimées en termes de ces derniers [8]. Cela contredit l'idée de l'intégrité de l'électron comme quasiparticule sous l'activation d'interactions. Les états possédant un ordre topologique, comme les systèmes de Hall quantique fractionnaires, sont généralement décrits par une phase fractionalisée [9].

La phase liquide de spin quantique (QSL) retrouvée dans certains aimants quantiques montre par exemple ce phénomène de fractionalisation [8]. Il s'agit d'un aimant qui, même à basse température, ne développe pas d'ordre magnétique. Cela survient dans les aimants dits « frustrés » où l'énergie d'interaction ne peut être minimisée localement pour tous les constituants. Par exemple, tel que montré à la Fig. 0.1(a), il n'est pas possible de minimiser l'énergie d'interaction de chaque paire dans un ensemble de trois spins où l'énergie spin-spin est minimisée par anti-alignement. L'état minimisant globalement l'énergie est plutôt obtenu en formant des paires de spins intriqués, plus précisément des singulets entre deux spins 1/2 tel que montré à la Fig. 0.1(b). Dans ce cas, le fait de détruire l'intrication d'une paire de spins devient une excitation possible. Les deux spins 1/2 ainsi libérés, les spinons, sont les quasiparticules fractionalisées relativement au magnon, une excitation bosonique de spin 1 consistant à renverser un spin sur un seul site. Dans le système de spin frustré, les spinons sont couplés par un champ de jauge émergent provenant d'une excitation collective du système.

Il existe plusieurs réalisations de QSL décrites par diverses théories de jauge. Le liquide de spin de Dirac (DSL) est un exemple important et particulièrement intéressant dans le cas des aimants quantiques bidimensionnels. C'est le cas qui sera étudié dans cette thèse. Dans la limite infrarouge, ce système est décrit par l'électrodynamique quantique en $2+1$ dimensions (QED_3) avec $2N$ saveurs de fermions à deux composantes sans masse, soit une théorie de jauge abélienne U(1). Dans un langage adapté aux aimants quantiques, les fermions correspondent aux spinons qui émergent par la fractionalisation. Le nombre de saveurs $2N$ correspond aux deux polarisations magnétiques de l'électron et à N vallées dans l'espace des impulsions. Dans les aimants typiques, on compte $N = 2$ [10–12] ou $N = 4$ [10] vallées en impulsions. Les liquides de spin-orbital de Dirac présentent quant à eux 4 polarisations

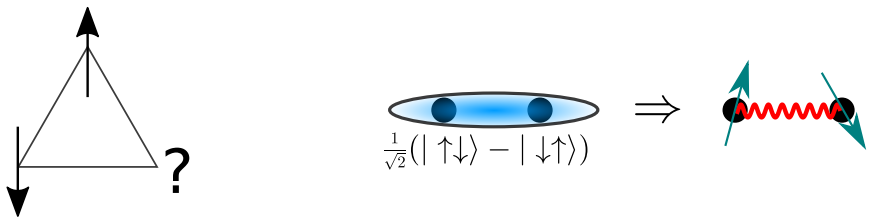

Figure 0.1. (a) Frustration « géométrique ». Il est impossible d'anti-aligner trois spins simultanément pour minimiser toutes les énergies d'interaction plus proche voisin antiferromagnétique. (b) Un aimant frustré peut être excité en détruisant l'intrication d'une paire de spins. Les spins sous-jacents libérés sont les spinons et interagissent via un boson de jauge émergent.

d'un spin 3/2 effectif induit par une interaction spin-orbite, pour un total de 8 saveurs fermioniques dans les exemples des Réfs. [13–15].

Le DSL décrit par le modèle QED_3 avec $2N = 4$ saveurs a été utilisé pour décrire des aimants quantiques dans plusieurs contextes. Le modèle $J_1 - J_2$ de spin 1/2 sur réseau triangulaire, qui apparaît dans des chalcogénures à base de terre rare [1] [16–20], serait notamment décrit par un DSL selon des études par Monte Carlo variationnel (VMC) [12, 21, 22] et avec le groupe de renormalisation par la matrice densité (DMRG) [22]. L'AFM de Heisenberg de spin 1/2 sur réseau kagome, un modèle de spin potentiellement réalisé dans le Herbertsmithite [2] [23, 24] et le Barlowite avec substituts de zinc [3] [25], serait aussi décrit par un DSL selon des études par VMC [26–29], par DMRG [30, 31] et par réseaux de tenseurs [32, 33]. Ces résultats sont toutefois controversés. Ils sont notamment contredits par d'autres études numériques supportant quant à elles un liquide de spin « gappé » [34–40].[4] D'autre part, le DMRG est étendu aux systèmes bidimensionnels comme une méthode quasi-1d, ici sur un cylindre. Les limitations de taille finie sont particulièrement problématiques pour distinguer

[1] Chalcogénures à base de terre rare : $AReCh_2$(A = alcalin ou ion monovalent, Re = terre rare, Ch = O,S,Se)

[2] Herbertsmithite : $ZnCu_3(OH)_6Cl_2$

[3] Barlowite avec substituts de zinc : $ZnCu_3(OH)_6FBr$

[4] C'est-à-dire, un liquide de spin où les spinons sont massifs.

un état sans « gap » d'un état avec un petit « gap » où la longueur caractéristique excède la circonférence du cylindre [31].

Un aspect crucial du DSL a jusqu'à présent été omis. Puisque le contexte physique concerne l'émergence de QED_3 sur un réseau sous-jacent, le champ de jauge U(1) est compact et admet par conséquent des excitations topologiques nommées monopôles, soit des instantons en $2+1$ dimensions. Les opérateurs monopôles créant ces configurations constituent l'objet central de cette thèse. Un bref survol des monopôles est d'abord présenté, puis l'importance de ces objets est mise de l'avant.

0.1. Opérateurs monopôles

0.1.1. Origine sur le réseau

Dans les théories de jauge sur réseau, une variable qui intervient naturellement est la ligne de Wilson. Pour un champ de jauge U(1) noté A_μ, on a la forme suivante [5]

$$U(y,x;C) = \exp\left\{ i \int_C dz^\mu A_\mu(z) \right\} , \tag{0.1.1}$$

où C est un chemin entre les points x et y. En particulier, le transport covariant d'un point du réseau x vers un autre point atteint par un vecteur de maille $x + ae_{(\mu)}$ d'un champ de matière de charge 1 est assuré par une ligne de Wilson donnée par [41]

$$U_\mu(x) \equiv U(x + ae_{(\mu)},x) \approx \exp\{iaA_\mu(x)\} . \tag{0.1.2}$$

On peut ainsi bâtir un terme invariant de jauge et bilocal $\bar{\psi}(x + ae_{(\mu)})U_\mu(x)\psi(x)$ lié, dans la limite du continu, au terme de Dirac $\bar{\psi}(x)(\partial_\mu - iA_\mu(x))\psi(x)$. Dans cette formulation, le champ de jauge apparaît naturellement comme une variable périodique, correspondant à la formulation compacte du groupe de symétrie U(1).

Le terme cinétique du champ de jauge est obtenu avec une variable de plaquette. Par exemple, sur le réseau carré (voir la Fig. 0.2(a)), cette variable de plaquette est donnée par

$$\Pi_{\mu\nu}(x) = U_\mu(x)U_\nu(x + ae_{(\mu)})U_\mu^\dagger(x + ae_{(\nu)})U_\nu^\dagger(x) = \exp\left\{ ia^2 \left(\Delta_\mu A_\nu(x) - \Delta_\nu A_\mu(x)\right)\right\} , \tag{0.1.3}$$

[5] On travaille ici dans les unités où la charge électrique est $e = 1$.

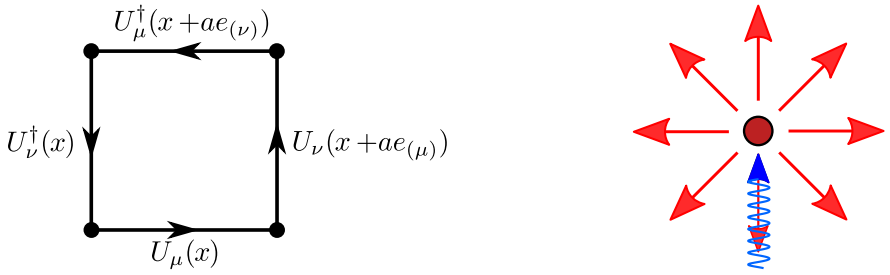

(a) (b)

Figure 0.2. (a) Variable de plaquette sur un réseau carré. (b) Schéma d'un monopôle de Dirac. Le flux de la source ponctuelle est en ligne droite, celui de la corde de Dirac est en ligne ondulée.

où on a défini la différence finie $\Delta_\mu A_\nu(x) = A_\nu(x+ae_{(\mu)}) - A_\nu(x)$. L'argument de l'exponentielle correspond au tenseur de Maxwell discret $F_{\mu\nu}(x) \equiv \Delta_\mu A_\nu(x) - \Delta_\nu A_\mu(x)$. La variable de plaquette est utilisée pour bâtir l'action sur réseau [42, 43]

$$\sum_{\mu,\nu} \mathrm{Re}\left\{1 - \Pi_{\mu\nu}(x)\right\} = \sum_{\mu,\nu}(1 - \cos a^2 F_{\mu\nu}(x))\,. \tag{0.1.4}$$

La limite du continu renvoie le terme de Maxwell, quadratique dans le tenseur de Maxwell.

En définissant le champ H^μ en termes du champ dual au tenseur de Maxwell $H^\mu = \frac{1}{2}\epsilon^{\mu\rho\lambda}F_{\rho\lambda} = \epsilon^{\mu\rho\lambda}\partial_\rho A_\lambda$, les équations de Maxwell sans sources sont données par

$$\frac{1}{2}\partial_\mu \epsilon^{\mu\nu\rho}F_{\nu\rho} = \nabla\cdot\boldsymbol{H} = 0\,, \quad \partial_\mu F^{\mu\nu} = (\nabla\times\boldsymbol{H})^\nu = 0\,. \tag{0.1.5}$$

Une solution non triviale est donnée par [42, 43]

$$H^\mu(x) = q\frac{x^\mu}{|x|^3} + 4\pi q\delta_3^\mu \delta(x_1)\delta(x_2)\theta(-x_3)\,, \tag{0.1.6}$$

où $2q \in \mathbb{Z}$. Cette dernière contrainte, la condition de Dirac, est nécessaire pour que la corde de Dirac, un objet singulier, soit invisible. Plus précisément, la périodicité du terme de Maxwell entrant dans l'argument d'un cosinus (0.1.4) annule l'effet de la corde si la charge q est un demi-entier. Ceci décrit un monopôle de Dirac à la position $x = 0$. Le deuxième terme correspond à la corde de Dirac qui compense le flux du premier terme, une source ponctuelle. Un schéma de la solution est montrée à la Fig. 0.2(b).

La formulation compacte de la théorie de jauge U(1) peut aussi être obtenue dans le continu. Le modèle de 't Hooft-Polyakov est une théorie de jauge non abélienne SU(2) qui

comporte un champ vectoriel de Higgs avec une auto-interaction. En réglant correctement la constante de couplage, une brisure spontanée de symétrie survient, où le champ de jauge est « Higgsé » et la symétrie est réduite SU(2) $\to$ U(1). Puisque le groupe de jauge SU(2) est compact, le sous-groupe U(1) obtenu par brisure de symétrie l'est aussi. Le groupe d'homotopie $\Pi_2(\mathrm{SU}(2)/\,\mathrm{U}(1))$ indique alors la présence d'une configuration topologique non triviale en trois dimensions [43, 44]. Pour un modèle en 3+1 dimensions, on parle d'une configuration statique qui correspond au monopôle de 't Hooft-Polyakov. Cela peut aussi être interprété comme un instanton dans le modèle euclidien en $2+1$ dimensions. Dans une certaine limite du modèle, on peut rendre très massive l'excitation de Higgs restante et se concentrer sur l'excitation du champ de jauge U(1).

0.1.2. Formulation en théorie des champs

Un point de vue plus moderne sur les opérateurs monopôles est présenté dans ce qui suit. L'opérateur monopôle est décrit comme un opérateur qui vient modifier les conditions frontières du champ de jauge pour produire le flux magnétique attendu.

On commence d'abord par formuler la fonction de partition d'une théorie de jauge U(1) pure sans monopôles, donnée par [6]

$$Z = \int \mathcal{D}A \exp\left\{-\int_x \left[-\frac{1}{2e^2}(\epsilon^{\mu\nu\rho}\partial_\nu A_\rho(x))^2\right]\right\}\,, \tag{0.1.7}$$

où $\int_x \equiv d^3x$ et on a réintroduit la charge électrique e. Il est possible de formuler cette fonction de partition en termes du tenseur de Maxwell

$$F_{\mu\nu}(x) = \partial_\mu A_\nu(x) - \partial_\nu A_\mu(x)\,. \tag{0.1.8}$$

Pour ce faire, il faut spécifier que le tenseur de Maxwell est un tenseur de rang 2 obtenu par la dérivée extérieure d'un tenseur de rang 1, $F = \mathrm{d}A$. Cela signifie que la dérivée extérieure du tenseur de Maxwell est nulle, $\mathrm{d}F = \mathrm{d}(\mathrm{d}A) = 0$. En notation tensorielle, cela implique que $\frac{1}{2}\epsilon^{\mu\nu\rho}\partial_\mu F_{\nu\rho}(x) = 0$, soit l'identité de Bianchi. La fonction de partition peut être écrite en termes de $F_{\mu\nu}$ en imposant cette contrainte à l'aide d'un boson auxiliaire σ qui agit comme

[6] Les modes de jauge purs (dus à l'invariance de jauge) devraient être éliminés. Cependant, pour une théorie de jauge abélienne, cela donne simplement un facteur supplémentaire pour la fonction de partition, donc cet effet peut être ignoré.

paramètre de Lagrange [45]

$$Z = \int \mathcal{D}F\mathcal{D}\sigma \exp\left\{-\int_x \left[-\frac{1}{4e^2}F_{\mu\nu}F^{\mu\nu} + \frac{i}{2\pi}\sigma\left(\frac{1}{2}\epsilon^{\mu\nu\rho}\partial_\mu F_{\nu\rho}\right)\right]\right\} . \tag{0.1.9}$$

L'intégrale de chemin est alors limitée aux configurations de champs de jauge respectant l'identité de Bianchi. Étant donné la condition de quantification de Dirac, $\int d^3x \frac{1}{2}\epsilon^{\mu\nu\rho}F_{\nu\rho} = 4\pi q$ avec $2q \in \mathbb{Z}$, il suit que σ est un champ compact avec une périodicité 2π. La fonction de partition est maintenant quadratique en termes du tenseur de Maxwell qui peut être intégré

$$Z = \int \mathcal{D}\sigma \exp\left\{-\int_x \frac{e^2}{8\pi^2}\partial_\mu\sigma\partial^\mu\sigma\right\} . \tag{0.1.10}$$

Le champ σ correspond au photon dual. Le modèle a une symétrie de « shift », $\sigma \to \sigma + \alpha$. Cette symétrie correspond à la symétrie $\mathrm{U}(1)_{\mathrm{top}}$, compacte puisque σ est 2π-périodique. Dans la formulation du modèle initial, cette symétrie est associée au courant topologique

$$J^\mu_{\mathrm{top}}(x) = \epsilon^{\mu\nu\rho}\partial_\nu A_\rho(x) . \tag{0.1.11}$$

L'existence d'un tel courant topologique survient en $2+1$ dimensions où le tenseur complètement antisymétrique a trois indices, dont deux se contractent avec la dérivée du champ de jauge. Les opérateurs chargés sous $\mathrm{U}(1)_{\mathrm{top}}$ sont les opérateurs monopôles $\mathcal{M}^\dagger_q(x)$ avec une charge q

$$\mathrm{U}(1)_{\mathrm{top}} : \mathcal{M}^\dagger_q(x) \to e^{i2q\alpha}\mathcal{M}^\dagger_q(x) . \tag{0.1.12}$$

Un opérateur monopôle peut donc être écrit en termes du photon dual comme $\mathcal{M}^\dagger_q(x) \sim e^{i2q\sigma(x)}$. L'action du courant topologique sur cet opérateur est donnée par [46]

$$J^\mu_{\mathrm{top}}(x)\mathcal{M}^\dagger_q(0) \sim q\frac{x^\mu}{|x|^3}\mathcal{M}^\dagger_q(0) + \text{termes moins singuliers} . \tag{0.1.13}$$

Le terme singulier correspond au champ d'un monopôle de Dirac de charge q. L'opérateur monopôle crée donc une configuration pour le flux topologique, plus spécifiquement

$$\partial_\mu J^\mu_{\mathrm{top}}(x) = \frac{1}{2}\epsilon^{\mu\nu\rho}\partial_\mu F_{\nu\rho}(x) = 4\pi q\delta^{(3)}(x - R) , \tag{0.1.14}$$

pour une charge placée en $x^\mu = R^\mu$.[7] Comparativement à la situation présentée précédemment, on a maintenant une violation de l'identité de Bianchi.[8] On peut insérer une telle

[7] De manière équivalente, on peut dire que le flux autour du point d'insertion sur une sphère S^2 est $\int_{S^2} d^2x J^0_{\mathrm{top}}(x) = 4\pi q$.

[8] Contrairement à la section précédente, l'effet de la corde de Dirac est exclu. C'est possible de le faire puisqu'elle ne contribue pas à l'action. L'équation de Maxwell a ainsi un terme de source pour décrire la

configuration dans la fonction de partition en modifiant la contribution du boson auxiliaire dans l'action

$$\frac{i}{2\pi}\int_x \sigma(x)\left[\frac{1}{2}\epsilon^{\mu\nu\rho}\partial_\mu F_{\nu\rho}(x) - 4\pi q\delta^{(3)}(x-R)\right] = \frac{i}{2\pi}\int_x \left[\sigma(x)\left(\frac{1}{2}\epsilon^{\mu\nu\rho}\partial_\mu F_{\nu\rho}\right)\right] - i2q\sigma(R)\,. \tag{0.1.15}$$

L'insertion du monopôle de charge q en $x^\mu = R^\mu$ correspond donc effectivement à l'ajout d'un terme $\mathcal{M}_q^\dagger(R) \sim e^{i2q\sigma(R)}$ dans la fonction de partition.

0.1.3. Autres propriétés importantes

Dans la théorie de jauge pure U(1) compacte en $2+1$ dimensions, les monopôles ont un effet de confinement [42, 43]. Ce modèle a d'abord été motivé par Polyakov comme un modèle jouet pour comprendre le confinement dans la chromodynamique quantique en $3+1$ dimensions (QCD), soit une théorie de jauge SU(3). L'importance des excitations topologiques pour le confinement dans les deux modèles [47] montre effectivement un lien intéressant. L'ajout de champs de matière sans masse, comme dans le modèle QED_3 étudié dans cette thèse, a pour effet d'écranter les monopôles. Pour un nombre suffisamment élevé de saveurs de champs de matière, le confinement peut ainsi être empêché [46, 48]. Le nombre critique pour obtenir une phase DSL stable a été évalué à $2N = 12$ [49], le nombre critique où le monopôle de charge minimale (et par conséquent, de dimension d'échelle minimale) devient non pertinent.[9] Ce résultat est cohérent avec les contraintes du « conformal bootstrap » établies par la suite [50, 51] et confirmé par une étude Monte Carlo [52]. Les impuretés contribuent à déstabiliser d'autant plus le DSL et à augmenter le nombre critique [53]. Sur les réseaux non bipartites, par contre, les symétries discrètes interdisent les monopôles de plus petites charges ($q = 1/2$ pour le réseau kagome et $q = 1/2, 1$ pour le réseau triangulaire [54]), ce qui abaisse ce nombre critique. Il demeure que le DSL $2N = 4$ sur réseau kagome considéré pourrait s'avérer instable [55], des résultats non perturbatifs seraient utiles pour clarifier la situation.

contribution ponctuelle du monopôle de Dirac. D'un autre point de vue, on peut simplement voir le terme de source dans l'équation de Maxwell comme la contribution de la corde de Dirac.

[9] Un opérateur « irrelevant », c'est-à-dire un opérateur dont la dimension d'échelle excède le nombre de dimensions d'espace-temps, ici 3.

L'existence de modes zéros fermioniques en présence d'un monopôle [56] est aussi une propriété importante. Plus précisément, on compte $2N \times 2|q|$ modes zéro pour un monopôle de charge q. Pour produire un opérateur monopôle sans charge fermionique (une condition nécessaire pour un opérateur invariant de jauge), ces modes doivent être à moitié remplis [46]. [10] De ce fait, en variant les saveurs des modes zéro qui « habillent » l'opérateur monopôle, on obtient une diversité d'opérateurs aux nombres quantiques non triviaux, correspondant au spin magnétique et aux vallées d'impulsion dans le contexte d'un aimant quantique. L'importance de l'« habillement » d'un mode zéro survient de manière similaire dans l'étude de la chaîne de polyacétylène. Ce système présente une brisure spontanée de symétrie Z_2 qui permet de former un mur de domaine. Il existe un mode zéro, nommé mode de Jackiw-Rebbi, localisé à la surface de ce dernier [57]. On conclut que ce soliton a une charge fractionalisée $\pm 1/2$, dépendamment si le mode zéro est occupé ou non. Dans le cas des monopôles dans QED_3, le nombre de saveurs fermionique $2N$ est pair [11], donnant aussi un nombre pair de modes zéros, une condition nécessaire pour obtenir un nombre fermionique nul.

0.1.4. Importance des monopôles

Le DSL avec $2N = 4$ saveurs a été décrit comme une phase parente permettant de comprendre le lien entre plusieurs paramètres d'ordre apparemment très différents, tant sur des réseaux bipartites (carré, nid d'abeilles) que non bipartites (triangulaire, kagome) [54]. Un ingrédient crucial dans cette description unifiée est la présence d'opérateurs monopôles. Les monopôles seront donc étudiés dans les transitions de phase quantiques hors d'un DSL. Plus spécifiquement, des transitions représentées par l'ajout de diverses interactions de type Gross-Neveu (GN) au modèle QED_3 sont considérées.

Ce type de modèle permet notamment de décrire la transition du DSL vers des ordres de type AFM ou VBS. Il s'agit d'une transition de confinement-déconfinement : alors que

[10] Ce résultat survient dans le cadre d'une quantification $\mathcal{CT}$ où les partenaires $\mathcal{CT}$ ont des nombres fermioniques opposés. Cette symétrie échange les particules et le trous. Pour avoir un opérateur au nombre fermionique nul, il faut un opérateur « habillé » par autant d'états fermioniques occupés que de trous. Si on requiert de plus que la dimension d'échelle de l'opérateur soit minimale, il faut remplir les états d'énergie minimale d'abord : on remplit toute la mer de Dirac (les états d'énergie négative, qui ont leur contrepartie en énergie positive), puis il reste la moitié des modes zéro à remplir.

[11] Ce choix est notamment nécessaire pour éviter l'anomalie de parité [58].

les spinons obtiennent une masse, leur effet d'écrantage est perdu [46, 59], laissant les monopôles proliférer et confiner le modèle [42, 43]. Cela signifie une recombinaison des spinons dans les phases ordonnées. Dans certains cas, ce sont même les monopôles, munis de nombres quantiques non triviaux provenant de leur « habillement » fermionique, qui jouent le rôle de paramètre d'ordre [11, 54, 60]. Certains types de masse impliquent néanmoins la présence d'un terme de Chern-Simons qui empêche la prolifération des monopôles. Dans ce cas, les spinons peuvent rester déconfinés, ce qui peut mener à des liquides de spin « gappés » présentant un ordre topologique [9].

Outre l'importance des opérateurs monopôles dans la description de certains matériaux quantiques, la place centrale que les monopôles occupent dans les dualités en théorie quantique champs (QFT) motive aussi grandement leur étude.[12] Ils apparaissent notamment dans la dualité particule-vortex [61] : les opérateurs de création de particules dans le modèle bosonique O(2) correspondent aux opérateurs monopôles (créant des vortex) du modèle CP^1 [13], et vice-versa. Les dualités en QFT donnent des outils supplémentaires dans l'étude des théories fortement couplées et ont attiré l'attention tant en physique de la matière condensée qu'en physique des hautes énergies [62, 63].

0.2. Plan de la thèse

La dimension d'échelle $\Delta_{\mathcal{M}_q}$ des opérateurs monopôles $\mathcal{M}_q^\dagger(x)$ au point critique quantique (QCP) d'une transition de phase est une quantité centrale étudiée dans chaque chapitre de la thèse. C'est l'exposant critique qui contrôle la fonction deux-points des opérateurs monopôles

$$\left\langle \mathcal{M}_q(x)\mathcal{M}_q^\dagger(y)\right\rangle \sim \frac{1}{|x-y|^{2\Delta_{\mathcal{M}_q}}}\,. \tag{0.2.1}$$

Puisqu'un QCP est décrit par une théorie conforme des champs (CFT), la correspondance état-opérateur peut être utilisée pour calculer la dimension d'échelle [64]. L'origine de cette correspondance est discutée dans l'annexe A. Utilisant cette correspondance, le calcul des dimensions d'échelle est traduit en termes du calcul de l'énergie de l'état fondamental d'une certaine CFT, ce qui est fait avec un développement en large-N. L'utilisation d'une telle

[12] De manière plus générale, les opérateurs de désordre topologique jouent un rôle central dans les dualités en QFT. Les opérateurs monopôles constituent un cas spécifique en $2+1$ dimensions.

[13] Le modèle CP^1 correspond au modèle abélien de Higgs avec deux bosons complexes. On appelle aussi ce modèle QED_3 scalaire (avec une contrainte non linéaire).

méthode appliquée aux monopôles remonte à la Réf. [65] où la dimension d'échelle dans QED_3 a été obtenue à l'ordre dominant en $1/N$.[14] La méthode a ensuite été utilisée à l'ordre sous-dominant en $1/N$ [49] et dans de nombreux autres modèles qui sont discutés dans les chapitres principaux de la thèse.

Le premier chapitre est motivé en partie par l'un des premiers matériaux identifiés comme un candidat QSL, le Herbertsmithite [23]. Avec ses plans d'atomes de cuivre, ce matériau forme un antiferroaimant d'Heinserberg sur réseau kagome. À proximité de ce présumé DSL, il existe un ordre antiferromagnétique coplanaire-120° dont le paramètre d'ordre est décrit par un opérateur monopôle [11, 54, 60]. Le monopôle en question a une polarisation maximale du spin magnétique induite par un habillement particulier en termes de modes zéros fermioniques. Il est condensé suite à l'apparition d'une masse de type spin-Hall induite par l'activation d'une interaction chiral Heisenberg Gross-Neveu (cHGN) qui dépend du spin magnétique [54, 59, 60].[15] Cette prolifération des monopôles mène au confinement des spinons, un phénomène lié à l'instabilité de la théorie de jauge pure U(1) [42, 43] tel que mentionné plus haut. La dimension d'échelle minimale parmi les opérateurs monopôles est obtenue au QCP, représenté par le modèle critique de QED_3-cHGN. Cette quantité est calculée pour plusieurs charges topologiques q de monopôle à l'ordre dominant dans un développement en $1/N$. Les dimensions d'échelle trouvées sont plus petites à ce QCP que dans le DSL représenté par QED_3. Une étude en renormalisation à une boucle est également réalisée pour le modèle non compact (sans monopôles) avec la régularisation dimensionnelle $d = 4 - \epsilon$. L'observabilité expérimentale de certains résultats est également explorée. L'implication des résultats pour la transition vers une phase VBS est également discutée.

Le deuxième chapitre concerne le même modèle, explorant plus en détail un aspect seulement effleuré dans le Chap. 1. L'activation de l'interaction cHGN brise partiellement une symétrie de saveurs de QED_3, $\mathrm{SU}(2N) \to \mathrm{SU}(2) \times \mathrm{SU}(N)$. Une levée partielle de la dégénérescence des dimensions d'échelles de monopôles survient alors au QCP. C'est la polarisation

[14] Le premier calcul de la dimension d'échelle d'un opérateur monopôle, réalisé dans le modèle CP^{N-1}, avait été fait sans cette méthode [48]. Les résultats ont par la suite été confirmés avec la correspondance état-opérateur [66].

[15] Une récente étude numérique du modèle $J_1 - J_2$ indique que cette transition de phase serait en fait (faiblement) du premier ordre. [67], ce qui changerait la description analytique du QCP. L'étude numérique est cependant menée pour une taille de réseau limitée.

magnétique des monopôles qui contrôle la hiérarchie : une polarisation maximale implique une dimension d'échelle minimale et vice-versa. Avec l'inclusion d'un paramètre de Lagrange, la dimension d'échelle minimale des monopôles est trouvée pour divers secteurs de spin magnétique à l'ordre dominant en $1/N$. Cette hiérarchie prédit notamment des exposants critiques différents pour les corrélations de type magnétique et de type liens de valence. La hiérarchie est également discutée à l'aide de la théorie des représentations. La représentation irréductible (irrep) de SU($2N$) formée par les monopôles dans QED_3 est réduite en une somme d'irreps de SU(2) $\times$ SU(N) au QCP. Pour chaque secteur de spin magnétique, une dégénérescence due au secteur de vallées d'impulsion est ainsi prédite.

Enfin, le troisième chapitre élargit une section d'abord présentée dans le Chap. 1. Elle concerne l'étude de la transition du DSL vers un liquide de spin chiral (CSL). Dans ce cas, c'est une interaction de type GN indépendante de la saveur qui est activée. L'ordre chiral est décrit par la masse fermionique symétrique induite par l'interaction. Contrairement à la situation dans l'AFM précédemment considérée, les spinons dans le CSL restent déconfinés, étant donné qu'un terme de Chern-Simons empêche la prolifération des monopôles. Dans le Chap. 1, on trouve que les monopôles au QCP décrit par QED_3-GN ont la même dimension d'échelle que dans QED_3 à l'ordre dominant en $1/N$. Le but du troisième chapitre est principalement d'obtenir les premières corrections quantiques avec l'ordre sous-dominant en $1/N$. De petites corrections positives sont trouvées. Celles-ci s'avèrent utiles pour tester des prédictions en théorie des champs. Notamment, une dualité entre les modèles QED_3-GN $|_{2N=2}$ et CP^1 prédite dans la Réf. [68] implique une symétrie SO(5). Les opérateurs organisés en multiplets analogues de SO(5) dans QED_3-GN et CP^1 devraient ainsi avoir la même dimension d'échelle. Les dimensions d'échelles des monopôles trouvées pour QED_3-GN $|_{2N=2}$ se comparent remarquablement bien aux autres dimensions d'échelle obtenues analytiquement dans la littérature. D'autre part, les résultats obtenus servent également à obtenir la dimension anormale des monopôles à un autre QCP, entre le DSL et un supraconducteur de type « s-wave », soit le QSL de type Z_2 [69, 70]. Cette transition est décrite par l'activation d'une interaction GN de type supraconducteur, soit le modèle QED_3-Z_2GN. Les dimensions anormales de monopôles trouvées pour ce cas sont également positives. En ajustant le comportement large-q des dimensions d'échelles des monopôles dans QED_3, QED_3-GN, et

QED_3-Z_2GN, le coefficient constant $O(q^0)$ trouvé concorde avec une prédiction universelle pour les CFTs ayant une symétrie globale U(1) [71].

Bibliographie

[1] K. von Klitzing, G. Dorda, and M. Pepper, Phys. Rev. Lett. **45**, 494 (1980), URL https://link.aps.org/doi/10.1103/PhysRevLett.45.494.

[2] K. von Klitzing, Rev. Mod. Phys. **58**, 519 (1986), URL https://link.aps.org/doi/10.1103/RevModPhys.58.519.

[3] D. C. Tsui, H. L. Stormer, and A. C. Gossard, Phys. Rev. Lett. **48**, 1559 (1982), URL https://link.aps.org/doi/10.1103/PhysRevLett.48.1559.

[4] J. K. Jain, Phys. Rev. B **41**, 7653 (1990), URL https://link.aps.org/doi/10.1103/PhysRevB.41.7653.

[5] T. Senthil, L. Balents, S. Sachdev, A. Vishwanath, and M. P. A. Fisher, Phys. Rev. B **70**, 144407 (2004), URL https://link.aps.org/doi/10.1103/PhysRevB.70.144407.

[6] T. Senthil, L. Balents, S. Sachdev, A. Vishwanath, and M. P. A. Fisher, Journal of the Physical Society of Japan **74**, 1 (2005), https://doi.org/10.1143/JPSJS.74S.1, URL https://doi.org/10.1143/JPSJS.74S.1.

[7] M. A. Metlitski and R. Thorngren, Phys. Rev. B **98**, 085140 (2018), URL https://link.aps.org/doi/10.1103/PhysRevB.98.085140.

[8] L. Savary and L. Balents, Reports on Progress in Physics **80**, 016502 (2016), URL https://doi.org/10.1088%2F0034-4885%2F80%2F1%2F016502.

[9] X.-G. Wen, Rev. Mod. Phys. **89**, 041004 (2017), URL https://link.aps.org/doi/10.1103/RevModPhys.89.041004.

[10] M. Hermele, T. Senthil, and M. P. A. Fisher, Phys. Rev. B **72**, 104404 (2005), URL https://link.aps.org/doi/10.1103/PhysRevB.72.104404.

[11] M. Hermele, Y. Ran, P. A. Lee, and X.-G. Wen, Phys. Rev. B **77**, 224413 (2008), URL https://link.aps.org/doi/10.1103/PhysRevB.77.224413.

[12] Y. Iqbal, W.-J. Hu, R. Thomale, D. Poilblanc, and F. Becca, Phys. Rev. B **93**, 144411 (2016), URL https://link.aps.org/doi/10.1103/PhysRevB.93.144411.

[13] P. Corboz, M. Lajkó, A. M. Läuchli, K. Penc, and F. Mila, Phys. Rev. X **2**, 041013 (2012), URL https://link.aps.org/doi/10.1103/PhysRevX.2.041013.

[14] V. Calvera and C. Wang, *Theory of Dirac spin liquids on spin-S triangular lattice : possible application to α-CrOOH(D)* (2020), 2012.09809.

[15] V. Calvera and C. Wang, *Theory of Dirac spin-orbital liquids : monopoles, anomalies, and applications to SU(4) honeycomb models* (2021), 2103.13405.

[16] M. Baenitz, P. Schlender, J. Sichelschmidt, Y. A. Onykiienko, Z. Zangeneh, K. M. Ranjith, R. Sarkar, L. Hozoi, H. C. Walker, J.-C. Orain, et al., Phys. Rev. B **98**, 220409 (2018), URL https://link.aps.org/doi/10.1103/PhysRevB.98.220409.

[17] W. Liu, Z. Zhang, J. Ji, Y. Liu, J. Li, X. Wang, H. Lei, G. Chen, and Q. Zhang, Chinese Physics Letters **35**, 117501 (2018), URL https://doi.org/10.1088/0256-307x/35/11/117501.

[18] L. Ding, P. Manuel, S. Bachus, F. Grußler, P. Gegenwart, J. Singleton, R. D. Johnson, H. C. Walker, D. T. Adroja, A. D. Hillier, et al., Phys. Rev. B **100**, 144432 (2019), URL https://link.aps.org/doi/10.1103/PhysRevB.100.144432.

[19] K. M. Ranjith, D. Dmytriieva, S. Khim, J. Sichelschmidt, S. Luther, D. Ehlers, H. Yasuoka, J. Wosnitza, A. A. Tsirlin, H. Kühne, et al., Phys. Rev. B **99**, 180401 (2019), URL https://link.aps.org/doi/10.1103/PhysRevB.99.180401.

[20] M. M. Bordelon, E. Kenney, C. Liu, T. Hogan, L. Posthuma, M. Kavand, Y. Lyu, M. Sherwin, N. P. Butch, C. Brown, et al., Nature Physics **15**, 1058 (2019), ISSN 1745-2481, URL https://doi.org/10.1038/s41567-019-0594-5.

[21] R. Kaneko, S. Morita, and M. Imada, Journal of the Physical Society of Japan **83**, 093707 (2014), https://doi.org/10.7566/JPSJ.83.093707, URL https://doi.org/10.7566/JPSJ.83.093707.

[22] S. Hu, W. Zhu, S. Eggert, and Y.-C. He, Phys. Rev. Lett. **123**, 207203 (2019), URL https://link.aps.org/doi/10.1103/PhysRevLett.123.207203.

[23] M. P. Shores, E. A. Nytko, B. M. Bartlett, and D. G. Nocera, Journal of the American Chemical Society **127**, 13462 (2005), ISSN 0002-7863, URL https://doi.org/10.1021/ja053891p.

[24] T.-H. Han, J. S. Helton, S. Chu, D. G. Nocera, J. A. Rodriguez-Rivera, C. Broholm, and Y. S. Lee, Nature **492**, 406 (2012), ISSN 0028-0836, 1476-4687, URL http://www.nature.com/articles/nature11659.

[25] Z. Feng, Z. Li, X. Meng, W. Yi, Y. Wei, J. Zhang, Y.-C. Wang, W. Jiang, Z. Liu, S. Li, et al., Chinese Physics Letters **34**, 077502 (2017), URL https://doi.org/10.1088%2F0256-307x%2F34%2F7%2F077502.

[26] Y. Ran, M. Hermele, P. A. Lee, and X.-G. Wen, Phys. Rev. Lett. **98**, 117205 (2007), URL https://link.aps.org/doi/10.1103/PhysRevLett.98.117205.

[27] Y. Iqbal, F. Becca, and D. Poilblanc, Phys. Rev. B **84**, 020407 (2011), URL https://link.aps.org/doi/10.1103/PhysRevB.84.020407.

[28] Y. Iqbal, F. Becca, S. Sorella, and D. Poilblanc, Phys. Rev. B **87**, 060405 (2013), URL https://link.aps.org/doi/10.1103/PhysRevB.87.060405.

[29] Y. Iqbal, D. Poilblanc, and F. Becca, Phys. Rev. B **91**, 020402 (2015), URL https://link.aps.org/doi/10.1103/PhysRevB.91.020402.

[30] Y.-C. He, M. P. Zaletel, M. Oshikawa, and F. Pollmann, Phys. Rev. X **7**, 031020 (2017), URL https://link.aps.org/doi/10.1103/PhysRevX.7.031020.

[31] W. Zhu, X. Chen, Y.-C. He, and W. Witczak-Krempa, Science Advances **4** (2018), URL https://advances.sciencemag.org/content/4/11/eaat5535.

[32] H. J. Liao, Z. Y. Xie, J. Chen, Z. Y. Liu, H. D. Xie, R. Z. Huang, B. Normand, and T. Xiang, Phys. Rev. Lett. **118**, 137202 (2017), URL https://link.aps.org/doi/10.1103/PhysRevLett.118.137202.

[33] S. Jiang, P. Kim, J. H. Han, and Y. Ran, SciPost Phys. **7**, 6 (2019), URL https://scipost.org/10.21468/SciPostPhys.7.1.006.

[34] H. C. Jiang, Z. Y. Weng, and D. N. Sheng, Phys. Rev. Lett. **101**, 117203 (2008), URL https://link.aps.org/doi/10.1103/PhysRevLett.101.117203.

[35] S. Yan, D. A. Huse, and S. R. White, Science **332**, 1173 (2011), ISSN 0036-8075, https://science.sciencemag.org/content/332/6034/1173.full.pdf, URL https://science.sciencemag.org/content/332/6034/1173.

[36] S. Depenbrock, I. P. McCulloch, and U. Schollwöck, Phys. Rev. Lett. **109**, 067201 (2012), URL https://link.aps.org/doi/10.1103/PhysRevLett.109.067201.

[37] H.-C. Jiang, Z. Wang, and L. Balents, Nature Physics **8**, 902 EP (2012), URL https://doi.org/10.1038/nphys2465.

[38] Z. Zhu and S. R. White, Phys. Rev. B **92**, 041105 (2015), URL https://link.aps.org/doi/10.1103/PhysRevB.92.041105.

[39] W.-J. Hu, S.-S. Gong, W. Zhu, and D. N. Sheng, Phys. Rev. B **92**, 140403 (2015), URL https://link.aps.org/doi/10.1103/PhysRevB.92.140403.

[40] J.-W. Mei, J.-Y. Chen, H. He, and X.-G. Wen, Phys. Rev. B **95**, 235107 (2017), URL https://link.aps.org/doi/10.1103/PhysRevB.95.235107.

[41] K. G. Wilson, Phys. Rev. D **10**, 2445 (1974), URL https://link.aps.org/doi/10.1103/PhysRevD.10.2445.

[42] A. M. Polyakov, Physics Letters B **59**, 82 (1975), ISSN 0370-2693, URL http://www.sciencedirect.com/science/article/pii/0370269375901628.

[43] A. M. Polyakov, Nuclear Physics B **120**, 429 (1977), ISSN 0550-3213, URL http://www.sciencedirect.com/science/article/pii/0550321377900864.

[44] G. 't Hooft, Nucl. Phys. B **79**, 276 (1974).

[45] D. Tong, *Gauge Theory. http ://www.damtp.cam.ac.uk/user/tong/gaugetheory.html*, URL http://www.damtp.cam.ac.uk/user/tong/gaugetheory.html.

[46] V. Borokhov, A. Kapustin, and X. Wu, Journal of High Energy Physics **2002**, 049 (2002), URL https://doi.org/10.1088/1126-6708/2002/11/049.

[47] J. Greensite, Progress in Particle and Nuclear Physics **51**, 1 (2003), ISSN 0146-6410, URL https://www.sciencedirect.com/science/article/pii/S0146641003900123.

[48] G. Murthy and S. Sachdev, Nuclear Physics B **344**, 557 (1990).

[49] S. S. Pufu, Phys. Rev. D **89**, 065016 (2014), URL https://link.aps.org/doi/10.1103/PhysRevD.89.065016.

[50] S. M. Chester and S. S. Pufu, Journal of High Energy Physics **2016**, 19 (2016), ISSN 1029-8479, URL https://doi.org/10.1007/JHEP08(2016)019.

[51] S. M. Chester, L. V. Iliesiu, M. Mezei, and S. S. Pufu, Journal of High Energy Physics **2018** (2018), ISSN 1029-8479, URL http://link.springer.com/10.1007/JHEP05(2018)157.

[52] N. Karthik and R. Narayanan, Phys. Rev. D **100**, 054514 (2019), URL https://link.aps.org/doi/10.1103/PhysRevD.100.054514.

[53] S. Dey, Phys. Rev. B **102**, 235165 (2020), URL https://link.aps.org/doi/10.1103/PhysRevB.102.235165.

[54] X.-Y. Song, C. Wang, A. Vishwanath, and Y.-C. He, Nature Communications **10**, 4254 (2019), ISSN 2041-1723, URL https://doi.org/10.1038/s41467-019-11727-3.

[55] E. Dyer, M. Mezei, and S. S. Pufu, *Monopole taxonomy in three-dimensional conformal field theories* (2013), arXiv:1309.1160.

[56] M. F. Atiyah and I. M. Singer, Bulletin of the American Mathematical Society **69**, 422 (1963), URL https://doi.org/.

[57] R. Jackiw and C. Rebbi, Phys. Rev. D **13**, 3398 (1976), URL https://link.aps.org/doi/10.1103/PhysRevD.13.3398.

[58] A. N. Redlich, Phys. Rev. Lett. **52**, 18 (1984), URL https://link.aps.org/doi/10.1103/PhysRevLett.52.18.

[59] P. Ghaemi and T. Senthil, Phys. Rev. B **73**, 054415 (2006), URL https://link.aps.org/doi/10.1103/PhysRevB.73.054415.

[60] Y.-M. Lu, G. Y. Cho, and A. Vishwanath, Phys. Rev. B **96**, 205150 (2017), URL https://link.aps.org/doi/10.1103/PhysRevB.96.205150.

[61] M. E. Peskin, Annals of Physics **113**, 122 (1978), ISSN 0003-4916, URL http://www.sciencedirect.com/science/article/pii/000349167890252X.

[62] N. Seiberg, T. Senthil, C. Wang, and E. Witten, Annals of Physics **374**, 395 (2016), ISSN 0003-4916, URL http://www.sciencedirect.com/science/article/pii/S0003491616301531.

[63] A. Karch and D. Tong, Phys. Rev. X **6**, 031043 (2016), URL https://link.aps.org/doi/10.1103/PhysRevX.6.031043.

[64] S. Rychkov, *EPFL Lectures on Conformal Field Theory in $D \geq 3$ Dimensions*, SpringerBriefs in Physics (Springer International Publishing, Cham, 2017), ISBN 978-3-319-43625-8, URL //www.springer.com/gp/book/9783319436258.

[65] V. Borokhov, A. Kapustin, and X. Wu, Journal of High Energy Physics **2002**, 044 (2002), URL https://doi.org/10.1088/1126-6708/2002/12/044.

[66] M. A. Metlitski, M. Hermele, T. Senthil, and M. P. A. Fisher, Phys. Rev. B **78**, 214418 (2008), URL https://link.aps.org/doi/10.1103/PhysRevB.78.214418.

[67] Y. Iqbal, F. Ferrari, A. Chauhan, A. Parola, D. Poilblanc, and F. Becca, *Gutzwiller-projected states for the j_1-j_2 Heisenberg model on the kagome lattice : achievements and pitfalls* (2021), 2108.02847.

[68] C. Wang, A. Nahum, M. A. Metlitski, C. Xu, and T. Senthil, Phys. Rev. X **7**, 031051 (2017), URL https://link.aps.org/doi/10.1103/PhysRevX.7.031051.

[69] N. Zerf, C.-H. Lin, and J. Maciejko, Phys. Rev. B **94**, 205106 (2016), URL https://link.aps.org/doi/10.1103/PhysRevB.94.205106.

[70] R. Boyack, C.-H. Lin, N. Zerf, A. Rayyan, and J. Maciejko, Phys. Rev. B **98**, 035137 (2018), URL https://link.aps.org/doi/10.1103/PhysRevB.98.035137.

[71] S. Hellerman, D. Orlando, S. Reffert, and M. Watanabe, Journal of High Energy Physics **2015**, 1 (2015), ISSN 1029-8479, arXiv:1505.01537, URL https://doi.org/10.1007/JHEP12(2015)071.

Chapitre 1

Transition from a Dirac spin liquid to an antiferromagnet : Monopoles in a QED_3-Gross-Neveu theory

É. Dupuis, M. B. Paranjape, et W. Witczak-Krempa, Phys. Rev. B, vol. 100, no. 9, p. 094443, Sep. 2019.

Abstract. We study the quantum phase transition from a Dirac spin liquid to an antiferromagnet driven by condensing monopoles with spin quantum numbers. We describe the transition in field theory by tuning a fermion interaction to condense a spin-Hall mass, which in turn allows the appropriate monopole operators to proliferate and confine the fermions. We compute various critical exponents at the quantum critical point (QCP), including the scaling dimensions of monopole operators by using the state-operator correspondence of conformal field theory. We find that the degeneracy of monopoles in QED_3 is lifted and yields a non-trivial monopole hierarchy at the QCP. In particular, the lowest monopole dimension is found to be smaller than that of QED_3 using a large N_f expansion where $2N_f$ is the number of fermion flavors. For the minimal magnetic charge, this dimension is $0.39N_f$ at leading order. We also study the QCP between Dirac and chiral spin liquids, which allows us to test a conjectured duality to a bosonic CP^1 theory. Finally, we discuss the implications of our results for quantum magnets on the Kagome lattice.

1.1. Introduction

Quantum spin liquids (QSLs) are strongly correlated phases of matter characterized by long-range entanglement, fractionalized excitations and, in some cases, topological order [1–3]. QSLs can arise in frustrated antiferromagnets where important quantum fluctuations lead to a highly entangled and non-magnetic ground state. In recent years, many candidate materials that may realize a QSL have been identified [3–7].

The fractionalized excitations of a QSL are said to be deconfined as they don't appear in ordered phases. One important aspect to better understand the fractionalized aspect of these phases of matter is to characterize their transition to confined phases, that is to characterize confinement-deconfinement phase transitions. In this respect, the U(1) Dirac spin liquid (DSL) or algebraic spin liquid, which potentially describes certain two-dimensional QSLs at low energy, is an interesting example. This theory corresponds to quantum electrodynamics in $2+1$ dimensions (QED_3) with typically $2N = 4$ massless fermions, called spinons, and an emergent U(1) gauge field. The U(1) gauge field is compact given the underlying lattice, and for this reason the spectrum of the DSL contains topological disorder operators known as monopole operators. These are the operators that may drive confinement. In a pure compact U(1) gauge theory, monopoles proliferate and confine the gauge field [8, 9]. The presence of massless fermions may screen the monopoles and prevent the confinement given a sufficiently large number of fermion flavors [10]. The stability of a QSL is thus determined by the relevance of monopole operators. Even if the spin liquid is intrinsically stable, monopole operators may still drive confinement if the fermions are gapped out at a phase transition. This is the situation considered in this paper.

The DSL phase has been used to describe quantum magnets in many contexts. On the triangular lattice, variational Monte Carlo (VMC) studies [11, 12] have shown that the ground state of a $J_1 - J_2$ Heisenberg antiferromagnet in the range $0.07 < J_2/J_1 < 0.15$ is given by the DSL. VMC studies [13–16] and other numerical methods [17, 18] also favor a DSL as the ground state of an Heisenberg antiferromagnet on the Kagome lattice. These results are not yet firmly established as contradicting studies find gapped spin liquids in both these contexts. The transition to a confined phase through monopole condensation was proposed for the DSL on the square lattice by Ghaemi and Senthil in Ref. [19]. A certain class of

monopole operators with spin quantum numbers may also give the correct order parameter for the $\boldsymbol{q} = 0$ antiferromagnet on the Kagome lattice [20].

Topological disorder operators such as the monopole operators play an important role in other contexts. For example, they are involved in the physics of deconfined quantum critical points (dQCPs) [21, 22]. The prototypical case study is the quantum critical point of the Néel-VBS phase transition on the square lattice which is described by the bosonic CP^1 theory where the condensing monopole operators which have lattice quantum numbers allows this non-Landau phase transition. The properties of the monopole operators in the CP^1 theory have been studied numerically in Refs. [23–25]. It is also important to note that dQCPs correspond to strongly correlated systems whose description may be reformulated as field theoritical dualities. A well known example is the particle-vortex duality [26, 27]. Recently, many new dualities have been found in $2 + 1$ dimensional gauge theories (earlier examples of this resurgence can be found in Refs. [28–30]). Studying critical properties of topological disorder operators provides useful data which may serve to verify conjectured dualities. Confinement-deconfinement transitions are also important in particle physics where the confinement of quarks into hadrons at low energy is a long-standing issue. In fact, the original motivation of Polyakov to study compact QED_3 was to obtain a toy model of confinement of quantum chromodynamics. These relations to deep advancements in quantum phases of matter and quantum field theories motivate further our study of monopole operators.

The objective of this paper is to provide a field theoretical characterization of the confinement-deconfinement transition from a DSL to an antiferromagnetic phase. We will study the properties of a quantum critical point (QCP) separating these phases, which is in fact a conformal field theory. The transition will be described with a Gross-Neveu like deformation of QED_3, where a fermion mass is condensed by tuning a fermion interaction. In turn, the gapped fermions no longer screen the monopole operators which can proliferate. Special attention is given to these topological operators. The central result of our work is the scaling dimension of monopole operators at the QCP. The field theory used to describe this confinement-deconfinement transition with the condensation of a spin-Hall mass was proposed in Ref. [31]. The idea was later generalized to include the condensation of any monopole operator following the condensation of an appropriate fermion bilinear [32].

The paper is structured as follows. In Sec. 1.2, we give the theoretical background for the monopole operators and the confinement-deconfinement transition driven by the condensation of a spin-Hall mass. To this end, we activate a chiral Heisenberg Gross-Neveu (cHGN) interaction term , i.e. the transition is described with the $\mathrm{QED}_3 - \mathrm{cHGN}$ model. In Sec. 1.3, we compute the lowest scaling dimension of monopole operators at the QCP using the state-operator correspondence. We find that the monopole scaling dimension is lower at the QCP than at the QED_3 fixed point. We also obtain an analytical approximation of the scaling dimension in the limit of large magnetic charge. In Sec. 1.4, we consider distinct fermionic dressings that define monopole operators with various quantum numbers, and show there is a hierarchy in the related scaling dimensions. In Sec. 1.5, we do the same analysis in a transition to a chiral spin liquid, where a mass respecting the full flavor group is condensed by activating a Gross-Neveu (GN) interaction. Extrapolating our results to $2N_f = 2$ allows us to test the duality between the $\mathrm{QED}_3 - \mathrm{GN}$ QCP and the bosonic CP^1 theory. In Sec. 1.6, we do a one-loop perturbative renormalization group analysis of the non-compact field theory describing the confinement-deconfinement transition. We find an infrared fixed point corresponding to the QCP and we compute various critical exponents. In Sec. 1.7, we discuss the implications of our results for the phase transition in the particular case of the Kagome Heisenberg lattice model. We summarize our results and discuss directions for future research in Sec. 1.8.

1.1.1. Summary of the main results

The main result of the paper is the computation of the scaling dimension of monopole operators when activating a chiral Heisenberg Gross-Neveu and a Gross-Neveu interaction. Using the state operator correspondence, we obtain these quantities at leading order in $1/N$ where $2N$ is the number of fermion flavors. We find in Sec. 1.3 and Sec. 1.5 that the minimal scaling dimension Δ_q of monopole operators with charge q in these theories are such that $\Delta_q^{\mathrm{QED}_3-\mathrm{cHGN}} < \Delta_q^{\mathrm{QED}_3-\mathrm{GN}} = \Delta_q^{\mathrm{QED}_3}$. The resulting scaling dimensions are evaluated numerically in Sec. 1.3. For example, taking the minimal magnetic charge $q = 1/2$, we find

$$\Delta_{q=1/2}^{\mathrm{QED}_3-\mathrm{cHGN}} = 2N \times 0.195 + \mathcal{O}(N^0)\,, \tag{1.1.1}$$

$$\Delta_{q=1/2}^{\mathrm{QED}_3-\mathrm{GN}} = 2N \times 0.265 + \mathcal{O}(N^0)\,. \tag{1.1.2}$$

Scaling dimensions up to $q = 5$ are also computed. The analytical form for these quantities obtained in the limit of a large monopole magnetic charge q computed in Sec. 1.3.4 is given by

$$\Delta_q^{\mathrm{QED}_3-\mathrm{cHGN}} = 2N\left(0.356q^{3/2} + 0.111q^{1/2} + \mathcal{O}(q^{-1/2})\right) + \mathcal{O}(N^0)\,, \tag{1.1.3}$$

$$\Delta_q^{\mathrm{QED}_3-\mathrm{GN}} = 2N\left(0.588q^{3/2} + 0.090q^{1/2} + \mathcal{O}(q^{-1/2})\right)\mathcal{O}(N^0)\,. \tag{1.1.4}$$

Crucially, in $\mathrm{QED}_3-\mathrm{cHGN}$ different types of monopole operators distinguished by their fermion zero modes dressing have different scaling dimensions, in contrast to QED_3. The origin of this difference is the presence of a spontaneously generated spin-Hall fermion mass on the sphere for $\mathrm{QED}_3-\mathrm{cHGN}$ as it is discussed Sec. 1.4. The largest scaling dimension among these monopole operators is given, at large q, by

$$\Delta_q^{\mathrm{QED}_3-\mathrm{cHGN};\uparrow} = 2N\left(1.248q^{3/2} + 0.0426q^{1/2} + \mathcal{O}(q^{-1/2})\right) + \mathcal{O}(N^0)\,. \tag{1.1.5}$$

The $\mathrm{SU}(2N_f)$-symmetric model $\mathrm{QED}_3-\mathrm{GN}$ is of particular interest for $2N = 2$ as this theory is conjectured to be dual to CP^1 model which is a bosonic model with a compact gauge field. This conjecture implies that the monopole operator with minimal magnetic charge on the fermionic side should, among others, have the same scaling dimension as the monopole operator or a Neel order on the bosonic side. With our large N result, we estimate $\Delta_{q=1/2}^{\mathrm{QED}_3-\mathrm{cHGN}}|_{2N=2} \sim 0.53$ which is not far off from the other scaling dimensions obtained in the literature as shown in Sec. 1.5.1.

A renormalization group study of the non-compact $\mathrm{QED}_3-\mathrm{cHGN}$ model is performed in Sec. 1.6 by studying the UV-completed Yukawa model ($\mathrm{QED}_3-\mathrm{cHGNY}$). We find the existence of the QCP and the phase diagram of this model using a $\epsilon = 4-d$ expansion at one-loop order. We also obtain the critical exponents of various operators.

1.2. Preliminaries

1.2.1. Monopole operators in QED_3

Let us consider QED_3 with $2N$ flavors of massless two-component Dirac fermions, ψ_A where $A = 1,2,\ldots 2N$. The flavors could correspond to magnetic spin and valley degrees of freedom, see Sec. 1.7 for a discussion of how they arise in the Kagome Heisenberg model.

These fermions can be organized as a spinor in flavor space, $\Psi = \left(\psi_1, \psi_2, \ldots, \psi_{2N}\right)^\intercal$. In Euclidean signature, the bare action reads

$$S_{\mathrm{QED}_3} = \int d^3x \left[-\bar{\Psi} \not{D}_a \Psi + \frac{1}{2e^2} \left(\epsilon_{\mu\nu\rho} \partial_\nu a_\rho\right)^2 \right] , \tag{1.2.1}$$

where a_μ is the U(1) gauge field, $\bar{\Psi} = \Psi^\dagger \gamma_0$ and $\not{D}_a$ is the gauge covariant derivative

$$\not{D}_a \Psi = \gamma_\mu \left(\partial_\mu - i a_\mu\right) \Psi \, . \tag{1.2.2}$$

The Dirac matrices γ_μ act on Lorentz spinor components and realize a two-dimensional representation of the Clifford algebra, $\{\gamma_\mu, \gamma_\nu\} = 2\delta_{\mu\nu} \mathbb{1}_2$. They can be chosen as $\gamma_\mu = (\tau_3, \tau_2, -\tau_1)$ where the τ_i are the Pauli matrices.

As it is written in Eq. (1.2.1), QED_3 has a global symmetry, $\mathrm{U}(1)_{\mathrm{top}}$, which is related to the conservation of the magnetic current $j^\mu_{\mathrm{top}}(x) = \frac{1}{2\pi} \epsilon^{\mu\nu\rho} \partial_\nu a_\rho(x)$. In the lattice regularization of this theory, it may no longer be the case that this current is conserved. Indeed, in the compact version of QED_3, a_μ is a periodic gauge field which takes values in the compact U(1) gauge group. This implies 2π quantization of the magnetic flux and the existence of instantons called monopole operators in this context. These operators insert integer multiples of the flux quantum and break the $\mathrm{U}(1)_{\mathrm{top}}$ symmetry. Non-compact QED_3 may still describe correctly the infrared (IR) limit of compact QED_3 if monopole operators are irrelevant. The theory is then said to exhibit an emergent $\mathrm{U}(1)_{\mathrm{top}}$ global symmetry in the infrared. Unless stated otherwise, we mean compact QED_3 when we simply write QED_3 throughout the paper.

Let $\mathcal{M}^\dagger_q(x)$ be a monopole operator with a $\mathrm{U}(1)_{\mathrm{top}}$ charge q at spacetime point x such that $2q \in \mathbb{Z}$. This disorder operator inserts a $4\pi q$ magnetic flux. More precisely, the Operator Product Expansion (OPE) of the magnetic current operator and the monopole operator yields the expected magnetic field for a magnetic monopole with charge q [10]

$$j^\mu_{\mathrm{top}}(x) \mathcal{M}^\dagger_q(0) \sim \frac{q}{2\pi} \frac{x^\mu}{|x|^3} \mathcal{M}^\dagger_q(0) + \cdots \, , \tag{1.2.3}$$

where the ellipsis denotes less singular terms as $|x| \to 0$. Apart from the magnetic flux they insert, another important property defining monopole operators is their gauge invariance. In particular, these operators must have a vanishing fermionic number. Among U(1) gauge invariant $4\pi q$-flux inserting operators, monopole operators are the most relevant, that is, they have the lowest scaling dimension. Only certain fermionic occupations can produce

such operators : Among the $4|q|N$ fermion zero modes existing in the monopole background [33], half of them must be filled. There are many ways to satisfy this condition, and all the distinct zero modes dressings define monopole operators with different quantum numbers but with equal scaling dimensions. In particular, for a minimal magnetic charge $q = 1/2$, there are precisely $\binom{2N}{N}$ monopole operators [10].

1.2.2. Confinement-deconfinement transition to an antiferromagnet

We mentioned in the last section that non-compact QED_3 provides an incomplete IR description of compact QED_3 if monopoles are relevant excitations. In fact, the theory is very different in this case. In pure U(1) compact gauge theory, monopole operators are relevant and condense. This leads to confinement and to the emergence of a mass gap [8, 34]. This effect can be prevented if there are enough massless fermion flavors to screen the monopoles. Indeed, at leading order in $1/N$, the monopole scaling dimension is proportional to N [10, 35] : The operator becomes irrelevant for a sufficiently large number of massless fermion flavors $2N$. Otherwise, the fermions confine. Even if monopoles turn out to be irrelevant and do not destabilize QSL phases in magnets described by emergent QED_3, they may play an important role elsewhere in the phase diagram. In particular, as new fermion interactions are tuned, fermion masses can be generated. In this case, the screening effect by fermions is lost and monopoles are free to proliferate.

For the rest of this section, we examine the aforementioned monopole proliferation subsequent to a fermion mass condensation. We study the deformation of compact QED_3 with a chiral Heisenberg Gross-Neveu (cHGN) interaction with coupling strength h

$$S_{\mathrm{QED}_3-\mathrm{cHGN}} = \int d^3x \left[-\bar{\Psi} \not{D}_a \Psi - \frac{h^2}{2} \left(\bar{\Psi} \boldsymbol{\sigma} \Psi \right)^2 \right] + \cdots , \tag{1.2.4}$$

where the ellipsis denotes the Maxwell free action and the contribution from monopole operators. Here, $\boldsymbol{\sigma}$ is a Pauli matrix vector acting on a SU(2) subspace of flavors. For definiteness, we introduce right now the language natural for quantum magnets. The SU(2) subspace in question consists of two magnetic spin degrees of freedom $\{\uparrow, \downarrow\}$. The other SU(N) subspace consists of valley degrees of freedom, i.e. locations of Dirac point in the Brillouin zone. QED_3

has the full flavor symmetry SU($2N$).[1] The cHGN interaction breaks down the global flavor symmetry, SU($2N$) $\to$ SU(2) $\times$ SU(N). This is broken further to SU(N) when a spin-Hall mass $\langle\bar{\Psi}\boldsymbol{\sigma}\Psi\rangle$ is condensed following the tuning of the coupling constant h. The condensate direction spontaneously chosen sets a preferred axis of quantization for the magnetic spin. Monopole operators which then condense have, accordingly, spin quantum numbers. We shall examine this point more thoroughly when we discuss the distinct flavors of monopole operators in Sec. 1.4.

We just described how an AFM order appears when, following the tuning of a spin-dependent fermion interaction, monopole operators proliferate. This mechanism was described in Ref. [31] in the contexts of Kagome antiferromagnets. It was also considered to describe a transition on the square lattice [19] where a SU(N)$_{\text{valley}}$ breaking interaction, $\delta\mathcal{L} \sim (\bar{\Psi}\mu_z\boldsymbol{\sigma}\Psi)^2$, is considered instead. This confinement of the DSL on the square lattice has also been studied numerically with quantum Monte Carlo [36]. An extended version of this mechanism involving general fermion bilinears was also considered in Ref. [32].

1.2.2.1. Spin-Hall mass condensation in the $1/N$ expansion. In what follows, we demonstrate, using a $1/N$ expansion, that a spin-Hall mass does condense when a sufficiently strong Gross-Neveu interaction is present. Performing a Hubbard-Stratonovich transformation on the action (1.2.4), we obtain

$$S'_{\text{QED}_3-\text{cHGN}} = \int d^3x \left[-\bar{\Psi}\left(\not{D}_a + \boldsymbol{\phi}\cdot\boldsymbol{\sigma}\right)\Psi + \frac{2N}{2h^2}\boldsymbol{\phi}^2\right], \tag{1.2.5}$$

where $\boldsymbol{\phi}$ is a three-component auxiliary bosonic field and we rescaled h^2 with the number of fermion flavors $2N$. The fermions can be integrated to get the usual determinant. Tracing out the valley subspace, the effective action becomes

$$S_{\text{eff}} = 2N_f\left(-\frac{1}{2}\ln\det\left(\not{D}_a + \boldsymbol{\phi}\cdot\boldsymbol{\sigma}\right) + \int d^3x \frac{1}{2h^2}\boldsymbol{\phi}^2\right), \tag{1.2.6}$$

where det is the determinant over the magnetic spin and the Dirac spaces. The saddle point solution for the gauge field is $a_\mu = 0$. We take a homogeneous ansatz for the saddle point value of the bosonic field $\langle\boldsymbol{\phi}\rangle = M\hat{n}$, where $\hat{n}$ is a unit vector. Eigenstates of the resulting determinant operator are plane waves and are used to obtain the saddle point equation for

[1] The center of SU($2N$) coincides with U(1) gauge transformations and we should quotient the symmetry group [32]. For simplicity, we keep the redundancy and refer to SU($2N$) as the flavor symmetry group.

M in a diagonalized form

$$2M\left(\frac{1}{2h^2}-\int\frac{d^3p}{(2\pi)^3}\frac{1}{p^2+M^2}\right)=0\,. \tag{1.2.7}$$

There is a trivial solution $M=0$ which represents the symmetric phase. A critical coupling h_c^{-2} defines the transition to the ordered phase $M>0$ through the relation

$$\frac{1}{2h_c^2}=\int\frac{d^3p}{(2\pi)^3}\frac{1}{p^2}=0\,, \tag{1.2.8}$$

where we used a zeta function regularization to evaluate the divergent integral. For future reference, we evaluate the effective action (1.2.6) at the critical point (1.2.8)

$$S^c_{\text{eff}}=-N\ln\det\left(\not{D}_a+\boldsymbol{\phi}\cdot\boldsymbol{\sigma}\right)\,. \tag{1.2.9}$$

In the ordered phase, the expectation value is $M=-2\pi h^{-2}$ for $h^{-2}<0$.

Before proceeding to the monopole calculation, we note that other quartic interactions that respect the symmetries of our theory, $(\bar{\Psi}\Gamma\Psi)^2$, could be considered. For example, the four-legged box diagram built with two gauge field propagators effectively generates a SU($2N_f$)-symmetric Gross-Neveu vertex $(\bar{\Psi}\Psi)^2$. This effect however is subleading in $1/N$, which is coherent with the fact that this interaction is irrelevant at large N at our fixed point, as is the case for the other quartic interactions. This justifies our choice of action to describe the QCP since we perform our monopole calculation at leading order in N_f.

1.3. Scaling dimensions of monopole operators

We established in Sec. 1.2.2 the existence of the large$-N$ QED$_3-$cHGN critical fixed point in the non-compact theory which leads to a spin-Hall mass condensation. In turn, this implies the proliferation of monopoles in the compact theory. Given the primordial role that monopole operators play in the quantum phase transition, we compute their scaling dimensions at the QCP. We shall restrict our computation to leading order in $1/N$.

Monopole operators are usually defined as operators with the lowest scaling dimension among $4\pi q$ flux-creating operators. In QED$_3$, there are many monopole operators due to the presence of fermion zero modes [10]. One important result we shall show in the next section is that the analogous operators in QED$_3-$cHGN develop a non-trivial hierarchy in their scaling dimensions. Nevertheless, we keep referring to those operators as monopole

operators. In the present section, we will compute the lowest scaling dimension among these monopole operators.

1.3.1. State-operator correspondence and $1/N$ expansion

A monopole operator $\mathcal{M}_q^\dagger$ is characterized by a scaling dimension $\Delta_{\mathcal{M}_q}$ which determines the power law decay of its two-point correlation function. The scaling dimension can be determined through the state-operator correspondence. This correspondence implies that the insertion of a local operator at the origin of flat spacetime can be mapped to a state of the conformal field theory (CFT) on $S^2 \times \mathbb{R}$ (see [37] for a clear and concise explanation of this correspondence). Specifically, the monopole operator with the lowest scaling dimension corresponds to the ground state of fermions in $\mathrm{QED}_3 - \mathrm{cHGN}$ living on S^2 in a background magnetic flux $4\pi q$. The relation also implies that the energy F_q of this ground state and the scaling dimension of this monopole operator $\Delta_q = \min(\Delta_{\mathcal{M}_q})$ are equal

$$\Delta_q = F_q \equiv -\ln Z_{S^2\times\mathbb{R}}[A^q]\,, \tag{1.3.1}$$

where A^q is an external gauge field yielding the magnetic flux $\int_{S^2} \mathrm{d}A^q = 4\pi q$. The notation F_q stands for free energy, which, in the present non-thermal setup, is the same as the ground state energy.[2] Our strategy to obtain the scaling dimension Δ_q will be to perform a $1/N$ expansion of the free energy

$$F_q = N F_q^{(0)} + F_q^{(1)} + \dots \tag{1.3.2}$$

We restrict our study to leading order in $1/N$ [3]

$$\Delta_q^{(0)} = F_q^{(0)}\,. \tag{1.3.3}$$

The state-operator correspondence was first used to compute the scaling dimension of a topological disorder operator in the context of QED_3 [10]. A similar computation was made for the bosonic theory CP^{N_b-1} [39]. The path integral formalism was also used to obtain $1/N$ corrections for QED_3 [40] and CP^{N_b-1} [41]. The ungauged version of CP^{N_b-1} was

[2] The free energy should be understood as a zero-temperature limit, $\lim_{\beta\to\infty}(-\ln Z_{S^2\times S^1_\beta}[A^q]/\beta)$ [38]. This definition is considered when needed later on.

[3] The appropriate relation is actually $\Delta_q^{(0)} = F_q^{(0)} - F_{q=0}^{(0)}$, but we find later on that for the case we study, $F_{q=0}^{(0)} = 0$.

also investigated using these techniques [42]. Monopole operators were also studied in non-abelian gauge theories, in presence of supersymmetries and in presence of a Chern-Simons term [38, 43–45].

1.3.2. Spectrum of the Dirac operator with a spin-Hall mass

In order to obtain the free energy F_q, we study the effective action obtained after integrating out the fermions. The analysis is similar to the one in Sec. 1.2.2, but we must now work on a sphere with a background magnetic flux. This latter consideration is incorporated through an external gauge field

$$A^q(x) = q(1-\cos\theta)\mathrm{d}\phi\,, \tag{1.3.4}$$

whose flux integral is $\int \mathrm{d}A^q = 4\pi q$. The gauge field only has an azimuthal component $A_\phi = q(1-\cos\theta)/\sin\theta$. The singular part at the south pole $\theta = \pi$ can be compensated by a Dirac string. The requirement that the Dirac string should be invisible imposes the Dirac condition $2q \in \mathbb{Z}$. On the other hand, the spacetime $S^2 \times \mathbb{R}$ is encoded in a non-trivial metric $g_{\mu\nu}(x)$ which we parameterize with (θ, ϕ, τ)

$$g_{\mu\nu}\mathrm{d}x^\mu \mathrm{d}x^\nu = \mathrm{d}\tau^2 + R^2\left(\mathrm{d}\theta^2 + \sin^2\theta \mathrm{d}\phi^2\right)\,, \tag{1.3.5}$$

where R is the radius of S^2. The metric can be decomposed as $g_{\mu\nu} = e^a_\mu e^b_\nu \eta_{ab}$, where η_{ab} is the flat spacetime metric and e^a_μ are the tetrad fields. A spin connection transporting the fermion fields on the curved spacetime can be found from the tetrad fields. The Dirac operator on $\mathbb{R}^3$ also has spin connections in spherical coordinates. However, these spin connections can be eliminated through a unitary transformation [46] and this corresponds to the basis used in Ref. [10] to define $\not{D}^{\mathbb{R}^3}_{a,A^q}$. The Dirac operator then obtained through the Weyl transformation $\mathbb{R}^3 \to S^2 \times \mathbb{R}$ is given by

$$\not{D}^{S^2\times\mathbb{R}}_{a,A^q} = e_b{}^\mu \gamma^b \left[\partial_\mu - \frac{1}{R}\delta^\tau_\mu - i\left(A^q_\mu + a_\mu\right)\right]\,, \tag{1.3.6}$$

where $\gamma^{\{1,2,3\}} = \tau^{\{r,\theta,\phi\}} = \boldsymbol{\tau}\cdot\{\hat{r},\hat{\theta},\hat{\phi}\}$. Also, the "time" τ on $S^2 \times \mathbb{R}$ is related to the radius r on $\mathbb{R}^3$ as $r = Re^{\tau/R}$ and the extra term correcting the "time" derivative above is obtained by acting with ∂_τ on the rescaling factor $e^{-\tau/R}$.

The critical effective action S^c_{eff} (1.2.9) with the modified Dirac operator, $\not{D}_a \to \not{D}^{S^2\times\mathbb{R}}_{a,A^q}$, becomes

$$S'^c_{\text{eff}} = -N \ln\det\left(\not{D}^{S^2\times\mathbb{R}}_{a,A^q} + \boldsymbol{\phi}\cdot\boldsymbol{\sigma}\right). \tag{1.3.7}$$

The saddle point condition for this modified effective action still implies a vanishing expectation value for the gauge field $\langle a_\mu\rangle = 0$. We take a homogeneous ansatz for the saddle point value of the bosonic field on the sphere with flux $4\pi q$, $\langle\boldsymbol{\phi}\rangle = M_q\hat{n}$, where $\hat{n}$ is a unit vector. Without loss of generality, we can orient the condensate such that $\hat{n} = \hat{z}$. Inserting this ansatz in the effective action (1.3.7), we find the leading order free energy

$$F^{(0)}_q = -\ln\det\left(\not{D}_{A^q} + M_q\sigma_z\right), \tag{1.3.8}$$

where $\not{D}_{A^q} \equiv \not{D}^{S^2\times\mathbb{R}}_{a,A^q}\Big|_{a=0}$.[4] The spectrum of the operator appearing inside the determinant in Eq. (1.3.8) must be found to obtain the leading order free energy $F^{(0)}_q$.

We first review how the spectrum of the Dirac operator $\not{D}_{A^q}$ was found in Refs. [10, 40] by using analogs of spherical harmonics [47] appropriate for describing spin-1/2 particles in the monopole background. A first step in the generalization is to define the generalized angular momentum $L^i_q = -i\epsilon_{ijk}x_j(\partial_k - A^q_k) - r^2\epsilon_{ijk}\partial_j A^q_k$ which includes the effect of the magnetic charge. The $SU(2)$ algebra remains after the generalization, $[L^i_q, L^j_q] = i\epsilon_{ijk}L^k_q$, so there exists eigenfunctions $Y_{q,\ell,m}(\theta,\phi)$, called monopole harmonics, which simultaneously diagonalize L^2_q and L^z_q [47]

$$L^2_q Y_{q,\ell,m} = \ell\,(\ell+1)\,Y_{q,\ell,m}\,, \qquad \ell = |q|, |q|+1, \ldots \tag{1.3.9}$$

$$L^z_q Y_{q,\ell,m} = m Y_{q,\ell,m}\,, \qquad m = -\ell, -\ell+1, \ldots, \ell\,. \tag{1.3.10}$$

From now on, we consider $q > 0$. As the Dirac operator acts on spinors, one must consider the total angular momentum $\boldsymbol{J}_q = \boldsymbol{L}_q + \boldsymbol{\tau}/2$ as well. Two-component spinors $S^\pm_{q,\ell,m}$ that diagonalize the operators $\{L^2_q, J^z_q, J^2_q\}$ are thus introduced

$$J^2_q S^\pm_{q,\ell,m} = j_\pm\,(j_\pm+1)\,S^\pm_{q,\ell,m}\,, \quad j_\pm = \ell \pm 1/2\,, \tag{1.3.11}$$

$$L^2_q S^\pm_{q,\ell,m} = \ell\,(\ell+1)\,S^\pm_{q,\ell,m}\,, \tag{1.3.12}$$

$$J^z_q S^\pm_{q,\ell,m} = (m+1/2) S^\pm_{q,\ell,m}\,. \tag{1.3.13}$$

[4] In this section, we simply write $\not{D}_{A^q}$ as we assume a curved spacetime $S^2\times\mathbb{R}$ whenever the external gauge field A^q is present.

Such spinors $S^{\pm}_{q,\ell,m}$, dubbed spinor monopole harmonics, are built using monopole harmonics as components [10, 40]

$$S^{+}_{q,\ell,m} = \begin{pmatrix} \sqrt{\frac{\ell+m+1}{2\ell+1}} Y_{q,\ell,m} \\ \sqrt{\frac{\ell-m}{2\ell+1}} Y_{q,\ell,m+1} \end{pmatrix}, \tag{1.3.14}$$

$$S^{-}_{q,\ell,m} = \begin{pmatrix} -\sqrt{\frac{\ell-m}{2\ell+1}} Y_{q,\ell,m} \\ \sqrt{\frac{\ell+m+1}{2\ell+1}} Y_{q,\ell,m+1} \end{pmatrix}. \tag{1.3.15}$$

These spinors can be organized as doublets $[S^{+}_{q,\ell-1,m}, \quad S^{-}_{q,\ell,m}]^{\intercal}$ with total angular momentum $j = \ell - 1/2$. Adding plane waves $e^{-i\omega\tau}$ to describe the "time" direction[5], the action of the Dirac operator on this basis is [10, 40]

$$\not{D}_{A^q} \begin{bmatrix} e^{-i\omega\tau} S^{+}_{q,\ell-1,m} \\ e^{-i\omega\tau} S^{-}_{q,\ell,m} \end{bmatrix} = -i \boldsymbol{O}_{q,\ell} \left(\omega + i \boldsymbol{P}_{q,\ell}\right) \begin{bmatrix} e^{-i\omega\tau} S^{+}_{q,\ell-1,m} \\ e^{-i\omega\tau} S^{-}_{q,\ell,m} \end{bmatrix} \tag{1.3.16}$$

where the matrices $\boldsymbol{O}_{q,\ell}$ and $\boldsymbol{P}_{q,\ell}$ are given by

$$\boldsymbol{O}_{q,\ell} = \frac{1}{\ell} \begin{bmatrix} -q & -R\varepsilon^0_\ell \\ -R\varepsilon^0_\ell & q \end{bmatrix}, \quad \boldsymbol{P}_{q,\ell} = \frac{\varepsilon^0_\ell}{\ell} \begin{bmatrix} R\varepsilon^0_\ell & -q \\ -q & -R\varepsilon^0_\ell \end{bmatrix} \tag{1.3.17}$$

and where $\varepsilon^0_\ell \equiv R^{-1}\sqrt{\ell^2 - q^2}$. For the minimal total angular momentum $j = q - 1/2$, only the spinor $S^{-}_{q,q,m}$ is defined[6] and the action of the Dirac operator on this mode reduces to

$$\not{D}_{A^q} \begin{bmatrix} 0 \\ e^{-i\omega\tau} S^{-}_{q,q,m} \end{bmatrix} = -i\omega \begin{bmatrix} 0 \\ e^{-i\omega\tau} S^{-}_{q,q,m} \end{bmatrix}. \tag{1.3.18}$$

This mode has a vanishing energy and thus corresponds to a fermion zero mode in the monopole background.

We now study the complete determinant operator with the contribution of the spin-Hall mass term appearing in Eq. (1.3.8). The additional term is diagonal in the spinor monopole

[5] We emphasize that this "time" dimension on $S^2 \times \mathbb{R}$ does not correspond to the original time dimension on $\mathbb{R}^{1,2}$.

[6] The other would-be spinor $S^{+}_{q,q-1,m}$ with $j = q - 1/2$ does not exist since $\ell = q - 1$ is smaller that the minimal angular momentum allowed for monopole harmonics (1.3.9).

harmonics basis. Therefore, we can still use this basis to compute the determinant operator

$$\ln\det\left(\not{D}_{A^q}+M_q\sigma_z\right)=\sum_{\sigma=\pm1}\int_{-\infty}^{\infty}\frac{d\omega}{2\pi}\times\Bigg[d_q\ln\left[-i\omega+M_q\sigma\right]+\sum_{\ell=q+1}^{\infty}d_\ell\ln\det\left[-i\boldsymbol{O}_{q,\ell}\left(\omega+i\boldsymbol{P}_{q,\ell}\right)+M_q\sigma\right]\Bigg], \tag{1.3.19}$$

where $d_\ell = 2\ell$ is the degeneracy coming from azimuthal quantum numbers. Simplifying further, we obtain

$$\begin{aligned}\ln\det\left(\not{D}_{A^q}+M_q\sigma_z\right)&=\sum_{\sigma=\pm1}\int_{-\infty}^{\infty}\frac{d\omega}{2\pi}\times\left[d_q\ln\left[\omega+iM_q\sigma\right]+\sum_{\ell=q+1}^{\infty}d_\ell\ln\left[\omega^2+(\varepsilon_\ell^0)^2+M_q^2\right]\right]\\&=\int_{-\infty}^{\infty}\frac{d\omega}{2\pi}\left[d_q\ln\left(\omega^2+M_q^2\right)+\sum_{\ell=q+1}^{\infty}2d_\ell\ln\left[\omega^2+\varepsilon_\ell^2\right]\right],\end{aligned} \tag{1.3.20}$$

where we removed inessential constants and we defined the mass-deformed eigenvalues

$$\varepsilon_\ell=R^{-1}\sqrt{\ell^2-q^2+M_q^2R^2}\,. \tag{1.3.21}$$

We now explicitly write the spectrum of the Dirac operator with a spin-Hall mass on the magnetically charged sphere found from (1.3.19)

$$\omega+i\sigma\varepsilon_q\,,\quad \ell=q\,, \tag{1.3.22}$$

$$\pm\sqrt{\omega^2+\varepsilon_\ell^2}\,,\quad \ell=\{q+1,q+2,\ldots\}\,, \tag{1.3.23}$$

where $\sigma\in\{-1,+1\}$. The $\pm$ modes for $\ell\geq q+1$ in (1.3.23) are referred to as conduction $(+)$ and valence $(-)$ modes. There is no such doubling of the $\ell=q$ modes in (1.3.22) which are descendants of the QED_3 zero modes. This is why we refer to these modes as "zero" modes even though they have non-vanishing energy $\pm\varepsilon_q=\pm M_q$ with the inclusion of the spin-Hall mass. We restate that the σ eigenvalue refers to magnetic spin orientation relative to the quantization axis defined by $\langle\boldsymbol{\phi}\rangle$. These "zero" modes are responsible for the first term in Eq. (1.3.20)

1.3.3. Scaling dimension computation

The free energy at leading order (1.3.8) is rewritten using the result (1.3.20) (from now on, we assume a positive magnetic charge $q > 0$),

$$F_q^{(0)} = -\int \frac{d\omega}{2\pi} \left[d_q \ln \left[\omega^2 + M_q^2 \right] + \sum_{\ell=q+1}^{\infty} 2 d_\ell \ln \left[\omega^2 + \varepsilon_\ell^2 \right] \right], \tag{1.3.24}$$

where the radius R of the sphere was eliminated by changing the integration variable $\omega \to \omega/R$, by rescaling the parameters $\{\varepsilon_\ell, F_q^{(0)}, M_q\} \to \{\varepsilon_\ell, F_q^{(0)}, M_q\}/R$ and by removing an inessential constant. The free energy (1.3.24) needs regularization. We first treat the diverging integral over frequencies by rewriting the integrand using the identity $\ln A = -\mathrm{d}A^{-s}/\mathrm{d}s|_{s=0}$ and doing an analytic continuation to $s = 0$. This procedure is presented in App. 1.A. The resulting free energy is

$$F_q^{(0)} = -d_q M_q - \sum_{\ell=q+1}^{\infty} 2 d_\ell \varepsilon_\ell \,. \tag{1.3.25}$$

By setting $M_q = 0$ in this free energy, we obtain the QED_3 results shown in Ref. [40].[7] This free energy (1.3.25) still needs regularization. The divergent sum is rewritten by adding and subtracting its diverging part

$$\begin{aligned} \sum_{\ell=q+1}^{\infty} d_\ell \varepsilon_\ell = & \sum_{\ell=q+1}^{\infty} \left[2\ell \sqrt{\ell^2 + M_q^2 - q^2} - 2\ell^2 - \left(M_q^2 - q^2 \right) \right] \\ & + 2 \sum_{\ell=q+1}^{\infty} \left[\ell^{2(1-s)} + \left(\frac{1}{2} - s \right) \left(M_q^2 - q^2 \right) \ell^{-2s} \right] \Bigg|_{s=0} . \end{aligned} \tag{1.3.26}$$

Now, only the last sum is divergent and we treat it with a zeta function regularization by using $\sum_{n=0}^{\infty} (n+a)^{-s} = \zeta(s,a)$. This sum then becomes $2\zeta(-2,q+1) + \left(M_q^2 - q^2 \right) \zeta(0,q+1)$, an expression for which a polynomial form may be found using Ref. [48]. The resulting finite expression is then inserted in (1.3.25) to obtain the regularized free energy

$$\begin{aligned} F_q^{(0)} = & - d_q M_q - \sum_{\ell=q+1}^{\infty} \left[2 d_\ell \varepsilon_\ell - d_\ell^2 - 2 \left(M_q^2 - q^2 \right) \right] \\ & + (2q+1) \left(M_q^2 - q(q-2)/3 \right) . \end{aligned} \tag{1.3.27}$$

[7] Our definition of $F_q^{(0)}$ has an extra factor of 2 because we defined the total number of fermion flavors as $2N$ but we expanded the free energy in powers of $1/N$ (1.3.2). This procedure is more natural since the spin degeneracy does not factor out like the valley degeneracy because of the "zero" modes.

We can then find the regularized gap equation, i.e. the saddle-point equation $\partial F_q^{(0)}/\partial M_q = 0$

$$-d_q + 2M_q(2q+1) - 2M_q \sum_{\ell=q+1}^{\infty} \left[d_\ell \varepsilon_\ell^{-1} - 2 \right] = 0 \,. \tag{1.3.28}$$

For a vanishing magnetic charge $q = 0$, the contribution from "zero" modes vanishes since $d_{q=0} = 0$. The saddle point equation then only has a trivial solution $M_{q=0} = 0$. This case coincides with QED_3 where there is no mass M_q to start with and the free energy vanishes, $F_{q=0}^{(0)} = 0$. For $q \neq 0$, the saddle point equation only has a non-trivial solution $M_q > 0$ which must be determined numerically.[8] The resulting mass M_q is then inserted in (1.3.27) to obtain the scaling dimension at leading order in $1/N$, $\Delta_q = N F_q^{(0)} + \mathcal{O}(N^0)$. The mass M_q and the scaling dimension of monopole operators in $\mathrm{QED}_3 - \mathrm{cHGN}$ and QED_3 are obtained for multiple values of q and are shown in Tab. 1.1. These numerical results are also plotted in Fig. 1.1 and Fig. 1.2 along with corresponding analytical approximations obtained in Sec. 1.3.4. The numerical and analytical results agree very well even for small values of q. We also note that the monopole operator scaling dimension is always smaller in $\mathrm{QED}_3 - \mathrm{cHGN}$ than in QED_3. The fact that $\Delta_q \leq \Delta_q^{\mathrm{QED}_3}$ is expected since the case $M_q = 0$ implies $\Delta_q = \Delta_q^{\mathrm{QED}_3}$ and sets an upper bound for the scaling dimension Δ_q. Setting $2N = 4$ gives an estimate on the scaling dimension of monopole operators for certain quantum magnets. One should be careful with these results as the expansion parameter is not small and corrections to the leading order may be important. Nevertheless, if we consider the monopole operator with a minimal magnetic charge $q = 1/2$, the lowest scaling dimension is

$$\Delta_{q=1/2} = 2N \cdot 0.19539 + \mathcal{O}(N^0) \,. \tag{1.3.29}$$

In the case $2N = 4$, which is interesting for application to quantum magnets, we find a strongly relevant operator

$$\Delta_{q=1/2}\Big|_{2N=4} \approx 0.78156 < 3 \,. \tag{1.3.30}$$

However, the monopole operator with the minimal magnetic charge is not allowed in many contexts, we discuss this matter in Sec. 1.7. We also note that the unitarity bound is violated

[8] If the "time" direction $\mathbb{R}$ is compactified on a circle S^1_β, a trivial solution does exist for $q > 0$. It persists as the radius β is taken to infinity to retrieve the real line. However, this solution is a *maximum* of free energy and does not determine Δ_q. See App. 1.B

Tableau 1.1. Numerical results for the mass M_q and the lowest scaling dimension of monopole operators in $\mathrm{QED}_3 - \mathrm{cHGN}$ and QED_3, respectively Δ_q and $\Delta_q^{\mathrm{QED}_3} = \Delta_q|_{M_q=0}$. These results are at leading order in $1/N$. We show the scaling dimensions per number of fermion flavors $2N$. These quantities are shown for the first few allowed values of the magnetic charge q.

q	M_q	$\frac{1}{2N}\Delta_q$	$\frac{1}{2N}\Delta_q^{\mathrm{QED}_3}$
0	0	0	0
0.5	0.27318	0.19539	0.26510
1.0	0.41395	0.46039	0.67315
1.5	0.51946	0.78471	1.18643
2.0	0.60728	1.15964	1.78690
2.5	0.68406	1.57928	2.46345
3.0	0.75311	2.03939	3.20837
3.5	0.81638	2.53671	4.01591
4.0	0.87510	3.06867	4.88154
4.5	0.93014	3.63315	5.80162
5.0	0.98211	4.22839	6.77309

for $2N < 2.56$ as $\Delta_{q=1/2} < 1/2$ [37]. It would be interesting to see if the violation persist with higher order corrections. This would shed light on the phase diagram of QED_3 at $2N_f = 2$.

For demonstration purpose, we plot in Fig. 1.3 the free energy for the minimal magnetic charge as a function of the mass $M_{q=1/2}$. The free energy minimum is identified and corresponds to the solution to the saddle point equation, $M_{q=1/2} = 0.27318$, as shown in Tab. 1.1. For large values of $M_{q=1/2}$, the sum in (1.3.27) can be approximated as an integral, and we find that the free energy grows as $F^{(0)}_{q=1/2} \sim 4(M_{q=1/2})^3/3$ at leading order in $M_{q=1/2}$.

Let us restate one important result. For $q \neq 0$, the gap equation determining the lowest scaling dimension of monopole operators involves a non-vanishing condensate $M_q \equiv \langle|\boldsymbol{\phi}|\rangle > 0$. We stress out that this does not imply a non-vanishing spin-Hall mass expectation value at the critical point of the phase transition. Our computation is done on a compact space using the state-operator correspondence and simply serves as way to compute the scaling dimension. The condensate is natural in this context since, once R is reintroduced by undoing

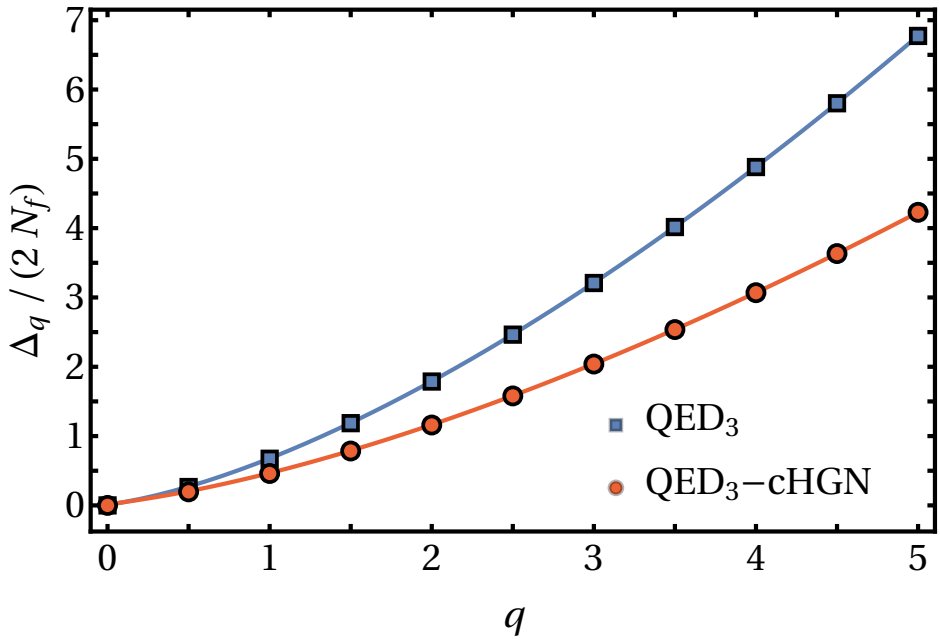

Figure 1.1. Lowest scaling dimension of monopole operators Δ_q per number of fermion flavors $2N$ as a function of the magnetic charge q. Analytical approximations in the large q limit of the scaling dimension in $\mathrm{QED}_3 - \mathrm{cHGN}$ and QED_3, respectively (1.3.39) and (1.3.40), are plotted in solid lines. These are compared to their respective numerical values shown in Tab. 1.1.

our previous rescaling (1.3.24), there is a characteristic length to build a non-vanishing mass $M_q \propto R^{-1}$.

1.3.4. Monopole scaling dimensions for large q

We now obtain an analytical approximation of the condensed mass M_q and the lowest scaling dimension of monopole operators Δ_q by studying the free energy $F_q^{(0)}$ in a large q limit. The structure of the expansion closely resembles what was done for the bosonic $\mathbb{C}P^{N-1}$ theory [41]. It is simpler to work with the unregularized free energy (1.3.25). We first change the summation index $\ell \to \ell + q + 1$ so that only the summand depends on q. The free energy then becomes

$$F_q^{(0)} = -2qM_q - 4\sum_{\ell=0}^{\infty}(\ell+q+1)\sqrt{(\ell+q+1)^2 - q^2 + M_q^2}\,. \tag{1.3.31}$$

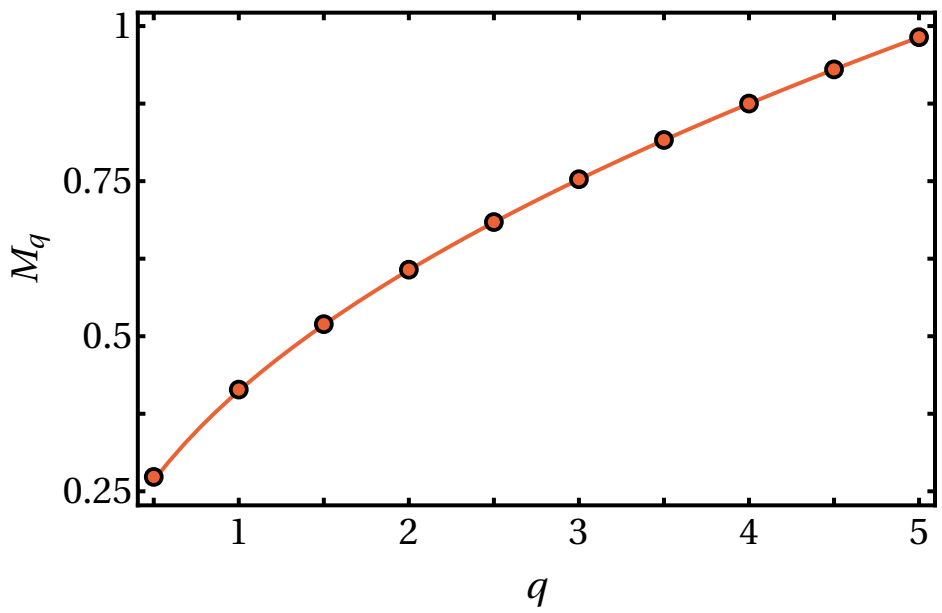

Figure 1.2. Mass $M_q \equiv \langle|\boldsymbol{\phi}|\rangle$ as a function of the magnetic charge q at leading order in $1/N$. The solid line corresponds to the large q analytical approximation of M_q (1.3.37). The circles are the numerical values of M_q shown in Tab. 1.1.

The saddle point equation $\partial F_q^{(0)}/\partial M_q = 0$ defining the mass M_q is, up to multiplicative factors,

$$q + 2M_q \sum_{\ell=0}^{\infty} \frac{\ell + q + 1}{\sqrt{(\ell + q + 1)^2 + M_q^2 - q^2}} = 0\,. \tag{1.3.32}$$

The gap equation can then be expanded in $1/q$. To solve this order by order in q, the mass squared order must take the following form

$$M_q^2 = 2\chi_0 q + \chi_1 + \mathcal{O}(q^{-1})\,. \tag{1.3.33}$$

With this ansatz, we expand Eq. (1.3.32) in powers of $1/q$. Using once again the zeta function regularization, the condition becomes

$$\begin{aligned} 0 = \; & 4q^{1/2}\left(2\zeta_{1/2} + \chi_0^{-1/2}\right) \\ & - q^{-1/2}\left(2\left(\chi_1 + \chi_0^2\right)\zeta_{3/2} + 4\chi_0\zeta_{1/2} - 6\zeta_{-1/2} + \chi_1\chi_0^{-3/2}\right) + \mathcal{O}(q^{-3/2})\,, \end{aligned} \tag{1.3.34}$$

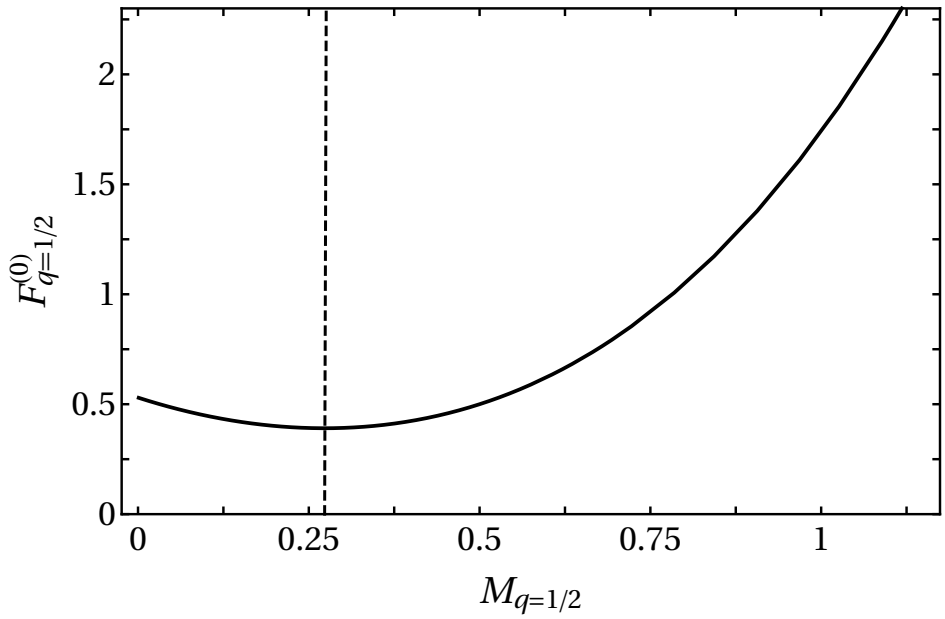

Figure 1.3. Leading order in $1/N$ of the free energy with minimal magnetic charge $F^{(0)}_{q=1/2}$ (1.3.27) as a function of the mass $M_{q=1/2}$. The appropriate value of the mass $M_{q=1/2}$ found with the saddle point equation (1.3.28) corresponds to the minimum of this function. For large mass, the free energy behaves as $F^{(0)}_{q=1/2} \sim 4(M_{q=1/2})^3/3$.

where we defined $\zeta_s \equiv \zeta(s, 1+\chi_0)$.[9] Solving (1.3.34) order by order, we find a transcendental condition defining χ_0 and a linear condition for χ_1

$$2\zeta_{1/2} + \chi_0^{-1/2} = 0\,, \tag{1.3.35}$$

$$\chi_1 + \frac{2\chi_0^{3/2}\left(\chi_0^2\zeta_{3/2} + 2\chi_0\zeta_{1/2} - 3\zeta_{-1/2}\right)}{1 + 2\chi_0^{3/2}\zeta_{3/2}} = 0\,. \tag{1.3.36}$$

Inserting the solution of (1.3.35, 1.3.36) into the mass ansatz (1.3.33), we find the mass squared $M_q^2 = 0.199q - 0.030 + \mathcal{O}(q^{-1})$ from which the mass is found to be

$$M_q = 0.446q^{1/2} - 0.0341q^{-1/2} + \mathcal{O}(q^{-3/2})\,. \tag{1.3.37}$$

As shown in Fig. 1.2, this asymptotic expansion is found to agree extremely well with the exact mass M_q, even at small magnetic charge q.

[9]Neglecting powers of ℓ compared to powers of q in the large$-\ell$ portion of the sum in condition (1.3.32) may seem problematic. These terms do appear to higher order in $1/q$ but cause no problem once properly regularized.

We repeat this procedure for the free energy. We insert the mass ansatz (1.3.33) in the free energy (1.3.31) and we perform a $1/q$ expansion

$$\begin{aligned}\frac{1}{2}F_q^{(0)} = &-\sqrt{2}q^{3/2}\left(2\zeta_{-1/2}+\chi_0^{1/2}\right)-\frac{q^{1/2}}{\sqrt{2}}\Bigg(\left(\chi_0^2+\chi_1\right)\zeta_{1/2}\\ &-6\chi_0\zeta_{-1/2}+5\zeta_{-3/2}+\frac{1}{2}\chi_1\chi_0^{-1/2}\Bigg)+\mathcal{O}(q^{-1/2})\,.\end{aligned} \tag{1.3.38}$$

Inserting the solution of (1.3.35, 1.3.36) in this result, we obtain the leading order scaling dimension (1.3.3)

$$\Delta_q = 2N\left(0.356q^{3/2}+0.111q^{1/2}+\mathcal{O}(q^{-1/2})\right)+\mathcal{O}(N^0)\,. \tag{1.3.39}$$

The scaling dimension for QED_3 is found by doing the same expansion but starting with $M_q = 0$

$$\Delta_q^{\mathrm{QED}_3} = 2N\left(0.588q^{3/2}+0.090q^{1/2}+\mathcal{O}(q^{-1/2})\right)+\mathcal{O}(N^0)\,. \tag{1.3.40}$$

Once again, these asymptotic expansions are in good agreement with the corresponding numerical results as shown in Fig. 1.1. Note that there is no term at order q^0 in the scaling dimensions at leading order in $1/N$ (1.3.39, 1.3.40). This is expected since all CFTs in $d = 2+1$ dimensions with a U(1) global charge should have the same q^0 term [49, 50]. As such, it can't depend on N. It thus has to vanish at order N.

We take a step back to appreciate the leading order relation $\Delta_q^{(0)} \sim q^{3/2}$. We recall that the theory is set on $S^2 \times \mathbb{R}$. The background magnetic flux on the sphere is $BR^2 = q$, where B is the magnetic field and R is the radius of the sphere. Taking $q \to \infty$ and $R \to \infty$ while keeping B finite, the theory is reduced to Dirac fermions on a plane in a uniform magnetic field. The eigenvalues are then given by relativistic Landau levels

$$E_n = \sqrt{2Bn + M_q^2} \approx R^{-1}q^{1/2}\sqrt{2n+2\chi_0}\,. \tag{1.3.41}$$

In terms of a free energy density $[\mathcal{F}_q] = [E]^3$, this means we have $\mathcal{F}_q \sim R^{-3}q^{3/2}$. The free energy should then scale as $F_q^{(0)} \sim R^2\mathcal{F}_q \sim R^{-1}q^{3/2}$. Reintroducing a missing power of R in (1.3.38) that was rescaled away in (1.3.24), this is indeed the relation we get. The behaviour $\Delta_q^{(0)} \sim q^{3/2}$ is then coherent with the large-q interpretation in terms of Landau levels.

1.4. Monopole dressing

In the previous section where we computed the lowest scaling dimension of monopole operators Δ_q, the fermionic occupation of the corresponding ground state was not explicited. In this section, we specify the "zero" modes dressing of this ground state and consider other possible "zero" modes dressings defining other monopole operators. We show a non-trivial hierarchy in the scaling dimensions of monopole operators in $\text{QED}_3 - \text{cHGN}$ that is not present in QED_3.

Monopole operators correspond to U(1) gauge invariant states which means they have a vanishing fermion number $\langle \hat{N} \rangle$. In a $\mathcal{CT}$ quantized theory where $\{CT, \hat{N}\} = 0$, this condition enforces half filling of the fermion modes. The monopole operators correspond to states where the Dirac sea is filled as well as half of the "zero" modes. This condition that was discussed in the case of QED_3 [10]. It is also valid in $\text{QED}_3 - \text{cHGN}$ where the spectrum has the same structure, as was shown in Sec. 1.3. One other consideration is that monopole operators should be Lorentz scalars. We shall focus on $q = 1/2$ monopoles where this is not an issue as the unique "zero" mode for each fermion flavor corresponds to a $j = 0$ Lorentz $\text{SU}(2)_{\text{rot}}$ singlet [10].

The energy spectrum of fermions in the monopole background (1.3.22, 1.3.23) shows that spin down "zero" modes have a lower energy than spin up "zero" modes. The monopole operator with the lowest scaling dimension Δ_q thus corresponds to the state with all the spin down "zero" modes occupied and all the spin up "zero" modes empty, as shown in Fig. 1.4. We refer to this operator as the ground state monopole. This fermionic configuration can also be read off the free energy (1.3.25) by rewritting it suggestively as

$$F_q^{(0)} = d_q\left(-M_q\right)\left(\frac{1}{2}\right) + d_q\left(M_q\right)\left(-\frac{1}{2}\right) + \sum_{\ell=q+1}^{\infty}\left[2d_\ell(-\varepsilon_\ell)\left(\frac{1}{2}\right) + 2d_\ell(\varepsilon_\ell)\left(-\frac{1}{2}\right)\right]. \quad (1.4.1)$$

This form puts emphasis on the fact that modes with positive (negative) energy are empty (filled), corresponding to an occupation factor $\langle c_n^\dagger c_n - 1/2\rangle = \mp 1/2$, where $c_n^\dagger$ are the creation operators for the fermion modes in the monopole background.

We now evaluate the scaling dimensions of monopole operators, which are defined by the various "zero" modes dressings. These operators can be built by annihilating some or all the spin down "zero" modes of the ground state monopole and creating an equal amount of spin up "zero" modes. Each such change increases the energy by $M_q - (-M_q) = 2M_q$.

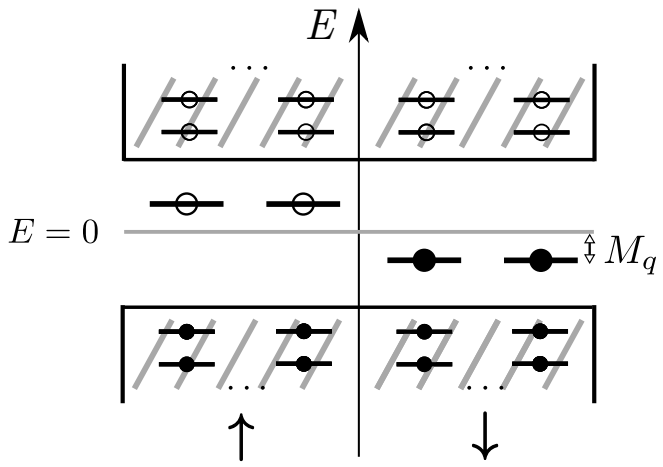

Figure 1.4. Schematic representation of the energy spectrum and fermionic occupation for the ground state monopole in presence of a spin-Hall mass $M_q\sigma^z$. The spectrum is shown for $2N = 4$ fermion flavors and minimal magnetic charge $q = 1/2$. Modes with spin up (down) are shown on left (right). A state of minimal energy is achieved by occupying all the Dirac sea as well as all the spin down zero modes which have energy $-M_q$.

We study explicitly excited monopole operators with minimal magnetic charge $q = 1/2$. For example, the first excited monopole operator, whose fermionic occupation is represented in Fig. 1.5(a), has a scaling dimension $\Delta^+_{q=1/2} = \Delta_{q=1/2} + 2M_{q=1/2}$. The monopole operator dressed with all the N spin up "zero" modes, represented in Fig.1.5(b), has the largest scaling dimension among monopole operators which is $\Delta^\uparrow_{q=1/2} = \Delta_{q=1/2} + 2NM_{q=1/2}$. Using the numerical results for the mass $M_{q=1/2}$ in Tab. 1.1, we find leading order scaling dimensions of excited monopole operators

$$\Delta^+_{q=1/2} - \Delta_{q=1/2} \approx 0.546 + \mathcal{O}(N^{-1})\,, \tag{1.4.2}$$

$$\Delta^\uparrow_{q=1/2} - \Delta_{q=1/2} \approx 2N(0.273) + \mathcal{O}(N^0)\,. \tag{1.4.3}$$

The first excited monopole scaling dimension is order $(1/N)^0$ larger than the ground state. This difference becomes relatively less important as N becomes large. On the other hand, the scaling dimension of the monopole operator dressed with all spin up "zero" modes is order N and the difference with the lowest scaling dimension grows larger as N is increased.

We can also find the range of the scaling dimensions analytically for large q. We consider the scaling dimension of the monopole operator dressed with all the $2Nq$ spin up "zero"

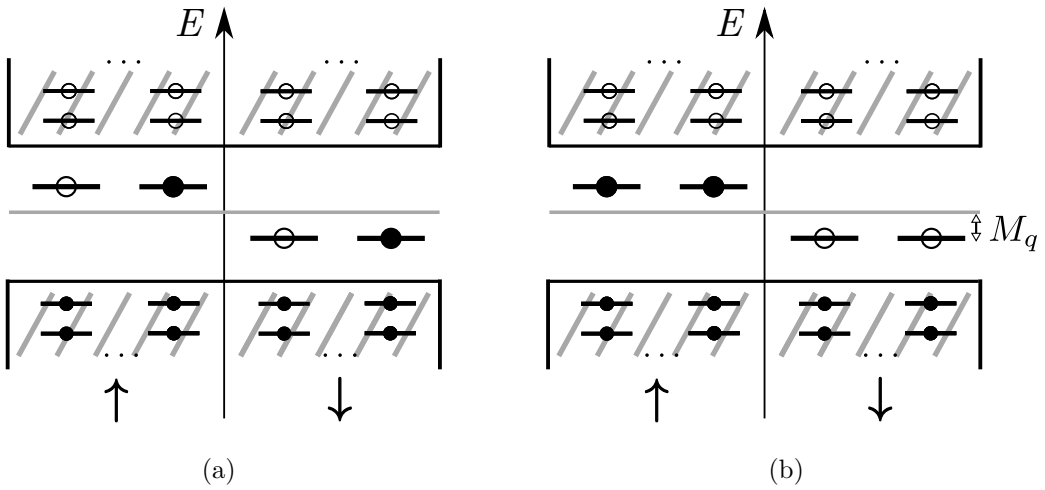

Figure 1.5. Schematic representation of the fermionic occupation of two excited monopole operators in presence of a spin-Hall mass $M_q\sigma^z$. Modes with spin up (down) are shown on left (right). The spectrum is shown for $2N = 4$ fermion flavors and minimal magnetic charge $q = 1/2$. a) First excited monopole operator ; b) Monopole operator dressed only with spin up "zero" modes.

modes

$$\Delta_q^{\uparrow} = \Delta_q + 4NqM_q\,. \tag{1.4.4}$$

Using large q results (1.3.37, 1.3.39), we find the leading order results in $1/N$

$$\Delta_q^{\uparrow} = 2N\left(1.248q^{3/2} + 0.0426q^{1/2} + \mathcal{O}(q^{-1/2})\right) + \mathcal{O}(N^0)\,. \tag{1.4.5}$$

The hierarchy observed in the scaling dimensions of monopole operators in $\mathrm{QED}_3 - \mathrm{cHGN}$ represents a symmetry lifting of the degenerate monopole multiplet in compact QED_3. The global $\mathrm{SU}(2N)$ flavor symmetry of QED_3 implies that monopole operators are organized in a completely antisymmetric representation of $\mathrm{SU}(2N)$ and consequently must have equal scaling dimensions [10]. Indeed, the symmetry is responsible for the degeneracy of the distinct zero modes dressings defining the monopole operators. When the spin-dependent interaction is added, the global symmetry is broken down $\mathrm{SU}(2N) \to \mathrm{SU}(2)_{\mathrm{spin}} \times \mathrm{SU}(N)_{\mathrm{valley}}$, and there is a symmetry lifting. This lifting is only partial since, for example, monopole operators with trivial spin quantum numbers remain degenerate, having the same scaling dimensions.

1.5. Comparison with SU($2N$) symmetric critical point

Other Gross-Neveu deformations of QED_3 yield distinct CFTs and different monopole operators. In this section, we study the monopole operators at the QCP between a DSL and a chiral spin liquid. In the latter phase, the fermions acquire the same mass, leading to a Chern-Simons term for the dynamical gauge field. This phase transition is driven by the interaction $(\bar{\Psi}\Psi)^2$,

$$S_{\text{QED}_3-\text{GN}} = \int d^3x \left[-\bar{\Psi} \not{D}_a \Psi - \frac{h^2}{2} \left(\bar{\Psi}\Psi \right)^2 \right] , \tag{1.5.1}$$

where a SU($2N$) symmetric mass is condensed for sufficiently strong coupling strength $h > h_c$.

The procedure to obtain the scaling dimensions of monopole operators must be modified. For this model, there is only a single pseudo-scalar boson ϕ entering the Hubbard-Stratonovich transform. The effective action at the critical point can be obtained in the same way we derived the analogous quantity for the spin-dependent case (1.3.7)

$$S''^c_{\text{eff}} = -N \ln \det \left(\not{D}^{S^2\times\mathbb{R}}_{a,A^q} + \phi \right) , \tag{1.5.2}$$

where we now work on $S^2 \times \mathbb{R}$ with the sphere pierced by a $4\pi q$ flux. Here, there is no constraint on the sign of the mass given by the expectation value of the bosonic field $M_q = \langle \phi \rangle$.

Another important difference when computing the lowest scaling dimension of monopole operators in this model is that a chemical potential μ must be introduced. This is used to enforce half-filling of the "zero" modes.[10] This was not necessary for the model with a spin-dependent interaction. The reason is that the chemical potential is by default set to zero. Thus, half of the "zero" modes are below this level and get filled up. In QED_3 [10, 40], the zero modes are also half filled as a chemical potential set to zero sits at the level of all the zero modes. This is not the case when a SU($2N$) symmetric interaction is activated since the "zero" modes all get shifted below the chemical potential if the boson condensate is non-zero. Thus, directly setting $\mu = 0$ only yields the correct fermionic occupation when there is an equal number of modes above and below zero energy.

[10] We will find that these modes have vanishing energy and are truly zero modes. However, it is simpler for the discussion that follows to assume that these modes might have non-zero energy, so we refer to them as "zero" modes at this point of the analysis.

The chemical potential can be incorporated within the path integral formalism. We first compactify the "time" direction to a circle S^1_β with a radius β. This radius is taken to infinity, $\beta \to \infty$, at the end of our computations. When working on this "thermal" circle, the modified relation between the monopole operator scaling dimension Δ_q and the free energy F_q for $\beta \gg 1$ is [45]

$$\Delta_q - \frac{1}{\beta}\ln(\Omega_q) + \mathcal{O}\left(e^{-c\beta}\right) = F_q \equiv -\frac{1}{\beta}\ln Z_{S^2\times S^1_\beta}[A^q]\,, \tag{1.5.3}$$

where Ω_q is the ground state degeneracy and c gives the energy spacing between the ground state and the first excited state.[11] On this space, the chemical potential can be defined as the homogeneous saddle point value of the imaginary gauge field $\langle a_\tau\rangle = -i\mu$. This approach was used in Ref. [45]. The chemical potential is a source for the fermion number $\Psi^\dagger\Psi$. Requiring a vanishing fermion number, we have the condition

$$\frac{1}{\beta}\frac{\delta \ln Z_{S^2\times S^1_\beta}[A^q]}{\delta\mu} = \langle N_{\text{fermions}}\rangle = 0\,. \tag{1.5.4}$$

This can also be written in terms of a saddle point equation. Once again, the spatial part of the gauge field has a vanishing expectation value $\langle a_i\rangle = 0$. We are left with our homogeneous ansatz $\langle a_\tau\rangle = -i\mu$ and $\langle\phi\rangle = M_q$,

$$\frac{\partial F_q^{(0)}}{\partial\mu} = 0\,, \tag{1.5.5}$$

$$\frac{\partial F_q^{(0)}}{\partial M_q} = 0\,, \tag{1.5.6}$$

where the leading order in $1/N$ of the free energy is

$$F_q^{(0)} = -\frac{1}{\beta}\ln\det\left(\not{D}^{S^2\times S^1_\beta}_{-i\mu,A^q} + M_q\right). \tag{1.5.7}$$

As the "time" direction is compact, the spectrum of the Dirac operator in Eq. (1.5.7) is now defined by Matsubara fermionic frequencies $\omega_n = (2\pi/\beta)(n+1/2)$ where $n \in \mathbb{Z}$. In contrast to our previous computations, the mass term is now spin symmetric in contrast to our previous computation. With these considerations, the previous result shown in Eq. (1.3.20) can be

[11] The identity operator ($q = 0$) should have a vanishing scaling dimension $\Delta_{q=0} = 0$ *and* no degeneracy, $\Omega_{q=0} = 1$. This can be guaranteed by a proper normalization, but just as in the spin-dependent case, it turns out to be unnecessary.

adapted so that (1.5.7) becomes

$$F_q^{(0)} = -\frac{2}{\beta}\sum_{n=-\infty}^{\infty}\left[d_q \ln\left[\omega_n - i\mu + iM_q\right] + \sum_{\ell=q+1}^{\infty} d_\ell \ln\left[(\omega_n - i\mu)^2 + \varepsilon_\ell^2\right]\right], \tag{1.5.8}$$

where as before ε_ℓ is given by Eq. (1.3.21) Regularizing the sum over Matsubara frequencies, we obtain

$$F_q^{(0)} = -\frac{2}{\beta}\left[d_q \ln\left[2\cosh\left(\frac{\beta(\mu - M_q)}{2}\right)\right] + \sum_{\ell=q+1}^{\infty} d_\ell \ln\left[2(\cosh(\beta\varepsilon_\ell) + \cosh(\beta\mu))\right]\right]. \tag{1.5.9}$$

The saddle point equations (1.5.5, 1.5.6) become

$$-d_q \tanh\left(\frac{\beta(\mu - M_q)}{2}\right) - \sum_{\ell=q+1}^{\infty} \frac{2d_\ell \sinh(\beta\mu)}{\cosh(\beta\varepsilon_\ell) + \cosh(\beta\mu)} = 0\,, \tag{1.5.10}$$

$$d_q \tanh\left(\frac{\beta(\mu - M_q)}{2}\right) - \sum_{\ell=q+1}^{\infty} \frac{2d_\ell \varepsilon_\ell^{-1} M_q \sinh(\beta\varepsilon_\ell)}{\cosh(\beta\varepsilon_\ell) + \cosh(\beta\mu)} = 0\,. \tag{1.5.11}$$

Taking $\mu = M_q$ eliminates the first term in both equations. These equations can be further simplified by taking the large β limit. The sum in the first equation vanishes to leading order in $1/\beta$ and the first saddle point equation is then satisfied for $\beta \to \infty$. In the same way, the second saddle point equation to leading order in $1/\beta$ with $\mu = M_q$ is given by

$$2M_q \sum_{\ell=q+1}^{\infty} d_\ell \varepsilon_\ell^{-1} = 0\,. \tag{1.5.12}$$

In this limit, this saddle point equation is only satisfied for $M_q = 0$, which implies a vanishing chemical potential $\mu = 0$. More directly, this means that the expectation value of the bosonic field vanishes, $\langle\phi\rangle = 0$. Thus, monopole operators at the symmetric QCP are dressed with true zero modes. One of the monopole ground states is shown in Fig. 1.6 Since there is no boson condensate, the fermion energies are unchanged when compared to those in QED_3. This means that we are left, at leading order in $1/N$, with the same scaling dimensions as in QED_3, $\Delta_q^{\mathrm{QED}_3\,-\,\mathrm{GN}} = \Delta_q^{\mathrm{QED}_3} + O(1/N^0)$. A similar result was obtained for the QCP between a DSL and a $\mathbb{Z}_2 -$ spin liquid [51].

We emphasize that this is a result at leading order in $1/N$. The presence of the bosonic field includes more quantum fluctuations that may change corrections at non-leading orders. We also note that the first condition $\mu = M_q$ is indeed the condition enforcing half-filling of the zero modes and is needed even if in the end, we find $\mu = M_q = 0$. Had we not included the chemical potential, we would minimize the free energy that has all the zero modes empty and we would find $M_q \neq 0$. In the case of the spin-dependent interaction we studied before,

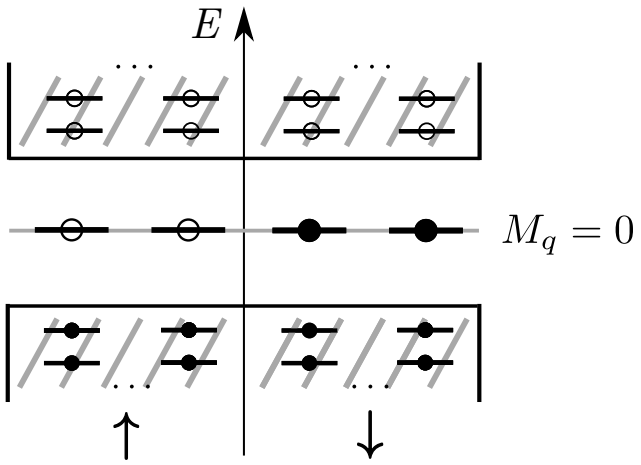

Figure 1.6. Schematic representation of the energy spectrum and fermionic occupation for one of the monopole ground state in the SU($2N$) symmetric QCP. The spectrum is shown for $2N = 4$ fermion flavors and minimal magnetic charge $q = 1/2$. The zero modes could be shifted by an energy M_q, but the saddle point equations force this quantity to vanish.

the saddle point solution for the chemical potential is $\mu = 0$, independently of the value of the mass M_q. We show this explicitly in App. 1.B. This is why the inclusion of a chemical potential was not necessary in this case.

1.5.1. Testing a duality with bosonic CP^1 model

The case of compact $\mathrm{QED}_3 - \mathrm{GN}$ theory with $2N = 2$ fermion flavors is of particular interest since it is conjectured to be dual to the CP^1 theory when both theories are tuned at their critical point, assuming the fixed points exist [22]. This latter theory describes $N_b = 2$ flavors of complex bosonic fields forming a SU(2) doublet $z = (z_1, z_2)^\intercal$ which satisfy a length constraint $z^\dagger z = 1$ and interact with a compact gauge field. This model notably describes a deconfined quantum critical point between Néel and VBS phases, which is relevant for quantum magnets on various lattices [52], with the case of square lattice being the prototype example of deconfined criticality [21]. Operators on one side of the conjectured duality have the same scaling dimension as their dual on the other side of the duality. More specifically, the duality relates a set of operators in the fermionic theory

$$\left[\mathrm{Re}\left(\psi_1^\dagger \widetilde{\mathcal{M}}_{q=1/2}\right), -\mathrm{Im}\left(\psi_1^\dagger \widetilde{\mathcal{M}}_{q=1/2}\right), \mathrm{Re}\left(\psi_2^\dagger \widetilde{\mathcal{M}}_{q=1/2}\right), \mathrm{Im}\left(\psi_2^\dagger \widetilde{\mathcal{M}}_{q=1/2}\right), \phi \right], \tag{1.5.13}$$

to a set of operators in the bosonic theory

$$\left[2\,\mathrm{Re}\,\mathcal{M}^{\mathrm{CP}^1}_{q=1/2}, 2\,\mathrm{Im}\,\mathcal{M}^{\mathrm{CP}^1}_{q=1/2}, z^\dagger\sigma_1 z, z^\dagger\sigma_2 z, z^\dagger\sigma_3 z\right]. \tag{1.5.14}$$

Here, $\psi^\dagger_{I=1,2}\widetilde{\mathcal{M}}_{q=1/2}$ is a monopole with a minimal magnetic charge $q=1/2$ dressed with one of the two fermion zero modes. On the bosonic side, $\mathcal{M}^{\mathrm{CP}^1}_{q=1/2}$ is the unique monopole operator with a minimal magnetic charge $q=1/2$. Additionally, both theories have global symmetries relating certain operators of these sets, i.e. some operators within a set have the same scaling dimension. Global U(1) symmetry relates the real and imaginary parts of monopole operators in both theories. Flavor symmetry on the fermionic side relates the two types of monopole operators while a SU(2) symmetry on the bosonic side implies that all three components of the bilinear $z^\dagger\boldsymbol{\sigma}z$ share the same scaling dimension. Taking into account these global symmetries and the conjectured duality, it is deduced that all operators above should have the same scaling dimension. Said otherwise, the duality predicts an emergent SO(5) symmetry at the fixed point of these theories. The duality can thus be tested by comparing the monopole scaling dimension obtained above to other scaling dimensions conjectured to be the same.

The scaling dimension of the monopole operator with $q=1/2$ in $\mathrm{QED}_3-\mathrm{GN}$ for $2N=2$ fermion flavors is $\Delta^{\mathrm{QED}_3-\mathrm{GN}}_{\mathcal{M}_{q=1/2}} = 2N(0.26510)+\mathcal{O}((1/N)^0)\sim 0.53$. We compare this value to results in the literature for the other scaling dimensions. For the monopole operator with minimal magnetic charge in the bosonic theory CP^{N_b-1} with $N_b=2$, it was found in a similar computation using the state-operator correspondence that $\Delta^{\mathrm{CP}^{N_b-1}}_{\mathcal{M}_{q=1/2}} = 0.1245922N_b+0.3815\sim 0.63$ [53]. In a functional renormalization group analysis [54], it was found that $\Delta_{\text{Néel}}\equiv\Delta_{z^\dagger\boldsymbol{\sigma}z}=0.61$. On the numerical front, the scaling dimensions of the VBS order parameter $\Delta_{\mathrm{VBS}}\equiv\Delta^{\mathrm{CP}^1}_{\mathcal{M}_{q=1/2}}$ and the Néel order parameter $\Delta_{\text{Néel}}$ were found to be in the range $\Delta_{\text{VBS, Néel}}\in[0.60,0.68]$ [55–59]. On the fermionic side, a large N expansion suggests that the scaling dimension of the boson is in the range $\Delta_\phi\in[0.59,0.65]$ [60]. These last results seem coherent together, and our 0.53 is not too far off. This being said, we only obtained the monopole scaling dimension at leading order in $1/N$. Higher order or non-perturbative calculations are needed to make a firmer statement.

1.6. Renormalization group analysis of the critical fixed point

We study more thoroughly the critical fixed point by considering the Yukawa theory that is the UV completion of the $\text{QED}_3 - \text{cHGN}$ model (1.2.5). This model is called $\text{QED}_3 - \text{cHGNY}$ and is defined by the following bare Euclidean lagrangian

$$\mathcal{L} = -\bar{\Psi}\partial\!\!\!/\Psi + \frac{1}{2}\left(\epsilon_{\mu\nu\rho}\partial_\nu a_\rho\right)^2 + \frac{1}{2}(\partial_\mu \boldsymbol{\phi})^2 + ie\bar{\Psi}a\!\!\!/\Psi + h\boldsymbol{\phi}\cdot\bar{\Psi}\boldsymbol{\sigma}\Psi + \frac{1}{2}m_\phi^2\boldsymbol{\phi}^2 + \lambda(\boldsymbol{\phi}^2)^2\,. \quad (1.6.1)$$

In this section, we consider the non-compact version of QED_3. As before, Ψ denotes the spinor with $2N$ flavors of two-component Dirac fermion field and $\boldsymbol{\phi}$ is a boson field with $N_b = 3$ components. We perform the renormalization group (RG) analysis for general N and N_b, and then we specialize to $N_b = 3$ and $2N = 4$, which are relevant parameters for certain quantum magnets. For simplicity, we keep referring to this model as $\text{QED}_3 - \text{cHGNY}$ although we don't fix $N_b = 3$ from the outset. RG studies for similar quantum field theories have been considered before. For example, a gauged theory with a valley-dependent cHGNY-like interaction, $\boldsymbol{\phi}\bar{\Psi}\mu_z\boldsymbol{\sigma}\Psi$, and with $2N = 4$ fermion flavors was studied to leading order in $\epsilon = 4 - d$ expansion [19]. Here, d is the spacetime dimension.

The analysis was also done in the ungauged theory, i.e. the cHGNY model, with general N at four-loop in the $\epsilon = 4 - d$ expansion [61] and to order $1/N^2$ [62]. The $\text{QED}_3 - \text{GNY}$ was also considered for general N using dimensional regularization at one-loop [63], three-loop [64] and four-loop [65] and to order $1/N^2$ [60, 66, 67]. In the last reference, a spin-dependent Yukawa interaction term with $N_b = 1$, $\phi\bar{\Psi}\sigma_z\Psi$, has also been considered. A theory with $N_b = 2$ bosons and an additional cubic self-interaction was also considered in Ref. [68]. See [69] for a comprehensive review on large$-N$ methods.

1.6.1. Setup

The first step in our RG study is to write the renormalized Euclidean lagrangian

$$\begin{aligned}\mathcal{L} = &-Z_\psi\bar{\Psi}\partial\!\!\!/\Psi + \frac{1}{2}Z_a\left(\epsilon_{\mu\nu\rho}\partial_\nu a_\rho\right)^2 + \frac{1}{2}Z_\phi(\partial_\mu\boldsymbol{\phi})^2 + Z_e\,(ie)\,\mu^{\frac{4-d}{2}}\bar{\Psi}a\!\!\!/\Psi \\ &+ Z_h h\mu^{\frac{4-d}{2}}\boldsymbol{\phi}\cdot\bar{\Psi}\boldsymbol{\sigma}\Psi + \frac{1}{2}Z_{m_\phi^2}m_\phi^2\mu^2\boldsymbol{\phi}^2 + Z_\lambda\lambda\mu^{4-d}(\boldsymbol{\phi}^2)^2\,,\end{aligned} \quad (1.6.2)$$

where we introduced wave function renormalization constants Z_ψ, Z_ϕ and Z_a as well as vertex renormalization constants Z_e, Z_h, $Z_{m_\phi^2}$ and Z_λ. Coupling constants are also rescaled

by powers of energy μ factoring out their naive scaling dimension. The renormalized fields are obtained by a rescaling of the bare fields $\Psi_0 = \sqrt{Z_\psi}\Psi, \quad \boldsymbol{\phi}_0 = \sqrt{Z_\phi}\boldsymbol{\phi}, \quad (a_\mu)_0 = \sqrt{Z_a}a_\mu$. Relations between the renormalized coupling constants $(e^2, h^2, \lambda) \equiv (c_1, c_2, c_3) = \boldsymbol{c}$ and the bare coupling constants are obtained

$$e^2 = e_0^2 \mu^{d-4} Z_a \,, \tag{1.6.3}$$

$$h^2 = h_0^2 \mu^{d-4} Z_\psi^2 Z_\phi Z_h^{-2} \,, \tag{1.6.4}$$

$$\lambda = \lambda_0 \mu^{d-4} Z_\phi^2 Z_\lambda^{-1} \,, \tag{1.6.5}$$

where the Ward identity, $Z_\psi^2 Z_e^{-2} = 1$, was used to simplify the renormalization of the gauge charge e^2. We also add a gauge fixing term $\mathcal{L}_{\text{g.f.}} = (\partial_\mu a_\mu)^2 / (2\xi)$ to ensure physical quantities are gauge independent. We have explicitly written a quadratic boson term since, as we discussed in Sec.1.2.2, the mass is the tuning parameter for the phase transition. We first study the RG flow equations at the critical value of the boson mass, $m_\phi^c = 0$. Later on, we incorporate the boson mass term, along with fermion bilinears, as perturbations away from the QCP.

By rescaling the energy $\mu \to \mu e^{-l}$ in (1.6.3 - 1.6.5), we can analyze how the coupling constants vary with the scale factor [70]. The RG flow equation are found by differentiating the renormalized coupling constants with respect to the scale factor, i.e. by obtaining the beta functions $\beta_{c_I} = \mathrm{d}c_I/\mathrm{d}l$ with $I \in \{1,2,3\}$

$$\beta_{e^2} \equiv \frac{\mathrm{d}e^2}{\mathrm{d}l} = (4 - d - \gamma_a)\, e^2 \,, \tag{1.6.6}$$

$$\beta_{h^2} \equiv \frac{\mathrm{d}h^2}{\mathrm{d}l} = (4 - d - 2\gamma_\psi - \gamma_\phi + 2\gamma_h)\, h^2 \,, \tag{1.6.7}$$

$$\beta_\lambda \equiv \frac{\mathrm{d}\lambda}{\mathrm{d}l} = (4 - d - 2\gamma_\phi + \gamma_\lambda)\, \lambda \,, \tag{1.6.8}$$

where the coefficients γ_{x_i} with $x_i \in \{\psi, \phi, a, h, \lambda\}$ are defined as

$$\gamma_{x_i} = -\frac{\mathrm{d}\ln Z_{x_i}}{\mathrm{d}l} \,. \tag{1.6.9}$$

The γ_{x_i} are obtained in App. 1.C, and allow to find the following flow equations at one-loop order

$$\frac{\mathrm{d}e^2}{\mathrm{d}l} = (4-d)\,e^2 - \frac{4N}{3}e^4\,, \tag{1.6.10}$$

$$\frac{\mathrm{d}h^2}{\mathrm{d}l} = (4-d)\,h^2 + 8\left(1-\frac{1}{d}\right)e^2h^2 - 2\left(N+2-\frac{2N_b}{d}\right)h^4\,, \tag{1.6.11}$$

$$\frac{\mathrm{d}\lambda}{\mathrm{d}l} = (4-d)\,\lambda - 4Nh^2\lambda + Nh^4 - 4\,(N_b+8)\,\lambda^2\,, \tag{1.6.12}$$

where the coupling constants have been rescaled to eliminate a loop integral factor. We will first find the fixed points of the RG flow, that is the critical coupling constants $(e_*^2, h_*^2, \lambda_*) \equiv \boldsymbol{c}_*$ for which the beta functions vanish, $\beta_{c_I} = 0$. The $\mathrm{QED}_3 - \mathrm{cHGNY}$ infrared fixed point corresponding to the QCP will be found, and we will obtain the corresponding critical exponents.

Note that adding other quartic interactions $\delta\mathcal{L} = (g_\Gamma^2/2)(\bar{\Psi}\Gamma\Psi)^2$ respecting the flavor and Lorentz symmetries of the theory does not affect the existence of the QCP. This can be seen in the UV completed theory where all these additional interactions are decoupled with auxiliary bosons. The flow equations of the corresponding Yukawa coupling g_Γ and of the boson self-interaction coupling λ_Γ take the form

$$\frac{\mathrm{d}g_\Gamma^2}{\mathrm{d}l} = (\cdots)g_\Gamma^2\,, \quad \frac{\mathrm{d}\lambda_\Gamma}{\mathrm{d}l} = (\cdots)g_\Gamma^2 + (\cdots)\lambda_\Gamma\,, \tag{1.6.13}$$

where the ellipses prefactors include constants and positive powers of the coupling constants. This means that there are fixed points for which these couplings vanish $(g_\Gamma, \lambda_\Gamma) = (0,0)$. Therefore, the critical exponents of the QCP can be studied within the $\mathrm{QED}_3 - \mathrm{cHGNY}$ model.

1.6.2. RG study in the $\epsilon = 4 - d$ expansion

We now use a dimensional regularization to control the RG flow. We study the theory at finite N by working near the upper critical number of spacetime dimensions $d = 4 - \epsilon$, where ϵ is treated as a small expansion parameter. Assuming the coupling constants are $\mathcal{O}(\epsilon)$, we

obtain the flow equations in the ϵ expansion

$$\frac{\mathrm{d}e^2}{\mathrm{d}l} = \epsilon e^2 - \frac{4N}{3} e^4 \,, \tag{1.6.14}$$

$$\frac{\mathrm{d}h^2}{\mathrm{d}l} = \epsilon h^2 + 6e^2 h^2 - (2N + 4 - N_b)\, h^4 \,, \tag{1.6.15}$$

$$\frac{\mathrm{d}\lambda}{\mathrm{d}l} = \epsilon\lambda + N h^4 - 4N h^2 \lambda - 4\,(N_b + 8)\,\lambda^2 \,. \tag{1.6.16}$$

The corresponding physical fixed points are shown in Tab. 1.2, where we have defined

$$\mathcal{K}_{N,N_b} = \left[4N_f^4 + 4\,(5N_b + 46)\,N_f^3 + 324\,(N_b + 8)\,N_f + \left(N_b^2 + 172N_b + 1348\right) N_f^2\right]^{1/2} , \tag{1.6.17}$$

$$\mathcal{K}'_{N,N_b} = \left[4N_f^2 + 4\,(5N_b + 28)\,N_f + (N_b - 4)^{\,2}\right]^{1/2} \,. \tag{1.6.18}$$

The linearized RG flow equations around a fixed point $\boldsymbol{c}^*$ yields a matrix equation for the coupling constant perturbations

$$\frac{\mathrm{d}}{\mathrm{d}l}(c_I - c_I^*) = \sum_{J=1,2,3} M_{IJ}\,(c_J - c_J^*) \,, \tag{1.6.19}$$

where $M_{IJ} = \frac{\partial \beta_{c_I}}{\partial c_J}\Big|_{\boldsymbol{c}=\boldsymbol{c}^*}$ is the stability matrix. Its eigenvectors yield proper directions in the space of couplings $\{e^2, h^2, \lambda\}$. The related eigenvalues λ_I indicate relevant ($\lambda_I > 0$), marginal ($\lambda_I = 0$), or irrelevant ($\lambda_I < 0$) perturbations. An infrared fixed point is characterized by irrelevant perturbations in all proper directions. For the theory under study, there is a unique infrared fixed point which, at order ϵ and for $N_b = 3$ is given by

$$e_*^2 = \frac{3}{4N}\epsilon \,, \tag{1.6.20}$$

$$h_*^2 = \frac{2N + 9}{2N\,(2N + 1)}\epsilon \,, \tag{1.6.21}$$

$$\lambda_* = \frac{-2N^2 - 17N + \mathcal{K}_{N,3}}{88N\,(2N + 1)}\epsilon \,, \tag{1.6.22}$$

where

$$\mathcal{K}_{N,3} = \left[N(4N^3 + 244N^2 + 1873N + 3564)\right]^{1/2} . \tag{1.6.23}$$

At this infrared fixed point, called $\mathrm{QED}_3 - \mathrm{cHGNY}$, all critical coupling constants are non-zero. Note in this case that the infrared fixed point is in the physical region $h^2 > 0$ only if $2N - N_b + 4 > 0$. The flow in the $(\lambda/\epsilon, h^2/\epsilon)$ plane with e^2 fixed to its two possible critical

values is shown Fig. 1.7. In particular, the flow from the QED_3 fixed point ($h^2 = \lambda = 0$) to the $\mathrm{QED}_3 - \mathrm{cHGNY}$ fixed point is shown in Fig. 1.7(a).

We also note that taking $\epsilon = 1$ and $N \gg 1$ yields the result of the $1/N$ expansion. For example, the QCP in this expansion is given by

$$e_*^2 = \frac{3}{4N}\,, \quad h_*^2 = \frac{1}{2N}\,, \quad \lambda_* = \frac{1}{4N}\,. \tag{1.6.24}$$

Note however that Wilson-Fisher type fixed points where $\lambda^* \sim O((1/N)^0)$ are not controlled by the $1/N$ expansion.

Tableau 1.2. Fixed points obtained at leading order in the $\epsilon = 4 - d$ expansion of RG flow equations (1.6.14 - 1.6.16). $\mathcal{K}_{N,N_b}$ and $\mathcal{K}'_{N,N_b}$ are defined in Eqs. (1.6.17, 1.6.18), respectively. There are six fixed points, where G stands for "Gaussian" and WF for "Wilson-Fisher".

Fixed points	e_*^2	h_*^2	λ_*
G	0	0	0
QED_3	$\frac{3}{4N_f}\epsilon$	0	0
WF	0	0	$\frac{1}{4\,(N_b+8)}\epsilon$
$\mathrm{QED}_3 - \mathrm{WF}$	$\frac{3}{4N_f}\epsilon$	0	$\frac{1}{4\,(N_b+8)}\epsilon$
cHGNY	0	$\frac{1}{2N-N_b+4}\epsilon$	$\frac{\mathcal{K}'_{N_f,N_b}-2N_f-N_b+4}{8\,(N_b+8)\,(2N_f-N_b+4)}\epsilon$
$\mathrm{QED}_3 - \mathrm{cHGNY}$	$\frac{3}{4N_f}\epsilon$	$\frac{2N_f+9}{2N\,(2N-N_b+4)}\epsilon$	$\frac{\mathcal{K}_{N_f,N_b}-2N_f^2-(N_b+14)\,N_f}{8N_f\,(N_b+8)\,(2N-N_b+4)}\epsilon$

1.6.2.1. Exponents at the quantum critical point . We now compute the critical exponents at the infrared fixed point. The scaling dimension of an operator $\mathcal{O}(x)$ at the QCP is defined by the following expectation value

$$\langle \mathcal{O}(x_1)\mathcal{O}^\dagger(x_2)\rangle \propto \frac{1}{|x_1 - x_2|^{2\Delta_\mathcal{O}}}\,. \tag{1.6.25}$$

Using scaling arguments, one can write a naive dimension $\Delta^0_\mathcal{O}$. This value is corrected by an anomalous dimension $\eta_\mathcal{O}$ once interactions are taken into account

$$\Delta_\mathcal{O} = \Delta^0_\mathcal{O} + \frac{\eta_\mathcal{O}}{2}\,. \tag{1.6.26}$$

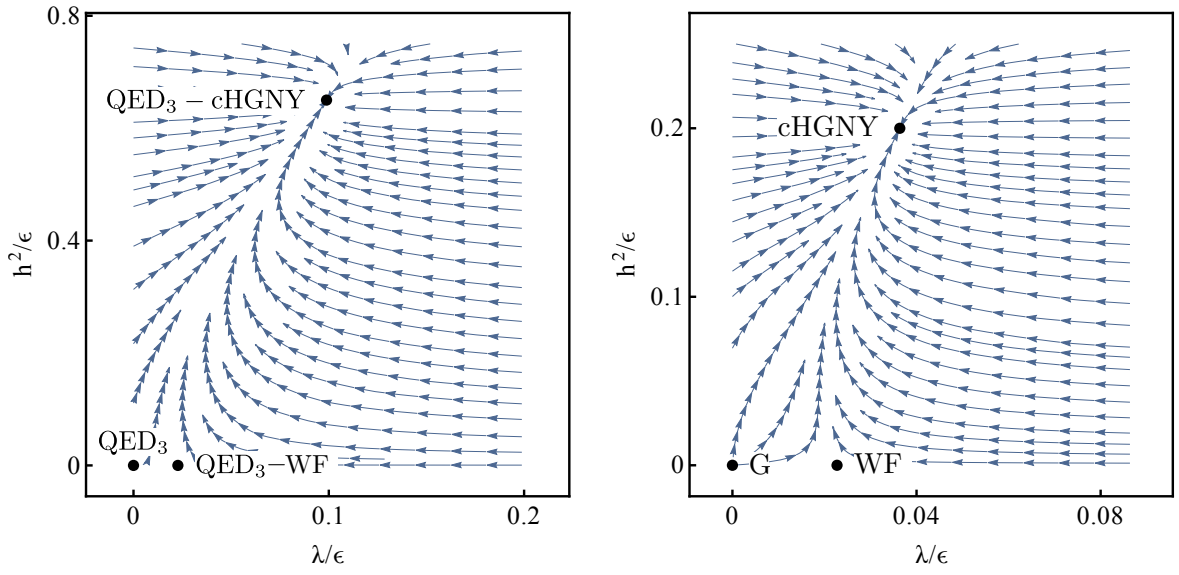

Figure 1.7. RG flow for $2N = 4$ and $N_b = 3$ in the $(\lambda/\epsilon, h^2/\epsilon)$ plane to leading order in $\epsilon = 4 - d$. a) Flow for $e^2 = 3\epsilon/4N$; b) Flow for $e^2 = 0$.

We start by studying the anomalous dimensions of the fields. These quantities are found by evaluating the corresponding coefficients γ_Φ (1.6.9) at the QCP, that is $\eta_\Phi = \gamma_\Phi|_{\boldsymbol{c}=\boldsymbol{c}_*^{\rm QCP}}$. First, we write the general expressions for these coefficients obtained in App. 1.C

$$\gamma_\phi = 2Nh^2\,, \tag{1.6.27}$$

$$\gamma_\psi = \left(d + \xi - 5 + \frac{4}{d}\right) e^2 + \left(1 - \frac{2}{d}\right) N_b h^2\,, \tag{1.6.28}$$

$$\gamma_a = \frac{4N}{3} e^2\,. \tag{1.6.29}$$

Replacing the coupling constants in Eqs. (1.6.27 - 1.6.29) by their critical value at the $\mathrm{QED}_3 - \mathrm{cHGNY}$ fixed point in Tab. 1.2, we obtain the anomalous dimensions

$$\eta_\phi = \frac{2N + 9}{2N - N_b + 4}\epsilon\,, \tag{1.6.30}$$

$$\eta_\psi = \frac{N_b\,(2N - 3\xi + 9) + 6\xi\,(N + 2)}{4N\,(2N - N_b + 4)}\epsilon\,, \tag{1.6.31}$$

$$\eta_a = \epsilon\,. \tag{1.6.32}$$

Note that the anomalous dimension of the fermion depends on the gauge fixing parameter ξ, but this is expected since it is not a gauge invariant quantity. The gauge field anomalous dimension is ϵ which implies that the one-loop corrected gauge field propagator is $\langle a_\mu(p)a_\nu(-p)\rangle \sim |p|^{-1}$ once we set $\epsilon = 1$. By setting $e_*^2 \neq 0$ in the gauge charge flow equation (1.6.6), it is seen that the one-loop result we found, $\eta_a = \epsilon$, is actually valid to all orders. This is again a consequence of the Ward identity. Now, setting $N_b = 3$ in the anomalous dimensions (1.6.30 - 1.6.31), we obtain

$$\eta_\phi = \frac{2N_f + 9}{2N_f + 1}\epsilon\,, \;\; \eta_\psi = \frac{3\,(2(\xi+1)N_f + \xi + 9)}{4N_f\,(2N_f+1)}\epsilon\,. \tag{1.6.33}$$

Setting $2N = 4$, we obtain

$$\eta_\phi = \frac{13}{5}\epsilon\,, \quad \eta_\psi = \frac{3\,(5\xi+13)}{40}\epsilon\,. \tag{1.6.34}$$

Setting $\epsilon = 1$, we find $\Delta_\phi = (d-2)/2 + \eta_\phi/2 \approx 1.8$.

We now study the scaling dimension of mass operators by introducing mass perturbations at the QCP

$$\Delta\mathcal{L} = \frac{1}{2}Z_{m_\phi^2} m_\phi^2 \boldsymbol{\phi}^2 + Z_{m_\psi} m_\psi \bar{\Psi}\Psi + Z_{\tilde{m}_\psi}\tilde{m}_\psi(\hat{\boldsymbol{n}}\cdot\bar{\Psi}\boldsymbol{\sigma}\Psi)\,, \tag{1.6.35}$$

where $\hat{\boldsymbol{n}}$ is a unit vector indicating the direction of the spin-Hall bilinear perturbation. We do not include a valley-Hall bilinear $\bar{\Psi}\mu_A\Psi$, where $A \in \{1,2,\ldots N\}$, since its scaling dimension is the same as the SU($2N$) symmetric bilinear $\bar{\Psi}\Psi$ at leading order in $\epsilon = 4-d$. The masses we introduced can be related to bare masses like we did with the other coupling constants

$$m_\phi^2 = \left(m_\phi^2\right)_0 \mu^2 Z_\phi Z_{m_\phi^2}^{-1}\,, \tag{1.6.36}$$

$$m_\psi = (m_\psi)_0\,\mu Z_\psi Z_{m_\psi}^{-1}\,, \tag{1.6.37}$$

$$\tilde{m}_\psi = (\tilde{m}_\psi)_0\,\mu Z_\psi Z_{\tilde{m}_\psi}^{-1}\,. \tag{1.6.38}$$

The RG flow equations follow from these relations are

$$\frac{\mathrm{d}m_\phi^2}{\mathrm{d}l} = \left(2 - \gamma_\phi + \gamma_{m_\phi^2}\right) m_\phi^2\,, \tag{1.6.39}$$

$$\frac{\mathrm{d}m_\psi}{\mathrm{d}l} = \left(1 - \gamma_\psi + \gamma_{m_\psi}\right) m_\psi\,, \tag{1.6.40}$$

$$\frac{\mathrm{d}\tilde{m}_\psi}{\mathrm{d}l} = \left(1 - \gamma_\psi + \gamma_{\tilde{m}_\psi}\right) \tilde{m}_\psi\,, \tag{1.6.41}$$

where the γ_{x_i} with $x_i \in \{\phi, \psi, m_\phi^2, m_\psi, \tilde{m}_\psi\}$ are defined in Eq. (1.6.9). Using results of App. 1.C, the RG flow equations become

$$\frac{\mathrm{d}m_\phi^2}{\mathrm{d}l} = \left(2 - 2Nh^2 - 4\left(N_b + 2\right)\lambda\right) m_\phi^2 \,, \tag{1.6.42}$$

$$\frac{\mathrm{d}m_\psi}{\mathrm{d}l} = \left(1 + 4\left(\frac{d-1}{d}\right)e^2 + 2N_b\left(\frac{1-d}{d}\right)h^2\right) m_\psi \,, \tag{1.6.43}$$

$$\frac{\mathrm{d}\tilde{m}_\psi}{\mathrm{d}l} = \left(1 + 4\left(\frac{d-1}{d}\right)e^2 + 2\left(\frac{N_b-d}{d}\right)h^2\right) \tilde{m}_\psi \,. \tag{1.6.44}$$

When the coupling constants are evaluated at their $\mathrm{QED}_3 - \mathrm{cHGN}$ critical value, the RG flow of the masses is controlled by the scaling dimension of the related mass operators at the QCP

$$\frac{\mathrm{d}m_\phi^2}{\mathrm{d}l} = (d - \Delta_{\phi^2}) m_\phi^2 \,, \tag{1.6.45}$$

$$\frac{\mathrm{d}m_\psi}{\mathrm{d}l} = (d - \Delta_{\bar{\Psi}\Psi}) m_\psi \,, \tag{1.6.46}$$

$$\frac{\mathrm{d}\tilde{m}_\psi}{\mathrm{d}l} = (d - \Delta_{\bar{\Psi}\sigma_a\Psi}) \tilde{m}_\psi \,. \tag{1.6.47}$$

We first study the $\boldsymbol{\phi}^2$ perturbation. The phase transition is controlled by the mass m_ϕ^2 auxiliary boson and the correlation length exponent $\nu^{-1} = d - \Delta_{\phi^2}$ is obtained by evaluating (1.6.42) at the QCP

$$\begin{aligned} \nu^{-1} = \; & 2 - \frac{2N_f + 9}{2N - N_b + 4}\epsilon \\ & - \frac{\left(N_b + 2\right)\left(\mathcal{K}_{N,N_b} - N_f\left(2N + N_b + 14\right)\right)}{2N_f\left(N_b + 8\right)\left(2N - N_b + 4\right)}\epsilon \,. \end{aligned} \tag{1.6.48}$$

Setting $N_b = 3$, we obtain

$$\nu^{-1} = 2 - \frac{34N_f^2 + 113N_f + 5\mathcal{K}_{N,3}}{22N_f\left(2N_f + 1\right)}\epsilon \,, \tag{1.6.49}$$

which gives the correct $N \to \infty$ limit : $\nu = 1$. Setting $2N = 4$, we obtain

$$\nu^{-1} = 2 - 4.577\epsilon \,. \tag{1.6.50}$$

Setting $\epsilon = 1$, our one-loop result yields a negative correlation length exponent, suggesting strong quantum fluctuations as the physical dimension is approached. This is was also observed for the $\mathrm{QED}_3 - \mathrm{GNY}$ model in Ref. [63] where a dimensional regularization around $d = 2 + \epsilon$ was also performed to do an interpolation and obtain a positive correlation length

exponent. One could also go further in the loop expansion to see if a physical result in the $\epsilon \to 1$ limit follows. However, an estimate for ν can be obtained by inverting ν^{-1}

$$\nu = \frac{1}{2} + \frac{34N_f^2 + 113N_f + 5\mathcal{K}_{N,3}}{88N_f\,(2N_f+1)}\epsilon \bigg|_{2N=4} = \frac{1}{2} + 1.144\epsilon\,. \tag{1.6.51}$$

Setting $\epsilon = 1$ now yields the positive result $\nu = 1.644$. Inverting this exponent once again, we obtain the scaling dimension of ϕ^2 which is given by $\Delta_{\phi^2} = d - \nu^{-1} \approx 2.392$. At $\epsilon = 1$, these are mere estimates, and a more refined treatment is needed to obtain controlled exponents.

We now turn our attention to the fermion bilinears perturbations. Evaluating (1.6.43, 1.6.44) with critical couplings of the $\mathrm{QED}_3 - \mathrm{cHGN}$ fixed point shown at leading order in ϵ in Tab. 1.2, we find the scaling dimensions at the QCP are given by

$$\Delta_{\bar{\Psi}\Psi} = 3 - \frac{4N^2 - (5N_b - 17)N - 18(N_b - 1)}{2N\,(2N - N_b + 4)}\epsilon\,, \tag{1.6.52}$$

$$\Delta_{\bar{\Psi}\sigma_a\Psi} = 3 - \frac{4N - N_b + 13}{2\,(2N - N_b + 4)}\epsilon\,. \tag{1.6.53}$$

Setting $N_b = 3$, we obtain

$$\Delta_{\bar{\Psi}\Psi} = 3 - \frac{2N^2 + N - 18}{N\,(2N+1)}\epsilon\,, \tag{1.6.54}$$

$$\Delta_{\bar{\Psi}\sigma_a\Psi} = 3 - \frac{2N_f + 5}{2N_f + 1}\epsilon\,. \tag{1.6.55}$$

Setting $2N = 4$, this becomes

$$\Delta_{\bar{\Psi}\Psi} = 3 + \frac{4}{5}\epsilon\,, \quad \Delta_{\bar{\Psi}\sigma_a\Psi} = 3 - \frac{9}{5}\epsilon\,. \tag{1.6.56}$$

Once we set $\epsilon = 1$, the spin-Hall bilinear is relevant at the QCP, $\Delta_{\bar{\Psi}\sigma_a\Psi} = 1.2$, but the symmetric bilinear is not, $\Delta_{\bar{\Psi}\Psi} = 3.8$. This contradicts what we obtain by taking the large N limit in (1.6.54) since the scaling dimension $\Delta_{\bar{\Psi}\Psi}|_{N\to\infty} = 3 - \epsilon$ then implies a relevant operator for $\epsilon = 1$. It is expected that higher order corrections in $\epsilon = 4 - d$ would render $\bar{\Psi}\Psi$ relevant.

The critical exponents we found are compiled in Tab. 1.3. In principle, many of our scaling dimensions should agree with the results in Ref. [19] for $2N = 4$ and $N_b = 3$ since the theory considered in this case is almost the same. We find small discrepancies attributable the RG flow equation for the Yukawa coupling, i.e. using their normalization, our Eq. (1.6.15) doesn't match Eq. (27) in Ref. [19]. Fortunately, the mismatch comes from diagrams which are independent of the number of boson components, thus we can compare with studies of

the $\text{QED}_3 - \text{GNY}$ model (see for example Ref. [63]) which confirm our result. We did other verifications for different regions of the parameter space of our theory. First, we considered the ungauged theory $e^2 = 0$ where the QCP point is given by the cHGNY fixed point. Setting $N_b = 3$, the fixed points, the RG flow equations and the critical exponents match those of the cHGNY model presented in Ref. [61]. The fermion bilinear scaling dimensions, which were not computed in this last reference, match the leading order results in $1/N$ of [62]. We also verified the gauged theory when $N_b = 1$. In this model, the spin-Hall bilinear scaling dimension $\Delta_{\bar{\Psi}\sigma_a\Psi}$ is equal, at one-loop order, to the symmetric bilinear scaling dimension $\Delta_{\bar{\Psi}\Psi}$ in $\text{QED}_3 - \text{GNY}$. We find agreement with the results obtained in $\epsilon = 4 - d$ expansions presented in Refs. [61, 63], and by taking the large N limit in our ϵ expansion and comparing to results obtained with large N expansions in Refs. [66, 67, 71]. As noted in Ref. [65], the result for $\Delta_{\bar{\Psi}\Psi}$ disagrees with the one presented in [72]. We find that the latter result would be obtained if the renormalization of the fermion mass included a Hartree diagram. This contribution is not generated in Wilsonian RG.

Tableau 1.3. Critical exponents at the $\text{QED}_3 - \text{cHGNY}$ fixed point with $N_b = 3$ at leading order in $\epsilon = 4 - d$. $\mathcal{K}_{N,3}$ is defined in (1.6.23). The scaling dimension of valley-Hall bilinears is $\Delta_{\bar{\Psi}\mu_A\Psi} = \Delta_{\bar{\Psi}\Psi}$ where $A \in \{1,2,\dots N\}$.

		$2N = 4$	$2N = 4$ $\epsilon = 1$
η_ϕ	$\dfrac{2N+9}{2N+1}\epsilon$	2.6ϵ	2.6
ν	$\dfrac{1}{2} + \dfrac{34N_f^2 + 113N_f + 5\mathcal{K}_{N,3}}{88N_f\,(2N_f+1)}\epsilon$	$\dfrac{1}{2} + 1.144\epsilon$	1.644
$\Delta_{\bar{\Psi}\Psi}$	$3 - \dfrac{2N^2+N-18}{N\,(2N+1)}\epsilon$	$3 + 0.8\epsilon$	3.8
$\Delta_{\bar{\Psi}\sigma_a\Psi}$	$3 - \dfrac{2N_f+5}{2N_f+1}\epsilon$	$3 - 1.8\epsilon$	1.2

1.7. Quantum phase transition in the Kagome magnet

The $\text{QED}_3 - \text{cHGN}$ model considered in the previous sections finds a natural application in quantum magnets where the underlying lattice implies the compactness of the emergent gauge field and the existence of the monopole operators. We specialize our analysis to the

quantum magnet on the Kagome lattice. We first review how a DSL emerges as a possible ground state of the Kagome Heisenberg Antiferromagnet (KHAFM) model. This simple Hamiltonian serves as a starting point to describe the magnetic Cu atoms in Hebertsmithite $ZnCu_3(OH)_6Cl_2$ [73]. We also review the confinement-deconfinement transition from this DSL to a $\boldsymbol{q} = 0$ coplanar antiferromagnetic phase. We then examine the properties of the monopole operators perturbations which drive this quantum phase transition.

1.7.1. Emergent QED_3

The Hamiltonian of the KHAFM is

$$H_H = J_1 \sum_{\langle ij \rangle} \boldsymbol{S}_i \cdot \boldsymbol{S}_j \,, \tag{1.7.1}$$

where $J_1 > 0$ gives the coupling strength of AFM interactions between nearest neighbors of the Kagome lattice. The emergent fractional spin excitations and gauge field in this model arise due to fractionalization. This phenomenon is studied using a parton construction. The spin operator on site i is decomposed as

$$\boldsymbol{S}_i = \frac{1}{2} f^\dagger_{i,s} \boldsymbol{\sigma}_{ss'} f_{i,s'} \,, \tag{1.7.2}$$

where $f_{i,s}$ is a slave-fermion (spinon) with spin $s \in \{\uparrow, \downarrow\}$ and $\boldsymbol{\sigma}$ is a vector of Pauli matrices acting on this spin space. The spinon variables introduce a U(1) gauge redundancy[12] through the symmetry transformation $f_{i,s} \to e^{i\theta_i} f_{i,s}$. The new Hilbert space is doubled compared to the original spin model, therefore an occupation constraint, $f^\dagger_{i,s} f_{i,s} = 1$, must be imposed. A QSL arises when spinon and gauge degrees of freedom are deconfined. The ground state of the KHAFM is not yet well established. Many numerical studies indicate a U(1) spin liquid for the ground state [13, 15–17, 74, 75] while other investigations point towards a $\mathbb{Z}_2$ spin liquid [76–81]. In the latter class of spin liquids, the U(1) gauge symmetry is broken due to a non-vanishing expectation value of spinon pairs $\langle f_i^\dagger f_j^\dagger \rangle$.

We focus our attention on U(1) spin liquids. Using the spinon decomposition (1.7.2) and applying the occupation constraint, the Hamiltonian developed around the hopping

[12] There is a larger SU(2) gauge symmetry, but the U(1) subgroup is sufficient for our discussion.

expectation value $\langle f_{is}^{\dagger} f_{js} \rangle \neq 0$ becomes

$$\tilde{H}_{\mathrm{H}} = -\sum_{\langle ij \rangle} t_{ij} e^{i a_{ij}} f_i^{\dagger} f_j + \mathrm{h.c.}\,, \tag{1.7.3}$$

where the sum on spin indices is now implicit, $t_{ij} = J_1 \langle f_i^{\dagger} f_j \rangle / 2$ and a_{ij} are the phase fluctuations around the expectation value $\langle f_i^{\dagger} f_j \rangle$. The U(1) gauge symmetry is preserved if the phase fluctuation transforms as $a_{ij} \to a_{ij} + \theta_i - \theta_j$. This degree of freedom is thus a dynamical U(1) gauge field.

Among the possible realizations of a U(1) spin liquid, the candidate ground state is obtained with the π-flux pattern of the bond orders which is depicted in Fig. 1.8. This

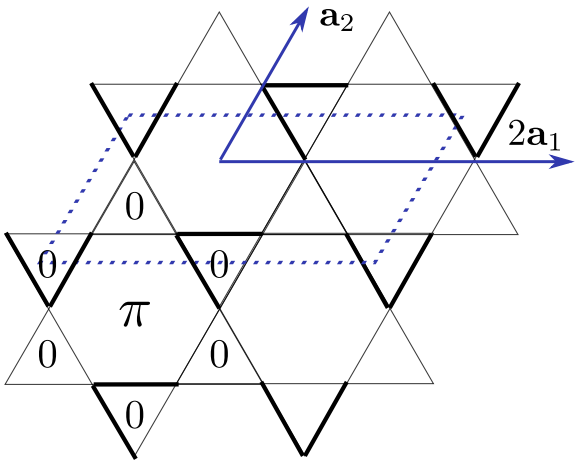

Figure 1.8. π-flux pattern on the Kagome lattice. Bold bonds and regulard bonds have opposite signs for their corresponding hopping parameters.

pattern defines the ground-state called U(1) Dirac spin liquid (DSL) and which has 4 Dirac cones at the Fermi level [82]. The low energy limit is described by QED_3 with $2N = 4$ flavors of massless two-component Dirac fermions, two spin components and two nodes $\pm\boldsymbol{Q}$ in momentum space [82]. An eight-component spinor regrouping all degrees of freedom can be written as $\Psi = (\psi_{\uparrow,\boldsymbol{Q}}, \psi_{\uparrow,-\boldsymbol{Q}}, \psi_{\downarrow,\boldsymbol{Q}}, \psi_{\downarrow,-\boldsymbol{Q}})^{\intercal}$. Vectors of Pauli matrices acting on $\mathrm{SU}(2)_{\mathrm{spin}}$ and $\mathrm{SU}(2)_{\mathrm{valley}}$ subspaces, respectively labeled as $\boldsymbol{\sigma}$ and $\boldsymbol{\mu}$, allow to form spin and valley vectors, $\bar{\Psi}\boldsymbol{\sigma}\Psi$ and $\bar{\Psi}\boldsymbol{\mu}\Psi$. Specifically, the third Pauli matrices in each subspace act as $\sigma_z = |\uparrow\rangle\langle\uparrow| - |\downarrow\rangle\langle\downarrow|$ and $\mu_z = |+\boldsymbol{Q}\rangle\langle+\boldsymbol{Q}| - |-\boldsymbol{Q}\rangle\langle-\boldsymbol{Q}|$. In similar fashion, Dirac matrices acting on the two-dimension spinor space are represented by Pauli matrices, $\gamma_\mu = (\tau_3, \tau_2, -\tau_1)$. The

transformations of these fermions under Kagome lattice symmetries and time reversal are shown in Tab. 1.4 [20].

Tableau 1.4. Transformation properties of spinons under discrete symmetries of the KHAFM [20] where $\mu_{C_6} = (\mu_1 + \mu_2 - \mu_3)/\sqrt{3}$ and $\mu_{\mathcal{R}_y} = -(\mu_1 + \mu_3)/\sqrt{2}$.

	$T_{\boldsymbol{a}_1}$	$T_{\boldsymbol{a}_2}$	$\mathcal{R}_y$	C_6	$\mathcal{T}$
$\Psi \to$	$i\mu_2\Psi$	$i\mu_3\Psi$	$\exp\left(\frac{i\pi}{2}\mu_{\mathcal{R}_y}\right)(i\tau_1)\,\Psi$	$\exp\left(\frac{2\pi i}{3}\mu_{C_6}\right)\exp\left(\frac{i\pi}{6}\tau_3\right)\Psi$	$(i\sigma_2)\,(-i\mu_2)\,(i\tau_2)\,\Psi$

1.7.2. Antiferromagnetic order parameter

We now modify the lattice model to include a next-nearest neighbor AFM coupling J_2. The resulting Hamiltonian describes the spin$-1/2$ $J_1 - J_2$ Heisenberg model

$$H' = J_1 \sum_{\langle ij \rangle} \boldsymbol{S}_i \cdot \boldsymbol{S}_j + J_2 \sum_{\langle\langle ij \rangle\rangle} \boldsymbol{S}_i \cdot \boldsymbol{S}_j \,. \tag{1.7.4}$$

When the ratio J_2/J_1 is sufficiently large, the Kagome frustrated magnet orders to a $\boldsymbol{q} = 0$ AFM coplanar phase [16, 83, 84] shown in Fig. 1.9. The order parameter can be described

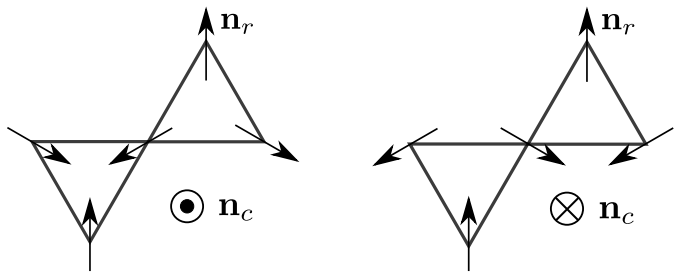

Figure 1.9. Antiferromagnetic $\boldsymbol{q} = 0$ non-collinear phase with a complex order parameter $\boldsymbol{n} = \boldsymbol{n}_r + i\,(\boldsymbol{n}_r \times \boldsymbol{n}_c)$ with a) positive chirality ; b) negative chirality.

as a complex vector $\boldsymbol{n} = \boldsymbol{n}_r + i\,(\boldsymbol{n}_r \times \boldsymbol{n}_c)$ whose real part encodes the orientation of the spin on one of Kagome's three sub-lattices. On each triangle, the two remaining spins are separated by 120° angles with chirality determined by $\boldsymbol{n}_c$. The transformation properties of this vector are shown in Tab. 1.5.

Tableau 1.5. Transformation properties of the $\boldsymbol{q} = 0$ coplanar AFM order $\boldsymbol{n}$ shown in Fig. 1.9 under Kagome lattice discrete symmetries and time reversal[20].

	$T_{\boldsymbol{a}_1}$	$T_{\boldsymbol{a}_2}$	R_y	C_6	$\mathcal{T}$
$\boldsymbol{n} \to$	$\boldsymbol{n}$	$\boldsymbol{n}$	$\boldsymbol{n}^*$	$e^{\frac{2\pi i}{3}}\boldsymbol{n}$	$-\boldsymbol{n}^*$

We now show that monopole operators with spin quantum numbers have the same transformation properties as the AFM order parameter shown in Tab. 1.5. This was first argued in Ref. [20]. A comprehensive study of the quantum numbers of monopole operators on the square, triangular honeycomb and Kagome lattices can be found in Ref. [32, 85]. One important contribution of this work was to verify numerically the contribution of the $\mathrm{U}(1)_{\mathrm{top}}$ charge for the space rotation. This amounts to deducing how the topologically charged Dirac sea transforms under the system symmetries. This result can be combined with the transformation properties of the zero modes creation operators to obtain the transformation properties of flux operators. This approach is well explained in Ref. [86]. We apply this procedure to the case of the Kagome lattice.

Here, we restrict the discussion to monopoles with minimal magnetic charge $q = 1/2$. This means there are four zero modes, two of which must be filled. The $q = 1/2$ flux operators take the form

$$\Phi_+^\dagger \sim f_{+;s,v}^\dagger f_{+;s',v'}^\dagger \widetilde{\mathcal{M}}_+^\dagger \,, \tag{1.7.5}$$

where the label + gives the sign of the magnetic charge, $f_{+;s,v}^\dagger$ is a zero mode creation operator and $\widetilde{\mathcal{M}}_+^\dagger$ defines a *bare* 2π-flux creating operator, an operator similar to a monopole operator but with all the zero modes empty (in what follows, we refer to it as the bare monopole operator). The six different zero modes filling can be organized as a triplet of $\mathrm{SU}(2)_{\mathrm{valley}}$ and a triplet of $\mathrm{SU}(2)_{\mathrm{spin}}$, yielding three valley-type and three spin-type flux operators :

$$\Phi_{+;1,2,3}^\dagger = \frac{1}{2} f_{+;s,v}^\dagger \left[(i\sigma_2)_{ss'} \left(i\mu_2\mu_{1,2,3}\right)_{vv'} \right] f_{+;s',v'}^\dagger \widetilde{\mathcal{M}}_+^\dagger \,, \tag{1.7.6}$$

$$\Phi_{+;4,5,6}^\dagger = \frac{i}{2} f_{+;s,v}^\dagger \left[(i\sigma_2\sigma_{1,2,3})_{ss'} \left(i\mu_2\right)_{vv'} \right] f_{+;s',v'}^\dagger \widetilde{\mathcal{M}}_+^\dagger \,, \tag{1.7.7}$$

where the global phases are chosen to reproduce the flux operators introduced in [32]. We focus on spin-type flux operator for which we introduce the following short-hand notation

$$(\Phi^\dagger_{+;4}, \Phi^\dagger_{+;5}, \Phi^\dagger_{+;6}) \equiv \boldsymbol{\Phi}^\dagger_{+;S} \equiv \boldsymbol{F}^\dagger_{+;S} \widetilde{\mathcal{M}}^\dagger_+ \,. \tag{1.7.8}$$

The flux operator with spin down quantum number is

$$\frac{1}{2}\left(\Phi^\dagger_{+,4} - i\Phi^\dagger_{+;5}\right) = i f^\dagger_{+;\downarrow,-\boldsymbol{Q}} f^\dagger_{+;\downarrow,\boldsymbol{Q}} \widetilde{\mathcal{M}}^\dagger_+ \,. \tag{1.7.9}$$

We define monopole operators, similar to Ref. [86], as combinations of flux creation operators and anti-flux destruction operators, e.g. spin-type monopole operators are given by

$$\begin{aligned} \boldsymbol{s}^\dagger &\equiv (s^\dagger_1\,, s^\dagger_2\,, s^\dagger_3) \\ &= \left(\Phi^\dagger_{+;4} + \Phi_{-;4}\,,\ \Phi^\dagger_{+;5} + \Phi_{-;5}\,,\ \Phi^\dagger_{+;6} + \Phi_{-;6}\right) . \end{aligned} \tag{1.7.10}$$

The transformations properties of these operators are obtained as follows. The transformation properties of the zero modes creation operators $\boldsymbol{F}^\dagger_{+;S}$ can be found using Tab. 1.4. As for the bare monopole $\widetilde{\mathcal{M}}^\dagger_+$, its transformations are partially constrained by symmetries and the requirement that flux operators $\Phi^\dagger_+$ and anti-flux operators $\Phi^\dagger_-$ transform between themselves. This does not completely fix $\mathrm{U}(1)_{\mathrm{top}}$ phases which were determined numerically in Refs. [20, 32] and analytically [85]. From these transformations, one can then find how flux operators and monopole operators transform under symmetries. The transformation properties of all the operators mentioned above are shown in Tab. 1.6. The definition of spin-type monopole operators was chosen (1.7.10) such that these operators are odd under time reversal. Note that the C_6 transformation induces an additional phase common to all the monopole operators which can be dropped. By comparing Tab. 1.5 and Tab. 1.6, we see that the spin triplet monopole $\boldsymbol{s}^\dagger$ is the right operator to produce the $\boldsymbol{q} = 0$ AFM order.

1.7.3. Quantum phase transition

The confinement-deconfinement mechanism introduced earlier is thus appropriate to describe the transition from the DSL to the $\boldsymbol{q} = 0$ coplanar AFM on the Kagome lattice. Following the condensation of a spin-Hall mass driven by the cHGN interaction, spin-type monopole operators proliferate [31] and condense the AFM order. In terms of lattice operators, the spin-Hall bilinear $\bar{\Psi}\boldsymbol{\sigma}\Psi$, or equivalently the auxiliary boson $\boldsymbol{\phi}$, corresponds to a vector spin chirality $V^a \sim \sum_{\langle ij\rangle\in\hexagon}\left(\vec{S}_i \times \vec{S}_j\right)^a$ [20], where $\hexagon$ denotes an hexagonal plaquette

Tableau 1.6. Transformation properties under Kagome lattice symmetries and time reversal of a bare monopole $\widetilde{\mathcal{M}}_+^\dagger$, of a spin-type combination of zero modes creation operators $\boldsymbol{F}_{+;S}^\dagger$ and the corresponding flux operators $\boldsymbol{\Phi}_{+;S}^\dagger$ and monopole operators $\boldsymbol{s}^\dagger$.

	$T_{\boldsymbol{a}_1}$	$T_{\boldsymbol{a}_2}$	R_y	C_6	$\mathcal{T}$
$\boldsymbol{F}_{+;S}^\dagger \to$	$\boldsymbol{F}_{+;S}^\dagger$	$\boldsymbol{F}_{+;S}^\dagger$	$-\boldsymbol{F}_{-;S}^\dagger$	$\boldsymbol{F}_{+;S}^\dagger$	$\boldsymbol{F}_{-;S}^\dagger$
$\widetilde{\mathcal{M}}_+^\dagger \to$	$\widetilde{\mathcal{M}}_+^\dagger$	$\widetilde{\mathcal{M}}_+^\dagger$	$\widetilde{\mathcal{M}}_-^\dagger$	$e^{\frac{2\pi i}{3}}\widetilde{\mathcal{M}}_+^\dagger$	$-\widetilde{\mathcal{M}}_-^\dagger$
$\boldsymbol{\Phi}_{+;\boldsymbol{s}}^\dagger \to$	$\boldsymbol{\Phi}_{+;\boldsymbol{s}}^\dagger$	$\boldsymbol{\Phi}_{+;\boldsymbol{s}}^\dagger$	$-\boldsymbol{\Phi}_{-;\boldsymbol{s}}^\dagger$	$e^{\frac{2\pi i}{3}}\boldsymbol{\Phi}_{+;\boldsymbol{s}}^\dagger$	$-\boldsymbol{\Phi}_{-;\boldsymbol{s}}^\dagger$
$\boldsymbol{s}^\dagger \to$	$\boldsymbol{s}^\dagger$	$\boldsymbol{s}^\dagger$	$\boldsymbol{s}$	$e^{\frac{2\pi i}{3}}\boldsymbol{s}^\dagger$	$-\boldsymbol{s}$

on the Kagome lattice. In this language, the transition is driven by the second neighbor antiferromagnetic interaction which condenses the vector spin chirality, which in turn allows the monopole operators to proliferate on the lattice.

We have just seen that lattice quantum numbers are important to identify the spin down monopole operator as the right operator to induce the AFM. They also determine which combinations of monopole operators transform trivially under all the symmetries of the DSL and thus constitute allowed perturbations in this phase. By inspection of Tab. 1.6, the sextupled spin down monopole operator, $\mathcal{O} = (s_1^\dagger - is_2^\dagger)^6 + \text{h. c.}$ is identified as a symmetry-allowed perturbation. This is reminiscent of the role that $n-$tupled monopole operators play for the Neel-VBS transition described by CP^{N_b-1} bosonic theory [21, 52, 87, 88]. The perturbation $\mathcal{O}' = s_1^\dagger s_2 + \text{h. c.}$ also respects the symmetries of the Kagome lattice. Among those symmetric perturbations built from spin down monopole operators $\mathcal{O}_s$, the one with the lowest scaling dimension $\Delta_{\mathcal{O}_s}$ controls the scale ξ_s of the AFM order. The spin-spin connected correlation function is controlled by this length scale ξ_s and the scaling dimension Δ_q of the spin down monopole operator (see Tab. 1.1), scaling as $\langle \boldsymbol{n}(\boldsymbol{r}) \cdot \boldsymbol{n}^\dagger(0)\rangle_c \sim 1/r^{2\Delta_q}$ for $r \ll \xi_s$.

Determining the scaling dimension of these monopole perturbations $\mathcal{O}_s$ for $2N = 4$ is important, as the quantum phase transition works out very differently whether these operators are relevant at the QCP or not [89]. If all allowed monopole perturbations $\mathcal{O}_s$ turn out irrelevant at the QCP — as is the case for all monopole operators in the large$-N$ limit — then these perturbations are dangerously irrelevant, and monopole operators only proliferate

once the spin-Hall mass is condensed. Said otherwise, the QCP is a simple fixed point with one relevant direction being controlled by the boson mass m_ϕ^2. The length scale ξ controlling the spin-Hall mass condensation is then determined by the critical exponent $\nu^{-1} = d - \Delta_{\phi^2}$. The vector spin chirality connected correlation function depends on this length scale ξ and on the scaling dimension Δ_V given by $\min(\Delta_\phi, \Delta_{\bar{\Psi}\sigma_a\Psi})$ (see Tab. 1.3) at leading order in the loop-expansion [19], scaling as $\langle \boldsymbol{V}(\boldsymbol{r}) \cdot \boldsymbol{V}(0)\rangle_c \sim 1/r^{2\Delta_V}$ for $r \ll \xi$. In this case where the monopole perturbation is a dangerously irrelevant operator, the two length scales ξ_s and ξ are interdependent [19]. At intermediate scales $\xi \ll L \ll \xi_s$, the system is described by a spin liquid where the spinons are gapped since a spin-Hall mass is condensed. At longer scale $L \gg \xi_s$, the spinons are confined and the system is well described by the AFM phase.

1.8. Conclusion

We have computed the scaling dimension of monopole operators at the QCP of a confinement-deconfinement transition between a DSL and an AFM phase in the large N expansion where $2N$ is the number of fermion flavors. We find that the lowest scaling dimension of monopole operators at the QCP is always smaller than at the QED_3 point. For the minimal magnetic charge, this scaling dimension is $\Delta_{q=1/2} = (2N)0.19539 + \mathcal{O}(N^0)$. We have considered other possible fermion "zero" modes dressings and found a hierachy in the scaling dimension of different monopole operators. We also computed the lowest scaling dimension and the range of the monopole operators scaling dimensions using a large q limit. In contrast, the case of the transition to a chiral spin liquid, where a $\text{SU}(2N)$ symmetric mass is condensed, was shown to have the same leading order scaling dimension as QED_3. To complement our large N analysis, we also studied the RG flow of QED_3 with a spin-dependent Yukawa coupling. We found the existence of the QCP and computed critical exponents at one-loop using the $d = 4 - \epsilon$ expansion. We characterized the QCP in the case of a Kagome quantum magnet.

We mainly focused on the transition from a DSL to an antiferromagnet and oriented our analysis towards its description. However, the results we obtained for the monopole scaling dimension would be the same with the introduction of a valley-dependent interaction $(\bar{\Psi}\boldsymbol{\mu}\Psi)^2$. We could do a similar development to obtain the scaling dimension of monopole operators. By performing a large N expansion with N the number of spin components, the same scaling dimensions are found. Now, the monopole operator with the lowest scaling

dimension is the monopole in the valley triplet with eigenvalue -1 under μ_z. The results at leading order $1/N$ is also unchanged whether we pick the $\mathrm{SU}(2)_{\mathrm{spin}}$ symmetric interaction $(\bar{\Psi}\boldsymbol{\sigma}\Psi)^2$ or an $\mathrm{SU}(2)_{\mathrm{spin}}$ symmetry breaking interaction like $(\bar{\Psi}\sigma_z\Psi)^2$. A similar adaptation can be made for a mixed spin-valley interaction like $(\bar{\Psi}\mu_z\sigma_z\Psi)^2$. In this case, the scaling dimension is also the same at leading order. It would also be interesting to extend the computation and obtain $\mathcal{O}(N^0)$ corrections using the same methods as in Refs. [40, 41].

Acknowledgements. We thank Yin-Chen He, Joseph Maciejko, Subir Sachdev, Sergueï Tchoumakov and Chong Wang for useful discussions. É.D. was funded by an Alexander Graham Bell CGS from NSERC. M.B.P. was funded by a Discovery Grant from NSERC. W.W.-K. was funded by a Discovery Grant from NSERC, a Canada Research Chair, a grant from the Fondation Courtois, and a "Établissement de nouveaux chercheurs et de nouvelles chercheuses universitaires" grant from FRQNT.

Note added. Shortly after this work was submitted, we became aware of Ref. [90], which partially overlaps with our work.

1.A. Regularization of the integrated logarithm

The divergent integral $\int d\omega \ln(\omega^2 + a^2)$ can be rewritten by using $\ln A = -\mathrm{d}A^{-s}/\mathrm{d}s|_{s=0}$. The resulting expression integrates to an hyper-geometric function

$$\begin{aligned}\int_{-\infty}^{\infty} d\omega \ln\left(\omega^2 + a^2\right) &= -\frac{\mathrm{d}}{\mathrm{d}s}\int d\omega \left(\omega^2 + a^2\right)^{-s}\Big|_{s=0} \\ &= 2\left(-\frac{\mathrm{d}}{\mathrm{d}s}a^{1-2s}\left[\omega \ {}_2F_1\left(\frac{1}{2}, s; \frac{3}{2}; -\omega^2\right)\right]_{\omega=\infty}\Big|_{s=0}\right), \end{aligned} \tag{1.A.1}$$

where it was assumed that $a > 0$, which is the case in the main text where $a = \{M_q, \varepsilon_\ell\}$. The analytic continuation then yields

$$\begin{aligned}\int_{-\infty}^{\infty} d\omega \ln\left(\omega^2 + a^2\right) &= 2\left(-\frac{\mathrm{d}}{\mathrm{d}s}a^{1-2s}\left(\frac{\sqrt{\pi}\Gamma\left(-s-\frac{1}{2}\right)}{2\Gamma(-s)}\right)\Big|_{s=0}\right) \\ &= 2\left(-a\frac{\mathrm{d}}{\mathrm{d}s}\left(-\pi s + O\left(s^2\right)\right)\Big|_{s=0}\right) = 2\pi a\,. \end{aligned} \tag{1.A.2}$$

Alternatively, we can also regularize this integral by introducing a frequency UV cut-off Λ and by keeping only the finite part as it is taken to infinity

$$\int_{-\Lambda}^{\Lambda} d\omega \ln\left(\omega^2 + a^2\right) = 4\Lambda\left(\ln(\Lambda) - 1\right) + 2\pi a + \mathcal{O}\left(\Lambda^{-1}\right) \to 2\pi a\,. \tag{1.A.3}$$

1.B. Saddle point equations for $\mathrm{QED}_3 - \mathrm{cHGN}$ in a thermal setup

In Sec. 1.3, we obtained the lowest scaling dimension Δ_q of monopole operators in $\mathrm{QED}_3 - \mathrm{cHGN}$. We did this by computing the leading order free energy $F_q^{(0)}$ (1.3.8) on $S^2 \times \mathbb{R}$ with appropriate magnetic flux. We saw that in the case of a $\mathrm{SU}(2N)$ symmetric interaction, the computation should be performed on a compactified "time" direction $\mathbb{R} \to S^1_\beta$. Here, we repeat the computation in the former theory now using the "thermal" setup,

$$\begin{aligned} F_q^{(0)} &= -\frac{1}{\beta} \ln \det \left[\not{D}_{-i\mu, A^q} + M_q \sigma_z \right] \\ &= -\frac{1}{\beta} \sum_{\sigma=\pm 1} \sum_{n \in \mathbb{Z}} \left[d_q \ln \left[\omega_n - i\mu + i\sigma M_q \right] + \sum_{\ell=q+1}^{\infty} d_\ell \ln \left[(\omega_n - i\mu)^2 + \varepsilon_\ell^2 \right] \right] , \end{aligned} \tag{1.B.1}$$

where as before ε_ℓ is given by Eq.(1.3.21) and ω_n are the Matsubara frequencies. First taking the sum over the magnetic spin degrees of freedom and then regularizing the sum on Matsubara frequencies, this expression becomes

$$\begin{aligned} F_q^{(0)} &= -\frac{1}{\beta} \sum_{n \in \mathbb{Z}} \left[d_q \ln \left[(\omega_n - i\mu)^2 + M_q^2 \right] + \sum_{\ell=q+1}^{\infty} 2 d_\ell \ln \left[(\omega_n - i\mu)^2 + \varepsilon_\ell^2 \right] \right] \\ &= -\frac{1}{\beta} \left[d_q \ln \left[2 \left(\cosh(\beta M_q) + \cosh(\beta \mu) \right) \right] + \sum_{\ell=q+1}^{\infty} 2 d_\ell \ln \left[2 \left(\cosh(\beta \varepsilon_\ell) + \cosh(\beta \mu) \right) \right] \right] . \end{aligned} \tag{1.B.2}$$

The saddle point equations are

$$0 = \frac{\partial F_q^{(0)}}{\partial \mu} = -d_q \left(\frac{\sinh(\beta \mu)}{\cosh(\beta M_q) + \cosh(\beta \mu)} \right) - \sum_{\ell=q+1}^{\infty} 2 d_\ell \left(\frac{\sinh(\beta \mu)}{\cosh(\beta \varepsilon_\ell) + \cosh(\beta \mu)} \right) , \tag{1.B.3}$$

$$0 = \frac{\partial F_q^{(0)}}{\partial M_q} = -d_q \left(\frac{\sinh(\beta M_q)}{\cosh(\beta M_q) + \cosh(\beta \mu)} \right) - \sum_{\ell=q+1}^{\infty} 2 d_\ell \varepsilon_\ell^{-1} M_q \left(\frac{\sinh(\beta \varepsilon_\ell)}{\cosh(\beta \varepsilon_\ell) + \cosh(\beta \mu)} \right) . \tag{1.B.4}$$

The first saddle point equation is solved with $\mu = 0$. This is the reason why the formalism used in the present section is unnecessary, as it was mentioned in Sec. 1.5. Setting $\mu = 0$ in the second saddle point equation yields

$$0 = \left. \frac{\partial F_q^{(0)}}{\partial M_q} \right|_{\mu=0} = -d_q \left(\frac{\sinh(\beta M_q)}{1 + \cosh(\beta M_q)} \right) - \sum_{\ell=q+1}^{\infty} 2 d_\ell \varepsilon_\ell^{-1} M_q \left(\frac{\sinh(\beta \varepsilon_\ell)}{1 + \cosh(\beta \varepsilon_\ell)} \right) . \tag{1.B.5}$$

We get the interesting result that $M_q = 0$ is a solution of this saddle point equation. This solution was not observed by working directly on $S^2 \times \mathbb{R}$. Assuming $M_q > 0$, the saddle point equation at leading order in $1/\beta$ yields the following condition

$$0 = d_q + \sum_{\ell=q+1}^{\infty} 2 d_\ell \varepsilon_\ell^{-1} M_q \,, \tag{1.B.6}$$

A non trivial solution $M_q \neq 0$ can be found numerically as in the main text. We distinguish the trivial and non-trivial solutions by studying the second derivatives of the free energy at these points. The second derivative in the μ direction designates imaginary fluctuations of the gauge field and as such has no physical signification. We only compute the second derivative in the M_q direction

$$\left.\frac{\partial^2 F_q^{(0)}}{\partial M_q^2}\right|_{\mu=0} = -d_q \left(\frac{\beta}{1+\cosh(\beta M_q)}\right) - \sum_{\ell=q+1}^{\infty} 2 d_\ell \left(\frac{\left(\varepsilon_\ell^2 - M_q^2\right)\sinh\left(\beta\varepsilon_\ell\right) + \beta M_q^2 \varepsilon_\ell}{\varepsilon_\ell^3 \left(1+\cosh\left(\beta\varepsilon_\ell\right)\right)}\right) . \tag{1.B.7}$$

We study the cases $M_q \neq 0$ and $M_q = 0$ separately. We start with the former case. The second derivative at leading order in $1/\beta$ is

$$\left.\frac{\partial^2 F_q^{(0)}}{\partial M_q^2}\right|_{\mu=0, M_q\neq 0} = -2 \sum_{\ell=q+1} \frac{d_\ell \left(\varepsilon_\ell^2 - M_q^2\right)}{\varepsilon_\ell^3} \,. \tag{1.B.8}$$

Using the saddle point condition (1.B.6) obtained for large β, this can be reformulated as

$$\left.\frac{\partial^2 F_q^{(0)}}{\partial M_q^2}\right|_{\mu=0, M_q\neq 0} = d_q \frac{1}{M_q} + 2 \sum_{\ell=q+1}^{\infty} \frac{M_q^2}{\varepsilon_\ell^3} > 0 \,. \tag{1.B.9}$$

The non trivial solution $M_q \neq 0$ thus corresponds to a minimum. The case of a vanishing mass $M_q = 0$ is now studied. In the large β limit, the second derivative of the free energy at leading order in $1/\beta$ is given by

$$\left.\frac{\partial^2 F_q^{(0)}}{\partial M_q^2}\right|_{\mu=0, M_q=0} = -\frac{\beta}{4} < 0 \,. \tag{1.B.10}$$

Thus, when setting $\mu = 0$, $M_q = 0$ is a maximum.

1.C. Feynman diagrams computation

A RG study of the $\mathrm{QED}_3 - \mathrm{cHGNY}$ model was shown in Sec.1.6. In the present section, we compute the one-loop corrections to the wavefunction normalization and coupling constants of this QFT necessary to obtain the RG flow equations shown in the main text.

1.C.1. Feynman rules

We first write down the Feynman rules of the $\mathrm{QED}_3 - \mathrm{cHGNY}$ field theory defined by the lagrangian (1.6.1)

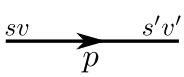

$$= G_{sv;s'v'}(p) \equiv \left\langle \psi_{sv}(p)\bar{\psi}_{s'v'}(p) \right\rangle = \delta_{ss'}\delta_{vv'}\frac{\not{p}}{p^2}\,, \tag{1.C.1}$$

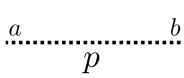

$$= D_{ab}(p) \equiv \langle \phi_a(p)\phi_b(-p)\rangle = \frac{\delta_{ab}}{p^2}\,, \tag{1.C.2}$$

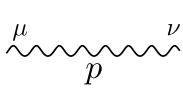

$$= \Pi_{\mu\nu}(p) \equiv \langle a_\mu(p)a_\nu(-p)\rangle = \frac{1}{p^2}\left(\delta_{\mu\nu} + (\xi - 1)\,\frac{p_\mu p_\nu}{p^2}\right)\,, \tag{1.C.3}$$

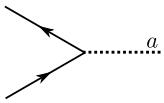

$$= h\sigma_a\,, \tag{1.C.4}$$

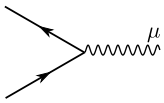

$$= ie\gamma_\mu\,, \tag{1.C.5}$$

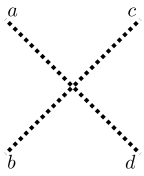

$$= 8\lambda\left(\delta_{ab}\delta_{cd} + \delta_{ac}\delta_{bd} + \delta_{ad}\delta_{bc}\right)\,, \tag{1.C.6}$$

where ξ is the gauge-fixing parameter for the gauge field a_μ. Here, ψ_{sv} is a two-component Dirac spinor with magnetic spin s and valley index v. The mass perturbations can also be treated as interactions with the following Feynman rules

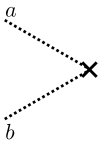

$$= m_\phi^2\delta_{ab}\,, \tag{1.C.7}$$

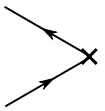

$$= m_\psi\,, \tag{1.C.8}$$

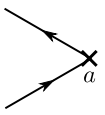

$$= \tilde{m}_\psi\sigma_a\,. \tag{1.C.9}$$

1.C.2. Computation of one-loop Feynman diagrams

We now compute the one-loop Feynman diagrams using the Feynman rules in Sec.1.C.1. First, let us introduce shorthand notation. The diagrams involve a momentum shell loop

integral factor $\tilde{I}$

$$\tilde{I} = \int_{k=\Lambda e^{-l}}^{k=\Lambda} \frac{\mathrm{d}^d k}{(2\pi)^d} \frac{1}{k^4} = \left(\frac{\int \mathrm{d}\Omega_{d-1}}{(2\pi)^d} \Lambda^{d-4} \right) \mathrm{d}l \,. \tag{1.C.10}$$

The momentum space measure is also abbreviated as $(\mathrm{d}\mathbf{k}) \equiv d^d k / (2\pi)^d$. As we write the Feynman diagrams, we identify the corresponding correction to the normalization factors, δZ_{x_i} with $x_i \in \{\psi, \phi, a, e, h, \lambda\}$.

1.C.2.1. Three-point functions. We compute the vertex diagrams shown in Fig. 1.10

(a) (b) (c) (d)

Figure 1.10. One-loop vertex diagrams.

$$[1.10(a)] = h\sigma_a \left(\delta Z_h^{(\phi)} \right) = h^3 \int (\mathrm{d}\mathbf{k})\, \sigma^b G(k) \sigma_a G(k) \sigma^c D_{bc}(k) = h\sigma_a \left(-h^2 \left(N_b - 2 \right) \tilde{I} \right) , \tag{1.C.11}$$

$$[1.10(b)] = h\sigma_a \left(\delta Z_h^{(a)} \right) = h\,(ie)^2 \int (\mathrm{d}\mathbf{k})\, \gamma^\mu G(k) \sigma_a G(k) \gamma^\nu \Pi_{\mu\nu}(k) = h\sigma_a \left(-e^2 \left(d + \xi - 1 \right) \tilde{I} \right) , \tag{1.C.12}$$

$$[1.10(c)] = ie\gamma^\alpha \left(\delta Z_e^{(\phi)} \right) = ie\,(-h)^2 \int (\mathrm{d}\mathbf{k})\, \sigma^b G(k) \gamma^\alpha G(k) \sigma^c D_{bc}(k) = ie\gamma^\alpha \left(-h^2 N_b \left(\frac{d-2}{d} \right) \tilde{I} \right) . \tag{1.C.13}$$

The last diagram involves a longer computation

$$
\begin{aligned}
[1.10(d)] &= ie\gamma^\alpha \left(\delta Z_e^{(a)}\right) \\
&= ie\,(ie)^2 \int (\mathrm{d}\mathbf{k})\, \gamma^\mu G(k)\gamma^\alpha G(k)\gamma^\nu \Pi_{\mu\nu}(k) \\
&= ie\,(ie)^2 \int (\mathrm{d}\mathbf{k})\, \frac{1}{k^4}\gamma^\mu\gamma^\lambda\gamma^\alpha\gamma^\rho\gamma^\nu \left[\frac{1}{d}\delta^{\mu\nu}\delta^{\lambda\rho} + \left(\frac{\xi-1}{d\,(d+2)}\right)\left(\delta^{\mu\nu}\delta^{\lambda\rho} + \delta^{\mu\lambda}\delta^{\nu\rho} + \delta^{\mu\rho}\delta^{\nu\lambda}\right)\right] \\
&= ie\,(ie)^2 \int (\mathrm{d}\mathbf{k})\, \frac{1}{k^4}\left(\frac{(d-2)^2}{d}\gamma^\alpha + \left(\frac{\xi-1}{d\,(d+2)}\right)\big[(d-2)^2\,\gamma^\alpha + d^2\gamma^\alpha \right. \\
&\quad \left. + \gamma^\rho\,(4\delta^{\alpha\rho} - (4-d)\,\gamma^\alpha\gamma^\rho)\big]\right) \\
&= ie\gamma^\alpha \left(-e^2\left(d - 5 + \frac{4}{d} + \xi\right)\tilde{I}\right), \qquad (1.C.14)
\end{aligned}
$$

where we used gamma identities

$$\gamma^\mu\gamma^\alpha\gamma^\beta\gamma^\mu = 4\delta^{\alpha\beta} - (4-d)\,\gamma^\alpha\gamma^\beta\,, \qquad (1.C.15)$$

$$\gamma^\mu\gamma^\nu\gamma^\rho\gamma^\lambda\gamma^\mu = -2\gamma^\lambda\gamma^\rho\gamma^\nu + (4-d)\,\gamma^\nu\gamma^\rho\gamma^\lambda\,, \qquad (1.C.16)$$

and a symmetrization of momentum components appearing in loop integrals,

$$k^\lambda k^\rho \to \frac{k^2}{d}\delta^{\lambda\rho}\,, \qquad (1.C.17)$$

$$k^\alpha k^\beta k^\gamma k^\delta \to \frac{k^4}{d\,(d+2)}\left(\delta^{\alpha\beta}\delta^{\gamma\delta} + \delta^{\alpha\gamma}\delta^{\beta\delta} + \delta^{\alpha\delta}\delta^{\beta\gamma}\right). \qquad (1.C.18)$$

1.C.2.2. Two-point functions. The two-point diagrams are shown in Fig. 1.11. The boson

(a) (b) (c) (d)

Figure 1.11. One-loop two-point diagrams.

contribution to the fermion self-energy is

$$\begin{aligned}\delta Z_{\psi}^{(\phi)} = -\frac{\partial}{\partial \not{p}}[1.11(a)] &= -\left(\gamma^{\mu}\right)^{-1}\frac{\partial}{\partial p^{\mu}}\left((h)^{2}\int(\mathrm{d}\mathbf{k})\,\sigma^{b}G(p-k)\sigma^{c}D_{bc}(k)\right)\\ &= \left(\gamma^{\mu}\right)^{-1}(h)^{2}\int(\mathrm{d}\mathbf{k})\,\sigma^{b}G(p-k)\frac{\partial G^{-1}(p-k)}{\partial p^{\mu}}G(p-k)\sigma^{c}D_{bc}(k)\\ &= \left(\gamma^{\mu}\right)^{-1}(h)^{2}\int(\mathrm{d}\mathbf{k})\,\sigma^{b}G(p-k)\gamma^{\mu}G(p-k)\sigma^{c}D_{bc}(k)\\ &\underset{p\to 0}{=}\delta Z_{e}^{(\phi)}\,. \end{aligned} \tag{1.C.19}$$

Similarly, the gauge field contribution is related to another vertex correction

$$\delta Z_{\psi}^{(A)} = -\frac{\partial}{\partial \not{p}}[1.11(b)] = \delta Z_{e}^{(A)}\,. \tag{1.C.20}$$

These results are the one-loop version of the Ward identity. As for the boson $\boldsymbol{\phi}$ self-energy, it only gets a one-loop contribution by the fermion

$$\begin{aligned}[1.11(c)] = p^{2}\delta_{ab}\left(-\delta Z_{\phi}^{(\psi)}\right) &= -(h)^{2}\int(\mathrm{d}\mathbf{k})\,\mathrm{tr}\,\sigma_{a}G(k)\sigma_{b}G(k+p)\\ &= -(h)^{2}\left(d_{\sigma}d_{\mu}d_{\gamma}\right)\delta_{ab}\int(\mathrm{d}\mathbf{k})\,\frac{k\cdot(k+p)}{k^{2}\left(k+p\right)^{2}}\\ &= -(h)^{2}\left(d_{\sigma}d_{\mu}d_{\gamma}\right)\delta_{ab}\int_{0}^{1}\mathrm{d}x\int(\mathrm{d}\mathbf{k})\,\frac{(k-px)\cdot(k+p\left(1-x\right))}{\left[k^{2}+p^{2}x\left(1-x\right)\right]^{2}}\\ &= p^{2}\delta_{ab}\left(2Nh^{2}\tilde{I}\right)\,, \end{aligned} \tag{1.C.21}$$

where d_{σ}, d_{μ} and d_{γ} are the size of the respective SU(2) representations, respectively $2, N$ and 2, and where we introduced a Feynman parameter x. The gauge field also only gets a

correction from the fermion

$$
\begin{aligned}
[1.11(d)] &= \left(p^2\delta_{\mu\nu} - p_\mu p_\nu/p^2\right)\left(-\delta Z_a^{(\psi)}\right) \\
&= -(ie)^2 \int (\mathrm{d}\mathbf{k})\, \mathrm{tr}\, \gamma^\mu G(k) \gamma^\nu G(k+p) \\
&= e^2 \int \mathrm{d}x \int (\mathrm{d}\mathbf{k})\, \frac{\mathrm{tr}\, \gamma^\mu \left(\not{k} - \not{p}x\right) \gamma^\nu \left[\left(\not{k} + \not{p}\,(1-x)\right)\right]}{\left[k^2 + p^2 x\,(1-x)\right]^2} \\
&= e^2 \int \mathrm{d}x \int (\mathrm{d}\mathbf{k})\, \frac{\mathrm{tr}\, \frac{(2-d)}{d} k^2 \gamma^\mu \gamma^\nu - x\,(1-x)\, p^\alpha p^\beta \gamma^\mu \gamma^\alpha \gamma^\nu \gamma^\beta}{\left[k^2 + p^2 x\,(1-x)\right]^2} \\
&= 4Ne^2 \int \mathrm{d}x \int (\mathrm{d}\mathbf{k})\, \frac{\frac{(2-d)}{d} k^2 \delta_{\mu\nu} - x\,(1-x)\, p^\alpha p^\beta \left(\delta^{\mu\alpha}\delta^{\nu\beta} - \delta^{\mu\nu}\delta^{\alpha\beta} + \delta^{\mu\beta}\delta^{\alpha\nu}\right)}{\left[k^2 + p^2 x\,(1-x)\right]^2} \\
&= 4Ne^2 \int \mathrm{d}x \int (\mathrm{d}\mathbf{k})\, \frac{\delta_{\mu\nu}\left[\frac{(2-d)}{d} k^2 - p^2\right] + 2x\,(1-x)\left(\delta_{\mu\nu} p^2 - p^\mu p^\nu\right)}{\left[k^2 + p^2 x\,(1-x)\right]^2}\,. \qquad (1.\mathrm{C}.22)
\end{aligned}
$$

The polarization tensor should be proportional to the transverse tensor $\delta_{\mu\nu} - p_\mu p_\nu/p^2$. This form cannot be achieved with a cut-off regularization which breaks Lorentz invariance. Terms that don't satisfy this form are removed. Since a $p_\mu p_\nu$ term cannot be generated by expansion of the denominator, the $p_\mu p_\nu$ term in the numerator serves as a reference to single out the polarization tensor

$$
\begin{aligned}
[1.11(d)] = \left(p^2\delta_{\mu\nu} - p_\mu p_\nu/p^2\right)\left(-\delta Z_a^{(\psi)}\right) &= \left(p^2\delta_{\mu\nu} - p_\mu p_\nu/p^2\right)\left(4Ne^2\left(\int \mathrm{d}x\; 2x\,(1-x)\right)\tilde{I}\right) \\
&= \left(p^2\delta_{\mu\nu} - p_\mu p_\nu/p^2\right)\left(\frac{4N}{3} e^2 \tilde{I}\right)\,. \qquad (1.\mathrm{C}.23)
\end{aligned}
$$

1.C.2.3. Four-point function. The four-point diagrams are shown in Fig. 1.12.

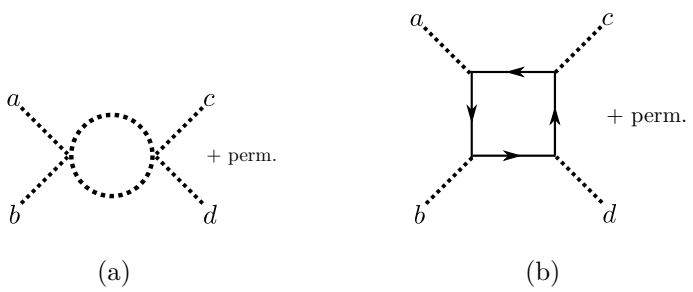

Figure 1.12. One-loop four-point diagrams.

The boson autointeraction's correction has a contribution from the boson

$$\begin{aligned}[1.12(a)] &= 8\lambda\left(\delta_{ab}\delta_{cd}+\delta_{ac}\delta_{bd}+\delta_{ad}\delta_{bc}\right)\left(\delta Z_{\lambda}^{\phi}\right)\\ &= \frac{1}{2}\left[8\lambda\left(\delta_{ab}\delta_{ef}+\delta_{ae}\delta_{bf}+\delta_{af}\delta_{be}\right)\right]\left[8\lambda\left(\delta_{cd}\delta_{ef}+\delta_{ce}\delta_{df}+\delta_{cf}\delta_{de}\right)\right]\tilde{I}+\text{perm.}\\ &= 8\lambda\left(\delta_{ab}\delta_{cd}+\delta_{ac}\delta_{bd}+\delta_{ad}\delta_{bc}\right)\left(4\left(N_b+8\right)\lambda\tilde{I}\right)\,, \end{aligned} \tag{1.C.24}$$

where the factor 1/2 is a symmetry factor. The fermion also contributes to the correction

$$\begin{aligned}[1.12(b)] &= 8\lambda\left(\delta_{ab}\delta_{cd}+\delta_{ac}\delta_{bd}+\delta_{ad}\delta_{bc}\right)\left(\delta Z_{\lambda}^{\psi}\right)\\ &= -h^4\left(\operatorname{tr}\sigma_a\sigma_b\sigma_c\sigma_d+\operatorname{tr}\sigma_d\sigma_c\sigma_b\sigma_a\right)\tilde{I}\\ &= 8\lambda\left(\delta_{ab}\delta_{cd}+\delta_{ac}\delta_{bd}+\delta_{ad}\delta_{bc}\right)\left(-h^4\lambda^{-1}N\tilde{I}\right)\,. \end{aligned} \tag{1.C.25}$$

1.C.2.4. Mass perturbations. Diagrams corresponding to mass perturbation are shown in Fig. 1.13. Some of the one-loop diagrams for the bilinear perturbations can be related to

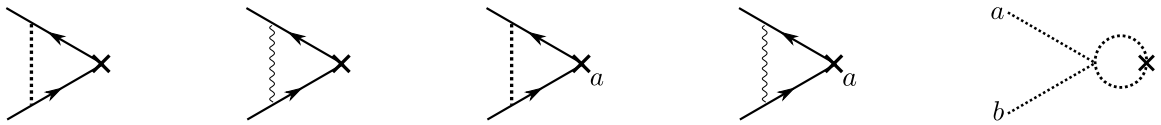

(a) (b) (c) (d) (e)

Figure 1.13. One-loop diagrams corresponding to mass perturbations.

previously computed diagrams

$$[1.13(a)] = m_\psi\left(\delta Z_{m_\psi}^{(\phi)}\right) \quad = m_\psi N_b\frac{1}{\left(\left(2-N_b\right)h\operatorname{tr}\mathbb{1}\right)}\operatorname{tr}\sigma_a[1.10(a)]_a = m_\psi\left(N_b h^2\tilde{I}\right)\,, \tag{1.C.26}$$

$$[1.13(b)] = m_\psi\left(\delta Z_{m_\psi}^{(a)}\right) \quad = m_\psi\frac{1}{\left(h\operatorname{tr}\mathbb{1}\right)}\operatorname{tr}\sigma_a[1.10(b)]_a = m_\psi\left(-\left(d+\xi-1\right)e^2\tilde{I}\right)\,, \tag{1.C.27}$$

$$[1.13(c)] = \tilde{m}_\psi\sigma_a\left(\delta Z_{\tilde{m}_\psi}^{(\phi)}\right) = \tilde{m}_\psi h^{-1}[1.10(a)]_a = \tilde{m}_\psi\sigma_a\left(-\left(N_b-2\right)h^2\tilde{I}\right)\,, \tag{1.C.28}$$

$$[1.13(d)] = \tilde{m}_\psi\sigma_a\left(\delta Z_{\tilde{m}_\psi}^{(a)}\right) = \tilde{m}_\psi h^{-1}[1.10(b)]_a = \tilde{m}_\psi\sigma_a\left(-\left(d+\xi-1\right)e^2\tilde{I}\right)\,. \tag{1.C.29}$$

Only the $\boldsymbol{\phi}$ field mass correction requires a new computation

$$\begin{aligned}[1.13(e)] = m_\phi^2\delta_{ab}\left(\delta Z_{m_\phi^2}^{(\phi)}\right) &= \frac{1}{2}8\lambda\left(\delta_{ab}\delta_{cd}+\delta_{ac}\delta_{bd}+\delta_{ad}\delta_{bc}\right)\left(m_\phi^2\delta_{cd}\right)\int\left(\mathrm{d}\mathbf{k}\right)\frac{1}{k^4}\\ &= m_\phi^2\delta_{ab}\left(4\left(N_b+2\right)\lambda\right)\tilde{I}\,. \end{aligned} \tag{1.C.30}$$

1.C.3. Results

The renormalization constants are obtained by summing the corrections found above, $Z_{x_i} = 1 + \sum_{\Phi=\phi,\psi,a} \delta Z_{x_i}^{(\Phi)}$ where $x_i \in \{\psi, \phi, a, e, h, \lambda\}$. In turn, this allows us to obtain the coefficients $\gamma_{x_i} = -\mathrm{d}\ln Z_{x_i}/\mathrm{d}l \approx -\mathrm{d}Z_{x_i}/\mathrm{d}l$ defined in the main text in Eq. (1.6.9) which are given by

$$\gamma_\phi = 2Nh^2\,, \tag{1.C.31}$$

$$\gamma_\psi = \left(d - 5 + \frac{4}{d} + \xi\right) e^2 + N_b \left(\frac{d-2}{d}\right) h^2\,, \tag{1.C.32}$$

$$\gamma_a = \frac{4N}{3} e^2\,, \tag{1.C.33}$$

$$\gamma_e = \gamma_\psi\,, \tag{1.C.34}$$

$$\gamma_h = (d + \xi - 1)\, e^2 + (N_b - 2)\, h^2\,, \tag{1.C.35}$$

$$\gamma_\lambda = -4\,(N_b + 8)\,\lambda + N h^4 \lambda^{-1}\,, \tag{1.C.36}$$

$$\gamma_{m_\phi^2} = -4(N_b + 2)\lambda\ , \tag{1.C.37}$$

$$\gamma_{m_\psi} = (d + \xi - 1)e^2 - N_b h^2\,, \tag{1.C.38}$$

$$\gamma_{\tilde{m}_\psi} = (d + \xi - 1)e^2 + (N_b - 2)\, h^2\,, \tag{1.C.39}$$

where we have eliminated the loop integral factor by rescaling the coupling constants

$$(e^2, h^2, \lambda) \to \left(\frac{\int \mathrm{d}\Omega_{d-1}}{(2\pi)^d} \Lambda^{d-4}\right)^{-1} (e^2, h^2, \lambda)\,. \tag{1.C.40}$$

Bibliographie

[1] W. X. Gang, *Quantum field theory of many-body systems : from the origin of sound to an origin of light and electrons* (Oxford University Press, Oxford, 2007).

[2] L. Balents, Nature **464**, 199 EP (2010), URL `https://doi.org/10.1038/nature08917`.

[3] Y. Zhou, K. Kanoda, and T.-K. Ng, Rev. Mod. Phys. **89**, 025003 (2017), URL `https://link.aps.org/doi/10.1103/RevModPhys.89.025003`.

[4] W. Witczak-Krempa, G. Chen, Y. B. Kim, and L. Balents, Annual Review of Condensed Matter Physics **5**, 57 (2014), `https://doi.org/10.`

1146/annurev-conmatphys-020911-125138, URL https://doi.org/10.1146/annurev-conmatphys-020911-125138.

[5] M. R. Norman, Rev. Mod. Phys. **88**, 041002 (2016), URL https://link.aps.org/doi/10.1103/RevModPhys.88.041002.

[6] L. Savary and L. Balents, Reports on Progress in Physics **80**, 016502 (2016), URL https://doi.org/10.1088%2F0034-4885%2F80%2F1%2F016502.

[7] H. Takagi, T. Takayama, G. Jackeli, G. Khaliullin, and S. E. Nagler (2019), arXiv:1903.08081.

[8] A. M. Polyakov, Nuclear Physics B **120**, 429 (1977), ISSN 0550-3213, URL http://www.sciencedirect.com/science/article/pii/0550321377900864.

[9] M. Paranjape, *The Theory and Applications of Instanton Calculations*, Cambridge Monographs on Mathematical Physics (Cambridge University Press, 2017).

[10] V. Borokhov, A. Kapustin, and X. Wu, Journal of High Energy Physics **2002**, 049 (2002), URL https://doi.org/10.1088/1126-6708/2002/11/049.

[11] R. Kaneko, S. Morita, and M. Imada, Journal of the Physical Society of Japan **83**, 093707 (2014), https://doi.org/10.7566/JPSJ.83.093707, URL https://doi.org/10.7566/JPSJ.83.093707.

[12] Y. Iqbal, W.-J. Hu, R. Thomale, D. Poilblanc, and F. Becca, Phys. Rev. B **93**, 144411 (2016), URL https://link.aps.org/doi/10.1103/PhysRevB.93.144411.

[13] Y. Ran, M. Hermele, P. A. Lee, and X.-G. Wen, Phys. Rev. Lett. **98**, 117205 (2007), URL https://link.aps.org/doi/10.1103/PhysRevLett.98.117205.

[14] Y. Iqbal, F. Becca, and D. Poilblanc, Phys. Rev. B **84**, 020407 (2011), URL https://link.aps.org/doi/10.1103/PhysRevB.84.020407.

[15] Y. Iqbal, F. Becca, S. Sorella, and D. Poilblanc, Phys. Rev. B **87**, 060405 (2013), URL https://link.aps.org/doi/10.1103/PhysRevB.87.060405.

[16] Y. Iqbal, D. Poilblanc, and F. Becca, Phys. Rev. B **91**, 020402 (2015), URL https://link.aps.org/doi/10.1103/PhysRevB.91.020402.

[17] Y.-C. He, M. P. Zaletel, M. Oshikawa, and F. Pollmann, Phys. Rev. X **7**, 031020 (2017), URL https://link.aps.org/doi/10.1103/PhysRevX.7.031020.

[18] H. J. Liao, Z. Y. Xie, J. Chen, Z. Y. Liu, H. D. Xie, R. Z. Huang, B. Normand, and T. Xiang, Phys. Rev. Lett. **118**, 137202 (2017), URL https://link.aps.org/doi/10.

1103/PhysRevLett.118.137202.

[19] P. Ghaemi and T. Senthil, Phys. Rev. B **73**, 054415 (2006), URL https://link.aps.org/doi/10.1103/PhysRevB.73.054415.

[20] M. Hermele, Y. Ran, P. A. Lee, and X.-G. Wen, Phys. Rev. B **77**, 224413 (2008), URL https://link.aps.org/doi/10.1103/PhysRevB.77.224413.

[21] T. Senthil, L. Balents, S. Sachdev, A. Vishwanath, and M. P. A. Fisher, Phys. Rev. B **70**, 144407 (2004), URL https://link.aps.org/doi/10.1103/PhysRevB.70.144407.

[22] C. Wang, A. Nahum, M. A. Metlitski, C. Xu, and T. Senthil, Phys. Rev. X **7**, 031051 (2017), URL https://link.aps.org/doi/10.1103/PhysRevX.7.031051.

[23] M. S. Block, R. G. Melko, and R. K. Kaul, Phys. Rev. Lett. **111**, 137202 (2013), URL https://link.aps.org/doi/10.1103/PhysRevLett.111.137202.

[24] G. J. Sreejith and S. Powell, Phys. Rev. B **92**, 184413 (2015), URL https://link.aps.org/doi/10.1103/PhysRevB.92.184413.

[25] S. Pujari, F. Alet, and K. Damle, Phys. Rev. B **91**, 104411 (2015), URL https://link.aps.org/doi/10.1103/PhysRevB.91.104411.

[26] M. E. Peskin, Annals of Physics **113**, 122 (1978), ISSN 0003-4916, URL http://www.sciencedirect.com/science/article/pii/000349167890252X.

[27] C. Dasgupta and B. I. Halperin, Phys. Rev. Lett. **47**, 1556 (1981), URL https://link.aps.org/doi/10.1103/PhysRevLett.47.1556.

[28] D. T. Son, Phys. Rev. X **5**, 031027 (2015), URL https://link.aps.org/doi/10.1103/PhysRevX.5.031027.

[29] N. Seiberg, T. Senthil, C. Wang, and E. Witten, Annals of Physics **374**, 395 (2016), ISSN 0003-4916, URL http://www.sciencedirect.com/science/article/pii/S0003491616301531.

[30] A. Karch and D. Tong, Phys. Rev. X **6**, 031043 (2016), URL https://link.aps.org/doi/10.1103/PhysRevX.6.031043.

[31] Y.-M. Lu, G. Y. Cho, and A. Vishwanath, Phys. Rev. B **96**, 205150 (2017), URL https://link.aps.org/doi/10.1103/PhysRevB.96.205150.

[32] X.-Y. Song, C. Wang, A. Vishwanath, and Y.-C. He, Nature Communications **10**, 4254 (2019), ISSN 2041-1723, URL https://doi.org/10.1038/s41467-019-11727-3.

[33] M. F. Atiyah and I. M. Singer, Bulletin of the American Mathematical Society **69**, 422 (1963), URL https://doi.org/.

[34] A. M. Polyakov, Physics Letters B **59**, 82 (1975), ISSN 0370-2693, URL http://www.sciencedirect.com/science/article/pii/0370269375901628.

[35] M. Hermele, T. Senthil, M. P. A. Fisher, P. A. Lee, N. Nagaosa, and X.-G. Wen, Phys. Rev. B **70**, 214437 (2004), URL https://link.aps.org/doi/10.1103/PhysRevB.70.214437.

[36] X. Y. Xu, Y. Qi, L. Zhang, F. F. Assaad, C. Xu, and Z. Y. Meng (2018), arXiv:1807.07574.

[37] S. Rychkov, *EPFL Lectures on Conformal Field Theory in $D \geq 3$ Dimensions*, SpringerBriefs in Physics (Springer International Publishing, Cham, 2017), ISBN 978-3-319-43625-8, URL //www.springer.com/gp/book/9783319436258.

[38] E. Dyer, M. Mezei, and S. S. Pufu, *Monopole taxonomy in three-dimensional conformal field theories* (2013), arXiv:1309.1160.

[39] M. A. Metlitski, M. Hermele, T. Senthil, and M. P. A. Fisher, Phys. Rev. B **78**, 214418 (2008), URL https://link.aps.org/doi/10.1103/PhysRevB.78.214418.

[40] S. S. Pufu, Phys. Rev. D **89**, 065016 (2014), URL https://link.aps.org/doi/10.1103/PhysRevD.89.065016.

[41] E. Dyer, M. Mezei, S. S. Pufu, and S. Sachdev, Journal of High Energy Physics **2015** (2015), ISSN 1029-8479, URL http://link.springer.com/10.1007/JHEP06(2015)037.

[42] S. S. Pufu and S. Sachdev, Journal of High Energy Physics **2013** (2013), ISSN 1029-8479, URL http://link.springer.com/10.1007/JHEP09(2013)127.

[43] V. Borokhov, A. Kapustin, and X. Wu, Journal of High Energy Physics **2002**, 044 (2002), URL https://doi.org/10.1088/1126-6708/2002/12/044.

[44] Đ. Rađivcević, Journal of High Energy Physics **2016**, 131 (2016), ISSN 1029-8479, URL https://doi.org/10.1007/JHEP03(2016)131.

[45] S. M. Chester, L. V. Iliesiu, M. Mezei, and S. S. Pufu, Journal of High Energy Physics **2018** (2018), ISSN 1029-8479, URL http://link.springer.com/10.1007/JHEP05(2018)157.

[46] A. Briggs, H. E. Camblong, and C. R. Ordóñez, International Journal of Modern Physics A **28**, 1350047 (2013), https://doi.org/10.1142/S0217751X13500474, URL https://doi.org/10.1142/S0217751X13500474.

[47] T. T. Wu and C. N. Yang, Nuclear Physics B **107**, 365 (1976), ISSN 0550-3213, URL https://www.sciencedirect.com/science/article/pii/0550321376901437.

[48] *Nist digital library of mathematical functions*, http ://dlmf.nist.gov/, Release 1.0.21 of 2018-12-15, URL http://dlmf.nist.gov/.

[49] S. Hellerman, D. Orlando, S. Reffert, and M. Watanabe, Journal of High Energy Physics **2015**, 1 (2015), ISSN 1029-8479, arXiv:1505.01537, URL https://doi.org/10.1007/JHEP12(2015)071.

[50] A. de la Fuente, Journal of High Energy Physics **2018**, 41 (2018), ISSN 1029-8479, URL https://doi.org/10.1007/JHEP08(2018)041.

[51] R. Boyack, C.-H. Lin, N. Zerf, A. Rayyan, and J. Maciejko, Phys. Rev. B **98**, 035137 (2018), URL https://link.aps.org/doi/10.1103/PhysRevB.98.035137.

[52] M. A. Metlitski and R. Thorngren, Phys. Rev. B **98**, 085140 (2018), URL https://link.aps.org/doi/10.1103/PhysRevB.98.085140.

[53] E. Dyer, M. Mezei, S. S. Pufu, and S. Sachdev, Journal of High Energy Physics **2016**, 111 (2016), ISSN 1029-8479, URL https://doi.org/10.1007/JHEP03(2016)111.

[54] L. Bartosch, Phys. Rev. B **88**, 195140 (2013), URL https://link.aps.org/doi/10.1103/PhysRevB.88.195140.

[55] A. W. Sandvik, Phys. Rev. Lett. **98**, 227202 (2007), URL https://link.aps.org/doi/10.1103/PhysRevLett.98.227202.

[56] R. G. Melko and R. K. Kaul, Phys. Rev. Lett. **100**, 017203 (2008), URL https://link.aps.org/doi/10.1103/PhysRevLett.100.017203.

[57] R. K. Kaul and A. W. Sandvik, Phys. Rev. Lett. **108**, 137201 (2012), URL https://link.aps.org/doi/10.1103/PhysRevLett.108.137201.

[58] S. Pujari, K. Damle, and F. Alet, Phys. Rev. Lett. **111**, 087203 (2013), URL https://link.aps.org/doi/10.1103/PhysRevLett.111.087203.

[59] A. Nahum, J. T. Chalker, P. Serna, M. Ortuño, and A. M. Somoza, Phys. Rev. X **5**, 041048 (2015), URL https://link.aps.org/doi/10.1103/PhysRevX.5.041048.

[60] R. Boyack, A. Rayyan, and J. Maciejko, Phys. Rev. B **99**, 195135 (2019), URL https://link.aps.org/doi/10.1103/PhysRevB.99.195135.

[61] N. Zerf, L. N. Mihaila, P. Marquard, I. F. Herbut, and M. M. Scherer, Phys. Rev. D **96**, 096010 (2017), URL https://link.aps.org/doi/10.1103/PhysRevD.96.096010.

[62] J. A. Gracey, Phys. Rev. D **97**, 105009 (2018), URL https://link.aps.org/doi/10.1103/PhysRevD.97.105009.

[63] L. Janssen and Y.-C. He, Phys. Rev. B **96**, 205113 (2017), URL https://link.aps.org/doi/10.1103/PhysRevB.96.205113.

[64] B. Ihrig, L. Janssen, L. N. Mihaila, and M. M. Scherer, Phys. Rev. B **98**, 115163 (2018), URL https://link.aps.org/doi/10.1103/PhysRevB.98.115163.

[65] N. Zerf, P. Marquard, R. Boyack, and J. Maciejko, Phys. Rev. B **98**, 165125 (2018), URL https://link.aps.org/doi/10.1103/PhysRevB.98.165125.

[66] J. A. Gracey, Phys. Rev. D **98**, 085012 (2018), URL https://link.aps.org/doi/10.1103/PhysRevD.98.085012.

[67] S. Benvenuti and H. Khachatryan, Journal of High Energy Physics **2019**, 214 (2019), ISSN 1029-8479, URL https://doi.org/10.1007/JHEP05(2019)214.

[68] M. M. Scherer and I. F. Herbut, Phys. Rev. B **94**, 205136 (2016), URL https://link.aps.org/doi/10.1103/PhysRevB.94.205136.

[69] J. A. Gracey, International Journal of Modern Physics A **33**, 1830032 (2018).

[70] S. Sachdev, *Quantum Phase Transitions* (Cambridge University Press, UK, 2011), ISBN 9781139500210.

[71] L. Iliesiu, F. Kos, D. Poland, S. S. Pufu, D. Simmons-Duffin, and R. Yacoby, Journal of High Energy Physics **2016**, 120 (2016), ISSN 1029-8479, URL https://doi.org/10.1007/JHEP03(2016)120.

[72] G. Tarnopolsky, L. Fei, S. Giombi, and I. R. Klebanov, Progress of Theoretical and Experimental Physics **2016** (2016), ISSN 2050-3911, URL https://dx.doi.org/10.1093/ptep/ptw120.

[73] M. P. Shores, E. A. Nytko, B. M. Bartlett, and D. G. Nocera, Journal of the American Chemical Society **127**, 13462 (2005), ISSN 0002-7863, URL https://doi.org/10.1021/ja053891p.

[74] P. Sindzingre and C. Lhuillier, EPL (Europhysics Letters) **88**, 27009 (2009), URL https://doi.org/10.1209/0295-5075/88/27009.

[75] W. Zhu, X. Chen, Y.-C. He, and W. Witczak-Krempa, Science Advances **4** (2018), URL https://advances.sciencemag.org/content/4/11/eaat5535.

[76] H. C. Jiang, Z. Y. Weng, and D. N. Sheng, Phys. Rev. Lett. **101**, 117203 (2008), URL https://link.aps.org/doi/10.1103/PhysRevLett.101.117203.

[77] O. Götze, D. J. J. Farnell, R. F. Bishop, P. H. Y. Li, and J. Richter, Phys. Rev. B **84**, 224428 (2011), URL https://link.aps.org/doi/10.1103/PhysRevB.84.224428.

[78] S. Yan, D. A. Huse, and S. R. White, Science **332**, 1173 (2011), ISSN 0036-8075, https://science.sciencemag.org/content/332/6034/1173.full.pdf, URL https://science.sciencemag.org/content/332/6034/1173.

[79] H.-C. Jiang, Z. Wang, and L. Balents, Nature Physics **8**, 902 EP (2012), URL https://doi.org/10.1038/nphys2465.

[80] S. Depenbrock, I. P. McCulloch, and U. Schollwöck, Phys. Rev. Lett. **109**, 067201 (2012), URL https://link.aps.org/doi/10.1103/PhysRevLett.109.067201.

[81] J.-W. Mei, J.-Y. Chen, H. He, and X.-G. Wen, Phys. Rev. B **95**, 235107 (2017), URL https://link.aps.org/doi/10.1103/PhysRevB.95.235107.

[82] M. B. Hastings, Phys. Rev. B **63**, 014413 (2000), URL https://link.aps.org/doi/10.1103/PhysRevB.63.014413.

[83] S.-S. Gong, W. Zhu, L. Balents, and D. N. Sheng, Phys. Rev. B **91**, 075112 (2015), URL https://link.aps.org/doi/10.1103/PhysRevB.91.075112.

[84] F. Kolley, S. Depenbrock, I. P. McCulloch, U. Schollwöck, and V. Alba, Phys. Rev. B **91**, 104418 (2015), URL https://link.aps.org/doi/10.1103/PhysRevB.91.104418.

[85] X.-Y. Song, Y.-C. He, A. Vishwanath, and C. Wang, Physical Review X **10** (2020), ISSN 2160-3308, URL http://dx.doi.org/10.1103/PhysRevX.10.011033.

[86] J. Alicea, Phys. Rev. B **78**, 035126 (2008), URL https://link.aps.org/doi/10.1103/PhysRevB.78.035126.

[87] N. Read and S. Sachdev, Phys. Rev. B **42**, 4568 (1990), URL https://link.aps.org/doi/10.1103/PhysRevB.42.4568.

[88] J. Lee and S. Sachdev, Phys. Rev. Lett. **114**, 226801 (2015), URL https://link.aps.org/doi/10.1103/PhysRevLett.114.226801.

[89] J. Y. Lee, Y.-Z. You, S. Sachdev, and A. Vishwanath, Phys. Rev. X **9**, 041037 (2019), URL https://link.aps.org/doi/10.1103/PhysRevX.9.041037.

[90] N. Zerf, R. Boyack, P. Marquard, J. A. Gracey, and J. Maciejko, Phys. Rev. B **100**, 235130 (2019), URL https://link.aps.org/doi/10.1103/PhysRevB.100.235130.

Chapitre 2

Monopole hierarchy in transitions out of a Dirac spin liquid

É. Dupuis et W. Witczak-Krempa, Annals of Physics, p. 168496, Mai 2021.

Abstract. Quantum spin liquids host novel emergent excitations, such as monopoles of an emergent gauge field. Here, we study the hierarchy of monopole operators that emerges at quantum critical points (QCPs) between a two-dimensional Dirac spin liquid and various ordered phases. This is described by a confinement transition of quantum electrodynamics in two spatial dimensions (QED_3 Gross-Neveu theories). Focusing on a spin ordering transition, we get the scaling dimension of monopoles at leading order in a large-N expansion, where $2N$ is the number of Dirac fermions, as a function of the monopole's total magnetic spin. Monopoles with a maximal spin have the smallest scaling dimension while monopoles with a vanishing magnetic spin have the largest one, the same as in pure QED_3. The organization of monopoles in multiplets of the QCP's symmetry group $SU(2) \times SU(N)$ is shown for general N.

2.1. Introduction

Anderson first proposed the idea of a quantum spin liquid, an insulator state emerging in frustrated quantum magnets [1]. To formulate this, he used the idea of a resonating valence bond theory which describes a highly entangled state. It was later realized that these kinds of systems can indeed host exotic phases of matter with fractional excitations and emergent

gauge fields that evade Landau paradigms. These states motivated the study of gauge theories in a condensed matter context. An important example is the Dirac spin liquid (DSL) which is described by quantum electrodynamics in $2+1$ dimensions (QED_3) with $2N$ flavors of gapless Dirac fermions, with typically $2N = 4$ Dirac cones in quantum magnets.

The formulation of the QED_3 model is rather simple, i.e. an abelian gauge field coupled to fermionic matter. Nevertheless, it is a strongly coupled theory with a non-trivial IR limit. The model flows to an interacting fixed point for N large enough while its exhibits a chiral symmetry breaking below some finite number of fermion flavors [2–5]. Many recent investigations still explore this dynamical mass generation as well as other aspects of QED_3 [6–13]. When the UV divergences of QED_3 are regularized by a lattice, as it is naturally the case in condensed matter systems, one also has to account for the compact nature of the U(1) gauge field. [1] This aspect implies the existence of topological disorder operators called monopole or instanton operators [14].

While monopoles confine the gauge field in a pure gauge theory [15], a sufficient number of massless matter flavors screening the monopoles prevents their proliferation. The scaling dimensions of monopoles operators determine whether or not monopoles are relevant and destabilize the QED_3 phase. Computations at leading order [14] and subleading order [16] in $1/N$ using the state-operator correspondence indicate a stable theory for $2N \geq 12$. This result was recently confirmed with Monte Carlo in the non-compact QED_3 where monopoles are probed using the background field method [17]. Conformal bootstrap bounds relating simply and doubly charged monopoles also yield coherent results [18, 19]. To characterize the stability of a DSL, it should also be known which monopole charges are allowed by lattice symmetries. The first results in this regard were obtained on the square and Kagome lattices [20, 21] and were followed by a comprehensive analysis of the monopole transformation properties under many lattice symmetries [22, 23].

Monopole operators have been studied in many other contexts with and without supersymmetry, including non-abelian gauge theories and Chern-Simons Matter theories [19, 24–28]. In fact, monopole operators were first studied in a bosonic theory, the CP^1 model. This is the prototype model for deconfined criticality [29–32], i.e. QCPs with emergent enlarged symmetry and fractionalized excitations separating classical Landau phases. The monopoles

[1] Throughout the text, the theories we describe are assumed to be compact unless stated otherwise.

in this model describe a valence bond solid (VBS) order. Their scaling dimension have been obtained at leading order [33, 34] and subleading order [35, 36] in $1/N_b$, at order $\mathcal{O}(q^0 N_b^0)$ in the $1/q$ and $1/N_b$ expansion [37], and with numerical methods on various lattices [38–40]. Another interesting aspect of this model is its conjectured duality with the QED_3-Gross-Neveu model (QED_3-GN) with $N = 2$ fermion flavors [41]. The non-compact realization of this latter model has been studied in Refs. [42–47]. In the compact version of QED_3-GN, the scaling dimension of monopole operators at leading order in $1/N$ were found to be the same as in QED_3 [48, 49].

The QED_3-GN model also underlies an important aspect of the DSL, which is that this phase has been described as the parent state for many spin liquids [22, 23, 50]. Indeed, the QED_3-GN model describes the QPT from the DSL to a chiral spin liquid which is induced by tuning a flavor symmetry preserving a Gross-Neveu interaction in QED_3 [51]. By tuning other Gross-Neveu like interactions in QED_3, it is also possible to describe transitions to confined phases. As a flavor-dependent fermion self-interaction is tuned, fermions become gapped and their screening effect is lost, letting monopoles proliferate [52, 53].[2] This leads to an interesting scenario in the Kagome Heisenberg antiferromagnet whose ground state is putatively described by the DSL with $N = 2$ valleys [54]. The confinement of this QSL to a coplanar antiferromagnet is described by QED_3 with a chiral Heisenberg Gross-Neveu interaction (QED_3-cHGN). In this model, a spin-Hall mass is condensed which in turn drives the condensation of monopoles with spin quantum numbers yielding the antiferromagnetic order [21, 53].

Monopole scaling dimensions in QED_3-cHGN were obtained at leading order in $1/N$ in Ref. [48]. The minimal monopole scaling dimension obtained is lower than in QED_3. A hierarchy among monopole operators with different quantum numbers was also found, but a proper complete treatment is still lacking. The objective of this paper is to put the hierarchy on a formal footing both qualitatively and quantitatively. An improved characterization of monopole scaling dimensions in QED_3-cHGN will yield further analytical results which offer more testing ground for experimental and numerical explorations of this system. Similarly, a

[2] This scheme does not apply to QED_3-GN where the symmetric fermion mass generates a Chern-Simons term which prevents monopole proliferation.

hierarchy of monopole operators was described in Chern-Simons Matter theories for monopoles with varying Lorentz spins.[3] At leading order in $1/N$, these operators share the same scaling dimension, but the degeneracy is lifted by higher order corrections. This effect was also seen in the conformal bootstrap [19]. The hierarchy considered in this work is instead among monopoles with different flavor quantum numbers. The degeneracy lifting is natural as the QED_3 flavor symmetry is partially broken at the QCP, i.e. in the QED_3-cHGN model.

The paper is organized as follows. In the following section, we define the QED_3-cHGN theory, and review the role of monopole operators and how different monopole types are distinguished by the fermionic self-interaction in this model. In Sec. 2.3, we obtain the scaling dimensions of monopoles as a function of their total magnetic spin to put the monopole hierarchy on a formal footing. In Sec. 2.4, the scaling dimensions of monopoles are computed with an analytical approximation valid for large values of the topological charge. We interpret these results in Sec. 2.5 as a degeneracy lifting of monopoles in QED_3 as we organize monopoles in multiplets of the reduced flavor symmetry group describing QED_3-cHGN. In Sec. 2.6, we summarize our results. In App. 2.A and App. 2.B, more general forms of the gap equations appearing in Sec. 2.3 are studied to justify the restricted analysis presented in the main text. In App. 2.C, it is shown why a particular region of parameters spaces does not yield solutions of the gap equations. In App. 2.D, the diverging sums appearing in Sec. 2.3 are regularized. In App. 2.E, the representation of monopoles with minimal topological charge for the $N = 2$ QCP is explicitly constructed. In App. 2.F, we show the detailed computations yielding the symmetry reduction shown in Sec. 2.5. We also discuss how the analysis in this section may be extended to $q > 1/2$.

2.2. Model

Let us consider $2N$ flavors of massless two-component Dirac fermions, ψ_A where $A = 1,2,\ldots,2N$. In a condensed matter language, these degrees of freedom correspond to the magnetic spin $\uparrow,\downarrow$ and N nodes in momentum space, typically $N = 2$ in quantum magnets. These fermions correspond to the spinons, the spin-1/2 quasiparticles emerging from the

[3] Monopole operators are not necessarily Lorentz scalars in Ref. [19] as opposed to the stricter definition provided in Ref. [14].

fractionalization of a spin-1 excitations in a quantum magnet. As crucially noted by Baskaran and Anderson [55], such a parton decomposition has a local gauge symmetry, which in turn implies the existence of a gauge field in the low energy description. In particular, we consider the QED$_3$-cHGN model, whose action in Euclidean signature is given by

$$S = \int d^3x \Big[-\bar{\Psi} \not{D}_a \Psi - \frac{h^2}{2} \left(\bar{\Psi} \boldsymbol{\sigma} \Psi \right)^2 \Big] + \dots \,. \tag{2.2.1}$$

The fermions are organized in a flavor spinor, $\Psi = \left(\psi_1, \psi_2, \dots, \psi_{2N} \right)^{\mathsf{T}}$. The adjoint spinor is given by $\bar{\Psi} = \Psi^\dagger \gamma^0$, where the Dirac matrices γ^μ act on Lorentz spinor components and may be written in terms of Pauli matrices τ_i as $\gamma^\mu = (\tau_3, \tau_2, -\tau_1)$. The gauge covariant derivative $\not{D}_a$ acting on fermions is given by

$$\not{D}_a = \gamma^\mu \left(\partial_\mu - i a_\mu \right) \,, \tag{2.2.2}$$

where a_μ is a U(1) gauge field. The cHGN interaction term has a coupling strength h and is defined with a Pauli matrix vector $\boldsymbol{\sigma}$ acting on the SU(2) magnetic spin subspace. The ellipsis denotes the Maxwell free action and the contribution from monopole operators $\mathcal{M}_q^\dagger$.

These topological disorder operators owe their existence to the compact nature of the U(1) gauge field which implies a 2π quantization of the gauge field's flux. Monopole operators insert integer multiples of the quantum flux $4\pi q$ where $2q \in \mathbb{Z}$. Formally, the charge q may defined by the action of the topological current operator $j^\mu_{\text{top}}(x) = \frac{1}{2\pi} \epsilon^{\mu\nu\rho} \partial_\nu a_\rho(x)$ on the monopole operator $\mathcal{M}_q^\dagger$ that can be developed with the operator product expansion [14]

$$j^\mu_{\text{top}}(x) \mathcal{M}_q^\dagger(0) \sim \frac{q}{2\pi} \frac{x^\mu}{|x|^3} \mathcal{M}_q^\dagger(0) + \cdots \,, \tag{2.2.3}$$

where the ellipsis denotes less singular terms as $|x| \to 0$. The prefactor corresponds to the magnetic field of a Dirac monopole with charge q. We emphasize that a monopole operator creates a topological configuration in the *emergent* gauge field which is not related to magnetism in the original system.

We can first begin the description of the quantum phase transition (QPT) by analyzing the non-compact QED$_3$-cHGN model. For a sufficiently strong coupling strength $h > h_c$, a spin-Hall mass is condensed $\hat{n} \cdot \langle \bar{\Psi} \boldsymbol{\sigma} \Psi \rangle > 0$. By using a zeta regularization to find the critical coupling, the effective action at the quantum critical point (QCP) is given by [48]

$$S^c_{\text{eff}} = -N \ln \det \left(\not{D}_a + \boldsymbol{\phi} \cdot \boldsymbol{\sigma} \right) \,, \tag{2.2.4}$$

where $\boldsymbol{\phi}$ is an auxiliary vector boson decoupling the cHGN interaction.

However, this picture is incomplete. Even if the monopole operators at the QCP are irrelevant and a $\mathrm{U}(1)_{\mathrm{top}}$ global symmetry emerges in the infrared, the monopole operators will be dangerously irrelevant. While gapless matter in QED_3 may screen the monopoles [14] and prevent the confinement observed in a pure U(1) gauge theory [56], the situation changes as fermions are gapped. Their screening effect is lost following the condensation of the spin-Hall mass which in turn drives the proliferation of spin-polarized monopoles [52, 53]. This confines the fermions, or in the context of quantum magnets, recombines the spinons that are fractionalized excitations of the underlying spin system. Monopole operators are thus an essential ingredient to properly understand this confinement-deconfinement transition.

A monopole at the QCP is characterized by its scaling dimension $\Delta_{\mathcal{M}_q}$ that controls the scaling behaviour of the two-point correlation function

$$\langle \mathcal{M}_q(x)\mathcal{M}_q^\dagger(0)\rangle \sim \frac{1}{|x|^{2\Delta_{\mathcal{M}_q}}}\,. \tag{2.2.5}$$

Since the model at the QCP is a conformal field theory, the state-operator correspondence can be used to obtain this critical exponent [57]. More precisely, the correspondence implies that within the set of $4\pi q$ flux operators, the minimal scaling dimension Δ_q is equal to the ground state of an alternate theory, namely the QED_3-GN model defined on $S^2 \times \mathbb{R}$ with a flux $\Phi = 4\pi q$ piercing the two-sphere. The external gauge field sourcing this flux $\Phi = \int \mathrm{d}A^q$ may be written as

$$A^q(x) = q(1-\cos\theta)\mathrm{d}\phi\,, \tag{2.2.6}$$

or $A^q_\phi = q(1-\cos\theta)/\sin\theta$ in components notation. The singularity at $\theta = \pi$ can be compensated by a Dirac string which imposes the Dirac condition on the topological charge $2q \in \mathbb{Z}$ as the string must remain invisible. By computing the free energy of this alternate theory, the scaling dimension Δ_q was computed at leading order in $1/N$ [48]. This scaling dimension obtained is smaller than in QED_3 and, specifically for the minimal monopole charge, is given by $\Delta_{1/2} = 2N \times 0.195 + \mathcal{O}(1/N^0)$.

As mentioned earlier, spin-polarized monopoles are favored by the spin-Hall mass condensation and yield the order parameter. It is useful to compare how different types of monopole operators behave at the QCP. We first precise what is meant by "types" of monopoles. While all monopole operators with a charge q insert the same flux, they are distinguished by the

different possible fermion modes dressings that define supplementary quantum numbers. The fermion occupation also determines Lorentz and gauge properties. For example, a flux operator with a vanishing fermion number is constructed by filling half of the fermion modes [14, 48]. Among these fermion modes, there are $4|q|N$ special fermion zero modes which owe their existence to the topological charge q of the flux operators [58]. By filling all negative energy modes and half of the zero modes, a flux operator with vanishing fermion number *and* a minimal scaling dimension is obtained. The zero modes occupation can be further constrained to select only operators with a vanishing Lorentz spin. This means that varying which zero modes are dressed defines a set of distinct $4\pi q$ flux operators which are Lorentz scalars, and have equal and minimal scaling dimensions. Those are the monopole operators of QED_3 [14].

The situation is slightly different in QED_3-cHGN. In the mean field theory, monopoles at the QCP are described by a non-vanishing spin-Hall mass $\langle \boldsymbol{\phi} \rangle_{A^q, S^2 \times \mathbb{R}} = M_q \hat{n}$ coming from the cHGN interaction.[4] This parameter most notably confers a non-vanishing energy to the zero modes. This affects the scaling dimension of a monopole which is lowered by anti-aligning the spin-Hall mass and the monopole magnetic spin polarization. Monopoles with different "zero" modes [5] occupation may then have different scaling dimensions, i.e. there is a monopole hierarchy in QED_3-cHGN. While the hierarchy was partly explored though this prism in Ref. [48], here we provide a more complete and accurate discussion on this point. Notably, here the spin-Hall mass is not fixed by the monopole with the lowest scaling dimension, it can instead vary in amplitude and orientation for each type of monopole. In this manner, we characterize the hierarchy among monopoles operators by obtaining the scaling dimension as a function of the monopole magnetic spin s in Sec. 2.3. We then show in Sec. 2.5 how monopoles are organized as irreducible representations of the QCP symmetry group $\text{SU}(2) \times \text{SU}(N)$ and how this makes contact with the scaling dimension results.

[4] We emphasize that a spin-Hall mass is condensed for the system of fermions put on the compactified spacetime $S^2 \times \mathbb{R}$, where the sphere is pierced by a $4\pi q$ flux. In the original flat space formulation describing the confinement-deconfinement transition, the fermions are gapless at the QCP.

[5] Since these modes do not have a vanishing energy but nevertheless keep their topological origin and their chiral aspect, we refer to them as "zero" modes.

2.3. Scaling dimension with fixed spin

2.3.1. Constraining the monopole magnetic spin

We now determine the scaling dimension of monopole operators $\mathcal{M}_{q;s}$ with topological charge q and with magnetic spin s. The minimal scaling dimension in this sector, $\Delta_{q;s}$, is obtained through the state-operator correspondence

$$\Delta_{q;s} = \lim_{\beta\to\infty} F_{q;s} \equiv -\lim_{\beta\to\infty} \beta^{-1} \ln Z_s[A^q]\,, \tag{2.3.1}$$

where $F_{q;s}$ is the rescaled free energy. The partition function and free energy define a ground state for an alternate version of the QED_3-cHGN action at the QCP (2.2.4). As discussed in the previous section, this alternate model is defined on a compactified spacetime $S^2 \times S^1_\beta$, where the "time" [6] direction is also taken compact as it is regularized on a "thermal" circle with radius β. Additionally, an external magnetic field A^q (2.2.6) is added to encode the flux of the monopole operator. Finally, the magnetic spin s of the monopole operator is selected by the inclusion of a Lagrange multiplier field μ_S in the action

$$S^c_{S^2\times S^1_\beta}[A^q] + \beta\mu_S\Big(s(s+1) - \boldsymbol{\mathcal{S}}^2\Big)\,, \tag{2.3.2}$$

where we introduced the total spin operator (averaged over time)

$$\boldsymbol{\mathcal{S}} = \beta^{-1}\int_{S^2\times S^1_\beta} \bar{\Psi}\gamma_0\tfrac{\boldsymbol{\sigma}}{2}\Psi\,. \tag{2.3.3}$$

More explicitly, this operator may be written as $\boldsymbol{\mathcal{S}} = \beta^{-1}\int_{S^2\times S^1_\beta}\Psi^\dagger\tfrac{\boldsymbol{\sigma}}{2}\Psi$. The lagrange multiplier equation yields the constraint $\langle\boldsymbol{\mathcal{S}}^2\rangle = s(s+1)$ which sets the magnetic spin of the monopole operator.

Since a monopole operator is dressed with half of the $4|q|N$ fermion "zero" modes, its maximal spin is $s_{\max} = |q|N$. This corresponds to configurations where only "zero" modes with the same spin-1/2 polarization are filled. On the other hand, a monopole with a minimal spin $s_{\min} = 0$ is obtained by dressing an equal proportion of "zero" modes with opposite spins.[7] The magnetic spin of a monopole obtained by filling the Dirac sea and half of the

[6] Here and throughout the text, we put quotes to emphasize that this is not the original time direction on $\mathbb{R}^3$ but rather the real direction obtained with conformal transformation $\mathbb{R}^3 \to S^2\times\mathbb{R}$.

[7] In fact, this is not possible for odd N as one "zero" mode always remains unmatched, i.e. $s_{\min} = 1/2$. However, this effect is subleading in $1/N$ and we only focus on the leading order.

zero modes is thus bounded as

$$0 \leq s \leq |q|N\,. \tag{2.3.4}$$

2.3.2. Free energy at leading order in $1/N$

The interaction added in Eq. (2.3.2) to the QED$_3$-cHGN action to constrain the total monopole spin is quartic in fermions and can be decoupled with an auxiliary boson field $\boldsymbol{\chi}$. As the spin-squared interaction is not diagonal in spacetime $\boldsymbol{\mathcal{S}}^2 = \beta^{-2}(\int_x \bar{\Psi}\gamma_0\frac{\boldsymbol{\sigma}}{2}\Psi \cdot \int_y \bar{\Psi}\gamma_0\frac{\boldsymbol{\sigma}}{2}\Psi)$, we should in principle introduce the boson in the same way. However, as we only seek to describe the free energy at leading order, we may replace the spin interaction with a diagonal formulation $\boldsymbol{\mathcal{S}}^2 \to V\beta^{-1}\int_x(\bar{\Psi}\gamma_0\frac{\boldsymbol{\sigma}}{2}\Psi)^2$, where $V = \int_{S^2}\sqrt{g}d^2x$ is the area of the two-sphere S^2. This will not affect the results as the expectation value is taken to be homogeneous. The auxiliary boson may then be introduced as the following resolution of the identity

$$\int \mathcal{D}\boldsymbol{\chi}\exp\Big\{-\int\frac{\boldsymbol{\chi}^2}{2V}\Big\} = \int \mathcal{D}\boldsymbol{\chi}\exp\Big\{-\int\frac{1}{2V}\Big(\boldsymbol{\chi} - V\sqrt{2\mu_S}\Big(\bar{\Psi}\gamma_0\frac{\boldsymbol{\sigma}}{2}\Psi\Big)\Big)^2\Big\}\,. \tag{2.3.5}$$

For later convenience, we note that the equation of motion for $\boldsymbol{\chi}$ relates the expectation value of the boson to the spin polarization as

$$\frac{\langle\boldsymbol{\chi}\rangle}{\sqrt{2\mu_S}} = V\langle\bar{\Psi}\gamma_0\frac{\boldsymbol{\sigma}}{2}\Psi\rangle\,. \tag{2.3.6}$$

With this auxiliary boson $\boldsymbol{\chi}$ (and the boson $\boldsymbol{\phi}$ decoupling the cHGN interaction in the original model QED$_3$-cHGN), fermions in the action (2.3.2) can be integrated out, yielding the following effective action

$$S'^c_{\text{eff}} = -N\ln\det\Big(\not{D}_{a,A^q} - \sqrt{\tfrac{\mu_S}{2}}\boldsymbol{\chi}\cdot\gamma_0\boldsymbol{\sigma} + \boldsymbol{\phi}\cdot\boldsymbol{\sigma}\Big) + \beta\mu_S s(s+1) + \int\frac{\boldsymbol{\chi}^2}{2V}\,. \tag{2.3.7}$$

We can now compute the free energy (2.3.1) using a large-N expansion corresponding to a saddle point expansion of the effective action. The leading order will be obtained by computing the saddle point value of the effective action

$$F^{\text{L.O.}}_{q;s} = NF^{(0)}_{q;s} = \frac{1}{\beta}S'^c_{\text{eff}}\Big|_{\text{Saddle pt.}}\,. \tag{2.3.8}$$

We take the saddle point configurations to be homogeneous. The two auxiliary bosons are SU(2)$_{\text{Spin}}$ vectors [8] and one of them may be oriented along $\hat{z}$ without loss of generality.

[8] By SU(2)$_{\text{Spin}}$ vectors, we only refer to the spin flavor group without specifying transformation properties under time reversal.

We orient the first auxiliary boson $\boldsymbol{\phi}$ along a general unit vector $\hat{n}$,

$$\langle \boldsymbol{\phi} \rangle = M_q \hat{n} \,, \tag{2.3.9}$$

where $M_q > 0$ is a spin-Hall mass.[9] The second boson can then be written simply as

$$\langle \boldsymbol{\chi} \rangle = P_z \hat{z} = \sqrt{2\mu_S} m_s \hat{z} \,, \tag{2.3.10}$$

where the spin polarization m_s (2.3.6) can be positive, negative or zero. As for the dynamical gauge field, gauge invariance requires its expectation value to vanish $\langle a_\mu \rangle = 0$.[10]

These mean field ansatz are inserted in the effective action. The free energy can be further simplified by recognizing that the spin variables scale as N since their magnitude can be formulated as a fraction of the total number of fermion "zero" modes (2.3.4). With this in mind, a subleading term in the total spin charge $s(s+1) = s^2 + \mathcal{O}(N^1)$ is dropped and the total spin and spin polarization s, $m_s \to Ns, Nm_s$ are rescaled. The rescaled total spin is thus bounded from above by $s_{\max} = q$, i.e. $s_{\max} = 1/2$ for the minimal topological charge. The free energy then becomes

$$F^{(0)}_{q;s} = f_{q;s} + \frac{\mu'}{m_s}\Big(s^2 + m_s^2\Big) \,, \tag{2.3.11}$$

where $f_{q;s}$ is the determinant operator

$$f_{q;s} = -\beta^{-1} \ln \det\Big(\not{D}_{-i\mu'\sigma_z, A^q} + M_q \hat{n} \cdot \boldsymbol{\sigma} \Big) \,, \tag{2.3.12}$$

and where we defined

$$\mu' = \mu_S m_s \,. \tag{2.3.13}$$

The saddle point parameters must solve the gap equations and minimize the free energy. Before determining them, we need to reexpress the free energy by developing the determinant operator. In QED$_3$-cHGN [48], the basis of spinor monopole harmonics can be used to diagonalize the determinant operator. The procedure is a simple generalization of the pure QED$_3$ case [16, 24]. Here, the formulation is a bit more involved since the spin-Hall mass and the spin polarization are not necessarily along the same axis. The analysis of the gap equations

[9] The spin-Hall mass could be written as $M_{q;s}$ since its value will depend on the magnetic spin s. We omit this index for simplicity.

[10] In fact, the gauge field may have a non-trivial holonomy on the "thermal" circle $i\int_0^\beta d\tau \langle a_0 \rangle \neq 0$. However, in the zero "temperature" limit, it is sufficient to take $\langle a_0 \rangle = 0$. See App. 2.A

for a general orientation of the spin-Hall mass $\boldsymbol{M_q} = M_q(\sin\vartheta\cos\varphi, \sin\vartheta\sin\varphi, \cos\vartheta)$ is presented in App. 2.B. Free energy minima are found for $(\vartheta = 0, m_s < 0)$ and $(\vartheta = \pi, m_s > 0)$, that is anti-aligned auxiliary bosons. The only other solution is found for $\vartheta = \pi/2$, but it yields a larger scaling dimension and can thus be discarded as it does not correspond to a global minimum of the free energy. This confirms that the monopole with the minimal scaling dimension has anti-aligned spin-Hall mass condensate and spin polarization, as interpreted in Ref. [48]. In the main text, we present the analysis for the simplified ansatz $\boldsymbol{M}_q = M_q\hat{z}$, where $M_q > 0$.

The determinant operator (2.3.12) can be diagonalized by introducing spinor monopole harmonics $S^{\pm}_{q,\ell,m}$. These functions diagonalize generalized total spinor operator $J_q^2 \to j_\pm(j_\pm + 1)$, where $j_\pm = \ell \pm 1/2$. The azimuthal and magnetic quantum numbers, respectively $\ell \in \{|q|, |q|+1, \ldots\}$ and $m \in \{-\ell, -\ell+1, \ldots \ell\}$, define the eigenvalues of L_q^2 and L_q^z which are diagonalized by monopole harmonics [59] which serve as components of the spinor monopole harmonics. For minimal angular momentum $\ell = |q|$, only the $S^{\pm}_{q,|q|,m}$ spinor exists and it corresponds to a zero mode of the Dirac operator. In the $j = \ell - 1/2$ basis $(S^{+}_{q;\ell-1,m}, S^{-}_{q;\ell,m})^\intercal$, the Dirac operator becomes a matrix with c-number entries [14]. As for the spin-Hall mass, its contribution is diagonal in this basis as noted in Ref. [48]. The resulting diagonal determinant operator therein is adapted by shifting the Matsubara frequency to account for the presence of the spin chemical potential

$$f_{q;s} = -\frac{1}{\beta}\sum_{\sigma=\pm1}\sum_{n\in\mathbb{Z}}\Big[d_q \ln\big(\omega_n - i\mu'\sigma + i\sigma M_q\big) + \sum_{\ell=q+1}^{\infty} d_\ell \ln\Big(\big(\omega_n - i\mu'\sigma\big)^2 + \varepsilon_\ell^2\Big)\Big], \qquad (2.3.14)$$

where ε_ℓ is the energy and d_ℓ is the degeneracy

$$\varepsilon_\ell = \sqrt{\ell^2 - q^2 + M_q^2}\,, \quad d_\ell = 2\ell\,, \qquad (2.3.15)$$

and ω_n are the fermionic Mastubara frequencies

$$\omega_n = \frac{2\pi}{\beta}(n + 1/2)\,, \quad n \in \mathbb{Z}\,. \qquad (2.3.16)$$

Note that the energy ε_ℓ is dimensionless as we choose units where the radius of the two-sphere $\sqrt{V/(4\pi)}$ is equal to one. Also, we have supposed that the topological charge is positive $q > 0$. In the end, the monopole scaling dimension is independent of the sign of the charge. Taking

the sum over Mastubara frequencies[11], Eq. (2.3.14) is simplified to

$$f_{q;s} = -\beta^{-1}\left[d_q \ln\Big(2\left[1+\cosh(\beta(M_q-\mu'))\right]\Big) + \sum_{\ell=q+1}^{\infty} 2d_\ell \ln\Big(2\left[\cosh(\beta\varepsilon_\ell)+\cosh(\beta\mu')\right]\Big)\right]. \tag{2.3.17}$$

2.3.3. Solving the gap equations

We now obtain the gap equations by varying the free energy with respect to the original saddle point parameters M_q, μ_S, P_z

$$\partial_{M_q} f_{q;s} = 0\,, \tag{2.3.18}$$

$$\tfrac{1}{2} m_s \partial_{\mu'} f_{q;s} + s^2 = 0\,, \tag{2.3.19}$$

$$\sqrt{\tfrac{\mu_S}{2}}\partial_{\mu'} f_{q;s} + P_z = 0\,. \tag{2.3.20}$$

The last gap equation could be solved with $\mu_S = P_z = 0$, but this yields unphysical results (see App. 2.C). Instead, if we take $\mu_S \neq 0$ and $P_z \neq 0$, the third gap equation can be written as

$$\partial_{\mu'} f_{q;s} = -2m_s\,, \tag{2.3.21}$$

where we used Eq. (2.3.10). The LHS can be developed explicitly as

$$\partial_{\mu'} f_{q;s} = d_q\left(\frac{\sinh(\beta(M_q-\mu'))}{1+\cosh(\beta(M_q-\mu'))}\right) - 2\sum_{\ell=q+1}^{\infty} d_\ell\left(\frac{\sinh(\beta\mu')}{\cosh(\beta\varepsilon_\ell)+\cosh(\beta\mu')}\right). \tag{2.3.22}$$

By taking μ' as

$$\mu' = M_q + \beta^{-1}\ln\left(\frac{1+2m_s/d_q}{1-2m_s/d_q}\right)\,, \tag{2.3.23}$$

the sum in Eq. (2.3.22) vanishes at leading order in $1/\beta$ since $\mu' < \varepsilon_{q+1}$ while the first term in Eq. (2.3.22) yields the required result (2.3.21). Inserting this in the second gap equation (2.3.19), we obtain

$$m_s^2 = s^2\,. \tag{2.3.24}$$

[11] We may define $\tilde{M}_q = M_q - \mu'$ in the first term and $\tilde{\mu} = \mu\sigma$ in the second term, and directly read results from Ref. [48]

This means that the polarization is maximized. We turn to the remaining gap equation for M_q. The derivative of the determinant operator with respect to M_q is given by

$$\partial_{M_q} f_{q;s} = -d_q \left(\frac{\sinh(\beta(M_q - \mu'))}{1 + \cosh(\beta(M_q - \mu'))} \right) - 2M_q \sum_{\ell=q+1}^{\infty} \frac{d_\ell \varepsilon_\ell^{-1} \sinh(\beta\varepsilon_\ell)}{\cosh(\beta\varepsilon_\ell) + \cosh(\beta\mu')} \,. \tag{2.3.25}$$

Inserting in this expression the result for μ' (2.3.23), the first gap equation (2.3.18) becomes $2m_s - 2M_q \sum_\ell d_\ell \epsilon_\ell^{-1} = 0$. A positive solution for M_q can only be found for $m_s < 0$. This shows, as mentioned above, that the spin polarization and the spin-Hall mass should be anti-aligned. Taking $m_s = -s$, the gap equation then becomes

$$-2s - 2M_q \sum_{\ell=q+1}^{\infty} d_\ell \epsilon_\ell^{-1} = 0 \,. \tag{2.3.26}$$

This equation can be solved for any allowed spin $0 \leq s \leq d_q/2$. We discuss its solutions later on.

We first turn to the computation of the free energy and the scaling dimension. Using the solution for μ' (2.3.23), the determinant operator (2.3.12) at leading order in $1/\beta$ is given by $-2\sum_\ell d_\ell \varepsilon_\ell$. The rest of the free energy (2.3.11) is reexpressed using $\mu' = M_q + \mathcal{O}(1/\beta)$ and $m_s = -s$ [12]. Taking the zero "temperature" limit of the resulting free energy, we obtain the scaling dimension at leading order in $1/N$

$$\Delta_{q;s} = -2N \left(sM_q + \sum_{\ell=q+1}^{\infty} d_\ell \varepsilon_\ell \right) + \mathcal{O}(1/N^0) \,. \tag{2.3.27}$$

2.3.4. Scaling dimension and spin-Hall mass

The last result (2.3.27) shows how monopoles with the largest spin s have a minimal contribution of the spin-Hall mass to their scaling dimension. The only remaining parameter is the spin-Hall mass M_q as other fields were evaluated. This mass can be obtained by solving numerically a regularized version of the gap equation (2.3.26). Inserting this result in a regularized version of Eq. (2.3.27), the monopole scaling dimension with spin s is found. Both regularized expressions are shown in App. 2.D. Here, we simply show their solutions for multiple values of s.

[12] Combining Eqs. (2.3.10) and (2.3.13), we may note that $P_z = \sqrt{2\mu' m_s}$, which, since $\mu' > 0$ and $m_s < 0$, is imaginary. As $\boldsymbol{\chi}$ is an auxiliary boson introduced as a resolution of the identity (2.3.5), an imaginary expectation value poses no problem : A gaussian integral shifted in the complex plane yields the same result.

The spin-Hall mass M_q and the scaling dimension $\Delta_{q;s}$ for the minimal topological charge $q = 1/2$ are shown as a function of the total magnetic spin s in Fig. 2.1. For the maximal

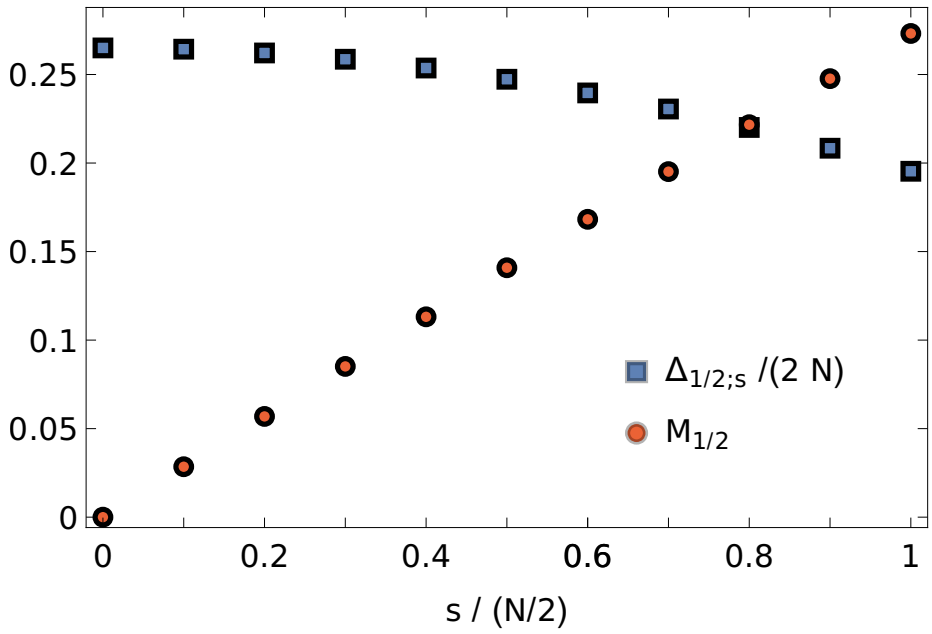

Figure 2.1. Scaling dimension $\Delta_{q;s}$ per number of fermion flavors $2N$ and spin-Hall mass M_q as a function of the magnetic spin s for a minimal topological charge $q = 1/2$. The spin is expressed as a fraction of its maximal value $s_{\max} = N/2$. Here, the spin s is not rescaled by N.

spin $s_{\max} = d_q/2$, the gap equation and the minimal scaling dimension in the $4\pi q$ sector of QED$_3$-cHGN found in Ref. [48] are retrieved, that is $\Delta_{q;s_{\max}} = \Delta_q^{\text{QED}_3\text{-cHGN}}$. More explicitly, the scaling dimension is given by

$$\Delta_{q;s_{\max}} = -N\Big(d_q M_q + 2\sum_\ell d_\ell \varepsilon_\ell\Big)\Big|_{\text{Saddle pt.}} + \mathcal{O}(N^0)\,, \tag{2.3.28}$$

where the spin-Hall mass is evaluated at its saddle point value found by solving the gap equation (2.3.26) for $s = s_{\max}$. The last expression for $\Delta_{q;s_{\max}}$ yields the minimal scaling dimension $\Delta_q^{\text{QED}_3\text{-cHGN}}$ found in Ref. [48]. For a minimal spin $s_{\min} = 0$, the mass at saddle point vanishes. In turn, this means that the leading order scaling dimension corresponds to the monopole scaling dimension in pure QED$_3$, $\Delta_{q;s_{\min}} = \Delta_q^{\text{QED}_3}$, or, more explicitly,

$$\Delta_{q;0} = -2N\sum_\ell d_\ell \varepsilon_\ell|_{M_q=0} + \mathcal{O}(N^0)\,. \tag{2.3.29}$$

The scaling dimension ranges between these values for intermediate values of the spin $s_{\min} < s < s_{\max}$

$$\Delta_q^{\text{QED}_3\text{-cHGN}} \leq \Delta_{\mathcal{M}_q}^{\text{QED}_3\text{-cHGN}} \leq \Delta_q^{\text{QED}_3}\,, \quad \text{L.O. in } 1/N\,. \tag{2.3.30}$$

This result includes the effect of fermion occupation on the mass M_q. This aspect was neglected in Ref. [48] where the mass was considered fixed in orientation and amplitude, defined as to yield the smallest possible lower bound for scaling dimensions in the $4\pi q$ sector. The operator corresponding to this minimal scaling dimension was dubbed "spin down" monopole and other monopoles were obtained by modifying its "zero" modes occupation. Here, by finding an optimal spin-Hall mass parameter in each spin sector, a smaller upper boundary on monopole scaling dimensions in QED_3-cHGN (2.3.30) is found. This is schematized in Fig. 2.2 for the case $q = 1/2$ and $N = 2$.

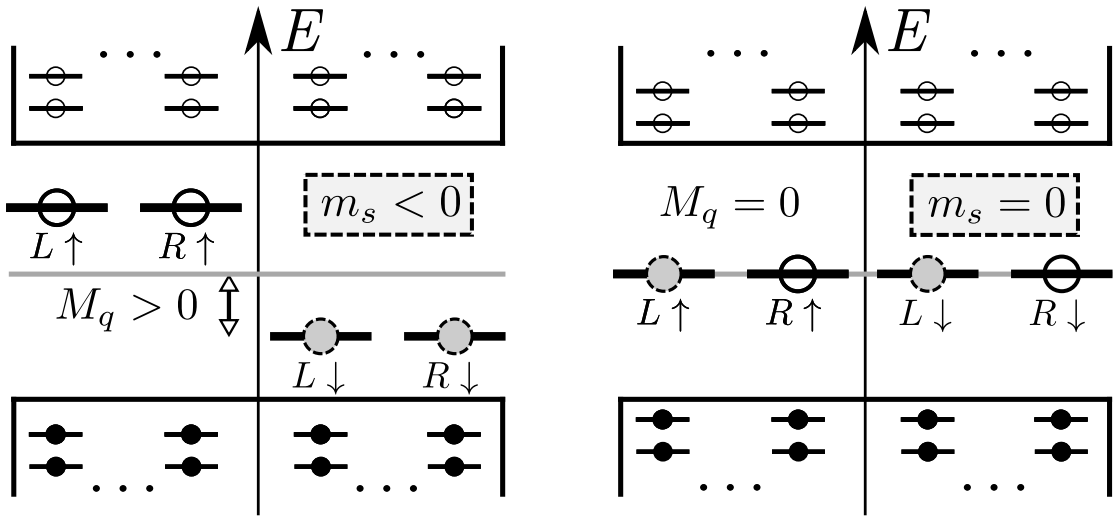

(a) (b)

Figure 2.2. Schematic representation of the fermion modes dressing of monopole operators with $N = 2$ valleys $v = L, R$ and a minimal topological charge $q = 1/2$. (a) The $s = 1, m_s = -1$ monopole is described by a non-vanishing spin-Hall mass $\langle\bar{\Psi}\boldsymbol{\sigma}\Psi\rangle \propto M_q\hat{z}$ where $M_q > 0$. (b) A spin singlet monopole ($s = m_s = 0$) is described by a vanishing spin-Hall mass $M_q = 0$. Here, the monopole polarized along the L valley is shown.

This hierarchy is characterized explicitly for various values of magnetic spin and topological charge. Monopole scaling dimensions obtained numerically are shown in Fig. 2.3. Every

$q = 1/2$ monopole has a smaller scaling dimension than monopoles with larger topological charges q. This is not necessarily the case for other monopoles, e.g. $\Delta_{4;s_{\min}} > \Delta_{5;s_{\max}}$. Analytical approximations for the scaling dimensions obtained with a large-q expansion and shown in Table 2.1 are also plotted in Fig. 2.3. There is a good agreement with the numerical results even for small values of the topological charge.

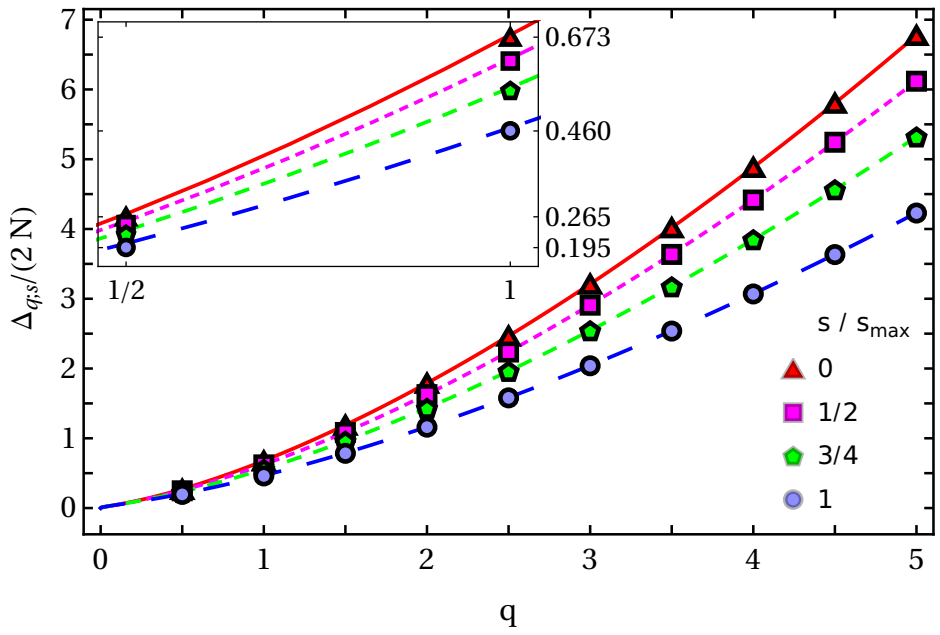

Figure 2.3. Scaling dimension $\Delta_{q;s}$ per number of fermion flavors $2N$ as a function of q for $s/s_{\max} = \{0, 1/2, 3/4, 1\}$ where $s_{\max} = qN$. The lines correspond to analytical approximations of the scaling dimensions obtained through a large-q expansion and shown in Table 2.1.

2.4. Scaling dimensions for large-q

The scaling dimension of monopole operators may also be approximated by an analytical expression obtained with a large-q expansion. The expansion was presented in Ref. [48] for the monopole with maximal spin and minimal scaling dimension. Building on this result, analytical approximations were also proposed for other types of monopoles, but these results again neglected the backreaction of the "zero" modes occupation on the spin-Hall mass. Here, we show the proper analysis for any magnetic spin s.

To start this computation, we may read the unregularized free energy (at zero temperature) off the scaling dimension (2.3.27) with the relation $\Delta_{q;s} = NF^{(0)}_{q;s} + \dots$ By changing

the summation index $\ell \to \ell + q + 1$, the free energy becomes

$$F_q^{(0)} = -4qM_q\tilde{s} - 4\sum_{\ell=0}^{\infty}(\ell+q+1)\sqrt{(\ell+q+1)^2 - q^2 + M_q^2}\,, \tag{2.4.1}$$

where we introduced $\tilde{s} \equiv s/s_{\max}$ in order to factorize the dependence on q. The saddle point equation is then given by

$$-4q\tilde{s} - 4M_q\sum_{\ell=0}^{\infty}\frac{\ell+q+1}{\sqrt{(\ell+q+1)^2 + M_q^2 - q^2}} = 0\,. \tag{2.4.2}$$

Inserting the following mass squared ansatz

$$M_q^2 = 2\chi_0 q + \chi_1 + \mathcal{O}(q^{-1})\,, \tag{2.4.3}$$

the free energy (2.4.1) and the gap equation (2.4.2) can be expanded in powers of $1/q$, respectively

$$\begin{aligned}\frac{1}{2}F_q^{(0)} = -2\sqrt{2}q^{3/2}\left(\zeta_{-1/2} + \tilde{s}\chi_0^{1/2}\right) - \frac{q^{1/2}}{\sqrt{2}}\Big(\left(\chi_0^2 + \chi_1\right)\zeta_{1/2} \\ - 6\chi_0\zeta_{-1/2} + 5\zeta_{-3/2} + \tilde{s}\chi_1\chi_0^{-1/2}\Big) + \mathcal{O}(q^{-1/2})\,.\end{aligned} \tag{2.4.4}$$

and

$$\begin{aligned}0 = \ 4q^{1/2}\left(\zeta_{1/2} + \tilde{s}\chi_0^{-1/2}\right) - q^{-1/2}\Big(\left(\chi_1 + \chi_0^2\right)\zeta_{3/2} \\ + 2\chi_0\zeta_{1/2} - 3\zeta_{-1/2} + \tilde{s}\chi_1\chi_0^{-3/2}\Big) + \mathcal{O}(q^{-3/2})\,,\end{aligned} \tag{2.4.5}$$

where $\zeta_n \equiv \zeta(n, 1+\chi_0)$ is the zeta function used to regularize $\sum_{l=0}(l + (1+\chi_0))^{-n}$. The gap equation at leading order yields a transcendental condition defining χ_0 while χ_1 is determined by a linear condition at next-to-leading order

$$\zeta_{1/2} + \tilde{s}\chi_0^{-1/2} = 0\,, \tag{2.4.6}$$

$$\chi_1 + \frac{2\chi_0^{3/2}\left(\chi_0^2\zeta_{3/2} + 2\chi_0\zeta_{1/2} - 3\zeta_{-1/2}\right)}{\tilde{s} + \chi_0^{3/2}\zeta_{3/2}} = 0\,. \tag{2.4.7}$$

We solve these equations by fixing s and by finding numerically the values of χ_0 and χ_1. These coefficients yield the value of the spin-Hall mass and are inserted in the free energy (2.4.4).[13] The resulting monopole scaling dimensions at leading order in $1/N$ for various magnetic spin s are shown in Table 2.1. The lines in Fig. 2.3 giving the monopole scaling

[13] As noted in last section, the gap equation (2.4.2) for $s = 0$ is solved for a vanishing spin-Hall mass $M_q = 0$. In this case, we must simply take $\chi_0 = \chi_1 = 0$.

Tableau 2.1. Analytical approximation of the monopole scaling dimensions for $s/s_{\max} = \{0, 1/2, 3/4, 1\}$ obtained in the large-q expansion.

$\frac{s}{s_{\max}}$	$\frac{\Delta_{q;s}}{2N} + \mathcal{O}(q^{-1/2}) + \mathcal{O}(N^{-1})$
1	$0.356q^{3/2} + 0.111q^{1/2}$
3/4	$0.455q^{3/2} + 0.103q^{1/2}$
1/2	$0.528q^{3/2} + 0.096q^{1/2}$
0	$0.588q^{3/2} + 0.090q^{1/2}$

dimensions against q are plotted using these analytic approximations.

Note that the absence of the $\mathcal{O}(q^0)$ term in $\Delta_{q;s}$ is expected. In $2+1$-dimensional CFTs with a U(1) global charge q, the q^0 contribution in the large-q expansion of the scaling dimension is predicted to be universal. It must thus be independent of the number of fermion flavors $2N$ defining our specific model [37, 60], i.e. the $\mathcal{O}(q^0 N^1)$ in the large-N and large-q expansion of $\Delta_{q;s}$ must vanish.

2.5. Hierarchy as degeneracy lifting

The hierarchy shown in Eq. (2.3.30) is now analyzed from the point of view of symmetry. Our non-perturbative analysis does not depend on a large-N expansion. The multiplet organization of monopoles at the QCP is obtained by showing how monopoles in the DSL reorganize as the flavor symmetry of QED_3 is broken to the flavor symmetry of QED_3-cHGN. To make contact with the scaling dimensions obtained in the last section, it is important to recognize that the spin-Hall mass is a $\text{SU}(2)_{\text{Spin}}$ vector.

The cHGN interaction $\delta\mathcal{L} \sim (\bar{\Psi}\boldsymbol{\sigma}\Psi)^2$ inducing the confinement-deconfinement transition breaks down the flavor symmetry of QED_3 as

$$\text{SU}(2N) \to \text{SU}(2) \times \text{SU}(N)\,. \tag{2.5.1}$$

While monopoles in QED_3 are all related by $\text{SU}(2N)$ rotations and share the same scaling dimension, this is not the case in $\text{QED}_3 - \text{cHGN}$. The hierarchy of monopole operators in $\text{QED}_3 - \text{cHGN}$ observed in the previous section may be explained as a degeneracy lifting of monopoles in QED_3.

Monopoles in QED_3 are organized as irreducible representations (irreps) of the flavor symmetry group $\text{SU}(2N)$. We focus our attention of monopoles with a minimal topological charge $q = 1/2$. This is the simplest case as monopole operators are then automatically Lorentz scalars [14]. The case with a larger topological charge is briefly discussed in App. 2.F. It is useful to first define a bare monopole operator $\mathcal{M}^\dagger_{\text{Bare}}$ creating a 2π flux background and filled only with negative energy modes. A monopole operator is then obtained by adding in half of the $2N$ zero modes creation operators $c^\dagger_{I_i}$

$$\mathcal{M}^\dagger_{I_1\dots I_N} = c^\dagger_{I_1}\dots c^\dagger_{I_N}\mathcal{M}^\dagger_{\text{Bare}}\,, \quad I_i \in \{1,2,\dots,2N\}\,. \tag{2.5.2}$$

Given the antisymmetric commutation relations between the fermionic creation operators, the expression above clearly shows how $q = 1/2$ monopoles in QED_3 form the rank-N completely antisymmetric irrep of $\text{SU}(2N)$.

2.5.1. Multiplets at the QCP for $N = 2$

We first discuss the monopole hierarchy for a finite N situation to provide some intuition. While the discussion is centered on symmetries and not dynamics, we do need to assume that the QCP still exists at finite N. We focus on the case with $N = 2$ valleys $v = L$,R which is the most relevant to quantum magnets. Monopole operators then have two zero modes creation operators and may be expressed in the following form

$$c^\dagger A (c^\dagger)^\intercal \mathcal{M}^\dagger_{\text{Bare}}\,, \tag{2.5.3}$$

where A acts on vectors in flavor space $c^\dagger = \left(c^\dagger_{\uparrow,L}, c^\dagger_{\uparrow,R}, c^\dagger_{\downarrow,L}, c^\dagger_{\downarrow,R}\right)$. At the QED_3-cHGN QCP, monopoles are organized as triplets [21, 22]

$$\boldsymbol{\mathcal{M}}^\dagger_{\text{Spin}} = c^\dagger \left(\sigma_y \boldsymbol{\sigma} \otimes \mu_y\right) (c^\dagger)^\intercal \mathcal{M}^\dagger_{\text{Bare}}\,, \tag{2.5.4}$$

$$\boldsymbol{\mathcal{M}}^\dagger_{\text{Nodal}} = c^\dagger \left(\sigma_y \otimes \mu_y \boldsymbol{\mu}\right) (c^\dagger)^\intercal \mathcal{M}^\dagger_{\text{Bare}}\,, \tag{2.5.5}$$

where $\boldsymbol{\sigma}$ and $\boldsymbol{\mu}$ are Pauli matrices vectors respectively acting on magnetic spin and nodal subspaces (in our notation, $\mu_z = |L\rangle\langle L| - |R\rangle\langle R|$ and σ_z has the usual definition $|\uparrow\rangle\langle\uparrow| - |\downarrow\rangle\langle\downarrow|$). In particular, the spin triplet forms the order parameter $\hat{n}\cdot\langle i\boldsymbol{\mathcal{M}}^\dagger_{\text{Spin}}\rangle$ for coplanar antiferromagnetic phase of the Kagome heisenberg antiferromagnet [21, 53].

More formally, monopoles in QED_3 (2.5.3) form the rank-2 completely antisymmetric irrep, that we note by its dimension **6**. Following the symmetry reduction (2.5.1), this irrep

is reduced in irreps $(\boldsymbol{m}, \boldsymbol{n})$ with dimension $m \times n$ of the QCP subgroup $\mathrm{SU}(2)_{\mathrm{Spin}} \times \mathrm{SU}(2)_{\mathrm{Nodal}}$

$$\mathbf{6} \to (\mathbf{3}, \mathbf{1}) \oplus (\mathbf{1}, \mathbf{3}) \ . \tag{2.5.6}$$

The spin and nodal triplet, respectively $(\mathbf{3}, \mathbf{1})$ and $(\mathbf{1}, \mathbf{3})$, have total magnetic spin given by $S = 1$ and $S = 0$. They are the finite-N analogues of $q = 1/2$ monopoles with $s_{\max} = 1$ and $s_{\min} = 0$, respectively, described in Sec. 2.3

$$\mathcal{M}^{\dagger}_{1/2;s_{\max}} \to (\mathbf{3}, \mathbf{1}) \ , \quad \mathcal{M}^{\dagger}_{1/2;s_{\min}} \to (\mathbf{1}, \mathbf{3}) \ . \tag{2.5.7}$$

As we perform a $\mathrm{SU}(2)_{\mathrm{Spin}}$ rotation, the "zero" modes occupation is modified and so does the orientation of the spin-Hall mass. For example, a spin flip exchanges spin down and spin up "zero" modes, changing the polarization sign of a monopole, i.e. $\mathcal{M}^{\dagger}_{q;s,m_s} \to \mathcal{M}^{\dagger}_{q;s,-m_s}$. With this transformation, the sign of the spin-Hall mass also changes $\langle \bar{\Psi} \sigma_z \Psi \rangle \to -\langle \bar{\Psi} \sigma_z \Psi \rangle$, which leaves the scaling dimension unchanged. The spin flip is schematically shown in Fig. 2.4. In

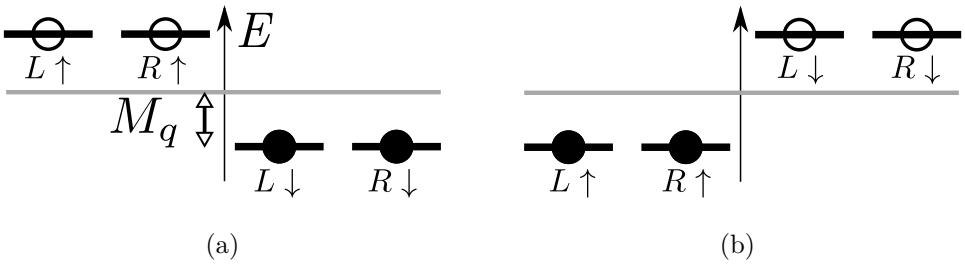

Figure 2.4. Schematic representation of the fermion zero modes dressing of monopole operators with $N = 2$ valleys $v = L, R$ and a minimal topological charge $q = 1/2$. (a) The $s = 1, m_s = -1$ monopole with spin-Hall mass $\langle \bar{\Psi} \boldsymbol{\sigma} \Psi \rangle \propto M_q \hat{z}$ can be rotated to (b) the $s = 1, m_s = -1$ monopole with spin-Hall mass $\langle \bar{\Psi} \boldsymbol{\sigma} \Psi \rangle \propto -M_q \hat{z}$.

App. 2.E, we explore the explicit realization of monopoles suggested in Eqs. (2.5.4 -2.5.5) and we also obtain a representation of the $\mathrm{SU}(2) \times \mathrm{SU}(2)$ generators. Acting with these on the monopoles, it can be seen that these operators indeed form a reducible representation of this group. We also build explicitly the rotation shown in Fig. 2.4, and the rotation that sends the quantization axis in the $x - y$ plane.

2.5.2. Multiplets at the QCP for general N

We now give a description of the monopole hierarchy for general N. Again, our starting point is the organization of monopoles in QED_3. As noted above, these monopoles form the rank-N antisymmetric tensor of SU($2N$) (2.5.2). In terms of a Young tableau, this may be written as a single column of N boxes

$$N\left\{\begin{array}{c}\square\\ \vdots\\ \square\end{array}\right. . \tag{2.5.8}$$

The organization of monopole operators at the QED_3-cHGN QCP can then be understood by finding how this SU($2N$) irrep reduces as a representation of the subgroup $\mathrm{SU}(2)\times\mathrm{SU}(N)$.

In the last section, we discussed the case $N = 2$ where the rank-2 completely antisymetric irrep **6** of SU(4) is reduced to the representation $(\mathbf{3},\mathbf{1}) \oplus (\mathbf{1},\mathbf{3})$ of $\mathrm{SU}(2) \times \mathrm{SU}(2)$. The following Young tableaux schematize this reduction (2.5.6)

$$\begin{array}{c}\square\\ \square\end{array}_{\mathbf{6}} \to \left(\square\square_{\mathbf{3}}, \begin{array}{c}\square\\ \square\end{array}_{\mathbf{1}}\right) \oplus \left(\begin{array}{c}\square\\ \square\end{array}_{\mathbf{1}}, \square\square_{\mathbf{3}}\right), \tag{2.5.9}$$

where the bold subscripts indicate the respective irrep's dimension. The reduction can also be written explicitly for general N. The rank-N completely antisymmetric irrep (2.5.8) is reduced as

$$N\left\{\begin{array}{c}\square\\ \vdots\\ \square\end{array}\right. \to \bigoplus_{b=0}^{\lfloor N/2\rfloor}\left(\begin{array}{c} \overbrace{\square\cdots\square\cdots\square}^{N-b}\\ \underbrace{\square\cdots\square}_{b}\end{array} , \; N-b\left\{\begin{array}{c}\square\square\\ \vdots\;\vdots\\ \square\square\\ \vdots\\ \square\end{array}\right\} b \right), \tag{2.5.10}$$

This is coherent with results in Ref. [61] where this reduction is obtained up to $N = 8$,[14] or with the output of a recent symbolic computation package for representation theory [62]. This result was stated in Ref. [19] where the organization of flux operators in Lorentz symmetry multiplets was discussed. We give the proof of this result (2.5.10) in App. 2.F.

The previous notation highlights well that the RHS of Eq. (2.5.10) is simply the sum over all pairs of conjugate Young tableaux with N boxes, $(\Upsilon_\nu, \Upsilon_{\tilde{\nu}})$, where the first diagram Υ_ν has a maximum of two rows since it must be a SU(2) irrep. This plays a key role when

[14] Using the notation employed in Ref. [61], Eq. (2.5.10) can be reexpressed as $(1^N) \to \bigoplus_{b=0}^{\lfloor N/2\rfloor}\Big((N-b,b),(2^b,1^{N-2b})\Big)$.

proving Eq. (2.5.10). This total number of boxes also corresponds to the number of fermion zero modes dressing the monopole. Indeed, the monopole may be noted as $\mathcal{M}^{\dagger}_{\sigma_1 v_1, \sigma_2 v_2, \ldots, \sigma_N v_N}$. The $\mathrm{SU}(2)_{\mathrm{Spin}}$ irrep encodes symmetry relations between spin indices σ_i, and the same goes for valley indices v_i and the $\mathrm{SU}(N)_{\mathrm{Nodal}}$ irrep. In the simplest case where $b = 0$, the irrep becomes

$$\left(\underbrace{\square \cdots \square}_{N} \, , \, N \left\{ \begin{array}{c} \square \\ \vdots \\ \square \end{array} \right. \right). \tag{2.5.11}$$

The corresponding monopole simply transforms symmetrically in its spin indices and antisymmetrically in its valley indices. That is, the monopole is a valley singlet and a spin multiplet with maximal spin. For other values of b, the irreps describe mixed symmetries between the indices. Every box represents a spin or valley index which is antisymmetrized with its column neighbours and symmetrized with its row neighbours. The antisymmetry of Eq. (2.5.10)'s LHS is realized in each of the RHS irreps through the following prescription : i) Match pairs of antisymmetrized spins (columns with two boxes) with pairs of symmetrized valleys (rows with two boxes) ii) Match the remaining symmetrized spins with the remaining antisymmetrized valleys.

To gain a better physical intuition, it is useful to label the Young tableaux in Eq. (2.5.10) with the magnetic spin s instead of a number of boxes b. The dimension of the $\mathrm{SU}(2)_{\mathrm{Spin}}$ irrep is $N - 2b + 1$. This number should naturally be identified with $2s + 1$. Also, we can eliminate every column of two boxes for the $\mathrm{SU}(2)_{\mathrm{Spin}}$ irreps which correspond to antisymmetrized pairs of spins. Ignoring those "bounded" spin indices by removing their corresponding boxes obscurs the underlying zero modes dressing, but it puts the $\mathrm{SU}(2)_{\mathrm{Spin}}$ irreps in a more familiar form. The remaining boxes correspond to the "free" spin indices that form the spin-s multiplet. With this, the monopole representation at the QCP can be written as

$$\bigoplus_{s=(N \bmod 2)/2}^{N/2} \left(\underbrace{\square \cdots \square}_{2s} \, , \, \tfrac{N}{2}+s \left\{ \begin{array}{c} \square\square \\ \vdots \;\; \vdots \\ \square\square \\ \vdots \\ \square \end{array} \right\} \tfrac{N}{2}-s \right). \tag{2.5.12}$$

For the maximal spin $s = N/2$, the valley irrep is a singlet, as noted earlier in Eq. (2.5.11).

2.5.2.1. Degeneracy in each magnetic spin sector. The degeneracy of monopoles at the QCP for each magnetic spin sector is found in what follows. To do so, we compute the

dimension of the reduced irreps in Eq. (2.5.12), which is given by the product of the spin and valley irreps' dimensions. The dimension of the spin irrep is the usual spin degeneracy $2s+1$. As for the valley irrep, it can first be observed that it is generated through a tensor product of completely antisymmetric tensors

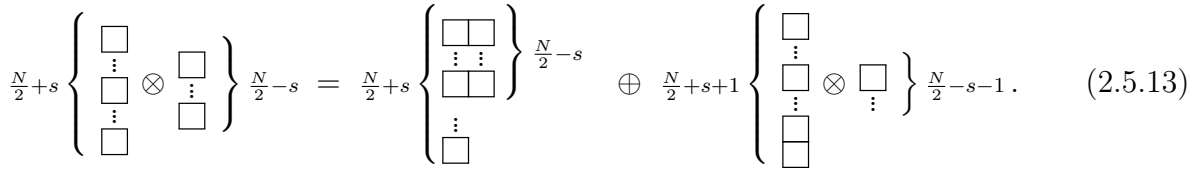

(2.5.13)

The valley irrep's dimension can be obtained by computing the dimensions of the other representations in this relation. Each composite antisymmetric tensor has a dimension given by a binomial factor. Specifically, the dimension of the SU(N) irrep corresponding to a single column of b boxes is $\binom{N}{b}$. The tensor product's dimension is simply the product of these binomial factors. The dimension of the valley irrep is then

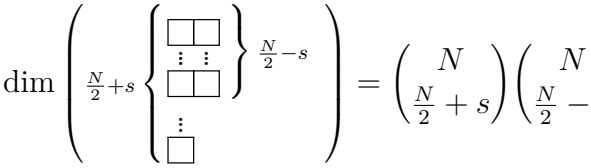

$$= \binom{N}{\frac{N}{2}+s}\binom{N}{\frac{N}{2}-s} - \binom{N}{\frac{N}{2}+s+1}\binom{N}{\frac{N}{2}-s-1}. \tag{2.5.14}$$

We can then obtain the total degeneracy of monopoles in each magnetic spin sector

$$\Omega_s = (2s+1) \times \left[\binom{N}{\frac{N}{2}+s}\binom{N}{\frac{N}{2}-s} - \binom{N}{\frac{N}{2}+s+1}\binom{N}{\frac{N}{2}-s-1} \right]. \tag{2.5.15}$$

In App. 2.F, we confirm this result with a method appropriate for general Young tableaux. We also show that the total dimension of the reduced irreps is equal to the original antisymmetric irrep in SU($2N$), that is $\sum_s \Omega_s = \binom{2N}{N}$.

We briefly reformulate the last result. The factor $2s+1$ comes from the possible spin polarizations of the monopole. As for the valley sector, we take as a starting point two antisymmetric tensors $A_{v_1,v_2,\ldots,v_{N/2+s}} \tilde{A}_{v'_1,v'_2,\ldots,v'_{N/2-s}}$ that assign valley indices to the N zero modes. This corresponds to the tensor product in the LHS of Eq. (2.5.13). The $2s$ supplementary valley indices in the first tensor can be attributed to the $2s$ "free" spin indices which give the monopole its magnetic polarization. Indeed, these "free" spin indices form a symmetric multiplet and must be matched with antisymmetrized valley indices to yield an antisymmetric state. On the other hand, the remaining $N-2s$ "bounded" spin indices (the boxes eliminated in Eq. (2.5.12)) form antisymmetrized spin pairs that should be matched with symmetrized valley pairs. Thus, every configuration with at least one pair of antisymmetrized

valley indices matched to an antisymmetrized spin pair should be removed. Such configurations can be written as $A_{v_1',v_1,v_2,\ldots,v_{N/2+s}}\tilde{A}_{v_2',v_3',\ldots,v_{N/2-s}'}$, which is the tensor product in the RHS of Eq. (2.5.13). It then follows that distinct spin pairs are also related by antisymmetrized valley indices, which yields the overall antisymmetric state.

2.5.2.2. Reduction for $N = 3$. Using the result in Eq. (2.5.10), we can retrieve the reduction of monopoles at the QCP for $N = 3$ that was discussed in Ref. [49]. In this case, the flavor symmetry breaking is $\mathrm{SU}(6) \to \mathrm{SU}(2)_{\mathrm{Spin}} \times \mathrm{SU}(3)_{\mathrm{Nodal}}$. Monopoles in QED_3 are organized as the rank-3 antisymmetric representation **20** of SU(6). At the QCP, this is decomposed as

$$\ydiagram{1,1,1}_{\mathbf{20}} \to \left(\ydiagram{3}_{\mathbf{4}}, \ydiagram{1,1,1}_{\mathbf{1}}\right) \oplus \left(\ydiagram{2,1}_{\mathbf{2}}, \ydiagram{2,1,1}_{\mathbf{8}}\right), \tag{2.5.16}$$

which agrees with Ref. [61]. The total dimension of the reduced irreps is $4 \times 1 + 2 \times 8 = 20$, as required. The largest $\mathrm{SU}(2)_{\mathrm{Spin}}$ spin is $s_{\max} = 3/2$ since $q = 1/2$ and $N = 3$ (see Eq. (2.3.4)). It corresponds to a spin quadruplet, the **4** in Eq. (2.5.16). This irrep represents monopoles with the lowest scaling dimension. As noted before, the fact that N is odd yields a non-vanishing minimal with $s_{\min} = 1/2$, the **2** in Eq. (2.5.16). As three "zero" modes must be filled, the lowest polarization that can be obtained is by paring two modes in a singlet, leaving one remaining spin that forms the doublet.

2.6. Conclusion

We characterized the hierarchy of monopole operators in QED_3-cHGN. Using the state-operator correspondence, we obtained the scaling dimensions of monopoles as a function of their magnetic spin at leading order in $1/N$. The spin-Hall mass parameter generated by the critical fermion self-interaction allows to lower the scaling dimension of monopoles, and this effect is more pronounced for monopoles with larger magnetic spins. The minimal scaling dimension identified in Ref. [48] corresponds to monopoles with a maximal magnetic spin. Monopoles with a vanishing spin have the largest scaling dimension which is the same as in QED_3. This hierarchy is natural from the point of view of symmetry as monopoles at the QCP are organized as irreps of $\mathrm{SU}(2) \times \mathrm{SU}(N)$ which are labeled by the magnetic spin. These irreps were obtained explicitly for $q = 1/2$ monopoles at the QCP by finding the branching rules of $\mathrm{SU}(2N) \to \mathrm{SU}(2) \times \mathrm{SU}(N)$ to reduce the monopole irrep formed in QED_3. This also

allowed to obtain the degeneracies remaining at the QCP following the degeneracy lifting. It would be interesting to improve the analysis for $q > 1/2$ that was began in App. 2.F.

The hierarchy of monopole operators for $2N = 4$ Dirac cones could be observed in the transition from a DSL to an antiferromagnet putatively realized in the Kagome Heisenberg antiferromagnet. The antiferromagnetic order is described by the condensation of the spin triplet monopoles [21, 22], whose scaling dimension is $\Delta_{q=1/2,s=1} = 2N \times 0.195 + O(N^0) \sim 0.78$. This controls the scaling behaviour of spin-spin correlation functions. On the other hand, bond-bond correlation functions are controlled by valley triplet monopoles, that is, spin singlet monopoles with scaling dimension $\Delta_{q=1/2,s=0} = 2N \times 0.265 + O(N^0) \sim 1.06$. We emphasize that these results are approximations, being the leading order of a $1/N$ expansion. One could also compare these observables in the vicinity of the QCP between the same DSL and a VBS order. In this case, the ordered phase is described by valley monopoles proliferating following the condensation of a valley-Hall mass in QED_3 [21, 22]. The transition is in the $O(2)$ universality class, as opposed to $O(3)$ for the antiferromagnetic one. However, this difference plays no role at leading order in $1/N$ and the hierarchy is simply inverted, with bond-bond correlations related to the smallest scaling dimension 0.78. Next-to-leading order corrections would be necessary to predict a difference.

The results in this work could be tested numerically. With the many recent numerical investigations of QED_3 with Monte Carlo [17, 63–65] and conformal bootstrap [18, 19], it would be interesting to see similar investigations in the QED_3-GN-like models.

Acknowledgements. We thank Jaume Gomis and Sergueï Tchoumakov for useful discussions. É.D. was funded by an Alexander Graham Bell CGS from NSERC. W.W.-K. was funded by a Discovery Grant from NSERC, a Canada Research Chair, a grant from the Fondation Courtois, and a "Établissement de nouveaux chercheurs et de nouvelles chercheuses universitaires" grant from FRQNT.

2.A. Holonomy of the gauge field

Let us also consider the holonomy of the gauge field on the "thermal" circle.

$$\alpha = \frac{i}{V} \int_{S^2 \times S^1_\beta} d^3x \sqrt{g}\, a_0 \,. \tag{2.A.1}$$

In our mean field ansatz, we now leave open the possibility of a non-trivial expectation value of the gauge field

$$\langle a_0 \rangle = -i\beta^{-1}\alpha\,. \tag{2.A.2}$$

Modifying Eq. (2.3.14) accordingly, the determinant operator becomes

$$\begin{aligned} f_{q;s} = &-\beta^{-1}\sum_{\sigma=\pm1}\sum_{n\in\mathbb{Z}}\Bigg[d_q \ln\Big(\omega_n - i\beta^{-1}\alpha - i\mu'\sigma + i\sigma M_q\Big) \\ &+ \sum_{\ell=q+1}^{\infty} d_\ell \ln\Bigg(\Big(\omega_n - i\beta^{-1}\alpha - i\mu'\sigma\Big)^2 + \varepsilon_\ell^2\Bigg)\Bigg]\,. \end{aligned} \tag{2.A.3}$$

Taking the sum over the mastubara frequencies, the same logic in passing from Eq. (2.3.14) to Eq. (2.3.17) is used

$$\begin{aligned} f_{q;s} = -\beta^{-1}\Bigg[&d_q \ln\Big(2\left[\cosh(\alpha) + \cosh(\beta(M_q - \mu'))\right]\Big) \\ &+ \sum_{\ell=q+1}^{\infty}\sum_{\sigma=\pm1} d_\ell \ln\Big(2\left[\cosh(\beta\varepsilon_\ell) + \cosh\Big(\beta(\sigma\mu' + \beta^{-1}\alpha)\Big)\right]\Big)\Bigg]\,. \end{aligned} \tag{2.A.4}$$

The gap equation for a_0 is

$$\begin{aligned} 0 = \beta\frac{\partial f_{q;s}}{\partial\alpha} = &-d_q\frac{\sinh(\alpha)}{\cosh(\alpha) + \cosh(\beta(M_q - \mu'))} \\ &- \sum_{\ell=q+1}^{\infty}\sum_{\sigma=\pm1}\frac{\sinh(\beta(\sigma\mu' + \beta^{-1}\alpha))}{\cosh(\beta\varepsilon_\ell) + \cosh(\beta(\sigma\mu' + \beta^{-1}\alpha))}\,. \end{aligned} \tag{2.A.5}$$

This vanishes for $\alpha = 0, i\pi$. Inserting this solution in the determinant operator, we obtain

$$\begin{aligned} f^{\pm}_{q;s} = -\beta^{-1}\Bigg[&d_q \ln\Big(2\left[\pm1 + \cosh(\beta(M_q - \mu'))\right]\Big) \\ &+ \sum_{\ell=q+1}^{\infty} 2d_\ell \ln\Big(2\left[\cosh(\beta\varepsilon_\ell) \pm \cosh(\beta\mu')\right]\Big)\Bigg]\,. \end{aligned} \tag{2.A.6}$$

With this, we can proceed to solve the remaining gap equations to find the other mean field parameters in these two cases for $M_q^{\pm}, \mu_S^{\pm}, \Sigma^{\pm}$. At leading order in $1/\beta$, the effective action evaluated at both these saddle points is the same. The partition function obtained by summing over these two saddle points then yields an extra factor of 2, $Z \approx 2e^{-\beta N F^{(0)}_{q;s}}$ where $F^{(0)}_{q;s}$ was found in the main text. We could directly ignore this as $\ln 2 = \mathcal{O}(\beta^0 N^0)$ and the factor does not contribute to the leading order results

$$Z_s[A^q] = \exp\Big\{-\beta N F^{(0)}_{q;s} + \mathcal{O}(\beta^1 N^0, N^1\beta^0)\Big\}\,. \tag{2.A.7}$$

However, it is more interesting to remark that this factor is cancelled with a proper normalization. When computing the scaling dimension $\Delta_{q;s}$, we should actually use the normalized partition function

$$\Delta_{q;s} = -\beta^{-1} \lim_{\beta\to\infty} \ln\left(\frac{Z_s[A^q]}{Z_0[0]}\right) . \tag{2.A.8}$$

Normally, this vacuum parition function is not mentioned, as the free energy usually vanishes, leaving a trivial normalization factor $Z_0[0] = 1$. However, on the "thermal" circle, the non-trivial holonomy also contributes to this partition function. By setting $q = 0$ (and $\mu' = 0$) in the gap equation for a_0, the two solutions for holonomies $\alpha = 0, i\pi$ remain. In this case, $Z_0[0] = 2$, which exactly cancels the extra factor in $Z_s[A^q]$.

2.B. General spin-Hall mass

In this section, we find the monopole scaling dimension using a more general ansatz than the one employed in Sec. 2.3. We let the auxiliary bosons have different orientations. We keep $\boldsymbol{\chi}$ along $\hat{z}$ while the spin-Hall mass is oriented more generally as $\boldsymbol{M}_q = M_q\hat{n}$. The more general determinant operator in Eq. (2.3.12) then becomes

$$\begin{aligned} f_{q;s} = -\beta^{-1} \sum_{n\in\mathbb{Z}} \Bigg[& d_q \ln\det\left[-i(\omega - i\mu'\sigma_z) + \boldsymbol{M}_q\cdot\boldsymbol{\sigma}\right] \\ & + \sum_{\ell=q+1}^{\infty} d_\ell \ln\det\left[-i\boldsymbol{O}_{q,\ell}\left(\omega - i\mu'\sigma_z + i\boldsymbol{P}_{q,\ell}\right) + \boldsymbol{M}_q\cdot\boldsymbol{\sigma}\right] \Bigg] , \end{aligned} \tag{2.B.1}$$

where the matrices $\boldsymbol{O}_{q,\ell}$ and $\boldsymbol{P}_{q,\ell}$ are given by [14, 48]

$$\begin{aligned} \boldsymbol{O}_{q,\ell} &= \frac{1}{\ell}\begin{pmatrix} -q & -\sqrt{\ell^2-q^2} \\ -\sqrt{\ell^2-q^2} & q \end{pmatrix} , \\ \boldsymbol{P}_{q,\ell} &= \frac{\sqrt{\ell^2-q^2}}{\ell}\begin{pmatrix} \sqrt{\ell^2-q^2} & -q \\ -q & -\sqrt{\ell^2-q^2} \end{pmatrix} . \end{aligned} \tag{2.B.2}$$

The spin-Hall mass $\boldsymbol{M}_q$ may be parameterized by its norm M_q and two angles (ϑ, φ) for its orientation $\hat{n}$

$$M_q\hat{n} = M_q\left(\sin\vartheta\cos\varphi, \sin\vartheta\sin\varphi, \cos\vartheta\right) . \tag{2.B.3}$$

The determinant operator can be diagonalized in the magnetic spin subspace

$$\begin{aligned} f_{q;s} = -\beta^{-1}\Bigg(& d_q \ln\left[2\left(1+\cosh\left(\beta\sqrt{M_q^2\sin^2\vartheta+(M_q\cos\vartheta-\mu')^2}\right)\right)\right] \\ & + 2\sum_{\sigma=\pm1}\sum_{\ell=q+1}^{\infty} d_\ell \ln\left[2\cosh\left(\frac{\beta}{2}\epsilon_{\ell,\vartheta,\sigma}\right)\right]\Bigg)\,, \end{aligned} \tag{2.B.4}$$

where

$$\epsilon_{\ell,\vartheta,\sigma} = \sqrt{\left(\sqrt{\ell^2-q^2+M_q^2\cos^2\vartheta}+\sigma\mu'\right)^2+M_q^2\sin^2\vartheta}\,. \tag{2.B.5}$$

For convienience, we may write this as

$$\epsilon_{\ell,\vartheta,\sigma} \equiv \sqrt{(\varepsilon_{\ell,\vartheta}+\sigma\mu')^2+M_q^2\sin^2\vartheta}\,, \tag{2.B.6}$$

where

$$\varepsilon_{\ell,\vartheta} = \sqrt{\ell^2-q^2+M_q^2\cos^2\vartheta}\,. \tag{2.B.7}$$

For $\vartheta = 0,\pi$, this corresponds to the eigenvalue ε_ℓ defined in the main text.

We note that the determinant operator (2.B.4) is independent of φ which indicates an azimutal symmetry. By setting $\vartheta = 0$, the determinant operator used in the main text (2.3.17) is retrieved. As shown in Eq. (2.3.11), the full free energy expression is given by $F^{(0)}_{q;s} = f_{q;s} + \frac{\mu'}{m_s}\left(s^2+m_s^2\right)$. Inserting Eq. (2.B.4) in this last expression, it is found that the free energy is invariant under

$$\vartheta \to \pi - \vartheta\,, \quad m_s \to -m_s\,, \tag{2.B.8}$$

where the last transformation also implies $\mu' \to -\mu'$ (2.3.13). This means that $\vartheta = \pi$ and $m_s = s$ is a solution with the same free energy as the $\vartheta = 0$ and $m_s = -s$ solution found in the main text. For this second solution, the spin polarization and the spin-Hall mass are still anti-aligned.

For later convenience, we write explicitly the free energy. We may already take the large-β limit for the non-zero modes as ℓ^2-q^2 is order $\mathcal{O}(\beta^0)$ which lets us take $\log\left[2\cosh\left(\beta\epsilon_{\ell,\vartheta,\sigma}/2\right)\right] \to \beta\epsilon_{\ell,\vartheta,\sigma}/2$. In this limit, the free energy is given by

$$\begin{aligned} F^{(0)}_{q;s} = & -\beta^{-1} d_q \ln\left[2\left(1+\cosh\left(\beta\sqrt{M_q^2\sin^2\vartheta+(M_q\cos\vartheta-\mu')^2}\right)\right)\right] \\ & + \frac{\mu'}{m_s}\left(s^2+m_s^2\right) - \sum_{\sigma=\pm1}\sum_{\ell=q+1}^{\infty} d_\ell \epsilon_{\ell,\vartheta,\sigma}\,. \end{aligned} \tag{2.B.9}$$

2.B.1. Gap equations

The gap equations are obtained by varying $F^{(0)}_{q;s}$ with respect to the original saddle point parameters $M_q, \mu_S, P_z, \vartheta$. In this more general case, the gap equations for μ_S and P_z,

$$\tfrac{1}{2} m_s \partial_{\mu'} f_{q;s} + s^2 = 0\,, \tag{2.B.10}$$

$$\sqrt{\tfrac{\mu_S}{2}}\left(\partial_{\mu'} f_{q;s} + 2m_s\right) = 0\,, \tag{2.B.11}$$

can still be combined to yield the condition $m_s^2 = s^2$ if $\mu_s \neq 0$. We are then left with a system of three gap equations

$$\partial_{M_q} f_{q;s} = 0\,, \tag{2.B.12}$$

$$\partial_{\mu'} f_{q;s} - 2m_s = 0\,, \tag{2.B.13}$$

$$\partial_{\vartheta} f_{q;s} = 0\,, \tag{2.B.14}$$

where the second equation is the gap equation for P_z divided by $\sqrt{\mu_S/2}$. The explicit expression for the gap equations is given by

$$-\left(\frac{M_q - \mu' \cos\vartheta}{M_q \cos\vartheta - \mu'}\right) C - \frac{M_q}{2} \sum_{\sigma} \sum_{\ell} d_\ell \left(\frac{\varepsilon_{\ell,\vartheta} + \cos^2\vartheta \mu' \sigma}{\varepsilon_{\ell,\vartheta}\, \epsilon_{\ell,\vartheta,\sigma}}\right) = 0\,, \tag{2.B.15}$$

$$C - 2m_s - \frac{1}{2} \sum_{\sigma} \sum_{\ell} d_\ell\, \sigma \left(\frac{\varepsilon_{\ell,\vartheta} + \mu' \sigma}{\epsilon_{\ell,\vartheta,\sigma}}\right) = 0\,, \tag{2.B.16}$$

$$-\left(\frac{\mu' M_q \sin\vartheta}{M_q \cos\vartheta - \mu'}\right) C + \frac{M_q^2 \mu' \sin\vartheta\cos\vartheta}{2} \sum_{\sigma} \sum_{\ell} d_\ell \frac{\sigma}{\varepsilon_{\ell,\vartheta}} \frac{1}{\epsilon_{\ell,\vartheta,\sigma}} = 0\,, \tag{2.B.17}$$

where C is defined as

$$C = \frac{d_q \left(M_q \cos\vartheta - \mu'\right) \tanh\left(\frac{1}{2}\beta \sqrt{\mu'^2 - 2\mu' M_q \cos\vartheta + M_q^2}\right)}{\sqrt{\mu'^2 - 2\mu' M_q \cos\vartheta + M_q^2}}\,. \tag{2.B.18}$$

2.B.2. Analytical solutions for $\vartheta \in \{0, \pi/2, \pi\}$

We first focus on the cases $\vartheta \in \{0, \pi/2, \pi\}$. For these angles, the sum over non-"zero" modes in the ϑ gap equation (2.B.17) does not contribute as it is proportional to $\sin\vartheta\cos\vartheta \to 0$. The sum in the second gap equation (2.B.16) also vanishes if we suppose that $\mu' < \varepsilon_\ell$ for $\vartheta = 0, \pi$ and $\mu' \sim \mathcal{O}(1/\beta)$ for $\vartheta = \pi/2$. In this case, $(\varepsilon_{\ell,\vartheta} + \mu'\sigma)/\epsilon_{\ell,\vartheta,\sigma} \to 1$ and the two terms in the sum over σ cancel each other. Later on, we see that this assumption does allow to find

a solution. The gap equations then become

$$-\left(\frac{M_q-\mu'\cos\vartheta}{M_q\cos\vartheta-\mu'}\right)C-\frac{M_q}{2}\sum_\sigma\sum_\ell d_\ell\left(\frac{\varepsilon_{\ell,\vartheta}+\cos^2\vartheta\mu'\sigma}{\varepsilon_{\ell,\vartheta}\,\epsilon_{\ell,\vartheta,\sigma}}\right)=0\,, \tag{2.B.19}$$

$$C-2m_s=0\,, \tag{2.B.20}$$

$$-\left(\frac{\mu' M_q\sin\vartheta}{M_q\cos\vartheta-\mu'}\right)C=0\,. \tag{2.B.21}$$

The gap equation for ϑ (2.B.21) is solved trivially for $\vartheta=0,\pi$. If $\vartheta=\pi/2$, it requires $M_q=0$. As for the second equation derived from $\partial F_q^{(0)}/\partial P_z$ (2.B.20), it is solved with the following μ'

$$\mu'=M_q\cos\vartheta+\beta^{-1}\ln\left(\frac{1+2m_s/d_q}{1-2m_s/d_q}\right)\,. \tag{2.B.22}$$

Using all previous results, the remaining gap equation becomes

$$-2\,\mathrm{sgn}(\cos\vartheta)m_s-2M_q\sum_\ell d_\ell\varepsilon_\ell^{-1}=0\,, \tag{2.B.23}$$

where $\mathrm{sgn}(0)=0$. For $\vartheta=\pi/2$, the first term vanishes and the gap equation is solved since it was established that $M_q=0$ for this angle. For $\vartheta=0,\pi$ and $m_s=-\,\mathrm{sgn}(\cos\vartheta)s$, we retrieve the same gap equation as in the main text (2.3.26). Putting together all the previous results, we can also find back the scaling dimension in Eq. (2.3.27). As for $\vartheta=\pi/2$, the only term that contributes to the free energy (2.3.11) at leading order in $1/\beta$ is the sum over non-"zero" modes. Thus, the free energy becomes

$$F^{(0)}_{q;s}\big|_{\vartheta=\pi/2}=-2\sum_\ell d_\ell\varepsilon_\ell|_{M_q=0}+\mathcal{O}(1/\beta)\,. \tag{2.B.24}$$

This is the free energy we would obtain in QED_3. The scaling dimension for $\vartheta=\pi/2$ is thus larger than for $\vartheta=0,\pi$. This solution should thus be discarded as it is not a global minimum.

2.B.3. Numerical study for $0<\vartheta<\frac{\pi}{2}$

We found two minima of free energy for $\vartheta=0,\pi$ and a maximum for $\vartheta=\pi/2$. Other values of ϑ cannot be solved so simply. This is because the sum over non-"zero" modes contributions doesn't simplify like it does for $\vartheta\in\{0,\pi/2,\pi\}$. In this case, we resort to solving the gap equations numerically.

We search the root of the three gap equations (2.B.15 - 2.B.17) yielding the solution for M_q, μ' and ϑ (the solution for the polarization is already known, $m_s = -2s\,\mathrm{sgn}(\cos\vartheta)$). Had we not taken the large-β limit for non-"zero" modes starting from Eq. (2.B.9), the sums would also contain a factor $\tanh(\beta\epsilon_{\ell,\vartheta,\sigma}/2)$. We reinstate this factors in our numerical analysis as we take finite beta. We will set $q = 1/2$ and $s = s_{\max}/2$, but the situation is similar for other topological charges and magnetic spins.

To solve the gap equations, we first seek a solution of the first two gap equations with a fixed value for ϑ. We then insert the solutions for M_q and μ' and the fixed value of ϑ in the last gap equation to see if it is satisfied, i.e. $\partial F_q^{(0)}/\partial\vartheta$ should vanish. As shown in Fig. 2.5(a), the only would-be solution in the range $0 < \vartheta < \pi/2$ occurs when $\mu' = 0$. However, this contradicts the assumption that $\mu_S \neq 0$ unless we take $m_s = 0$. The full treatment of the four gap equations, without assuming $\mu_S \neq 0$, yields the same solution. In the case where $\mu' = 0$, the gap equation for μ_S yields the condition $m_s \cos\vartheta = -2s^2/d_q$. As we enforced $m_s = -s$ in the range $0 < \vartheta < \pi/2$, the numerical solution indeed occurs at $\vartheta = \arccos(2s/d_q)$, as shown in Fig. 2.5(a). However, as argued in the main text and further in App. App. 2.C, this solution has divergences in the second derivatives of the free energy and should be discarded.

A closer look at the situation near $\vartheta = 0$ is shown in Fig. 2.5(b). The solution obtained in the main text is recovered in this limit as $M_q \to 0.14$ and $\exp\{\beta(\mu' - M_q\cos\vartheta)\} \to 1/3$ which are the expected values for $q = 1/2$ and $s = s_{\max}/2$ (see Fig. 2.1 and Eq. (2.B.22) with $m_s = -s$).

As for the $\vartheta = \pi/2$ solution, Fig. 2.5(a) near $\pi/2$ is a bad starting point. Seeking solutions in another part of the parameters' space as shown in Fig. 2.6, we do recover the $\vartheta = \pi/2$ solution for which $M_q \to 0$, and, again, $\exp\{\beta(\mu' - M_q\cos\vartheta)\} \to 1/3$.

We found no other solutions numerically. This justifies our assumption in the main text where we worked only with $\vartheta = 0$.

2.C. Gap equations and $\mu' = 0$

In the main text, we obtained three gap equations (2.3.18-2.3.20) for M_q, μ_S and P_z, respectively. The third one can be solved for $\mu_S = P_z = 0$. This also means that $\mu' = 0$. The

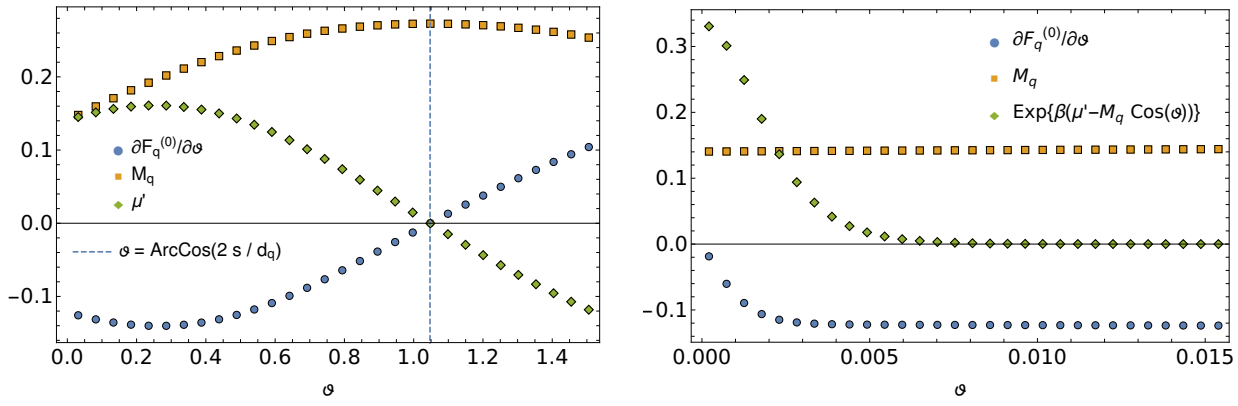

(a) (b)

Figure 2.5. Numerical investigation of possible solutions to the gap equations for a) $0 < \vartheta < \pi/2$ and b) near $\vartheta = 0$. We set $\beta = 10^4$. Values of M_q and μ' are found by solving Eqs. (2.B.15-2.B.16) at fixed ϑ. $\partial F_q^{(0)}/\partial\vartheta$ which yields the LHS of the remaining gap equation becomes 0 for $\vartheta = 0$ and $\vartheta = \arccos(2s/d_q)$.

first gap equation then simply becomes

$$-d_q - 2M_q \sum_{\ell=q+1}^{\infty} d_\ell \varepsilon_\ell^{-1} = 0\,, \tag{2.C.1}$$

which can be written as

$$-2s_{\max} - 2M_q \sum_{\ell=q+1}^{\infty} d_\ell \varepsilon_\ell^{-1} = 0\,. \tag{2.C.2}$$

This has the same form as the gap equation found in the main text (2.3.26) yields as a solution the maximal possible spin-Hall mass. As for the free energy, it also takes the form obtained in the main text for a maximal spin

$$F_{q;s}^{(0)} = -2M_q s_{\max} - 2\sum_{\ell=q+1} d_\ell \varepsilon_\ell + \mathcal{O}(\beta^{-1})\,. \tag{2.C.3}$$

This solution with $\mu' = 0$ thus seems to indicate a smaller scaling dimension that the one proposed in the main text where $s_{\max} \to s$. However, by inspecting the second derivatives of the free energy at this saddle point, divergences are found. The third gap equation can be derived with respect to μ_S

$$\frac{\partial^2 F_{q;s}^{(0)}}{\partial\mu_S \partial P_z} = \frac{1}{2\sqrt{\mu_S}}\partial_{\mu'} f_{q;s} + \frac{1}{2} m_s \sqrt{\frac{\mu_S}{2}}\partial_{\mu'}\partial_{\mu'} f_{q;s}\,. \tag{2.C.4}$$

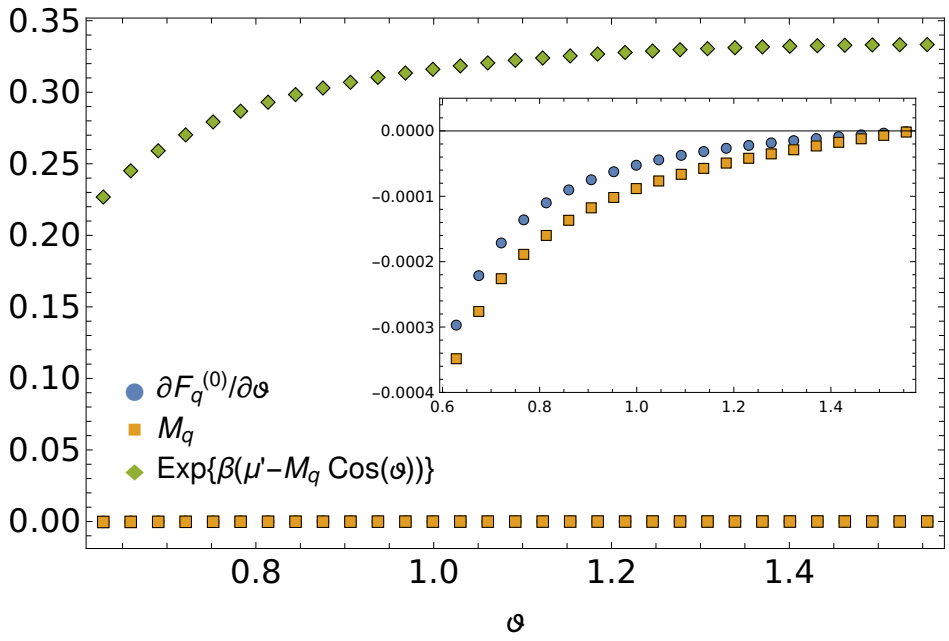

Figure 2.6. Numerical investigation of possible solutions to the gap equations for near $\vartheta = \pi/2$. Values of M_q and μ' are found by solving Eqs. (2.B.15-2.B.16) at fixed ϑ. We set $\beta = 10^4$. The solution at $\pi/2$ where $\partial F_q^{(0)}/\partial\vartheta \to 0$ lies in a different region of parameters' space than the one considered in Fig. 2.5(a). Here, $M_q \to 0$.

Developing this and taking the large-β limit, this becomes

$$\frac{\partial^2 F^{(0)}_{q;s}}{\partial\mu_S \partial P_z} = \frac{1}{2\sqrt{\mu_S}}\,, \tag{2.C.5}$$

which is singular. This shows how this solution has a bad behavior and should be ignored.

2.D. Regularized gap equation and scaling dimension

The free energy used to find the monopole scaling dimension has a diverging sum $\sum_{\ell=q+1}^{\infty} d_\ell \varepsilon_\ell$, where the degeneracy and energy are defined in Eq. (2.3.15). By obtaining the first two orders in the $1/\ell$ expansion of the summand

$$d_\ell \varepsilon_\ell = 2\ell^2 + (M_q^2 - q^2) + \mathcal{O}(\ell^{-2}) \equiv d_\ell \varepsilon_\ell^{\text{div}} + \mathcal{O}(\ell^{-2})\,, \tag{2.D.1}$$

the diverging sum can be rewritten as

$$\sum_{\ell=q+1}^{\infty} d_\ell \varepsilon_\ell = \sum_{\ell=q+1}^{\infty} d_\ell (\varepsilon_\ell - \varepsilon_\ell^{\text{div}}) + \sum_{\ell=q+1}^{\infty} d_\ell \varepsilon_\ell^{\text{div}}\,. \tag{2.D.2}$$

In this expression, the first sum is convergent

$$\sum_{\ell=q+1}^{\infty} d_\ell(\varepsilon_\ell - \varepsilon_\ell^{\rm div}) = \sum_{\ell=q+1}^{\infty} \left[d_\ell \varepsilon_\ell - \frac{1}{2} d_\ell^2 - (M_q^2 - q^2) \right] , \tag{2.D.3}$$

while the second sum is divergent

$$\sum_{\ell=q+1}^{\infty} d_\ell \varepsilon_\ell^{\rm div} = 2 \sum_{\ell=q+1}^{\infty} \left[\ell^{2(1-s)} + \left(\frac{1}{2} - s \right) \left(M_q^2 - q^2 \right) \ell^{-2s} \right] \Big|_{s=0} . \tag{2.D.4}$$

This divergent sum may be continued analytically to the Hurwitz zeta function $\sum_{k=0}^{\infty}(k+a)^{-s} = \zeta(s,a)$ [66]

$$\begin{aligned} \sum_{\ell=q+1}^{\infty} d_\ell \varepsilon_\ell^{\rm div} &= 2 \sum_{\ell=0}^{\infty} (\ell + (q+1))^2 + \left(M_q^2 - q^2 \right) \sum_{\ell=0}^{\infty} (\ell + (q+1))^0 \\ &= 2\zeta(-2,q+1) + \left(M_q^2 - q^2 \right) \zeta(0,q+1) \end{aligned} \tag{2.D.5}$$

Replacing the zeta functions with their polynomial expressions, we obtain

$$\sum_{\ell=q+1}^{\infty} d_\ell \varepsilon_\ell^{\rm div} = \frac{1}{2}(2q+1) \left(\frac{q(q-2)}{3} - M_q^2 \right) . \tag{2.D.6}$$

Using these results, we obtain the regularized version of the gap equation (2.3.27)

$$\begin{aligned} \frac{\Delta_{q;s}}{2N} = &-2s d_q M_q + (2q+1) \left(M_q^2 - \frac{q(q-2)}{3} \right) \\ &- \sum_{\ell=q+1}^{\infty} \left[2 d_\ell \varepsilon_\ell - d_\ell^2 - 2 \left(M_q^2 - q^2 \right) \right] , \end{aligned} \tag{2.D.7}$$

where the spin-Hall mass M_q is determined by the regularized version of the gap equation (2.3.26)

$$-2s d_q + 2M_q \left(2q + 1 - \sum_{\ell=q+1}^{\infty} \left[d_\ell \varepsilon_\ell^{-1} - 2 \right] \right) = 0 . \tag{2.D.8}$$

2.E. Representation of $q = 1/2$ monopoles for $N = 2$

We can generally write a monopole operator as

$$\mathcal{M}_I^\dagger = D_I^\dagger \mathcal{M}_{\rm Bare}^\dagger , \tag{2.E.1}$$

where $D_I^\dagger$ is an operator that creates half of all zero modes available. For $N = 2$ and $q = 1/2$, $D_I^\dagger$ corresponds to a zero modes creation operators bilinear $c^\dagger A_I (c^\dagger)^\intercal$ as in Eq. (2.5.3). Taking

the z axis as the spin quantization axis, monopoles in the helicity basis are written as follows

$$D^\dagger_\downarrow = \frac{1}{2}c^\dagger\left[\frac{1-\sigma_z}{2}\otimes i\mu_y\right](c^\dagger)^\intercal = \frac{1}{2}\left(c^\dagger_{L\downarrow}c^\dagger_{R\downarrow} - c^\dagger_{R\downarrow}c^\dagger_{L\downarrow}\right), \tag{2.E.2}$$

$$D^\dagger_\uparrow = \frac{1}{2}c^\dagger\left[\frac{1+\sigma_z}{2}\otimes i\mu_y\right](c^\dagger)^\intercal = \frac{1}{2}\left(c^\dagger_{L\uparrow}c^\dagger_{R\uparrow} - c^\dagger_{R\uparrow}c^\dagger_{L\uparrow}\right), \tag{2.E.3}$$

$$D^\dagger_{\uparrow\downarrow} = \frac{1}{2}c^\dagger\left[\frac{\sigma_x}{\sqrt{2}}\otimes i\mu_y\right](c^\dagger)^\intercal = \frac{1}{2}\left[\frac{\left(c^\dagger_{L\uparrow}c^\dagger_{R\downarrow} + c^\dagger_{L\downarrow}c^\dagger_{R\uparrow}\right)}{\sqrt{2}} - (L\leftrightarrow R)\right]. \tag{2.E.4}$$

For example, the spin down monopole acting on the vacuum $D^\dagger_\downarrow\mathcal{M}^\dagger_{\text{Bare}}|0\rangle$ may schematically be represented as shown in Fig. 2.7.

Figure 2.7. Schematic representation of the spin down monopole with the fermion zero modes occupation.

We may reorganize the monopoles in the real vector basis used in the main text in Eqs. (2.5.4) and (2.5.5)

$$\begin{pmatrix} \mathcal{M}_\downarrow - \mathcal{M}_\uparrow \\ -i\left(\mathcal{M}_\downarrow + \mathcal{M}_\uparrow\right) \\ \sqrt{2}\mathcal{M}_{\uparrow\downarrow} \end{pmatrix} = \frac{1}{2}c^\dagger\left[\sigma_y\boldsymbol{\sigma}\otimes\mu_y\right](c^\dagger)^\intercal\mathcal{M}^\dagger_{\text{Bare}}. \tag{2.E.5}$$

The same can be done for monopoles in the nodal triplet by simply exchanging spin and valley indices $\uparrow,\downarrow\leftrightarrow L,R$.

2.E.1. SU(2) × SU(2) generators

Generators T_a of the SU(4) algebra may be realized with one zero mode creation operator and one zero mode destruction operator

$$T_a = c^\dagger\mathcal{O}_a c. \tag{2.E.6}$$

For example, we may identify the raising spin operator, which is part of the $\text{SU(2)}_{\text{Spin}}\otimes\text{SU(2)}_{\text{Nodal}}$ subalgebra of SU(4), as

$$\mathfrak{s}_+ = \frac{1}{2}c^\dagger\left(\left(\sigma_x + i\sigma_y\right)\otimes\mathbb{1}\right)c = c^\dagger_{L\uparrow}c_{L\downarrow} + c^\dagger_{R\uparrow}c_{R\downarrow}. \tag{2.E.7}$$

Under the action of this operator, the spin down monopole transforms in other monopoles in spin triplet while the monopoles in the nodal triplet are annhiliated

$$\mathfrak{s}_+\mathfrak{s}_+\mathcal{M}_\downarrow = \sqrt{2}\mathfrak{s}_+\mathcal{M}_{\uparrow\downarrow} = 2\mathcal{M}_\uparrow\,, \tag{2.E.8}$$

$$\mathfrak{s}_+\mathcal{M}_R = \mathfrak{s}_+\mathcal{M}_{LR} = \mathfrak{s}_+\mathcal{M}_L = 0\,. \tag{2.E.9}$$

The factors involved are the usual total magnetic spin eigenvalue $\sqrt{s(s+1)}$. One may also define the lowering spin and the azimutal spin number operators, respectively given by

$$\mathfrak{s}_- = \mathfrak{s}_+^\dagger\,, \quad \mathfrak{s}_z = \frac{1}{2}c^\dagger\left(\sigma_z \otimes \mathbb{1}\right)c = \frac{1}{2}(c_{L\uparrow}^\dagger c_{L\uparrow} - c_{L\downarrow}^\dagger c_{L\downarrow} + (L \leftrightarrow R))\,. \tag{2.E.10}$$

It is simple to show that these operators obey the SU(2) algebra commutation relations $[\mathfrak{s}_+, \mathfrak{s}_-] = 2\mathfrak{s}_z$. Again, analogous valley operators $\mathfrak{v}$ may be constructed by the exchange $\uparrow,\downarrow \leftrightarrow\ L, R$. The action of these SU(2) × SU(2) generators $\{\mathfrak{s}_-, \mathfrak{s}_z, \mathfrak{s}_+, \mathfrak{v}_-, \mathfrak{v}_z, \mathfrak{v}_+\}$ on the monopole operators is shown in Table 2.2. It is readily seen that the monopole spin and nodal triplets form a reducible representation of SU(2) × SU(2).

Tableau 2.2. The monopoles form a reducible representation $(\mathbf{3},\mathbf{1})\oplus(\mathbf{1},\mathbf{3})$ of SU(2)×SU(2) (helicity basis).

	$\mathcal{M}^\downarrow$	$\mathcal{M}^\uparrow$	$\mathcal{M}^{\uparrow\downarrow}$	$\mathcal{M}^R$	$\mathcal{M}^L$	$\mathcal{M}^{LR}$
$\frac{1}{\sqrt{2}}\mathfrak{s}_+$	$\mathcal{M}^{\uparrow\downarrow}$	0	$\mathcal{M}^\uparrow$	0	0	0
$\mathfrak{s}_z$	$-\mathcal{M}^\downarrow$	$\mathcal{M}^\uparrow$	0	0	0	0
$\frac{1}{\sqrt{2}}\mathfrak{s}_-$	0	$\mathcal{M}^{\uparrow\downarrow}$	$\mathcal{M}^\downarrow$	0	0	0
$\frac{1}{\sqrt{2}}\mathfrak{v}_+$	0	0	0	$\mathcal{M}^{LR}$	0	$\mathcal{M}^L$
$\mathfrak{v}_z$	0	0	0	$-\mathcal{M}^R$	$\mathcal{M}^L$	0
$\frac{1}{\sqrt{2}}\mathfrak{v}_+$	0	0	0	0	$\mathcal{M}^{LR}$	$\mathcal{M}^R$

2.E.2. Rotation of spin monopoles

We may explicitly show the rotation of spin monopoles mentioned in the main text. To do so, we first rexpress monopoles in the real vector representation (2.E.5) in the following

basis

$$\begin{pmatrix}1\\0\\0\end{pmatrix} = \frac{1}{\sqrt{2}}\left(\mathcal{M}_\downarrow - \mathcal{M}_\uparrow\right) , \quad \begin{pmatrix}0\\1\\0\end{pmatrix} = \frac{-i}{\sqrt{2}}\left(\mathcal{M}_\downarrow + \mathcal{M}_\uparrow\right) , \quad \begin{pmatrix}0\\0\\1\end{pmatrix} = \mathcal{M}_{\uparrow\downarrow} . \tag{2.E.11}$$

In this real basis, the angular momentum operators take the form $(J^I)_{jk} = \epsilon_{Ijk}$. Considering an SU(2) transformation of the fermions

$$\Psi \to e^{i\boldsymbol{\theta}\cdot\boldsymbol{\sigma}}\Psi , \tag{2.E.12}$$

we can find the transformation of the vector representations. The fermion bilinears and the monopoles transform a bit differently

$$\bar{\Psi}\sigma_i\Psi \to \bar{\Psi}e^{-i\boldsymbol{\vartheta}\cdot\boldsymbol{\sigma}}\sigma_i e^{i\boldsymbol{\vartheta}\cdot\boldsymbol{\sigma}}\Psi = R_{ij}\bar{\Psi}\sigma_j\Psi , \tag{2.E.13}$$

$$c^\dagger(i\sigma_y\sigma_i)(c^\dagger)^\intercal \to c^\dagger(i\sigma_y)e^{i\boldsymbol{\vartheta}\cdot\boldsymbol{\sigma}^\intercal}\sigma_i e^{-i\boldsymbol{\vartheta}\cdot\boldsymbol{\sigma}^\intercal}(c^\dagger)^\intercal = \tilde{R}_{ij}c^\dagger(i\sigma_y\sigma_j)(c^\dagger)^\intercal , \tag{2.E.14}$$

where $\tilde{R}_{ij} = R_{ij}|_{\vartheta_{x,z}\to-\vartheta_{x,z}}$ and we used the fact that $(\boldsymbol{\vartheta}\cdot\boldsymbol{\sigma})\sigma_y = -\sigma_y(\boldsymbol{\vartheta}\cdot\boldsymbol{\sigma}^\intercal)$. We will perform these rotations explicitly on the spin-Hall mass $\bar{\Psi}\sigma_z\Psi$ and the spin down monopole $\mathcal{M}_\downarrow$. In the real vector basis, they are expressed as

$$\bar{\Psi}\sigma_z\Psi = \begin{pmatrix}0\\0\\1\end{pmatrix} , \quad \mathcal{M}_\downarrow = \frac{1}{\sqrt{2}}\begin{pmatrix}-i\\1\\0\end{pmatrix} . \tag{2.E.15}$$

We can compare how these vectors rotate along the y axis. In this case, they are transformed by the same rotation matrix

$$R_{\vartheta_y} = \tilde{R}_{\vartheta_y} = \begin{pmatrix}\cos\vartheta_y & 0 & \sin\vartheta_y\\ 0 & 1 & 0\\ -\sin\vartheta_y & 0 & \cos\vartheta_y\end{pmatrix} . \tag{2.E.16}$$

We first consider a rotation $\vartheta_y = \pi/2$ that sends the quantization axis in the $x-y$ plane. The spin-Hall mass is rotated to $\bar{\Psi}\sigma_x\Psi$

$$R_{\vartheta_y=\pi/2}\left(\bar{\Psi}\sigma_z\Psi\right) = \begin{pmatrix}0 & 0 & 1\\ 0 & 1 & 0\\ -1 & 0 & 0\end{pmatrix}\begin{pmatrix}0\\0\\1\end{pmatrix} = \begin{pmatrix}1\\0\\0\end{pmatrix} = \bar{\Psi}\sigma_x\Psi . \tag{2.E.17}$$

As for the spin down monopole, it is rotated to a combination of all the monopoles (in the helicity basis) of the spin triplet

$$R_{\vartheta_y=\pi/2}\mathcal{M}_\downarrow = \frac{1}{\sqrt{2}}\begin{pmatrix} 0 & 0 & 1 \\ 0 & 1 & 0 \\ -1 & 0 & 0 \end{pmatrix}\begin{pmatrix} -i \\ 1 \\ 0 \end{pmatrix} = \frac{1}{\sqrt{2}}\begin{pmatrix} 0 \\ 1 \\ i \end{pmatrix} = \frac{1}{2}\left(\mathcal{M}_\downarrow + \mathcal{M}_\uparrow\right) - \frac{1}{\sqrt{2}}\mathcal{M}_{\uparrow\downarrow}\,. \quad (2.E.18)$$

This is an eigenstate of the angular momentum oriented along $\hat{x}$, $(J_x)_{ij} = \epsilon_{1ij}$. Indeed, $J_x R_{\pi/2}\mathcal{M}_\downarrow = -R_{\pi/2}\mathcal{M}_\downarrow$. This monopole operator now creates a state with $S_x = -1$ which minimizes the rotated spin-Hall mass $\bar{\Psi}\sigma_x\Psi$.

The $\vartheta_y = \pi$ rotation is more simple. In this case

$$R_{\vartheta_y=\pi}\bar{\Psi}\sigma_z\Psi = \begin{pmatrix} -1 & 0 & 0 \\ 0 & 1 & 0 \\ 0 & 0 & -1 \end{pmatrix}\begin{pmatrix} 0 \\ 0 \\ 1 \end{pmatrix} = -\bar{\Psi}\sigma_z\Psi\,, \quad (2.E.19)$$

$$R_{\vartheta_y=\pi}\mathcal{M}_\downarrow = \begin{pmatrix} -1 & 0 & 0 \\ 0 & 1 & 0 \\ 0 & 0 & -1 \end{pmatrix}\frac{1}{\sqrt{2}}\begin{pmatrix} -i \\ 1 \\ 0 \end{pmatrix} = \frac{1}{\sqrt{2}}\begin{pmatrix} i \\ 1 \\ 0 \end{pmatrix} = \mathcal{M}_\uparrow\,. \quad (2.E.20)$$

Thus, the mass is shifted $\bar{\Psi}\sigma_z\Psi \to -\bar{\Psi}\sigma_z\Psi$ while the spin down monopole is rotated to the spin up monopole $\mathcal{M}_\downarrow \to \mathcal{M}_\uparrow$, just as expected. This situation was shown in Fig. 2.4

2.E.3. Computing the spin-Hall energy

We may also explicitly compute the energy of the spin-Hall mass term for the state $|\psi_I\rangle = \mathcal{M}_I^\dagger|0\rangle$ in the three situations considered above. i) For the spin down monopole, the state is $\mathcal{M}_\downarrow^\dagger|0\rangle = |\downarrow\downarrow\rangle \equiv |s=1, m_s=-1\rangle$. The energy of the spin-Hall mass term oriented along $\hat{z}$ for this state is

$$M_q(\sigma_z \otimes \mathbb{1} + \mathbb{1} \otimes \sigma_z)\,|\downarrow\downarrow\rangle = -2M_q\,|\downarrow\downarrow\rangle\ . \quad (2.E.21)$$

ii) After the $\pi/2$ rotation, the related state may be written using (2.E.18)

$$R_{\vartheta_y=\pi/2}\mathcal{M}_\downarrow^\dagger|0\rangle = \frac{|\downarrow\downarrow\rangle + |\uparrow\uparrow\rangle - |\downarrow\uparrow\rangle - |\uparrow\downarrow\rangle}{2}\,, \quad (2.E.22)$$

while the spin-Hall mass becomes oriented along $\hat{x}$. Its energy contribution to this state remains $-2M_q$

$$M_q(\sigma_x \otimes \mathbb{1} + \mathbb{1} \otimes \sigma_x)\Big(R_{\vartheta_y=\pi/2}\mathcal{M}^\dagger_\downarrow |0\rangle\Big) \tag{2.E.23}$$

$$= M_q \frac{[(|\uparrow\downarrow\rangle + |\downarrow\uparrow\rangle - |\uparrow\uparrow\rangle - |\downarrow\downarrow\rangle) + (|\downarrow\uparrow\rangle + |\uparrow\downarrow\rangle - |\downarrow\downarrow\rangle - |\uparrow\uparrow\rangle)]}{2}$$

$$= -2M_q\Big(R_{\vartheta_y=\pi/2}\mathcal{M}^\dagger_\downarrow |0\rangle\Big)\,. \tag{2.E.24}$$

iii) Finally, after the π rotation, the state and the action of the spin-Hall mass are as expected

$$R_{\vartheta_y=\pi}\mathcal{M}^\dagger_\uparrow |0\rangle = |\uparrow\uparrow\rangle\ , \quad -M_q(\sigma_z \otimes \mathbb{1} + \mathbb{1} \otimes \sigma_z)\,|\uparrow\uparrow\rangle = -2M_q\,|\uparrow\uparrow\rangle\ . \tag{2.E.25}$$

2.F. General reduction problem

2.F.1. A relation with the permutation group

There is an ambiguity when discussing the reduction $\mathrm{SU}(2N) \to \mathrm{SU}(2) \times \mathrm{SU}(N)$ as the $\mathrm{SU}(2) \times \mathrm{SU}(N)$ subgroup of $\mathrm{SU}(2N)$ is not uniquely defined. The subgroup $\mathrm{SU}(2) \times \mathrm{SU}(N)$ describing the QED_3-cHGN model is not the same as the one obtained by the chain $\mathrm{SU}(2N) \supset \mathrm{SU}(N) \times \mathrm{SU}(N) \supset \mathrm{SU}(2) \times \mathrm{SU}(N)$. The two subgroups have different branching rules. In this regard, it is useful to consider a more general reduction problem

$$\mathrm{SU}(MN) \to \mathrm{SU}(M) \times \mathrm{SU}(N)\,, \tag{2.F.1}$$

where M and N are integers, and our case corresponds to $M = 2$ and $N = N$.

We note in passing that this embedding in a larger symmetry group is also used to find the multiplicity of flux operators that transform as Lorentz scalars. For topological charges larger than the minimum $q = 1/2$, the number of zero modes dressing a monopole (2.5.2) is $4|q|N$ rather than $2N$. However, starting with requirement that half of zero modes should be filled, it is natural to first build a rank-$2|q|N$ completely antisymmetric irrep of $\mathrm{SU}(4|q|N)$. As an intermediate step to reduce this to the real symmetry group $\mathrm{SU}(2) \times \mathrm{SU}(2N)$, one can consider the reduction $\mathrm{SU}(4|q|N) \to \mathrm{SU}(2|q|) \times \mathrm{SU}(2N)$ [14, 19, 26] which corresponds to setting $M = 2|q|$ and $N = 2N$.

The generators of SU(MN) may be parameterized by taking Kronecker products of the SU(M) and SU(N) generators

$$\mathrm{SU}(MN): \quad T_a^{MN} \in \{T_{a'}^M \otimes \mathbb{1}, \mathbb{1} \otimes T_{a''}^N, T_{a'}^M \otimes T_{a''}^N\}\,, \tag{2.F.2}$$

where $a \in \{1, \ldots, (MN)^2 - 1\}$, $a' \in \{1, \ldots, (M)^2 - 1\}$ and $a'' \in \{1, \ldots, (N)^2 - 1\}$. The subgroup SU($M$) $\times$ SU(N) is completely defined by the set of unbroken generators, which are

$$\mathrm{SU}(M) \times \mathrm{SU}(N): \quad \{T_{a'}^M \otimes \mathbb{1}, \mathbb{1} \otimes T_{a''}^N\}\,. \tag{2.F.3}$$

This represents the reduced symmetry group of the QED_3-cHGN QCP. While the spin-Hall term $\bar{\Psi}\boldsymbol{\sigma}\Psi$ transforms as a vector under the first generators $T_{a'}^M \otimes \mathbb{1}$, the cHGN interaction term $(\bar{\Psi}\boldsymbol{\sigma}\Psi)^2$ is a scalar built from this vector and thus transforms trivially. Once the unbroken generators are specified, it follows that the fundamental representation of SU(MN) simply reduces as the fundamental of SU(M) and SU(N)

$$\square \to (\square, \square)\ . \tag{2.F.4}$$

This may be understood with rank-1 tensors as a SU(MN) index $\alpha \in \{1, \ldots, MN\}$ can be decomposed in one SU(M) index $\sigma \in \{1, \ldots, M\}$ and one SU(N) index $v \in \{1, \ldots, N\}$

$$h_\alpha = h_{(\sigma v)} \equiv f_\sigma g_v\,. \tag{2.F.5}$$

We may also define rank-2 tensors in this manner, $h_{\alpha\beta} = f_{\sigma\eta} g_{vw}$. Defining symmetrized and anti-symmetrized tensor respectively as $t_{\{i,j\}} = \frac{1}{2}(t_{ij} + t_{ji})$ and $\frac{1}{2}t_{[i,j]} = \frac{1}{2}(t_{ij} - t_{ji})$, we may write explicitly the RHS of (2.5.9) as a tensor whose simplified form corresponds to the LHS of (2.5.9)

$$f_{\{\sigma,\eta\}} g_{[v,w]} + f_{[\sigma,\eta]} g_{\{v,w\}} = \frac{1}{2}\left(f_{\sigma\eta} g_{vw} - f_{\eta\sigma} g_{wv}\right) = h_{[\alpha,\beta]}\,. \tag{2.F.6}$$

This method is difficult to implement as the rank of the tensors is increased, i.e. the number of boxes in the Young diagrams is increased. However, this specific example has the merit of showcasing an important property of the reduction of interest (2.F.1) : The decomposition is independent of M and N. Indeed, the only information needed to show Eq. (2.F.6) is the SU(MN) index decomposition (2.F.5) which characterizes the reduction studied (2.F.1 , 2.F.3). This can be understood by inspecting the relation between the reduction SU(MN) $\to$ SU(M) $\times$ SU(N) and the finite permutation group of f objects S_f [61].

This independence also manifests by the fact that general reductions of $\mathrm{SU}(MN) \to \mathrm{SU}(M) \times \mathrm{SU}(N)$ may be built by taking products of the fundamental representation [61]. For example, by taking the product of the fundamental representation reduction (2.F.4) with itself

$$\square \otimes \square \to (\square \otimes \square, \square \otimes \square) \,, \tag{2.F.7}$$

one finds can write the reduction for $(1) \otimes (1) = (2) \oplus (1^2)$. By also developing the RHS, the reduction in Eq. (2.5.9) can be found. Given that this is the reduction of a reducible representation $(2) \oplus (1^2)$, the associations made between the LHS and RHS of (2.F.7) are not straightforward. However, this shows again that this decomposition is independent of the indices M and N as they were not involved in the computation[15] With this procedure, it is clear that a Young tableau in the $\mathrm{SU}(MN)$ side with f boxes generally reduces to Young tableaux of $\mathrm{SU}(M) \times \mathrm{SU}(N)$ with the same number f of boxes. Those properties hint at a the importance of the permutation group of f objects S_f in this reduction problem (2.F.1).

If we define Υ_λ as a certain diagram λ among Young tableaux with f boxes, then the general reduction (2.F.1) may be written as

$$\Upsilon_\lambda \to \bigoplus_{\nu,\rho} c_{\nu\rho\lambda} (\Upsilon_\nu, \Upsilon_\rho) \,, \tag{2.F.8}$$

where $c_{\nu\rho\lambda}$ is a coefficient of fractional parentage (CFP). The relation with S_f manifests itself through these CFPs : For each Young tableau Υ_λ, there is a corresponding irrep D_λ of S_f, and the CFP of Υ_λ in $(\Upsilon_\nu, \Upsilon_\rho)$ is the Clebsch-Gordan coefficient (CGC) of D_λ in the decomposition of the direct product representation $D_\nu \otimes D_\rho$ [61]

$$D_\nu \otimes D_\rho = \bigoplus_\lambda c_{\nu\rho\lambda} D_\lambda \,. \tag{2.F.9}$$

Since the characters χ of a direct product is the product of the characters

$$\chi_{\nu\otimes\rho} = \chi_\nu \chi_\rho \,, \tag{2.F.10}$$

these CGCs are simply given by

$$c_{\nu\rho\lambda} = \frac{1}{\dim(S_f)} \sum_r p_r \chi_\nu(\mathcal{C}_r) \chi_\rho(\mathcal{C}_r) \chi^*_\lambda(\mathcal{C}_r) \,, \tag{2.F.11}$$

[15] This general procedure may however include diagrams with too many rows and that are not allowed in either $\mathrm{SU}(M)$ or $\mathrm{SU}(N)$. These must simply be removed.

where $\chi_\nu(\mathcal{C}_r)$ is the character of D_ν and p_r is the number of group elements in a conjugacy class $\mathcal{C}_r$.

2.F.2. Clebsch-Gordan coefficients of the sign irrep

We seek to reduce the rank-N completely antisymmetric irrep of SU($2N$) which is a Young diagram with $f = N$ boxes. More precisely, this irrep corresponds to a single column of N boxes (2.5.8). This diagram corresponds to the sign irrep of S_N that we note D_{sign}. To find out how the rank-N completely antisymmetric irrep of SU($2N$) reduces, we must therefore find the CGCs $c_{\nu\rho\,\text{sign}}$ that give the contribution of D_{sign} in the reduction of $D_\nu \otimes D_\rho$.

Let D_ν be an irrep of S_N and $D_{\tilde{\nu}}$ its conjugate. Diagrammatically, these Young tableaux are the transposed of each other (e.g. the two diagrams in the RHS of Eq. 2.5.10). As the conjugate irrep $D_{\tilde{\nu}}$ is simply the direct product of the irrep ν with the sign irrep, $D_{\tilde{\nu}} = D_{\text{sign}} \otimes D_\nu$, its character is simply the product of their characters (2.F.10), i.e. $\chi_{\tilde{\nu}} = \chi_{\text{sign}}\chi_\nu$. Using this, the product of characters that define $c_{\nu\rho\,\text{sign}}$ (2.F.11) may be rewritten as

$$\chi_\nu(\mathcal{C}_r)\chi_\rho(\mathcal{C}_r)\chi^*_{\text{sign}}(\mathcal{C}_r) = \chi_\nu(\mathcal{C}_r)\chi_{\text{trivial}}(\mathcal{C}_r)\chi^*_{\tilde{\rho}}(\mathcal{C}_r)\,. \tag{2.F.12}$$

To obtain this, we also used that, for any equivalence class $\mathcal{C}_r$, the characters of the sign irrep are ± 1, implying that $|\chi_{\text{sign}}|^2 = 1 = \chi_{\text{trivial}}$, and more generally that the characters of the permutation group are real, $\chi_{\tilde{\rho}} = \chi^*_{\tilde{\rho}}$. This relation (2.F.12) implies that $c_{\nu\rho\,\text{sign}} = c_{\nu\,\text{trivial}\,\tilde{\rho}}$. The latter CGC gives the decomposition of $D_{\tilde{\rho}}$ in $D_\nu \otimes D_{\text{trivial}} = D_\nu$. Obviously, the coefficient is only non-"zero" if $\tilde{\rho} = \nu$, which in turn means that $c_{\nu\rho\,\text{sign}} = \delta_{\rho,\tilde{\nu}}$. More explicitly, this means that only pairs of conjugate irreps have a contribution from the sign irrep in their direct product decomposition

$$D_\nu \otimes D_\rho = \delta_{\rho,\tilde{\nu}} D_{\text{sign}} \oplus \dots\,. \tag{2.F.13}$$

This result (2.F.13) implies that the CFPs (2.F.8) are equal to one for every pair of irrep and its conjugate

$$\Upsilon_\lambda \to \bigoplus_\nu (\Upsilon_\nu, \Upsilon_{\tilde{\nu}})\,. \tag{2.F.14}$$

In the case of interest where $M = 2$ and $N = N$, we must exclude irreps of SU(2) $\times$ SU(N) where tableaux in the SU(2) side have more than two rows since they are not include in

SU(2). In the end, this corresponds exactly to the reduction we announced in Eq. (2.5.10). In App. 2.F.3, we explicitly check that the dimensions of these diagrams match.

2.F.3. Dimensions of the reduced irreps

We explicitly check the dimensions of irreps in the reduction of monopoles shown in the main text (2.5.10)

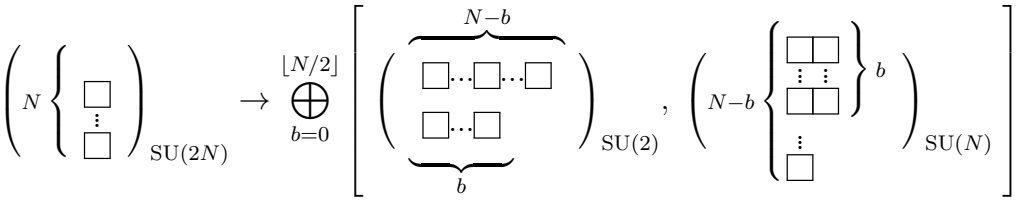

(2.F.15)

2.F.3.1. Dimensions of the $\mathrm{SU}(2) \times \mathrm{SU}(N)$ irreps. The SU(2) subdiagram simply has dimension $N - 2b + 1$

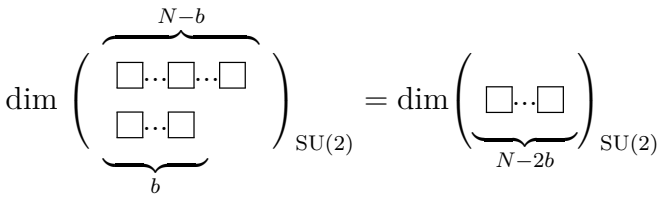

(2.F.16)

where we removed columns of two boxes which transform trivially in SU(2). The $\mathrm{SU}(N)$ diagrams requires more work. The dimension F/H of such a diagram is found using the factor over hooks rule [67]. The $\mathrm{SU}(N)$ Young tableau's boxes can be labeled as

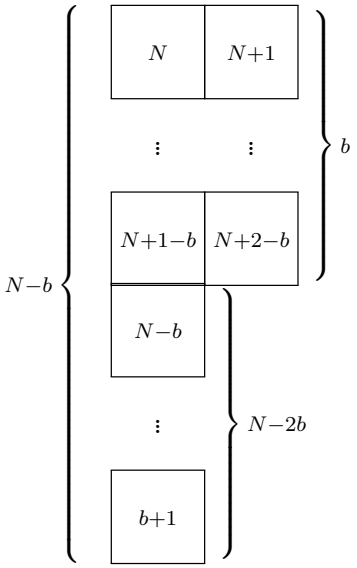

(2.F.17)

Then, the numerator F is the product of all the box labels in the Young tableau above. It can be decomposed as the product of labels in the first column and in the second

$$F = F_L \times F_R = \frac{(N)!}{b!} \times \frac{(N+1)!}{(N+1-b)!}\,. \tag{2.F.18}$$

As for the denominator H, the length of the hooks for each box must be multiplied. It is useful to decompose it in three sections

$$H = h_A \times h_B \times h_C = (N-2b)! \times \frac{(N-b+1)!}{(N-2b+1)!} \times b!\,, \quad N-b \left\{ \begin{array}{|c|c|} \hline B & C \\ \hline \end{array} \right\} b \left\{ \begin{array}{|c|c|} \hline B & C \\ \hline \end{array} \right. \left. \begin{array}{|c|} \hline A \\ \hline \end{array} \right\} N-2b \left. \begin{array}{|c|} \hline A \\ \hline \end{array} \right. \,. \tag{2.F.19}$$

Putting all together, this becomes

$$\begin{aligned} \dim\left(N-b \left\{ \begin{array}{|c|c|} \hline & \\ \hline \end{array} \right\} b \left\{ \begin{array}{|c|c|} \hline & \\ \hline \end{array} \right. \left. \begin{array}{|c|} \hline \\ \hline \end{array} \right\} \right)_{\mathrm{SU}(N)} &= \frac{\frac{(N)!}{b!} \times \frac{(N+1)!}{(N-b+1)!}}{(N-2b)! \times \frac{(N-b+1)!}{(N-2b+1)!} \times b!} \\ &= \frac{(N-2b+1)\,(N+1)}{(N-b+1)^2} \times \binom{N}{b}^2 . \end{aligned} \tag{2.F.20}$$

The total dimension of the $\mathrm{SU}(2) \times \mathrm{SU}(N)$ irrep is

$$\dim\left(\underbrace{\overbrace{\square \cdots \square \cdots \square}^{N-b}}_{b} \right)_{\mathrm{SU}(2)} \times \dim\left(N-b \left\{ \begin{array}{|c|c|} \hline & \\ \hline \end{array} \right\} b \left\{ \begin{array}{|c|c|} \hline & \\ \hline \end{array} \right. \left. \begin{array}{|c|} \hline \\ \hline \end{array} \right\} \right)_{\mathrm{SU}(N)} = \frac{(N-2b+1)^2\,(N+1)}{(N-b+1)^2} \times \binom{N}{b}^2 . \tag{2.F.21}$$

Replacing b with $N/2-s$, it can be verified that this result indeed corresponds to Eq. (2.5.15).

2.F.3.2. Total dimension. The dimension of the $\mathrm{SU}(2N)$ irrep should match the dimension of the $\mathrm{SU}(2) \times \mathrm{SU}(N)$ representation to which it is reduced

$$\dim\left(N \left\{ \begin{array}{|c|} \hline \\ \hline \end{array} \right. \left. \begin{array}{|c|} \hline \\ \hline \end{array} \right\} \right)_{\mathrm{SU}(2N)} = \sum_{b=0}^{\lfloor N/2 \rfloor} \dim\left(\underbrace{\overbrace{\square \cdots \square \cdots \square}^{N-b}}_{b} \right)_{\mathrm{SU}(2)} \times \dim\left(N-b \left\{ \begin{array}{|c|c|} \hline & \\ \hline \end{array} \right\} b \left\{ \begin{array}{|c|c|} \hline & \\ \hline \end{array} \right. \left. \begin{array}{|c|} \hline \\ \hline \end{array} \right\} \right)_{\mathrm{SU}(N)} . \tag{2.F.22}$$

Summing over the index b, we obtain the RHS of Eq. (2.F.22). The LHS of Eq. (2.F.22) is the dimension of the rank-N antisymmetric irrep of SU($2N$) which is $\binom{2N}{N}$. It is left to show that

$$\binom{2N}{N} = \sum_{b=0}^{\lfloor N/2 \rfloor} \frac{(N-2b+1)^2 (N+1)}{(N-b+1)^2} \times \binom{N}{b}^2 . \tag{2.F.23}$$

The RHS of Eq. (2.F.23) with even $N = 2x$ with $x \in \mathbb{Z}^+$ can be simplified to the expected result

$$\begin{aligned} \sum_{b=0}^{x} \frac{(N-2b+1)^2 (N+1)}{(N-b+1)^2} \times \binom{N}{b}^2 \Big|_{N=2x} &= \frac{\pi^{\frac{3}{2}} (2\,x)!^2 \left(x-\frac{1}{4}\right)! \left(x-\frac{3}{4}\right)!}{\left(x-\frac{1}{2}\right)!^3 x!^3 \Gamma\left(\frac{3}{4}\right) \Gamma\left(\frac{1}{4}\right)} \\ &= \frac{(4x)!}{(2x)!^2} = \binom{2N}{N}\Big|_{N=2x} . \end{aligned} \tag{2.F.24}$$

For odd N, we could not show (2.F.23) analytically, but it was confirmed numerically up to $N = 10^4 + 1$.

2.F.4. Monopoles with larger topological charges

The results in the present section directly apply to the study of monopole with a topological charge larger than the minimum $q = 1/2$. As we take a larger topological, more fermion zero modes become available. However, filling half of those $2d_qN$ zero modes will generate monopole with non vanishing Lorentz spins. This is still a good starting point : We define $4\pi q$ flux operators with vanishing fermion number by generalizing Eq. (2.5.2)

$$\Phi^\dagger_{I_1 \dots I_N} = c^\dagger_{I_1} \dots c^\dagger_{I_N} \mathcal{M}^\dagger_{\text{Bare}} , \quad I_i \in \{1, 2, \dots, 2d_qN\} . \tag{2.F.25}$$

These flux operators form the rank-d_qN completely antisymmetric tensor of SU($2d_qN$). In QED$_3$, it reduces in irreps of the symmetry group $\text{SU}(2)_{\text{rot}} \times \text{SU}(2N)$. Consider the following chain

$$\text{SU}(2d_qN) \supset \text{SU}(d_q) \times \text{SU}(2N) \supset \text{SU}(2) \times \text{SU}(2N) . \tag{2.F.26}$$

Then, a first step in reducing the antisymmetric irrep of SU($2d_qN$) is to first consider the reduction

$$\text{SU}(2d_qN) \to \text{SU}(d_q) \times \text{SU}(2N) . \tag{2.F.27}$$

This is just a subcase of the general reduction considered above (2.F.1) with $M = d_q$ and $N = 2N$. The reduction is then simply

$$(1^{d_q N}) \to \bigoplus_{\nu} (\Upsilon^q_\nu, \Upsilon^q_{\tilde{\nu}}) \ , \tag{2.F.28}$$

where $\Upsilon^q_\nu, \Upsilon^q_{\tilde{\nu}}$ are pairs of conjugate Young tableaux with $d_q N$ boxes, and Υ^q_ν has at most d_q rows. To obtain irreps in QED_3-cHGN, this should then be reduced as

$$\text{SU}(d_q) \times \text{SU}(2N) \to \text{SU}(2) \times \text{SU}(2N) \, . \tag{2.F.29}$$

Of course, we only need to know how the treat the reduction of the first subalgebra $\text{SU}(d_q) \to \text{SU}(2)$. At this point, SU(2) singlets may be selected and represent the monopole operators, i.e. flux operators with vanishing fermion number and that transform as Lorentz scalars

$$\text{SU}(2 d_q N) \to \text{SU}(2) \times \text{SU}(2N) \, , \tag{2.F.30}$$

$$(1^{d_q N}) \to \bigoplus_{\nu \in V_0} \Omega_\nu \, (\mathbf{1}, \Upsilon^q_{\tilde{\nu}}) \ , \quad V_0 = \{ \nu \mid (\Upsilon^q_\nu)_{\text{SU}(d_q)} \to \Omega_\nu \mathbf{1}_{\text{SU}(2)} \oplus \ldots \} \, , \tag{2.F.31}$$

where Ω_ν is a degeneracy to be determined. Then, we can proceed to the reduction of the flavor symmetry irreps with $\nu \in V_0$ just as we did in the main text for monopoles with $q = 1/2$

$$\text{SU}(2N) \to \text{SU}(2) \times \text{SU}(N) \, , \tag{2.F.32}$$

$$\Upsilon^q_{\tilde{\nu}} \to \qquad \ldots \, , \tag{2.F.33}$$

where the ellipsis indicates the various diagrams involved in the reduction. To our knowledge, there is no way to systematically obtain the reduction for general q like we did for general N and $q = 1/2$. We will simply examine the case $N = 2$. We consider the reduction given by

$$\text{SU}(4 d_q) \to \text{SU}(d_q) \times \text{SU}(4) \to \text{SU}(d_q) \times \text{SU}(2) \times \text{SU}(2) \, . \tag{2.F.34}$$

For the second smallest topological charge $q = 1$, the reduction is given by

$$\text{SU}(8) \to \text{SU}(2) \times \text{SU}(4) \, , \tag{2.F.35}$$

$$\ydiagram{1,1,1,1}_{\mathbf{70}} \to \left(\ydiagram{2,2}_{\mathbf{1}}, \ydiagram{2,2}_{\mathbf{20'}} \right) \oplus \left(\ydiagram{3,1}_{\mathbf{3}}, \ydiagram{2,1,1}_{\mathbf{15}} \right) \oplus \left(\ydiagram{4,1}_{\mathbf{5}}, \ydiagram{1,1,1,1}_{\mathbf{1}} \right) \, . \tag{2.F.36}$$

Keeping only the Lorentz singlet, we the decompose the multiplet $\mathbf{20'}$ of SU(4) in irreps of SU(2) × SU(2)

$$\mathrm{SU}(4) \to \mathrm{SU}(2) \times \mathrm{SU}(2)\,, \tag{2.F.37}$$

$$\mathbf{20'} \to (\mathbf{1},\mathbf{1}) \oplus (\mathbf{1},\mathbf{5}) \oplus (\mathbf{3},\mathbf{3}) \oplus (\mathbf{5},\mathbf{1})\,. \tag{2.F.38}$$

The first two irreps shows there is accidental degeneracy. One could continue for larger values of q, e.g. $q = 3/2$

$$\mathrm{SU}(12) \to \mathrm{SU}(3) \times \mathrm{SU}(4)\,, \tag{2.F.39}$$

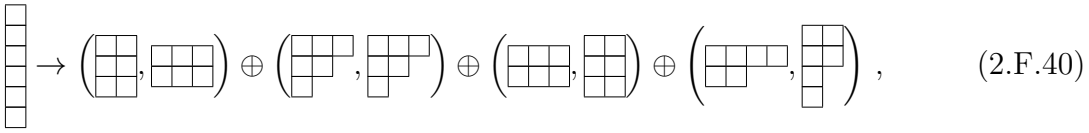

(2.F.40)

and so on. In these other cases, the first subalgebra must also be reduced to SU(2) in order to select Lorentz scalars.

Bibliographie

[1] P. Anderson, Materials Research Bulletin **8**, 153 (1973), ISSN 0025-5408, URL http://www.sciencedirect.com/science/article/pii/0025540873901670.

[2] R. D. Pisarski, Phys. Rev. D **29**, 2423 (1984), URL https://link.aps.org/doi/10.1103/PhysRevD.29.2423.

[3] C. Vafa and E. Witten, Communications in Mathematical Physics **95**, 257 (1984), ISSN 1432-0916, URL https://doi.org/10.1007/BF01212397.

[4] T. Appelquist, D. Nash, and L. C. R. Wijewardhana, Phys. Rev. Lett. **60**, 2575 (1988), URL https://link.aps.org/doi/10.1103/PhysRevLett.60.2575.

[5] T. Appelquist and L. C. R. Wijewardhana, Tech. Rep. hep-ph/0403250. UCTP-106-04, Cincinnati Univ. Dept. Phys., Cincinnati, OH (2004), URL http://cds.cern.ch/record/726218.

[6] J. Braun, H. Gies, L. Janssen, and D. Roscher, Phys. Rev. D **90**, 036002 (2014), URL https://link.aps.org/doi/10.1103/PhysRevD.90.036002.

[7] S. Giombi, I. R. Klebanov, and G. Tarnopolsky, Journal of Physics A : Mathematical and Theoretical **49**, 135403 (2016), URL https://doi.org/10.1088%2F1751-8113%2F49%2F13%2F135403.

[8] N. Karthik and R. Narayanan, Phys. Rev. D **93**, 045020 (2016), URL https://link.aps.org/doi/10.1103/PhysRevD.93.045020.

[9] L. Di Pietro, Z. Komargodski, I. Shamir, and E. Stamou, Phys. Rev. Lett. **116**, 131601 (2016), URL https://link.aps.org/doi/10.1103/PhysRevLett.116.131601.

[10] S. M. Chester and S. S. Pufu, Journal of High Energy Physics **2016**, 69 (2016), ISSN 1029-8479, URL https://doi.org/10.1007/JHEP08(2016)069.

[11] S. Giombi, G. Tarnopolsky, and I. R. Klebanov, Journal of High Energy Physics **2016**, 156 (2016), ISSN 1029-8479, URL https://doi.org/10.1007/JHEP08(2016)156.

[12] A. V. Kotikov, V. I. Shilin, and S. Teber, Phys. Rev. D **94**, 056009 (2016), URL https://link.aps.org/doi/10.1103/PhysRevD.94.056009.

[13] A. V. Kotikov and S. Teber, Phys. Rev. D **94**, 114011 (2016), URL https://link.aps.org/doi/10.1103/PhysRevD.94.114011.

[14] V. Borokhov, A. Kapustin, and X. Wu, Journal of High Energy Physics **2002**, 049 (2002), URL https://doi.org/10.1088/1126-6708/2002/11/049.

[15] A. M. Polyakov, Nuclear Physics B **120**, 429 (1977), ISSN 0550-3213, URL http://www.sciencedirect.com/science/article/pii/0550321377900864.

[16] S. S. Pufu, Phys. Rev. D **89**, 065016 (2014), URL https://link.aps.org/doi/10.1103/PhysRevD.89.065016.

[17] N. Karthik and R. Narayanan, Phys. Rev. D **100**, 054514 (2019), URL https://link.aps.org/doi/10.1103/PhysRevD.100.054514.

[18] S. M. Chester and S. S. Pufu, Journal of High Energy Physics **2016**, 19 (2016), ISSN 1029-8479, URL https://doi.org/10.1007/JHEP08(2016)019.

[19] S. M. Chester, L. V. Iliesiu, M. Mezei, and S. S. Pufu, Journal of High Energy Physics **2018** (2018), ISSN 1029-8479, URL http://link.springer.com/10.1007/JHEP05(2018)157.

[20] J. Alicea, Phys. Rev. B **78**, 035126 (2008), URL https://link.aps.org/doi/10.1103/PhysRevB.78.035126.

[21] M. Hermele, Y. Ran, P. A. Lee, and X.-G. Wen, Phys. Rev. B **77**, 224413 (2008), URL https://link.aps.org/doi/10.1103/PhysRevB.77.224413.

[22] X.-Y. Song, C. Wang, A. Vishwanath, and Y.-C. He, Nature Communications **10**, 4254 (2019), ISSN 2041-1723, URL https://doi.org/10.1038/s41467-019-11727-3.

[23] X.-Y. Song, Y.-C. He, A. Vishwanath, and C. Wang, Physical Review X **10** (2020), ISSN 2160-3308, URL http://dx.doi.org/10.1103/PhysRevX.10.011033.

[24] V. Borokhov, A. Kapustin, and X. Wu, Journal of High Energy Physics **2002**, 044 (2002), URL https://doi.org/10.1088/1126-6708/2002/12/044.

[25] V. Borokhov, Journal of High Energy Physics **2004**, 008 (2004), URL https://doi.org/10.1088%2F1126-6708%2F2004%2F03%2F008.

[26] E. Dyer, M. Mezei, and S. S. Pufu, *Monopole taxonomy in three-dimensional conformal field theories* (2013), arXiv:1309.1160.

[27] Đ. Radičević, Journal of High Energy Physics **2016**, 131 (2016), ISSN 1029-8479, URL https://doi.org/10.1007/JHEP03(2016)131.

[28] B. Assel, Journal of High Energy Physics **2019**, 74 (2019), ISSN 1029-8479, URL https://doi.org/10.1007/JHEP03(2019)074.

[29] T. Senthil, L. Balents, S. Sachdev, A. Vishwanath, and M. P. A. Fisher, Phys. Rev. B **70**, 144407 (2004), URL https://link.aps.org/doi/10.1103/PhysRevB.70.144407.

[30] T. Senthil, L. Balents, S. Sachdev, A. Vishwanath, and M. P. A. Fisher, Journal of the Physical Society of Japan **74**, 1 (2005), https://doi.org/10.1143/JPSJS.74S.1, URL https://doi.org/10.1143/JPSJS.74S.1.

[31] M. A. Metlitski and R. Thorngren, Phys. Rev. B **98**, 085140 (2018), URL https://link.aps.org/doi/10.1103/PhysRevB.98.085140.

[32] J. Y. Lee, Y.-Z. You, S. Sachdev, and A. Vishwanath, Phys. Rev. X **9**, 041037 (2019), URL https://link.aps.org/doi/10.1103/PhysRevX.9.041037.

[33] G. Murthy and S. Sachdev, Nuclear Physics B **344**, 557 (1990).

[34] M. A. Metlitski, M. Hermele, T. Senthil, and M. P. A. Fisher, Phys. Rev. B **78**, 214418 (2008), URL https://link.aps.org/doi/10.1103/PhysRevB.78.214418.

[35] E. Dyer, M. Mezei, S. S. Pufu, and S. Sachdev, Journal of High Energy Physics **2015** (2015), ISSN 1029-8479, URL http://link.springer.com/10.1007/JHEP06(2015)037.

[36] E. Dyer, M. Mezei, S. S. Pufu, and S. Sachdev, Journal of High Energy Physics **2016**, 111 (2016), ISSN 1029-8479, URL https://doi.org/10.1007/JHEP03(2016)111.

[37] A. de la Fuente, Journal of High Energy Physics **2018**, 41 (2018), ISSN 1029-8479, URL https://doi.org/10.1007/JHEP08(2018)041.

[38] M. S. Block, R. G. Melko, and R. K. Kaul, Phys. Rev. Lett. **111**, 137202 (2013), URL https://link.aps.org/doi/10.1103/PhysRevLett.111.137202.

[39] G. J. Sreejith and S. Powell, Phys. Rev. B **92**, 184413 (2015), URL https://link.aps.org/doi/10.1103/PhysRevB.92.184413.

[40] S. Pujari, F. Alet, and K. Damle, Phys. Rev. B **91**, 104411 (2015), URL https://link.aps.org/doi/10.1103/PhysRevB.91.104411.

[41] C. Wang, A. Nahum, M. A. Metlitski, C. Xu, and T. Senthil, Phys. Rev. X **7**, 031051 (2017), URL https://link.aps.org/doi/10.1103/PhysRevX.7.031051.

[42] L. Janssen and Y.-C. He, Phys. Rev. B **96**, 205113 (2017), URL https://link.aps.org/doi/10.1103/PhysRevB.96.205113.

[43] B. Ihrig, L. Janssen, L. N. Mihaila, and M. M. Scherer, Phys. Rev. B **98**, 115163 (2018), URL https://link.aps.org/doi/10.1103/PhysRevB.98.115163.

[44] J. A. Gracey, Phys. Rev. D **98**, 085012 (2018), URL https://link.aps.org/doi/10.1103/PhysRevD.98.085012.

[45] N. Zerf, P. Marquard, R. Boyack, and J. Maciejko, Phys. Rev. B **98**, 165125 (2018), URL https://link.aps.org/doi/10.1103/PhysRevB.98.165125.

[46] R. Boyack, A. Rayyan, and J. Maciejko, Phys. Rev. B **99**, 195135 (2019), URL https://link.aps.org/doi/10.1103/PhysRevB.99.195135.

[47] S. Benvenuti and H. Khachatryan, Journal of High Energy Physics **2019**, 214 (2019), ISSN 1029-8479, URL https://doi.org/10.1007/JHEP05(2019)214.

[48] É. Dupuis, M. B. Paranjape, and W. Witczak-Krempa, Phys. Rev. B **100**, 094443 (2019), URL https://link.aps.org/doi/10.1103/PhysRevB.100.094443.

[49] É. Dupuis, M. B. Paranjape, and W. Witczak-Krempa, in *Quantum Theory and Symmetries*, edited by M. B. Paranjape, R. MacKenzie, Z. Thomova, P. Winternitz, and W. Witczak-Krempa (Springer International Publishing, Cham, 2021), pp. 327–336, ISBN 978-3-030-55777-5.

[50] M. Hermele, T. Senthil, and M. P. A. Fisher, Phys. Rev. B **72**, 104404 (2005), URL https://link.aps.org/doi/10.1103/PhysRevB.72.104404.

[51] Y.-C. He, Y. Fuji, and S. Bhattacharjee, *Kagome spin liquid : a deconfined critical phase driven by $U(1)$ gauge fluctuation* (2015), arXiv:1512.05381.

[52] P. Ghaemi and T. Senthil, Phys. Rev. B **73**, 054415 (2006), URL https://link.aps.org/doi/10.1103/PhysRevB.73.054415.

[53] Y.-M. Lu, G. Y. Cho, and A. Vishwanath, Phys. Rev. B **96**, 205150 (2017), URL https://link.aps.org/doi/10.1103/PhysRevB.96.205150.

[54] M. B. Hastings, Phys. Rev. B **63**, 014413 (2000), URL https://link.aps.org/doi/10.1103/PhysRevB.63.014413.

[55] G. Baskaran and P. W. Anderson, Phys. Rev. B **37**, 580 (1988), URL https://link.aps.org/doi/10.1103/PhysRevB.37.580.

[56] A. M. Polyakov, Physics Letters B **59**, 82 (1975), ISSN 0370-2693, URL http://www.sciencedirect.com/science/article/pii/0370269375901628.

[57] S. Rychkov, *EPFL Lectures on Conformal Field Theory in $D \geq 3$ Dimensions*, SpringerBriefs in Physics (Springer International Publishing, Cham, 2017), ISBN 978-3-319-43625-8, URL //www.springer.com/gp/book/9783319436258.

[58] M. F. Atiyah and I. M. Singer, Bulletin of the American Mathematical Society **69**, 422 (1963), URL https://doi.org/.

[59] T. T. Wu and C. N. Yang, Nuclear Physics B **107**, 365 (1976), ISSN 0550-3213, URL https://www.sciencedirect.com/science/article/pii/0550321376901437.

[60] S. Hellerman, D. Orlando, S. Reffert, and M. Watanabe, Journal of High Energy Physics **2015**, 1 (2015), ISSN 1029-8479, arXiv:1505.01537, URL https://doi.org/10.1007/JHEP12(2015)071.

[61] C. Itzykson and M. Nauenberg, Rev. Mod. Phys. **38**, 95 (1966), URL https://link.aps.org/doi/10.1103/RevModPhys.38.95.

[62] R. Feger, T. W. Kephart, and R. J. Saskowski, *Lieart 2.0 – a mathematica application for lie algebras and representation theory* (2019), arXiv:1912.10969.

[63] N. Karthik, Phys. Rev. D **98**, 074513 (2018), URL https://link.aps.org/doi/10.1103/PhysRevD.98.074513.

[64] X. Y. Xu, Y. Qi, L. Zhang, F. F. Assaad, C. Xu, and Z. Y. Meng (2018), arXiv:1807.07574.

[65] X. Y. Xu, Y. Qi, L. Zhang, F. F. Assaad, C. Xu, and Z. Y. Meng, Phys. Rev. X **9**, 021022 (2019), URL https://link.aps.org/doi/10.1103/PhysRevX.9.021022.

[66] *Nist digital library of mathematical functions*, http ://dlmf.nist.gov/, Release 1.0.21 of 2018-12-15, URL `http://dlmf.nist.gov/`.

[67] H. M. Georgi, *Lie algebras in particle physics ; 2nd ed.*, Frontiers in Physics (Perseus, Cambridge, 1999).

Chapitre 3

Anomalous dimensions of monopole operators at the transition between Dirac and topological spin liquids

É. Dupuis, R. Boyack, et W. Witczak-Krempa, arXiv : 2108.05922, Août 2021.

Abstract. Monopole operators are studied at certain quantum critical points between a Dirac spin liquid and topological quantum spin liquids (QSLs) : chiral and Z_2 QSLs. These quantum phase transitions are described by conformal field theories (CFTs) : quantum electrodynamics in 2+1 dimensions with $2N$ flavors of two-component massless Dirac fermions and a four-fermion interaction term. For the transition to a chiral spin liquid, it is the Gross-Neveu interaction (QED_3-GN), while for the transition to the Z_2 QSL it is a superconducting pairing term (QED_3-Z_2GN). Using the state-operator correspondence, we obtain monopole scaling dimensions to sub-leading order in $1/N$. For monopoles with a minimal topological charge $q = 1/2$, the scaling dimension is $2N \times 0.26510$ at leading-order, with the quantum correction being 0.118911(7) for the chiral spin liquid, and 0.102846(9) for the Z_2 case. Although these two anomalous dimensions are nearly equal, the underlying quantum fluctuations possess distinct origins. The analogous result in QED_3 is also obtained and we find a sub-leading contribution of $-0.038138(5)$, which is slightly different from the value -0.0383 first obtained in the literature. The scaling dimension of a QED_3-GN monopole with minimal charge is very close to the scaling dimensions of other operators predicted to be equal by a

conjectured duality between QED_3-GN with $2N = 2$ flavors and the CP^1 model. Additionally, non-minimally charged monopoles with equal charges on both sides of the duality have similar scaling dimensions. By studying the large-q asymptotics of the scaling dimensions in QED_3, QED_3-GN, and QED_3-Z_2GN we verify that the constant $O(q^0)$ coefficient precisely matches the universal prediction for CFTs with a global U(1) symmetry.

3.1. Introduction

Gauge theories have taken an important place in modern condensed matter physics, in part due to their ability to provide a low-energy description of many quantum phases of matter. Gauge fields emerge as collective excitations that capture the highly entangled nature of certain strongly correlated systems. This is notably apparent in the case of frustrated two-dimensional magnets hosting quantum spin liquids and deconfined quantum critical points (dQCPs).

In these lattice systems, the emergent gauge field is compact, and, as a result, has topological excitations created by topological disorder operators. For a U(1) gauge field, these objects are called monopole or instanton operators and they play an essential role in many physical systems. Crucially, monopole proliferation confines the gauge field. This is the case in the pure U(1) gauge theory [1, 2]. In the presence of massless matter, however, monopoles are screened and confinement can be avoided if enough flavors of massless matter are present.

In particular, we will be first considering a transition from a U(1) Dirac spin liquid (DSL), which is described by QED_3 with $2N$ flavors of massless two-component Dirac fermions. Realizations of the U(1) DSL were formulated for the Kagome Heisenberg spin-1/2 magnet [3–8] and the $J_1 - J_2$ spin-1/2 model on the triangular lattice [9–11] with $2N = 4$ flavors. Dirac spin-orbital liquid with effective spin $j = 3/2$ and $2N = 8$ flavors have also been formulated for quantum magnets on honeycomb [12, 13] and triangular [14] lattices. For a large number of fermion flavors $2N$, it has been shown through a $1/N$ expansion that monopole operators are irrelevant [15], and thus the U(1) DSL is stable in this limit. Taking into account next-to-leading order corrections [16], the critical number of fermion flavors was estimated to be $2N_c = 12$, beyond which minimally charged monopoles become irrelevant. This result was confirmed by Monte Carlo computations [17] and is consistent with conformal bootstrap bounds [18, 19]. The addition of disorder renders the model more unstable [20].

Monopole operators also serve as order parameters in neighboring phases. For instance, in the CP^1 model, which describes the transition between an antiferromagnetic (AFM) phase and a valence bond solid (VBS), there are monopoles with lattice quantum numbers and their condensation results in VBS order [21–24]. It is in this model where the scaling dimension of monopole operators were first obtained [25]. Monopoles are also crucial in the U(1) DSL, a parent state for many spin liquids. In this fermionic theory, monopoles can carry different quantum numbers due to the existence of fermion zero modes [26] which may dress monopoles in various ways. Monopoles describe various VBS and AFM orders, depending on which lattice the U(1) DSL is formulated [27]. By tuning a flavor-dependent Gross-Neveu (GN) interaction, a fermion mass is generated and monopoles with specific quantum numbers condense [28]. In particular, the U(1) DSL on the Kagome lattice orders to an antiferromagnetic 120° coplanar order as monopoles dressed with a magnetic spin polarization condense [29, 30]. This confinement-deconfinement transition is described by the QED_3- chiral Heisenberg GN model (QED_3-cHGN), and the scaling dimensions of monopole operators at the quantum critical point (QCP) were obtained in Ref. [31]. In this case, the activation of the cHGN interaction breaks the flavor symmetry, resulting in a hierarchy among monopoles where the scaling dimension depends on the total magnetic spin of a monopole [32, 33].

The quantum criticality of the dQCP and the U(1) DSL with $2N = 4$ fermions were recently given a precise relation. It was shown that they can be formulated as so-called Stiefel liquids, which are related to non-linear sigma models in 2+1 dimensions with target manifolds $\mathrm{SO}(n) / \mathrm{SO}(4)$, where $n = 5$ and $n = 6$ for the dQCP and the U(1) DSL respectively [34]. Higher values are conjectured to realize non-lagrangian critical systems, for instance realizing a phase between a non-coplanar magnet and a VBS order when $n = 7$.

In this work, we will focus on transitions from the U(1) DSL to two topological quantum spin liquids (QSL) : a chiral spin liquid (CSL) as mentioned above, and a Z_2 QSL. The first transition is described by QED_3-GN [35, 36], where the CSL results from the condensation of a symmetric fermion mass induced by the GN interaction. This transition can be realized for the Kagome [37–40] and triangular [41–43] Heisenberg magnets with $2N = 4$ Dirac cones. The QCP for the non-compact QED_3-GN has been studied in Refs. [36, 44–48]. Even though a mass gap is condensed in the CSL, there is no confinement-deconfinement transition taking

place in the compact theory. Despite removing the screening effect of gapless modes, the symmetric condensed mass induces a Chern-Simons term in the infrared limit which gaps the monopoles and prevents their proliferation. The spinons in the gapped CSL thus remain deconfined. The CSL is a topologically ordered state that breaks time-reversal symmetry, and has robust chiral edge modes.

In contrast, the non-chiral Z_2 QSL is obtained when the fermionic spinons undergo a pairing instability to a gapped s-wave superconducting state. The U(1) gauge field is gapped through the Higgs mechanism, and gives place to a discrete Z_2 gauge field. In this case, fractionalization remains intact. This quantum phase transition was studied in Refs. [49, 50]. Earlier studies [30, 51] qualitatively described how a Z_2 QSL can be obtained from a Dirac QSL through a superconducting transition for the fermions, albeit without a fluctuating scalar field (Cooper pair field). In addition, Ref. [52] studied a similar model in the context of superconducting criticality in topological insulators. Interestingly, it turns out that, at leading-order in $1/N$, the monopoles have the same scaling dimension at both QCPs as in the U(1) DSL [31, 50]. In this work, we obtain the next-to-leading order correction to monopole scaling dimensions at those QCPs.

This study is also motivated by the duality between QED$_3$-GN with $2N = 2$ fermion flavors and CP^{N-1} with $N = 2$ complex boson flavors conjectured in Ref. [53] and further studied in Ref. [44]. This duality can be checked by comparing the scaling of monopole operators with various scaling dimensions that are predicted to be equal according to this duality. The good agreement obtained in the LO result [31] is further improved by the scaling dimension correction we obtain here for the QED$_3$-GN monopoles.

The paper is organized as follows. In the next section, we present the QED$_3$-GN model and show how the state-operator correspondence is used to obtain monopole scaling dimensions. In Sec. 3.3, the leading-order computation presented in Ref. [31] is reviewed. In Sec. 3.4, $1/N$ corrections to monopole scaling dimensions are computed. We also verify that the scaling dimensions satisfy a conjectured convexity property. In Sec. 3.5, we compare our results with the large-charge expansion obtained in Ref. [54] for CFTs. In Sec. 3.6, we study the QED$_3$-GN $\Leftrightarrow$ CP^1 duality [53]. In Sec. 3.7, we study monopole scaling dimensions at the transition to a Z_2 QSL, and obtain distinct values compared to the CSL. In Sec. 3.8, we briefly discuss other phase transitions that could be studied with this formalism, including

the QED$_3$-U(N) $\times$ U(N) GN, QED$_3$-chiral XY GN, and QED$_3$-cHGN QCPs. We conclude with a discussion of our results and an outlook. In Appendix 3.A, we review the phase transition from the U(1) DSL to the CSL in the non-compact model. In Apps. 3.B and 3.C, we give more details regarding how the kernels appearing in Sec. 3.4 are obtained and simplified with gauge invariance. The expansion of these kernels in terms of harmonics is detailed in Apps. 3.D and 3.E. We give detailed simplifications of the kernels used for the case of minimally charge monopoles in App. 3.F. In App. 3.G, some remainder coefficients used to analytically approximate sums over angular momenta are shown. In App. 3.H, we show how some contributions of fermion zero modes neglected in the main text vanish. In App. 3.I, the fitting procedure used to alleviate finite-size effects when computing monopole anomalous dimensions are described. In App. 3.J, we list monopole anomalous dimensions in QED$_3$, QED$_3$-GN, and QED$_3$-Z$_2$GN for topological charges up to $q = 13$.

3.2. Monopoles at transition between Dirac & chiral spin liquids

The action of the QED$_3$-GN model in euclidean flat spacetime is given by

$$S = \int d^3r \left[-\overline{\Psi}\gamma^\mu \left(\partial_\mu - iA_\mu\right) \Psi - \frac{h^2}{2}\left(\overline{\Psi}\Psi\right)^2 \right] + \cdots , \tag{3.2.1}$$

where Ψ is a $2N$ flavor spinor $\Psi = (\psi_1, \psi_2, \ldots \psi_{2N})^\intercal$ with each flavor ψ_i being a two-component Dirac fermion. For certain quantum magnets, where fermions emerge as fractionalized quasiparticles, the $2N$ flavors are related to two magnetic spin polarizations $s = \uparrow, \downarrow$ and N valley nodes per spin, $v = 1, \ldots, N$. Typical quantum magnets have $N = 2$ or 4 nodes, but here we keep N general and use it as an expansion parameter. The adjoint spinor is given by $\overline{\Psi} = \Psi^\dagger \gamma_0$, where the gamma matrices are defined in terms of the Pauli matrices by $\gamma_{x,y} = \sigma_{x,y}$, and $\gamma_0 = \sigma_z$. The fermions are coupled to a compact U(1) gauge field A_μ, and have a GN self-interaction with coupling strength h. The ellipsis denotes an irrelevant Maxwell term and the contribution of monopole operators $\mathcal{M}_q(x)$ that we discuss further in what follows.

In 2+1 dimensions, U(1) gauge theories have an extra global $\mathrm{U}_{\mathrm{top}}(1)$ symmetry associated with the following conserved current

$$J^{\mu}_{\mathrm{top}}(x) = \frac{1}{2\pi}\epsilon^{\mu\nu\rho}\partial_{\nu}A_{\rho}(x), \tag{3.2.2}$$

where "top" stands for topological. The operators charged under $\mathrm{U}_{\mathrm{top}}(1)$ are called topological disorder operators or instantons. In this $2+1$ dimensional context, we refer to them as monopole operators. These operators create topological configurations of the gauge field $\mathcal{A}^{q}_{\mu}$ with a quantized flux $\int dn_{\mu}\epsilon^{\mu\nu\rho}\partial_{\nu}\mathcal{A}^{q}_{\rho} = 4\pi q$, where the topological charge is a half-integer $q \in \mathbb{Z}/2$ as a result of the Dirac quantization condition [55]. These kinds of configurations are allowed in the compact formulation of the U(1) gauge group, which gives the correct description for emergent gauge theories in a condensed matter context. The monopole operators themselves can be defined by the action of the topological current on them :

$$J^{\mu}_{\mathrm{top}}(x)\mathcal{M}^{\dagger}_{q}(0) \sim \frac{q}{2\pi}\frac{x^{\mu}}{|x|^{3}}\mathcal{M}^{\dagger}_{q}(0) + \cdots, \tag{3.2.3}$$

where the ellipsis denotes less singular terms in the operator-product expansion (OPE) [15]. The resulting factor in front of the monopole operator corresponds to the magnetic field of a charge-q Dirac magnetic monopole.

The model in Eq. (3.2.1) describes a transition from a DSL to a CSL. For a sufficiently strong coupling, a chiral order develops due to the condensation of a fermion bilinear : $\langle\overline{\Psi}\Psi\rangle \neq 0$. This may be studied by introducing an auxiliary pseudo-scalar boson ϕ. The effective action at the quantum critical point (QCP), denoted by $S^{\mathrm{c}}_{\mathrm{eff}}$, is

$$S^{\mathrm{c}}_{\mathrm{eff}} = -N\ln\det\Big(\partial\!\!\!/ - iA\!\!\!/ + \phi\Big), \tag{3.2.4}$$

where ϕ is an auxiliary boson decoupling the GN interaction. More details are shown in App. 3.A.

In the compact version of QED_3-GN, monopole operators are also present at the QCP. The main goal of this paper is to compute their scaling dimension $\Delta_{\mathcal{M}_q}$, which controls the scaling of the monopole two-point correlation function :

$$\langle\mathcal{M}_{q}(x)\mathcal{M}^{\dagger}_{q}(y)\rangle \sim \frac{1}{|x-y|^{2\Delta_{\mathcal{M}_q}}}. \tag{3.2.5}$$

Since the QED_3-GN model at the QCP is a conformal field theory (CFT), the state-operator correspondence can be used to obtain these scaling dimensions [15]. This correspondence

relies on a radial quantization of the CFT and a conformal transformation mapping the dilatation operator $\hat{D}$ on $\mathbb{R}^3$ to a Hamiltonian $\hat{H}$ on $S^2 \times \mathbb{R}$. Denoting the usual radius on $\mathbb{R}^3$ as $r = e^{\tau}$,[1] the related Weyl transformation of the spacetime is written as

$$\left(ds^2\right)_{S^2\times\mathbb{R}} = e^{-2\tau}\left(ds^2\right)_{\mathbb{R}^3} = d\tau^2 + d\theta^2 + \sin^2\theta d\phi^2. \tag{3.2.6}$$

The scaling dimension of an operator $\mathcal{O}(x)$ then corresponds to the energy of some state $\hat{H}\left|\mathcal{O}\right\rangle = \Delta_{\mathcal{O}}\left|\mathcal{O}\right\rangle$ on this compactified spacetime. Specifically, the charge-q operator with the smallest scaling dimension corresponds to the ground state of the CFT on the compactified spacetime $S^2 \times \mathbb{R}$, where the sphere S^2 is pierced by $4\pi q$ flux. To implement this flux, an external gauge field is coupled to the fermions

$$\mathcal{A}^q = q\left(1 - \cos\theta\right)\mathrm{d}\phi, \tag{3.2.7}$$

or $\mathcal{A}^q_\phi = \left(1 - \cos\theta\right)/\sin\theta$ in component notation. The smallest scaling dimension of monopole operators in topological sector q is then given by [2]

$$\Delta_q = \lim_{\beta\to\infty} F_q = -\lim_{\beta\to\infty}\frac{1}{\beta}\ln Z\left[\mathcal{A}^q\right], \tag{3.2.8}$$

where F_q is the free energy and $Z\left[\mathcal{A}^q\right]$ is the partition function formulated on $S^2 \times S^1_\beta$, i.e., the previous spacetime but now with the "time" direction compactified to a "thermal" circle S^1_β with radius β. This formulation allows us to introduce the holonomy of the gauge field along this circle, written as

$$\alpha = i\beta^{-1}\int_{S^1_\beta} d\tau\ A_\tau. \tag{3.2.9}$$

The holonomy couples to the fermion number operator $\int d^2r\sqrt{g(r)}\Psi^\dagger\Psi = \hat{N}_{\text{fermions}}$ and acts as a chemical potential [19, 31]. The saddle-point equation of this holonomy constrains the fermion number to vanish

$$0 = \frac{1}{\beta}\left.\frac{\delta\ln Z\left[\mathcal{A}^q\right]}{\delta\alpha}\right|_{\text{s.p.}} = \left\langle\hat{N}_{\text{fermions}}\right\rangle, \tag{3.2.10}$$

where "s.p." stands for saddle-point. The holonomy thus serves as a Lagrange multiplier that ensures that a state with $\langle\hat{N}_{\text{fermions}}\rangle = 0$ is selected to correctly represent a gauge-invariant monopole operator [31].

[1] We work in natural units where the two-sphere radius is $R = 1$.

[2] More formally, we could write $\Delta_q = \lim_{\beta\to\infty}\left(F_q - F_0\right)$ as explained in Ref. [56]. However, it turns out that $\lim_{\beta\to\infty} F_0 = 0$.

The scaling dimension will be obtained using a large-N expansion. We first note that the partition function can be written as a path integral :

$$Z\left[\mathcal{A}^q\right] = e^{-\beta F_q} = \int \mathcal{D}\phi\mathcal{D}A_\mu \exp\left(-S_{\text{eff}}\left[\phi,A_\mu,\mathcal{A}^q_\mu\right]\right). \tag{3.2.11}$$

The effective action is now given by

$$S_{\text{eff}}\left[\phi,A_\mu,\mathcal{A}^q_\mu\right] = -2N \ln\det\left(\not{D}_{A+\mathcal{A}^q} + \phi\right), \tag{3.2.12}$$

where $\not{D}_{A+\mathcal{A}^q}$ is the gauge-covariant derivative on a curved spacetime including the external gauge field $\mathcal{A}^q_\mu$ sourcing the $4\pi q$ flux :

$$\not{D}_{A+\mathcal{A}^q} = e^\mu_b \gamma^b \left(\nabla_\mu - iA_\mu - i\mathcal{A}^q_\mu\right). \tag{3.2.13}$$

The gamma matrices γ^b still correspond to the Pauli matrices, as the spacetime index is normalized with a tetrad e^μ_b which encapsulates the information about the metric $g_{\mu\nu}e^\mu_b e^\nu_c = \delta_{bc}$. The path integral defining the partition function can be expanded around the saddle-point values of the auxiliary and gauge bosons :

$$\phi = \langle\phi\rangle + \sigma, \quad A_\mu = \langle A_\mu\rangle + a_\mu, \tag{3.2.14}$$

which are defined by the following saddle-point conditions

$$\left.\frac{\delta F_q}{\delta\phi}\right|_{\phi=\langle\phi\rangle, A_\mu=\langle A_\mu\rangle} = \left.\frac{\delta F_q}{\delta A_\mu}\right|_{\phi=\langle\phi\rangle, A_\mu=\langle A_\mu\rangle} = 0. \tag{3.2.15}$$

Taking the fluctuations to scale as $1/\sqrt{2N}$, the saddle-point expansion of the partition function is then

$$\int \mathcal{D}\phi\mathcal{D}A e^{-S_{\text{eff}}} = e^{-S_{\text{eff}}|_{\text{s.p.}}} \int \mathcal{D}\sigma\mathcal{D}a e^{-S^{(2)}_{\text{eff}}}, \tag{3.2.16}$$

where $S^{(2)}_{\text{eff}}$ is the second variation of the action. Integrating over the quadratic fluctuations, this gives us the $1/N$ expansion of the free energy :

$$2NF^{(0)}_q = \frac{1}{\beta} S_{\text{eff}}|_{\text{s.p.}}, \tag{3.2.17}$$

$$F^{(1)}_q = \frac{1}{\beta} \times \frac{1}{2} \ln\det\left[\frac{\delta^2 S_{\text{eff}}}{\delta(\sigma,a)\,\delta(\sigma,a)}\right]\Bigg|_{\text{s.p.}}. \tag{3.2.18}$$

Using the relation in Eq. (3.2.8), which follows from the state-operator correspondence, these first two terms of the free energy give the scaling dimension at next-to-leading order in $1/N$.[3]

[3]The expansion is in terms of the total number of fermion flavors, $2N$, such that $F_q = 2NF^{(0)}_q + F^{(1)}_q + O(1/N)$.

Since the fermionic mass condensed in the ordered phase is flavor-symmetric $\left\langle \overline{\Psi}\Psi \right\rangle$, the global flavor symmetry remains unbroken and monopole operators are organized as representations of SU($2N$). Just as for the various fermion bilinears and monopole correlation functions in the U(1) DSL [29, 57, 58], monopole correlation functions at the QCP between U(1) DSL and CSL related by this SU($2N$) symmetry share the same scaling dimension.[4] Depending on the lattice, various magnetic and VBS correlation functions will be described by minimally charged monopole operators [27], but they all share the same scaling dimension $2N \times 0.26510 + 0.118911(7) + O\left(N^{-1}\right)$, where the leading-order was found in Ref. [31] and the next-to-leading order is one of the main results of this work shown in Eq. (3.4.61). For typical quantum magnets, we have $2N = 4$ fermion flavors. The way that monopole scaling dimensions control observable correlation functions could also be compared at this QCP and deep in the U(1) DSL phase. In this latter case, scaling dimensions are those of monopoles in QED_3.

3.3. Review of $N = \infty$ theory

First, we review the computation of monopole scaling dimensions in QED_3-GN at leading-order in $1/N$ [31]. At this order, the free energy is given by the effective action in (3.2.12) at its saddle-point corresponding to a global minimum

$$F_q^{(0)} = -\frac{1}{\beta} \ln \det \left(\not{D}_{-i\alpha d\tau + \mathcal{A}^q} + \langle \phi \rangle \right), \tag{3.3.1}$$

where the trace over the $2N$ flavors has been taken and has canceled a prefactor of $(2N)^{-1}$. The expectation value of the pseudo-scalar field is taken to be homogeneous. The gauge field is also constant at the saddle-point, with a possible non-vanishing holonomy α on the thermal circle described in (3.2.9). The determinant operator is diagonalized by introducing monopole harmonics $Y_{q,\ell,m}(\hat{n})$, which are a generalization of spherical harmonics for a space with a charge at the center [59, 60]. For a fixed charge q, these functions form a complete basis. One important difference with these harmonics is that their angular momentum is now

[4] This degeneracy we described is among a flavor symmetry multiplet composed of monopoles with the smallest scaling dimension, which we focus on. We emphasize that monopoles with larger scaling dimensions can be built by dressing fermion modes with higher energies. For instance, a splitting of monopoles was obtained for QED_3 $q = 1$ monopoles as their scaling dimensions increases with Lorentz spin [19]. Notably, for a monopole with Lorentz spin of order $\sqrt{N}$, there is a $O(N^0)$ additional positive correction.

bounded below by this charge q. Using these functions to build appropriate eigenspinors, the eigenvalues of this determinant operator on $S^2 \times S^1_\beta$ in Eq. (3.3.1) are shown to be [15, 31]

$$-i \times \begin{cases} \omega_n - i\alpha + i\varepsilon_q & \ell = q, \\ \pm\sqrt{(\omega_n - i\alpha)^2 + \varepsilon_\ell^2} & \ell = q+1, q+2, \dots \end{cases} \tag{3.3.2}$$

where, for simplicity, we suppose $q > 0$ throughout. Here, $\omega_n = 2\pi\beta^{-1}(n + 1/2)$, for $n \in \mathbb{Z}$, are the fermionic Matsubara frequencies, and ε_ℓ are the energies of the modes for the quantized theory on $S^2 \times \mathbb{R}$:

$$\varepsilon_\ell = \sqrt{\ell^2 - q^2 + \langle\phi\rangle^2}. \tag{3.3.3}$$

More details on the diagonalization are presented in App. (3.D.2). Note that the energies are dimensionless, as we work in units where the radius of the sphere is 1. Each mode has the usual degeneracy that comes from the azimuthal symmetry, $d_\ell = 2\ell$. The free energy at leading-order then becomes

$$F_q^{(0)} = -\frac{1}{\beta}\sum_{n=-\infty}^{\infty}\left\{ d_q \ln\left[\omega_n - i\alpha + i\langle\phi\rangle\right] + \sum_{\ell=q+1}^{\infty} d_\ell \ln\left[(\omega_n - i\alpha)^2 + \varepsilon_\ell^2\right]\right\}. \tag{3.3.4}$$

The saddle-point equation for the holonomy, given in Eq. (3.2.15), yields the condition

$$-d_q \tanh\left(\frac{\beta}{2}(\alpha - \langle\phi\rangle)\right) - \sum_{\ell=q+1}^{\infty} \frac{2d_\ell \sinh(\beta\alpha)}{\cosh(\beta\varepsilon_\ell) + \cosh(\beta\alpha)} = 0, \tag{3.3.5}$$

which is solved for $\alpha = \langle\phi\rangle$ in the $\beta \to \infty$ limit. With this result, the second gap equation at leading-order in β is given by

$$2\langle\phi\rangle \sum_{\ell=q+1}^{\infty} d_\ell \varepsilon_\ell^{-1} = 0, \tag{3.3.6}$$

whose only solution is $\langle\phi\rangle = 0$. Therefore, the saddle-point values of both fields vanish.

Inserting this result in Eq. (3.3.4), the monopole scaling dimension at leading-order in $1/N$ is obtained from Eq. (3.2.8)[5]

$$\Delta_q = 2N \sum_{\ell=q+1}^{\infty} d_\ell E_{q,\ell} + O\left(N^0\right), \tag{3.3.7}$$

[5]More explicitly, the leading-order free energy is $\lim_{\beta\to\infty} F_q^{(0)} = 2\sum_{\ell=q+1}^{\infty} d_\ell E_{q,\ell}$. Using zeta regularization, it follows that the $q = 0$ case vanishes : $\lim_{\beta\to\infty} F_0^{(0)} = 4\sum_{\ell=1}^{\infty} \ell^2 = 4\zeta(-2) = 0$, as previously claimed.

where the energies at the saddle-point are defined as

$$E_{q,\ell} = \sqrt{\ell^2 - q^2}. \tag{3.3.8}$$

This is simply the leading-order scaling dimension of QED_3 [15] (which must still be regularized). For example, the scaling dimension of the monopole with minimal charge is $\Delta_{q=1/2} = 2N \times 0.265 + O\left(N^0\right)$. Here, a supplementary GN interaction is considered, but it does not come into play at this level of the expansion since $\langle\phi\rangle = 0$. Thus, monopoles in QED_3 and QED_3-GN have the same scaling dimensions at leading-order in $1/N$:

$$\Delta^{(0)}_{q,\,\mathrm{QED}_3} = \Delta^{(0)}_{q,\,\mathrm{QED}_3\text{-GN}}. \tag{3.3.9}$$

3.4. $1/N$ corrections

3.4.1. Setup

3.4.1.1. Real-space kernels. We now turn to the next-to-leading-order term in the free-energy expansion in Eq. (3.2.18). The free-energy correction is related to the second variation of the action by

$$\exp\left(-\beta F_q^{(1)}\right) = \int \mathcal{D}\sigma\mathcal{D}a \exp\left[-\frac{(2N)}{2}\int_{r,r'}\begin{pmatrix}\sigma(r) & a_\mu(r)\end{pmatrix}\begin{pmatrix}D^q(r,r') & H^q_{\mu'}(r,r') \\ H^q_\mu(r',r) & K^q_{\mu\mu'}(r,r')\end{pmatrix}\begin{pmatrix}\sigma(r') \\ a_{\mu'}(r')\end{pmatrix}\right], \tag{3.4.1}$$

where $\int_r \equiv \int d^3r\sqrt{g(r)}$ and we defined the following kernels

$$D^q(r,r') = \frac{1}{2N}\left.\frac{\delta^2 S_{\text{eff}}}{\delta\sigma(r)\delta\sigma(r')}\right|_{\text{s.p.}}, \tag{3.4.2}$$

$$K^q_{\mu\mu'}(r,r') = \frac{1}{2N}\left.\frac{\delta^2 S_{\text{eff}}}{\delta a^\mu(r)\delta a^{\mu'}(r')}\right|_{\text{s.p.}}, \tag{3.4.3}$$

$$H^q_{\mu'}(r,r') = \frac{1}{2N}\left.\frac{\delta^2 S_{\text{eff}}}{\delta\sigma(r)\delta a^{\mu'}(r')}\right|_{\text{s.p.}}, \tag{3.4.4}$$

where S_{eff} is defined in Eq. (3.2.12). The remaining scalar-gauge kernel[6] with mixed $a_\mu(r)$ and $\sigma(r')$ partial derivatives is obtained by exchanging coordinates r,r' in $H^q_{\mu'}(r,r')$, which

[6]Although $\sigma(r)$ is really a pseudo-scalar, we refer to it as a "scalar" when labeling related kernels for simplicity.

has mixed $\sigma(r)$ and $a_{\mu'}(r')$ partial derivatives; thus we write $H^q_\mu(r',r)$ in Eq. (3.4.1). In terms of the fermions in the original system, the kernels are given by

$$D^q(r,r') = \left\langle \overline{\psi}(r)\psi(r)\overline{\psi}(r')\,\psi(r')\right\rangle\Big|_{\text{s.p.}}, \tag{3.4.5}$$

$$K^q_{\mu\mu'}(r,r') = -\left\langle J_\mu(r)J_{\mu'}(r')\right\rangle\Big|_{\text{s.p.}}, \tag{3.4.6}$$

$$H^q_{\mu'}(r,r') = -i\left\langle \overline{\psi}(r)\psi(r)J_{\mu'}(r')\right\rangle\Big|_{\text{s.p.}}, \tag{3.4.7}$$

where ψ is a single fermion flavor and the current is

$$J_\mu(r) = \overline{\psi}(r)\gamma_\mu\psi(r). \tag{3.4.8}$$

This can be re-expressed in terms of the fermionic Green's function $G_q(r,r') = \left\langle \psi(r)\overline{\psi}(r')\right\rangle\Big|_{\text{s.p.}}$ and its hermitean conjugate $G^\dagger_q(r,r') = -\left\langle \psi(r')\,\overline{\psi}(r)\right\rangle\Big|_{\text{s.p.}}$. The Wick expansion of the kernels yields

$$D^q(r,r') = -\text{tr}\left[G_q(r,r')G^\dagger_q(r,r')\right], \tag{3.4.9}$$

$$K^q_{\mu\mu'}(r,r') = \text{tr}\left[\gamma_\mu G_q(r,r')\gamma_{\mu'}G^\dagger_q(r,r')\right], \tag{3.4.10}$$

$$H^q_{\mu'}(r,r') = i\text{tr}\left[G_q(r,r')\gamma_{\mu'}G^\dagger_q(r,r')\right], \tag{3.4.11}$$

where the cyclicity of the trace was used. The remaining prefactor $2N$ in Eq. (3.4.1) is cancelled as the fluctuation fields are rescaled $\sigma,a_\mu \to \sigma/\sqrt{2N}, a_\mu/\sqrt{2N}$ to control the expansion. The free-energy correction is then obtained by integrating the field fluctuations in Eq. (3.4.1). It is convenient to subtract the $q=0$ correction $F^{(1)}_0 = 0$,[7] therefore we write the general correction as

$$F^{(1)}_q = \frac{1}{2}\ln\left(\frac{\det' M^q}{\det' M^0}\right), \tag{3.4.12}$$

where we define the matrix kernel

$$M^q(r,r') = \begin{pmatrix} D^q(r,r') & H^q_{\mu'}(r,r') \\ H^q_\mu(r',r) & K^q_{\mu\mu'}(r,r') \end{pmatrix}. \tag{3.4.13}$$

[7]Since the scaling dimension of the identity operator vanishes, we have $\lim_{\beta\to\infty} F^{(1)}_0 = 0$. Computing $F^{(1)}_q - F^{(1)}_0$ requires less regularization procedures and automatically takes care of gauge fixing subtleties since the Fadeev-Popov ghost contribution is independent of the background flux $4\pi q$ in QED_3 [61].

3.4.1.2. Fourier transform. To compute the determinant operator, the kernels are expanded in terms of harmonics. For the gauge-gauge kernels, the vector spherical harmonics are introduced :

$$\mathfrak{a}^T_{\mu,\ell m}(\hat{n}) = \delta^0_\mu Y_{\ell m}(\hat{n}), \tag{3.4.14}$$

$$\mathfrak{a}^E_{\mu,\ell m}(\hat{n}) = \frac{1}{\sqrt{\ell(\ell+1)}} \nabla_\mu Y_{\ell m}(\hat{n}), \tag{3.4.15}$$

$$\mathfrak{a}^{\mu,B}_{\ell m}(\hat{n}) = \frac{1}{\sqrt{\ell(\ell+1)}} \frac{\epsilon^{0\mu\nu}}{\sqrt{g(r)}} \nabla_\nu Y_{\ell m}(\hat{n}). \tag{3.4.16}$$

As suggested by the notation, the B mode has zero divergence : $\nabla \cdot \vec{\mathfrak{a}}^B_{\ell m}(\hat{n}) = 0$, and the E mode has zero curl : $\nabla \times \vec{\mathfrak{a}}^E_{\ell m}(\hat{n}) = 0$. It is also useful to introduce 4-dimensional eigenfunctions,

$$\mathbb{Y}^D_{\ell m}(\hat{n}) = \begin{pmatrix} Y_{\ell m}(\hat{n}) \\ 0^\mu \end{pmatrix}, \quad \mathbb{Y}^X_{\ell m}(\hat{n}) = \begin{pmatrix} 0 \\ \mathfrak{a}^{\mu,X}_{\ell m}(\hat{n}) \end{pmatrix}, \tag{3.4.17}$$

where $X \in \{T,E,B\}$. In this basis, the matrix kernel $M^q(r,r')$ can be expanded as

$$M^q(r,r') = \int_{-\infty}^{\infty} \frac{d\omega}{2\pi} \sum_{\ell=0}^{\infty} \sum_{m=-\ell}^{\ell} e^{-i\omega(\tau-\tau')} \begin{pmatrix} \mathbb{Y}^D_{\ell m}(\hat{n}) \\ \mathbb{Y}^T_{\ell m}(\hat{n}) \\ \mathbb{Y}^E_{\ell m}(\hat{n}) \\ \mathbb{Y}^B_{\ell m}(\hat{n}) \end{pmatrix}^\intercal M^q_\ell(\omega) \begin{pmatrix} \mathbb{Y}^D_{\ell m}(\hat{n}')^\dagger \\ \mathbb{Y}^T_{\ell m}(\hat{n}')^\dagger \\ \mathbb{Y}^E_{\ell m}(\hat{n}')^\dagger \\ \mathbb{Y}^B_{\ell m}(\hat{n}')^\dagger \end{pmatrix}, \tag{3.4.18}$$

where we directly work on $S^2 \times \mathbb{R}$ (i.e., taking the limit $\beta \to \infty$ now) and where

$$M^q_\ell(\omega) = \begin{pmatrix} D^q_\ell & H^{q,T}_\ell & H^{q,E}_\ell & H^{q,B}_\ell \\ -H^{q,T*}_\ell & K^{q,TT}_\ell & K^{q,TE}_\ell & K^{q,TB}_\ell \\ -H^{q,E*}_\ell & K^{q,TE*}_\ell & K^{q,EE}_\ell & K^{q,EB}_\ell \\ -H^{q,B*}_\ell & K^{q,TB*}_\ell & K^{q,EB*}_\ell & K^{q,BB}_\ell \end{pmatrix}. \tag{3.4.19}$$

All of the arguments of the functions appearing in the matrix are ω. Note that the scalar-gauge kernel is imaginary, hence the reason for the signs in the first column of the matrix. This last point is shown explicitly in App. 3.B.

This kernel can be simplified by using $\mathcal{CT}$ invariance. The auxiliary boson ϕ, a pseudo-scalar, and the E,T modes of the gauge field are antisymmetric under $\mathcal{CT}$, while the B modes

are symmetric under $\mathcal{CT}$. This implies that the following kernels vanish [8]

$$K_\ell^{q,TB}(\omega) = K_\ell^{q,EB}(\omega) = H_\ell^{q,B}(\omega) = 0. \tag{3.4.20}$$

The U(1) gauge invariance also enables the kernel to be simplified. Using the conservation of the U(1) current, $\nabla_\mu J^\mu(r) = 0$, in Eqs. (3.4.6-3.4.7), it follows that

$$K_\ell^{q,TE}(\omega) = \frac{i\omega}{\sqrt{\ell(\ell+1)}} K_\ell^{q,TT}(\omega), \tag{3.4.21}$$

$$K_\ell^{q,EE}(\omega) = \frac{\omega^2}{\ell(\ell+1)} K_\ell^{q,TT}(\omega), \tag{3.4.22}$$

$$H_\ell^{q,E}(\omega) = \frac{i\omega}{\sqrt{\ell(\ell+1)}} H_\ell^{q,T}(\omega). \tag{3.4.23}$$

It should also be noted that among vector spherical harmonics, only $\mathfrak{a}^T_{\mu,\ell m}(\hat{n})$ is defined for $\ell = 0$. In this case, the only remaining gauge-gauge kernel is $K_0^{q,TT}(\omega)$, and it vanishes by gauge invariance. The computations to obtain these gauge invariance conditions are shown in App. 3.C. Using all these simplifications, the monopole scaling dimension correction is given by

$$\begin{aligned}\Delta^{(1)}_{q,\text{QED}_3\text{-GN}} = \frac{1}{2}\int_\omega \Bigg\{ &\ln\left(\frac{D_0^q(\omega)}{D_0^0(\omega)}\right) + \sum_{\ell=1}^{\infty}(2\ell+1) \\ &\times \ln\left[\frac{K_\ell^{q,B}(\omega)\left(D_\ell^q(\omega)K_\ell^{q,E}(\omega) + \left(1+\frac{\omega^2}{\ell(\ell+1)}\right)\left|H_\ell^{q,T}(\omega)\right|^2\right)}{K_\ell^{0,B}(\omega)D_\ell^0(\omega)K_\ell^{0,E}(\omega)}\right]\Bigg\},\end{aligned} \tag{3.4.24}$$

where $\int_\omega \equiv \int_{-\infty}^{\infty} d\omega/(2\pi)$ and we defined

$$K_\ell^{q,E}(\omega) \equiv K_\ell^{q,TT}(\omega) + K_\ell^{q,EE}(\omega), \tag{3.4.25}$$

$$K_\ell^{q,B}(\omega) \equiv K_\ell^{q,BB}(\omega). \tag{3.4.26}$$

Note that $H_\ell^{0,T}(\omega) = 0$ and thus it does not appear in the denominator.

By turning off the GN interaction in Eq. (3.4.24), the scalar-scalar kernel $D_\ell^q(\omega)$ and the scalar-gauge kernel $H_\ell^{q,T}(\omega)$ do not contribute, and the monopole scaling dimension correction in QED_3 [16] is recovered :

$$\Delta^{(1)}_{q,\,\text{QED}_3} = \frac{1}{2}\int_\omega \sum_{\ell=1}^{\infty}(2\ell+1)\ln\left[\frac{K_\ell^{q,B}(\omega)K_\ell^{q,E}(\omega)}{K_\ell^{0,B}(\omega)K_\ell^{0,E}(\omega)}\right], \tag{3.4.27}$$

[8] This result was also checked explicitly with the same method giving the values of non-vanishing kernels.

One can alternatively deactivate the gauge field, keeping only the scalar-scalar kernels, and obtain the pure GN model. Despite the absence of a gauge field in this model, one can still introduce an external gauge field with the $4\pi q$ flux, define a correlation function on this background configuration, and obtain the related critical exponent. This was notably achieved for the O(N) model in Ref. [61]. In a forthcoming publication, we shall also explore this avenue in the pure-GN model.

The relevant kernel Fourier coefficients to compute the monopole scaling dimensions in (3.4.24) and (3.4.27) are found by inverting Eq. (3.4.18) :

$$D^q_\ell(\omega) = \frac{4\pi}{2\ell+1}\int_r e^{i\omega\tau} D^q\left(r,0\right)\sum_m Y^*_{\ell m}(\hat{n})Y_{\ell m}\left(\hat{z}\right), \tag{3.4.28}$$

$$H^{q,T}_\ell(\omega) = \frac{4\pi}{2\ell+1}\int_r e^{i\omega\tau} H^q_0\left(r,0\right)\sum_m Y^*_{\ell m}(\hat{n})Y_{\ell m}\left(\hat{z}\right), \tag{3.4.29}$$

$$K^{q,E}_\ell(\omega) = \frac{4\pi}{2\ell+1}\int_r e^{i\omega\tau}\left[K^q_{00}\left(r,0\right)\sum_m Y^*_{\ell m}(\hat{n})Y_{\ell m}\left(\hat{z}\right) + K^q_{aa'}\left(r,0\right)\sum_m \mathfrak{a}^{a,E*}_{\ell m}(\hat{n})\mathfrak{a}^{a',E}_{\ell m}\left(\hat{z}\right)\right], \tag{3.4.30}$$

$$K^{q,B}_\ell(\omega) = \frac{4\pi}{2\ell+1}\int_r e^{i\omega\tau} K^q_{aa'}\left(r,0\right)\sum_m \mathfrak{a}^{a,B*}_{\ell m}(\hat{n})\mathfrak{a}^{a',B}_{\ell m}\left(\hat{z}\right), \tag{3.4.31}$$

where the second coordinates are fixed to $\tau' = 0$ and $\hat{n}' = \hat{z}$ without loss of generality, and normalized coordinates a,a' are introduced.

3.4.2. Anomalous dimensions

The anomalous dimensions of monopole operators (3.4.24, 3.4.27) are computed in this section. To do so, the kernel coefficients in Eqs. (3.4.28, 3.4.30, 3.4.31) must be obtained. These coefficients are built with real-space kernels (3.4.9-3.4.11) that depend on the fermionic Green's function at the saddle-point. The Green's function is defined by the action of the Dirac operator on it :

$$i\not{D}^{S^2\times\mathbb{R}}_{\mathcal{A}^q}(r)G_q(r,r') = -\delta(r-r'). \tag{3.4.32}$$

The eigenkernels in Eqs. (3.4.28, 3.4.30, 3.4.31), involving the sums on spherical harmonics or vector spherical harmonics, will also be needed.

3.4.2.1. $q = 0$ kernels. We first compute the expressions in the denominator of the scaling-dimension corrections (3.4.24, 3.4.27), that is, the $q = 0$ kernel coefficients. The eigenkernel in the scalar-scalar kernel (3.4.28) is just the sum of spherical harmonics, which is given by

the addition theorem

$$\sum_m Y^*_{\ell m}(\hat{n}) Y_{\ell m}(\hat{n}') = \frac{2\ell+1}{4\pi} P_\ell\left(\cos\gamma\right), \tag{3.4.33}$$

where

$$\cos\gamma \equiv \hat{n}\cdot\hat{n}' = \cos\theta\cos\theta' + \sin\theta\sin\theta'\cos\left(\phi-\phi'\right). \tag{3.4.34}$$

When working with $\hat{n}' = \hat{z}$, this is replaced by

$$x \equiv \cos\theta. \tag{3.4.35}$$

For the sums on vector spherical harmonics appearing in the gauge-gauge kernels (3.4.30, 3.4.31), a similar result is obtained in spherical coordinates $a = \hat{\theta}, \hat{\phi}, \hat{\tau}$ in Eqs. (3.E.4, 3.E.5) in App. 3.E and is formulated with the same Legendre polynomial and its first and second derivatives. This reproduces a result from Ref. [62].

The real-space kernel for $q = 0$ is also needed. In this case, the Green's function takes a simple form which is simply the conformally transformed $3D$ flat space Green's function [16] :

$$G_0\left(\tau-\tau',\hat{n},\hat{n}'\right) = \frac{i}{4\pi}\frac{1}{X^{3/2}}\vec{\gamma}\cdot\left(e^{\frac{1}{2}(\tau-\tau')}\hat{n} - e^{-\frac{1}{2}(\tau-\tau')}\hat{n}'\right), \tag{3.4.36}$$

where

$$X \equiv 2\cosh(\tau-\tau') - 2\cos\gamma. \tag{3.4.37}$$

The real-space kernels can then be obtained in normalized spherical coordinates. Inserting this Green's function, along with the eigenkernels, in Eqs. (3.4.28, 3.4.30, 3.4.31), the resulting $q = 0$ kernel coefficients are (setting $\tau' = 0$)

$$D^0_\ell(\omega) = \frac{1}{8\pi^2}\int_r e^{i\omega\tau} P_\ell(x)\frac{1}{X^4}, \tag{3.4.38}$$

$$K^{0,E}_\ell(\omega) = \frac{1}{32\pi^2}\int_r e^{i\omega\tau} P_\ell(x)\Big(-\nabla^2_{S^2} + \frac{1}{\ell(\ell+1)}\nabla^2_{S^2}\partial^2_\tau\Big)\frac{1}{X^2}, \tag{3.4.39}$$

$$K^{0,B}_\ell(\omega) = -\frac{1}{8\pi^2\ell(\ell+1)}\int_r e^{i\omega\tau} P_\ell(x)\nabla^2_{S^2}\frac{1}{X^4}, \tag{3.4.40}$$

where integration by parts was used to eliminate derivatives of $P_\ell(x)$. The differential operators acting on $e^{i\omega\tau}P_\ell(x)$ can be replaced with the corresponding eigenvalues $\nabla^2_{S^2} \to -\ell(\ell+1)$ and $\partial^2_\tau \to -\omega^2$ with further integration by parts. The remaining expressions contain Fourier transforms of the form $\int_r e^{i\omega\tau}P_\ell(x)X^p$ which were obtained in the appendix of Ref. [62]. Using

these results, the $q = 0$ kernel coefficients are simplified to

$$D_\ell^0(\omega) = \left(\ell^2 + \omega^2\right) \mathcal{D}_{\ell-1}(\omega), \tag{3.4.41}$$

$$K_\ell^{0,E}(\omega) = \frac{1}{2}\left(\ell(\ell+1) + \omega^2\right) \mathcal{D}_\ell(\omega), \tag{3.4.42}$$

$$K_\ell^{0,B}(\omega) = \frac{1}{2}\left(\ell^2 + \omega^2\right) \mathcal{D}_{\ell-1}(\omega), \tag{3.4.43}$$

where

$$\mathcal{D}_\ell(\omega) = \left| \frac{\Gamma\left(\frac{1+\ell+i\omega}{2}\right)}{4\Gamma\left(\frac{2+\ell+i\omega}{2}\right)} \right|^2. \tag{3.4.44}$$

Note that we have reproduced the gauge-gauge coefficients $K_\ell^{0,E}(\omega)$ and $K_\ell^{0,B}(\omega)$ given in Ref. [16] by using the methods of Ref. [62].

3.4.2.2. Anomalous dimensions for $q = 1/2$. For the minimal magnetic charge, the eigenkernels in Eqs. (3.4.28-3.4.31) are formulated using the same expression (3.4.33, 3.E.4, 3.E.5) as in the last section. In particular, the gauge-gauge kernels will be worked out in normalized spherical coordinates. As for the real-space kernels (3.4.9-3.4.11), they depend on the $q = 1/2$ fermionic Green's function defined through Eq. (3.4.32). The spectral decomposition of the Green's function in terms of spinors with monopole harmonics components is shown in App. 3.D.2. A generalized addition theorem for monopole harmonics involving the Jacobi Polynomials $P_\ell^{(0,2q)}(x)$ is then needed. Specifically, after taking the sum over the azimuthal quantum number, the Green's function for general q is given by [16][9]

$$\begin{aligned} G_q\left(\tau,\hat{n};\tau',\hat{n}'\right) = \frac{i}{2} e^{-i2q\Theta} \sum_{\ell=q}^{\infty} e^{-E_{q,\ell}|\tau-\tau'|} \Big\{ -\frac{E_{q,\ell}}{1-x} Q_{q,\ell}(x) \left(\hat{n}-\hat{n}'\right)\cdot\vec{\gamma} + \mathrm{sgn}(\tau-\tau') \\ \times \left[qQ_{q,\ell}(x)\mathbb{I} + Q'_{q,\ell}(x)\left(\hat{n}+\hat{n}'\right)\cdot\vec{\gamma} + i\frac{q}{1+x} Q_{q,\ell}(x)\left(\hat{n}\times\hat{n}'\right)\cdot\vec{\gamma} \right] \Big\}, \end{aligned} \tag{3.4.45}$$

where the energies $E_{q,\ell}$ were defined in Eq. (3.3.8) and where

$$Q_{q,\ell}(x) = \frac{(1+x)^q}{(4\pi)\,2^q} \begin{cases} P_{\ell-q}^{(0,2q)}(x) - P_{\ell-1-q}^{(0,2q)}(x), & \ell > q, \\ 1, & \ell = q. \end{cases} \tag{3.4.46}$$

The phase $e^{-i2q\Theta}$ comes from the generalized addition theorem and is defined in Eq. (3.D.19), but it is not involved in the computation since it is always cancelled by the opposite phase of the Green's function hermitean conjugate. The Green's function can be inserted

[9] There is a sign error in the first term of the Green's function in Ref. [16] that we corrected here. This sign does not affect the conclusions in Ref. [16].

in Eqs. (3.4.9-3.4.11) to obtain the real-space kernels, which, along with the eigenkernels (3.4.33, 3.E.4, 3.E.5), are inserted in Eqs. (3.4.28-3.4.31) to compute the four kernel coefficients. Defining $K_\ell^{q,D}(\omega) \equiv D_\ell^q(\omega)$ and $K_\ell^{q,T}(\omega) \equiv H_\ell^{q,T}(\omega)$, the kernel coefficients $K_\ell^{q,Z}(\omega)$ with $Z \in \{D,T,E,B\}$ are given by

$$K_\ell^{q,Z}(\omega) = \sum_{\ell',\ell''} \frac{4\pi A^Z \left(E_{q,\ell'} + E_{q,\ell''}\right)}{\omega^2 + \left(E_{q,\ell'} + E_{q,\ell''}\right)^2} \left[\frac{\mathcal{I}_1^Z}{2} + E_{q,\ell'} E_{q,\ell''} \mathcal{I}_2^Z\right] \equiv \sum_{\ell',\ell''}^{\infty} k_{\ell,\ell',\ell''}^{q,Z}(\omega), \tag{3.4.47}$$

where the prefactors are given by

$$A^Z = \left\{1, i, \tfrac{1}{\ell(\ell+1)}, \tfrac{1}{\ell(\ell+1)}\right\},\ Z \in \{D,T,E,B\}, \tag{3.4.48}$$

the integrals for scalar-scalar and scalar-gauge kernels are

$$\mathcal{I}_1^D = -2 \int dx P_\ell \left[q^2 \frac{1}{1+x} Q_{q,\ell'} Q_{q,\ell''} + (1+x)\, Q'_{q,\ell'} Q'_{q,\ell''}\right] \tag{3.4.49}$$

$$\mathcal{I}_2^D = -\int dx \frac{1}{1-x} P_\ell Q_{q,\ell'} Q_{q,\ell''}, \tag{3.4.50}$$

$$\mathcal{I}_1^T = -2q \int dx P'_\ell Q_{q,\ell'} Q_{q,\ell''}, \tag{3.4.51}$$

$$\mathcal{I}_2^T = 0, \tag{3.4.52}$$

and the integrals for gauge-gauge kernels reproduce the expressions obtained in Ref. [16][10]

$$\mathcal{I}_1^E = 2 \int dx \left\{\left[\frac{2\ell(\ell+1)P_\ell + (1-x)\, P'_\ell}{1+x}\right] q^2 Q_{q,\ell'} Q_{q,\ell''} - \left(1-x^2\right) P'_\ell Q'_{q,\ell'} Q'_{q,\ell''}\right\}, \tag{3.4.53}$$

$$\mathcal{I}_2^E = -\int dx \left(\frac{1+x}{1-x}\right) P'_\ell Q_{q,\ell'} Q_{q,\ell''}, \tag{3.4.54}$$

$$\mathcal{I}_1^B = 2 \int dx \left\{\left[P'_\ell - (1-x)\, P''_\ell\right] \left[q^2 Q_{q,\ell'} Q_{q,\ell''} - (1+x)^2\, Q'_{q,\ell'} Q'_{q,\ell''}\right]\right\}, \tag{3.4.55}$$

$$\mathcal{I}_2^B = \int dx \left[P'_\ell + (1+x)\, P''_\ell\right] Q_{q,\ell'} Q_{q,\ell''}. \tag{3.4.56}$$

These integrals can be performed exactly, see App. 3.F for more details. In the end, these quantities depend only on the angular momenta : $\mathcal{I}_1^Z$ (ℓ,ℓ',ℓ'') and $\mathcal{I}_2^Z$ (ℓ,ℓ',ℓ''). For $\ell' = \ell'' = q$, this computation requires more care since both energies vanish, and the integral over time leading to the prefactor in Eq. (3.4.47) instead yields a Dirac delta function $\delta(\omega)$. However,

[10] Here, our definitions for the integrals differ by a factor $(2\ell+1)/(4\pi)$, so that the Legendre polynomial appears $P_\ell(x)$ instead of $F_\ell(x) = [(2\ell+1)/(4\pi)]P_\ell(x)$ as in Ref. [16].

for $\ell' = \ell'' = q = 1/2$, the term in the bracket simply vanishes. When only one of ℓ' and ℓ' have their minimal value $q = 1/2$, there is a non-vanishing contribution to the anomalous dimension. In this case, only $\mathcal{I}_1^Z$ contributes, since the prefactor in front of $\mathcal{I}_2^Z$ in Eq. (3.4.47) vanishes. For $q = 1/2$, the contribution of zero modes in Eq. (3.4.47) vanishes with $\ell = \omega = 0$, otherwise it is given by

$$2\sum_{\ell'=3/2}^{\infty} k^{1/2,Z}_{\ell,\ell',1/2}(\omega) = -\frac{1}{4\pi}\frac{\sqrt{\ell(\ell+1)}}{\omega^2+\ell(\ell+1)} \times \{1,-i,0,1\}. \tag{3.4.57}$$

The remaining contribution consists in a sum on non-zero modes $\ell',\ell'' \geq 3/2$. The summand depends on $\mathcal{I}_1^Z(\ell,\ell',\ell'')$ and $\mathcal{I}_2^Z(\ell,\ell',\ell'')$ which are formed of three-J symbols in ℓ,ℓ' and ℓ'' (3.F.8-3.F.10). Thus, one of the sums, say on ℓ'', can be viewed as finite. Then, after taking the sum on ℓ'', the remaining summand tends to a constant for large ℓ'

$$\lim_{\ell'\to\infty}\sum_{\ell''=3/2}^{\infty} k^{1/2,Z}_{\ell,\ell',\ell''}(\omega) = \alpha^Z = -\frac{1}{4\pi} \times \{2,0,1,1\}. \tag{3.4.58}$$

Thus, for kernels with a non-zero asymptotic constant, the sum on ℓ' will be divergent. This is regularized with a zeta function regularization $\sum_{\ell=a}^{\infty} \ell^{-p} = \zeta(p,a)$, here specifically $\zeta(0,3/2) = -1$

$$-\alpha^Z + \sum_{\ell'=3/2}^{\infty}\left[-\alpha^Z + \sum_{\ell''=3/2}^{\infty} k^{1/2,Z}_{\ell,\ell',\ell''}(\omega)\right]. \tag{3.4.59}$$

The sum above is then finite and is computed numerically up to a cutoff ℓ'_c. The remainder is approximated with a large ℓ' expansion of the summand $-\alpha^Z + \sum_{\ell''} k^{1/2,Z}_{\ell,\ell',\ell''}(\omega) = \sum_{p=2}^{k} c^{1/2,Z}_{\ell,p}(\omega)\,(\ell')^{-p} + O\left(1/\ell'^{(k+1)}\right)$. Each power in the expansion is summed analytically from $\ell' = \ell'_c + 1$ to $\ell' = \infty$ with a zeta function. The coefficients $c^{1/2,Z}_{\ell,p}(\omega)$ are found by doing the expansion for a few fixed values of ℓ and deducing the general dependence on ℓ. It turns out that only even powers of $1/\ell'$ have non-vanishing coefficients $c^{1/2,Z}_{\ell,p}(\omega)$. We obtained the expansion up to $k = 18$. With this remainder, we found that a cutoff $\ell'_c = 300 + 1/2$ was sufficiently large to achieve the desired precision goals. The first few terms of the remainders for general q are shown in App. 3.G.

After performing the sums in Eqs. (3.4.57, 3.4.59), the kernel coefficients in Eq. (3.4.47) are computed and inserted in Eq. (3.4.24) (or Eq. (3.4.27) for the case of QED_3). The kernel coefficients in the denominator of the logarithm of the monopole anomalous dimension were obtained analytically in Eqs. (3.4.41-3.4.43). The remaining sum on ℓ and integral on ω are

computed up to a relativistic cutoff [16]

$$\ell(\ell+1)+\omega^2 \leq L\,(L+1)\,. \tag{3.4.60}$$

We obtained the anomalous dimension with a cutoff up to $L_{\max}=65$. A function of $1/L$ is then fitted to extract the value of the anomalous dimension as the full sum and integration are taken with $L\to\infty$. Fig. 3.1 shows a quartic function fitted with the data from $L\in[L_{\max}-10, L_{\max}]$. The anomalous dimension of a charge $q=1/2$ monopole in QED$_3$-GN extracted from this fit is $\Delta^{(1)}_{1/2,\,\text{QED}_3\text{-GN}}=0.11890$, whereas in QED$_3$ it is given by $\Delta^{(1)}_{1/2,\,\text{QED}_3}=-0.03814$. This reproduces the result in Ref. [16] up to a difference of order 10^{-4}.

While we extrapolated the result for $L\to\infty$ with a quartic fit, based on a cutoff of $L_{\max}=65$, varying the maximal relativistic cutoff can change the last digit in the result quoted above. For instance, $\Delta^{(1)}_{1/2,\,\text{QED}_3}|_{L_{\max}=50}=-0.03815$. In App. 3.I, we show how we computed anomalous dimensions for various $L_{\max}$ and used the trend as $L_{\max}\to\infty$ to estimate the anomalous dimensions and their errors. The error we quote in what follows reflects the uncertainties related to the extrapolations and not the precision of our computation which yields relatively negligible errors.

Using this method, the anomalous dimension of $q=1/2$ monopoles at next-to-leading order in the $1/N$ expansion in QED$_3$-GN is given by

$$\Delta^{(1)}_{1/2,\,\text{QED}_3\text{-GN}}=0.118911(7). \tag{3.4.61}$$

The scaling dimension of $q=1/2$ monopole operators in QED$_3$-GN is then given by $2N\times 0.26510+0.118911(7)+O\left(N^{-1}\right)$. In QED$_3$, the correction we found is

$$\Delta^{(1)}_{1/2,\,\text{QED}_3}=-0.038138(5). \tag{3.4.62}$$

With this estimated uncertainty of our result, it is clearer that there is a small discrepancy when comparing our result with the correction -0.0383 computed in Ref. [16]. Trying to replicate the method in Ref. [16], we used a cubic fit with data $L\in$ [5,45] and obtained -0.03823, which is closer to -0.0383.

3.4.2.3. Anomalous dimensions for general q. For larger topological charge q, many results used from App. 3.F are not easily generalized. In the previous section, the computations involved three different Jacobi polynomials that appear after taking the sum over an appropriate azimuthal quantum number. Here instead, the real-space kernels and the eigenkernels

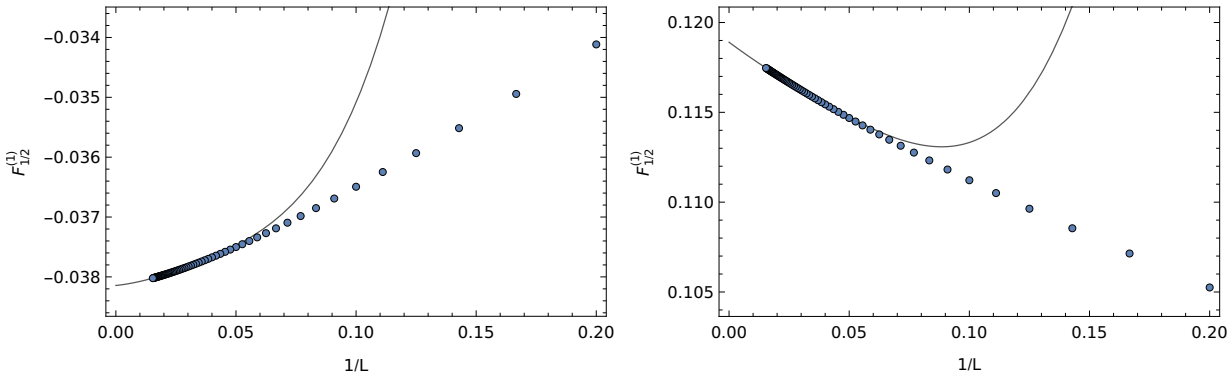

(a) (b)

Figure 3.1. Anomalous dimension of the $q=1/2$ monopole $\Delta^{(1)}_{1/2}$ (3.4.24, 3.4.27) as a function of the relativistic cutoff L (3.4.60) in (a) QED$_3$; (b) QED$_3$-GN. The points are obtained by numerically computing Eqs. (3.4.24, 3.4.27), and the solid line is a quartic fit in $1/L$ with the points $L \in [55, 65]$.

will be written explicitly as sums of monopole spherical harmonics, respectively with finite charge q and vanishing charge. This follows the alternative and more algorithmic method presented in Ref. [63].

For the real-space kernels, the required formulation already appears as an intermediate step in App. 3.D.2 when obtaining the Green's function in Eq. (3.4.45). The Green's function is a 2×2 matrix acting on particle-hole space with components given by the product of two monopole harmonics (3.D.16-3.D.18). Consequently, the real-space kernels are formulated as products of four monopole harmonics. As for the eigenkernels appearing in $D^q_\ell(\omega)$, $H^{q,T}_\ell(\omega)$, they are already expressed as the product of two spherical harmonics (3.4.28, 3.4.29). Only the gauge-gauge kernels then need a reformulation. In this case, a different basis $U^\mu_{\ell,m}(\hat{n})$,$V^\mu_{\ell,m}(\hat{n})$,$W^\mu_{\ell,m}(\hat{n})$ for the vector spherical harmonics can be introduced. These are eigenfunctions with respective total spin $j = \ell - 1$,ℓ and $\ell + 1$ [16]. Most importantly, the components of these harmonics are simply given by spherical harmonics (see App. 3.E.2). We discuss the relation with the previous basis shortly.

Before doing so, we note that, in this new formulation, the kernel coefficients are expressed as the integral of a product of four monopole harmonics and two spherical harmonics. To be more precise, half of these functions are conjugate harmonics, but they can all be expressed

as harmonics with the following relation

$$Y^*_{q,\ell,m}(\hat{n}) = (-1)^{q+m}\, Y_{-q,\ell,-m}(\hat{n}). \tag{3.4.63}$$

Just as we did in Sec. 3.4.2, the primed coordinates can be fixed as $\tau' = 0$ and $\hat{n}' = \hat{z}$ without loss of generality. As a result, half of the six harmonics are eliminated

$$Y_{q,\ell,m}\left(\hat{z}\right) = \delta_{q,-m}\sqrt{\frac{2\ell+1}{4\pi}}. \tag{3.4.64}$$

This removes every sum on azimuthal quantum numbers, which greatly simplifies the computation. There remains an integral over three harmonics

$$\begin{aligned}\int d\hat{n} Y_{q,\ell,m}(\hat{n}) Y_{q',\ell',m'}(\hat{n}) Y_{q'',\ell'',m''}(\hat{n}) = (-1)^{\ell+\ell'+\ell''} \\ \times\sqrt{\frac{(2\ell+1)\,(2\ell'+1)\,(2\ell''+1)}{4\pi}} \begin{pmatrix} \ell & \ell' & \ell'' \\ q & q' & q'' \end{pmatrix} \begin{pmatrix} \ell & \ell' & \ell'' \\ m & m' & m'' \end{pmatrix}.\end{aligned} \tag{3.4.65}$$

The explicit expressions for the kernel coefficients involve the sum of many such integrals and are not reproduced here.

Returning to the change of basis, the U,V,W vector spherical harmonics in the $j = \ell$ sector can be related to the harmonics previously introduced in Eqs. (3.4.14-3.4.16) by

$$\begin{pmatrix} U^\mu_{\ell+1,m}(\hat{n}) \\ W^\mu_{\ell-1,m}(\hat{n}) \\ V^\mu_{\ell,m}(\hat{n}) \end{pmatrix} = \begin{pmatrix} -\sqrt{\frac{\ell+1}{2\ell+1}} & \sqrt{\frac{\ell}{2\ell+1}} & 0 \\ \sqrt{\frac{\ell}{2\ell+1}} & \sqrt{\frac{\ell+1}{2\ell+1}} & 0 \\ 0 & 0 & i \end{pmatrix} \begin{pmatrix} \mathfrak{a}^{T,\mu}_{\ell m}(\hat{n}) \\ \mathfrak{a}^{E,\mu}_{\ell m}(\hat{n}) \\ \mathfrak{a}^{B,\mu}_{\ell m}(\hat{n}) \end{pmatrix} \equiv \mathcal{R} \begin{pmatrix} \mathfrak{a}^{T,\mu}_{\ell m}(\hat{n}) \\ \mathfrak{a}^{E,\mu}_{\ell m}(\hat{n}) \\ \mathfrak{a}^{B,\mu}_{\ell m}(\hat{n}) \end{pmatrix}. \tag{3.4.66}$$

The Fourier coefficients can also be transformed in this basis :

$$\mathcal{R} \begin{pmatrix} K^{q,TT}_\ell(\omega) & K^{q,TE}_\ell(\omega) & 0 \\ K^{q,TE*}_\ell(\omega) & K^{q,EE}_\ell(\omega) & 0 \\ 0 & 0 & K^{q,BB}_\ell(\omega) \end{pmatrix} \mathcal{R}^{-1} = \begin{pmatrix} K^{q,UU}_\ell(\omega) & K^{q,UW}_\ell(\omega) & 0 \\ K^{q,UW*}_\ell(\omega) & K^{q,WW}_\ell(\omega) & 0 \\ 0 & 0 & K^{q,VV}_\ell(\omega) \end{pmatrix}. \tag{3.4.67}$$

The matrix of eigenkernels keeps the same structure thanks to the block-diagonal form of the transformation matrix $\mathcal{R}$. This is expected, as we could also argue that the kernels $K^{q,UV}_\ell(\omega) = K^{q,WV}_\ell(\omega) = 0$ vanish because of CT invariance, as we did for $K^{q,TB}_\ell(\omega) = K^{q,EB}_\ell(\omega) = 0$. The relevant relations are then

$$K^{q,VV}_\ell(\omega) = K^{q,B}_\ell(\omega), \tag{3.4.68}$$

$$K^{q,UU}_\ell(\omega) + K^{q,WW}_\ell(\omega) = K^{q,E}_\ell(\omega). \tag{3.4.69}$$

The first relation is found by comparing the bottom-right components in Eq. (3.4.67) and using the definition of $K_\ell^{q,B}(\omega)$ (3.4.26), whereas the second relation is found by taking the trace of Eq. (3.4.67), using the first result in Eq. (3.4.68) and the definition of $K_\ell^{q,E}(\omega)$ (3.4.25). The kernels $K_\ell^{q,E}(\omega)$ and $K_\ell^{q,B}(\omega)$ can then be replaced in the scaling-dimension corrections (3.4.24-3.4.27) by their formulation in the new basis.

For general charge, the regularization of the kernels presented in Eqs. (3.4.58, 3.4.59) is still valid : Regulator terms $-1/(2\pi)$ and $-1/(4\pi)$ can be used respectively for the scalar-scalar and gauge-gauge kernels, while the scalar-gauge kernel does not require regularization. The contribution of the zero modes using this method is also very straightforward and algorithmic. However, there seems to be additional contributions coming from the combination of zero modes in both Green's function, $\ell' = \ell'' = q$. As discussed previously, this contribution is proportional to a Dirac Delta function $\delta(\omega)$ instead of the energy prefactor in Eq. (3.4.47). This contribution vanishes once integrated over ω (see App. 3.H). Numerical sums on ℓ' are obtained up to $\ell'_c = 200 + q$,[11] and the remainder is computed analytically with an expansion up to $1/\ell'^{18}$. In this case, the coefficients of the expansion also depend on the charge q and are found by fixing ℓ and q for a few values.

The anomalous dimension $\Delta_q^{(1)}$ for each charge are computed with a relativistic cutoff $L_{\max} = 35 + \lfloor q \rceil$, where $\lfloor q \rceil \equiv \text{Round}(q)$. Here, the convention is that half-integers are rounded to even numbers, e.g. $\lfloor 1/2 \rceil = 0$ and $\lfloor 3/2 \rceil = 2$. The value of $L_{\max}$ is modulated with the charge q to ensure that a regime with a tail-like behaviour, as observed in Fig. 3.1, is attained for larger charges. For the three minimal charges, we used a larger relativistic cutoff : We use $L_{\max} = 65$ for $q = 1/2$ (as in the last section) and $L_{\max} = 46{,}47$ for $q = 1, 3/2$.[12] We found that the results are robust as $L_{\max}$ is increased and more precise (see App. 3.I). The results for $L \in [L_{\max} - 6, L_{\max}]$ are used to fit a quartic function in $1/L$ to extrapolate the anomalous dimensions $\Delta_q^{(1)}$ as $L \to \infty$. The fits obtained for $q = 5/2$ monopoles in QED_3 and QED_3-GN are shown in Fig. 3.2 and yield scaling-dimension corrections $\Delta^{(1)}_{5/2,\,\text{QED}_3} = -1.0359$ and $\Delta^{(1)}_{5/2,\,\text{QED}_3\text{-GN}} = 0.6253$ as $L \to \infty$.

[11] We use a smaller cutoff for the general charge q which is still sufficient for the precision needed and less computationally intensive.

[12] In these cases, we use $\ell'_c = 300 + q$. For $q = 1/2$, we fit with $L \in [L_{\max} - 10, L_{\max}]$ (as in the last section) whereas we fit the $q = 1, 3/2$ cases with $L \in [L_{\max} - 6, L_{\max}]$ (as other charges in this section). The number of points used for the fits is discussed further in App. 3.I.

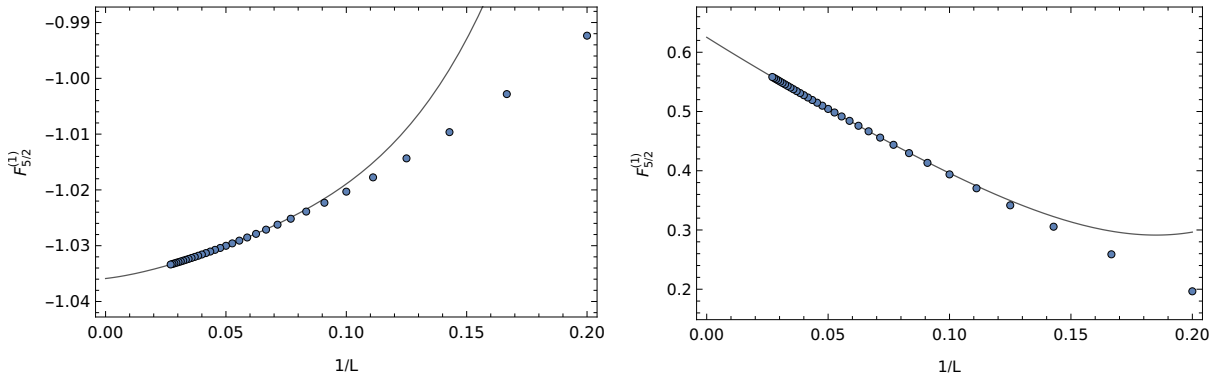

(a) (b)

Figure 3.2. Anomalous dimension of the $q = 5/2$ monopole $\Delta^{(1)}_{5/2}$ (3.4.24, 3.4.27) as a function of the relativistic cutoff L (3.4.60) in (a) QED$_3$; (b) QED$_3$-GN. The points are obtained by numerically computing Eqs. (3.4.24, 3.4.27) and the solid line is a quartic fit in $1/L$ with the points $L \in [L_{\max} - 6, L_{\max}]$, here $[31, 37]$.

As before, the uncertainty in the scaling dimension is estimated by varying $L_{\max}$ and estimating the anomalous dimension as $L_{\max} \to \infty$. More details are shown in App. 3.I . The resulting scaling dimensions up to $q = 7/2$ obtained in this way are shown in Tab. 3.1. Comparing the QED$_3$ monopoles' anomalous dimensions with the results in Ref. [61], discrepancies of order 10^{-4} to 10^{-3} are again observed for higher charges.

The $q = 1/2$ results obtained in Sec. 3.4.2.2 are successfully reproduced with the more general method. Monopole scaling dimensions up to $q = 13$ are shown in App. 3.J.

The next-to-leading order term in $1/N$ decreases the scaling dimension of monopoles in QED$_3$ whereas it increases for QED$_3$-GN. That is, quantum corrections help to stabilize the QED$_3$-GN model and destabilize QED$_3$. To understand the difference between both cases, it is useful to write the scaling dimension as

$$\Delta^{(1)}_{q,\,\text{QED}_3\text{-GN}} = \Delta^{(1)}_{q,\,\text{QED}_3} + \Delta^{(1)}_{q,\,\text{GN}} + \frac{1}{2}\int_\omega \sum_{\ell=1}^{\infty} (2\ell+1) \ln\left[1 + \frac{\left(1 + \frac{\omega^2}{\ell(\ell+1)}\right)\left|H^{q,T}_\ell(\omega)\right|^2}{D^q_\ell(\omega) K^{q,E}_\ell(\omega)}\right], \tag{3.4.70}$$

where $\Delta^{(1)}_{q,\,\text{GN}} = \frac{1}{2}\int_\omega \sum_{\ell=0}^{\infty} (2\ell+1) \log\left[D^q_\ell(\omega)/D^0_\ell(\omega)\right]$ is the contribution in the QED$_3$-GN anomalous dimension (3.4.24) coming exclusively from the pseudo-scalar field.[13] Computing

[13] It is also the expression for the anomalous dimension of monopoles in a pure GN model, hence the label.

Tableau 3.1. Leading-order and next-to-leading order in $1/N$ contributions to monopole scaling dimensions in QED_3, QED_3-GN, and QED_3-Z_2GN models. The latter model is discussed in Sec. 3.7. The leading-order result is the same in all models. The scaling dimension in a given model is $\Delta_q = 2N\Delta_q^{(0)} + \Delta_q^{(1)} + O\left(N^{-1}\right)$.

q	$\Delta_q^{(0)}$	$\Delta^{(1)}_{q,\,\mathrm{QED}_3}$	$\Delta^{(1)}_{q,\,\mathrm{QED}_3\text{-GN}}$	$\Delta^{(1)}_{q,\,\mathrm{QED}_3\text{-Z}_2\mathrm{GN}}$
1/2	0.26510	−0.038138(5)	0.118911(7)	0.102846(9)
1	0.67315	−0.19340(3)	0.23561(4)	0.18663(4)
3/2	1.18643	−0.42109(4)	0.35808(6)	0.26528(7)
2	1.78690	−0.70482(9)	0.4879(2)	0.3426(2)
5/2	2.46345	−1.0358(2)	0.6254(2)	0.4202(3)
3	3.20837	−1.4082(2)	0.7705(3)	0.4989(3)
7/2	4.01591	−1.8181(2)	0.9229(3)	0.5789(4)

$\Delta^{(1)}_{q,\,\mathrm{GN}}$ in the same way as we did for $\Delta^{(1)}_{q,\mathrm{QED}_3\text{-GN}}$ and $\Delta^{(1)}_{q,\,\mathrm{QED}_3}$, we found this contribution is positive $\Delta^{(1)}_{q,\,\mathrm{GN}} > 0$ and more important than the contribution coming exclusively from gauge fields $\left|\Delta^{(1)}_{q,\,\mathrm{GN}}\right| > \left|\Delta^{(1)}_{q,\,\mathrm{QED}_3}\right|$. As for the remaining scalar-gauge contribution in the second line of Eq. (3.4.70), it is also positive. To see this, we must show that the second term in the logarithm is positive. The numerator is explicitly positive. As for the denominator, we note that $\Delta^{(1)}_{q,\,\mathrm{GN}}$ is real, meaning that $D^q_\ell(\omega)$ and the $D^0_\ell(\omega)$ must have the same sign. The latter $q = 0$ kernel is positive, as seen from Eqs.(3.4.41, 3.4.44), meaning that $D^q_\ell(\omega) > 0$. The same goes for $K^{q,E}_\ell(\omega)$, thus the denominator is positive $D^q_\ell(\omega)K^{q,E}_\ell(\omega) > 0$. This does not come as a surprise as these kernels are diagonal entries in the Hessian matrix developed around a minimum saddle-point. The scalar-gauge kernel thus gives a positive contribution to the anomalous dimension in QED_3-GN. It then must be that the QED_3-GN monopole anomalous dimension is positive, $\Delta^{(1)}_{q,\,\mathrm{QED}_3\text{-GN}} > 0$, given what is known about each contribution on the RHS of Eq. (3.4.70). It would be desirable to understand heuristically why quantum fluctuations render monopoles less relevant at the QCP compared to deep in the Dirac spin liquid.

In the CP^{N-1} model, similar relations between the different contributions to the monopole anomalous dimension are found. A positive contribution coming only from the auxiliary boson was found numerically in Ref. [61]; the correction from the mixed scalar-gauge kernel can

be deduced as positive [62, 64], and the total anomalous dimension of monopoles in CP^{N-1} numerically found in Ref. [64] is also positive.

3.4.2.4. Convexity conjecture. It was recently conjectured that CFT operators charged under a global U(1) symmetry respect the following convexity relation

$$\Delta((n_1+n_2)n_0) \geq \Delta(n_1 n_0) + \Delta(n_2 n_0), \tag{3.4.71}$$

for some positive integer n_0 of order 1 [65]. We test this conjecture using the monopole operators that are charged under $\mathrm{U}(1)_{\mathrm{top}}$. Here, n_0,n_1,n_2 are integers, where in our notation $\Delta(2q) \equiv \Delta_q$. Using the scaling dimensions we obtained in Tab. 3.5 and extrapolating to finite N, we find this relation is respected for the monopoles under consideration in QED_3, QED_3-GN (and also for the case QED_3-Z_2GN presented later on) for any $2N \in \mathbb{Z}_+$ starting from $n_0 = 1$, i.e. the minimal possible value.

3.5. Large-charge universality

In CFTs with a global U(1) symmetry, the related charge q can be used as an expansion parameter by using effective-field-theory methods. It was shown that the lowest scaling dimension among charge-q operators has the following expansion at $q \gg 1$ [54] :

$$\Delta_q = c_{3/2} q^{3/2} + c_{1/2} q^{1/2} + \gamma_{\mathrm{U}(1)} + \ldots, \tag{3.5.1}$$

where the ellipsis denotes negative half-integer and integer powers of q [66]. While $c_{3/2}$ and $c_{1/2}$ depend on the specific QFT considered, the $O\left(q^0\right)$ coefficient is universal (theory independent) [54, 67] :

$$\gamma_{\mathrm{U}(1)} = -0.0937\ldots \tag{3.5.2}$$

This coefficient is obtained by computing the Casimir energy of the U(1) Goldstone mode. The Goldstone appears in the state-operator correspondence where the charged operator insertion is mapped to a state where the saddle-point configuration breaks the U(1) symmetry.

This analysis applies to monopole operators in theories with the global $\mathrm{U}_{\mathrm{top}}(1)$ symmetry group. Given the universality of the coefficient γ, no term at $O\left(q^0\right)$ should be present at leading-order in the $1/N$ expansion[14], since the leading-order term is proportional to N and thus non-universal. This was indeed observed in QED_3, and O(2)- and O(3)-QED_3-GN

[14]Here, the parameter N is used to designate either N complex boson flavors or $2N$ fermion flavors.

models[15] [31, 33] as well as in the CP^{N-1} model [62, 68].[16] Since QED_3 and QED_3-GN monopoles have the same leading-order scaling dimensions, as discussed in Sec. 3.3, this also applies to QED_3-GN monopoles.

Using the monopole anomalous dimensions $\Delta_q^{(1)}$, the $O\left(q^0\right)$ coefficient γ can be computed. This was done for the CP^{N-1} model in Ref. [68], where $\Delta_q^{(1)}$ was obtained for a hundred charges $q = 1/2,1,\ldots,50$ and the expected expansion (3.5.1) is fitted numerically to extract γ. A similar computation is performed here for monopoles in the QED_3-GN and QED_3 models. We fit all monopole anomalous dimensions in QED_3-GN and QED_3 shown in Tab. 3.5 by using the fitting function in Eq. (3.5.1) with powers down to q^{-1} [66]. The fits and the anomalous dimensions are shown in Fig. 3.3; note that the errors in the values of the anomalous dimension are smaller than the dots in the figure. Including more powers in the fitting function would yield significantly larger errors in the estimation of γ.

The value of γ obtained for each theory is consistent with the expected universal value (3.5.2)

$$\gamma_{\mathrm{QED}_3} = 1.02(4) \times \gamma_{\mathrm{U}(1)}, \tag{3.5.3}$$

$$\gamma_{\mathrm{QED}_3\text{-GN}} = 1.01(6) \times \gamma_{\mathrm{U}(1)}. \tag{3.5.4}$$

This is a nice consistency check of the anomalous scaling dimensions obtained in the last section.

The universal coefficient of the scaling dimension of U(1)-charged operators in Eq. (3.5.1) can also be formulated with the following sum rule [54]

$$q^2\Delta_q - \left(\frac{q^2}{2} + \frac{q}{4} + \frac{3}{16}\right)\Delta_{q-1} - \left(\frac{q^2}{2} - \frac{q}{4} + \frac{3}{16}\right)\Delta_{q+1} = -\frac{3}{8}\gamma_{\mathrm{U}(1)} + O\left(q^{-1/2}\right) = 0.0351\ldots \tag{3.5.5}$$

The RHS results from a cancellation of order $O(q^{3/2})$ and $O(q^{1/2})$ terms on the LHS. In comparison, the error on the LHS coming from the triplet Δ_{q-1},Δ_q,Δ_{q+1} is comparatively large, even more so as the coefficients in front of the scaling dimensions, which are of order q^2, become larger with increasing q. The resulting errors are too important to obtain a reliable

[15] These models are also known as QED_3 −chiral XY GN and QED_3 −chiral Heisenberg GN models, respectively.

[16] While Ref. [62] discusses only the $O\left(q^{3/2}\right)$ term of the large-q expansion, it is straightforward to use their analytical results to verify that no $O\left(Nq^0\right)$ term is present.

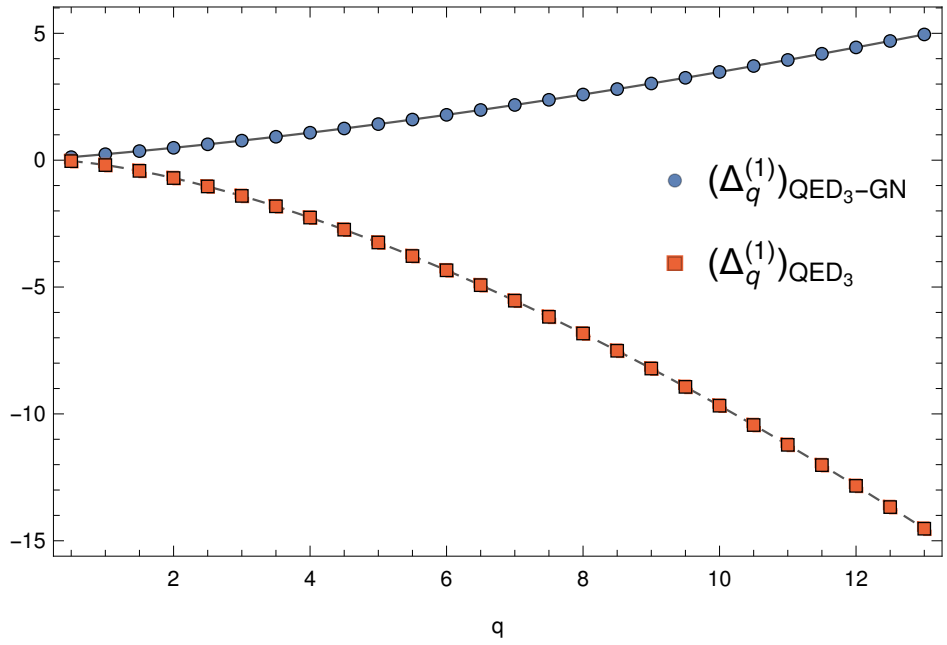

Figure 3.3. Anomalous dimensions of monopoles in QED_3-GN and QED_3 fitted with the large-q expansion (3.5.1). The points are the scaling dimension corrections obtained with a quartic fit in $1/L$. The solid and dashed lines are the fitting functions for QED_3-GN and QED_3, respectively, with a minimal power of q^{-1}.

fit of the large-q behaviour of this sum rule. Nevertheless, we did observe a good qualitative agreement for the scaling dimensions shown in Tab. 3.5.

3.6. CFT duality : QED_3-GN and CP^1 models

Another interesting application of our results concerns the duality between the QED_3-GN model with $2N = 2$ two-component Dirac fermion flavors and the CP^{N-1} model with $N = 2$ complex boson flavors [53]. Crucially, the duality between these models implies an emergent SO(5) symmetry. The following SO(5) multiplet in the $\text{QED}_3\text{-GN}\,|_{2N=2}$ model

$$\left(\text{Re}(\psi_1^\dagger \widetilde{\mathcal{M}}^f_{1/2}), -\text{Im}\left(\psi_1^\dagger \widetilde{\mathcal{M}}^f_{1/2}\right), \text{Re}(\psi_2^\dagger \widetilde{\mathcal{M}}^f_{1/2}), \text{Im}(\psi_2^\dagger \widetilde{\mathcal{M}}^f_{1/2}), \phi\right), \tag{3.6.1}$$

is dual to the following multiplet in the CP^1 model

$$\left(2\,\text{Re}(\mathcal{M}^b_{1/2}), 2\,\text{Im}(\mathcal{M}^b_{1/2}), z^\dagger\sigma_1 z, z^\dagger\sigma_2 z, z^\dagger\sigma_3 z\right). \tag{3.6.2}$$

Here $\widetilde{\mathcal{M}}^f_{1/2}$ are the $\text{QED}_3\text{-GN}\,|_{2N=2}$ minimally charged monopoles which must be dressed with an additional zero mode $\psi_1^\dagger$ or $\psi_2^\dagger$ on top of a Dirac sea in order to be gauge invariant.

These monopoles form an SU(2) doublet $\mathcal{M}^f_{1/2} = \left(\mathcal{M}^f_{1/2,\uparrow}, \mathcal{M}^f_{1/2,\downarrow}\right)^\intercal$. On the CP^1 side, z is an SU(2) doublet $z = (z_1, z_2)^\intercal$ where each flavor is a complex boson and $\mathcal{M}^b_{1/2}$ is the minimally charged monopole. The SO(5) symmetry means that all scaling dimensions within a multiplet should be equal, while operators identified by the duality should also have the same scaling dimension. Putting this together, this means that all the operators above should have the same scaling dimension. A decent agreement was already observed in Ref. [31], but the scaling dimension of QED_3-GN monopoles were obtained only at leading-order in $1/N$, with $\Delta_{\mathcal{M}^f_{1/2}} = 0.53$. Updating the comparison with the next-to-leading order correction, we find $\Delta_{\mathcal{M}^f_{1/2}} = 0.65$, which gives an even better agreement. For instance, the scaling dimension of the $q = 1/2$ monopole on the CP^1 side obtained at next-to-leading in $1/N$ is given by $\Delta_{\mathcal{M}^b_{1/2}} = 0.63$ [62, 64]. In contrast, if we extrapolate the large-N QED_3 result to $2N = 2$, we obtain a scaling dimension of 0.49, which is further from the CP^1 result, as expected since the two CFTs are not related by duality. The scaling dimensions of the other operators in the duality also show a good agreement coming from both analytical and numerical studies, as shown in Tab. 3.2.

In the same way, monopoles with the second smallest charge $q = 1$ were argued to be part of the symmetric traceless **14** representation of SO(5) [44, 69]. The various relevant scaling dimensions obtained with analytical methods are also compared in Tab. 3.3. Again there is a very good agreement between the scaling dimension of monopole operators, with $\Delta_{\mathcal{M}^f_1} = 1.58$ and $\Delta_{\mathcal{M}^b_1} = 1.50$. The agreement is weaker with other operators, but by taking into account Padé and Padé-Borel resummations the duality prediction seems quite reasonable. The scaling dimension related to auxiliary bosons Δ_{ϕ^2} and Δ_λ obtained using the large-N have greater discrepancy with $\Delta \sim 1$, but these expansions are not very well controlled. However, the same can be said about the monopole operator on the bosonic side. Overall, the duality for the **14** representation of SO(5) is not as convincing as for the **5**, but still reasonable for perturbative results. The scaling dimension of the Lagrange field obtained using the functional renormalization group also agrees reasonably well $\Delta_\lambda = 1.21$ [70].

The CP^1 model is a prototype for dQCPs and has received a great deal of attention, particularly in many numerical lattice studies. The value obtained for the correlation length exponent ν, related to the Lagrange field scaling dimension as $\Delta_\lambda = 3 - 1/\nu$, has varied greatly among many numerical works. Older results indicate $\Delta_\lambda \in [1.34, 1.67]$ [71, 72, 78, 79]

Tableau 3.2. Operators in the SO(5) **5** multiplets (3.6.1, 3.6.2) and their scaling dimensions. "VBS" and "Néel" make reference to operators whose scaling dimensions are obtained numerically on lattices. The results for monopole operators are obtained by using the state-operator correspondence at next-to-leading order in $1/N$. The scaling dimension of the auxiliary boson ϕ in QED$_3$-GN was obtained at order $1/N$ using the mean of Padé and Padé-Borel [0/1] resummations (non-resummed scaling dimension are unphysical). The scaling dimension of the fermionic monopole operator can also be resummed to $(0.59, 0.68)$, but not in the bosonic case. The operator $z^\dagger \boldsymbol{\sigma} z$ designates any of the boson bilinears, i.e. flavor spin-1 in the bosonic side. It was obtained at order $1/N^2$ in Ref. [69] and using functional renormalization group in Ref. [70].

$\mathcal{O}$	$\Delta_{\mathcal{O}}$	Ref.
$\mathcal{M}^f_{1/2}$	0.65	This work
$\mathcal{M}^b_{1/2}$	0.63	[64]
ϕ	$(0.59, 0.64)$	[47]
$z^\dagger \boldsymbol{\sigma} z$	0.64	[69]
	0.61	[70]
VBS, Néel	$[0.60, 0.68]$	[71–75]

which seems compatible with other scaling dimensions in Tab. 3.3. Unusual scaling behaviour and the "drifting" of ν with increasing lattice size [75] motivated further studies, and lower scaling dimensions have been found. The wide range of values obtained are shown in Tab. 3.4. Notably, a scaling dimension going down to $\Delta_\lambda = 0.75(1)$ by considering the presence of a second length scale [80]. Among other scenarios considered was that of a weakly first order transition. This possibility has also been discussed in a field theory context where the dual models QED$_3$-GN $|_{2N=2}$ and CP^{N-1} $|_{N=2}$ are possibly complex CFTs emerging from the collision of fixed points as the number of matter flavors is lowered below a critical level in Ref. [69, 81].

A similar tension between the results from field theory and lattice models was observed in Ref. [83] where the QED$_3$ $|_{2N=2}$ model was studied using conformal bootstrap. The duality to the easy-plane CP^1 model conjectured in Ref. [53] implies a self-duality and an emergent O(4) symmetry on both sides. While the conformal bootstrap study of QED$_3$ $|_{2N=2}$ is consistent

Tableau 3.3. Operators in the SO(5) symmetric traceless **14** multiplets and their scaling dimensions predicted to be equal according to the duality between QED$_3$-GN$|_{2N=2}$ and CP^1 models. The scaling dimensions presented are obtained analytically with the large-N expansion. Padé and Padé-Borel [0/1] resummations are shown in parenthesis (apart from Ref. [47], resummations are not obtained in the references cited). The symbol "$\times$" indicates unphysical results, i.e., negative scaling dimensions. The operator λ is the Lagrange multiplier field on the CP^1 side. Results for monopole operators are obtained using state-operator correspondence at order N^0, while other results were obtained at order N^{-1}. The resummed value for $\Delta_{\bar{\psi}\boldsymbol{\sigma}\psi}$ was obtained in Ref. [47] and is the same for $\Delta_{(z^*\boldsymbol{\sigma}z)(z^*\boldsymbol{\sigma}z)^\intercal}$ at this order.

$\mathcal{O}$	$\Delta_{\mathcal{O}}$	$(\Delta_{\mathcal{O}}^{\text{Padé}},\Delta_{\mathcal{O}}^{\text{Padé-Borel}})$	Ref.
$\mathcal{M}_1^f$	1.58	$(1.63, 1.75)$	This work
$\mathcal{M}_1^b$	1.50	$(\times, 0.24)$	[64]
$\bar{\psi}\boldsymbol{\sigma}\psi$	1.19	$(1.42, 1.51)$	[47, 69]
$\left(z^\dagger\boldsymbol{\sigma}z\right)\left(z^\dagger\boldsymbol{\sigma}z\right)^\intercal$	1.19	$(1.42, 1.51)$	[69]
ϕ^2	4.43	$(\times,1.02)$	[47, 69]
λ	$\times$	$(0.90, 1.11)$	[76, 77]

Tableau 3.4. Numerical determination of the correlation length exponent ν and the related scaling dimension $\Delta_\lambda = 3 - 1/\nu$ in lattice studies describing the CP^1 side.

ν	Δ_λ	Ref.
0.78(3)	1.72(5)	[71]
0.68(4)	1.52(9)	[72]
0.67(1)	1.51(3)	[79]
0.69(2)	1.55(5)	
0.62(2)	1.39(5)	[78]
0.54(5)	1.13(17)	[74]
[0.51,0.69]	[1.04,1.55]	[82]
0.468(6)	0.87(3)	[75]
0.455(2)	0.80(1)	[80]

with the self-duality and the emergent symmetry, it contradicts results from the lattice study of the easy-plane CP^1 model [84].

An interesting approach to understand these discrepancies could be that of pseudo-criticality, that is a weakly first-order transition with a generically long correlation length. In Ref. [85], a Wess-Zumino-Witten model in $2+\epsilon$ dimensions, with target space $S^{3+\epsilon}$, with global symmetry $\mathrm{SO}(4+\epsilon)$ has been shown to exhibit this behaviour and consistent with numerical results in the literature. A crucial point was that the physical dimension $d=3$ is close to the critical dimension $d=2.77$ where fixed points collide. Pseudo-criticality was also found in a loop model describing the easy-plane Néel-VBS transition [86].

Higher charge

The duality can be tested further by comparing monopoles on both sides of the duality. First, the relation between minimally charged monopoles is further discussed. This relation is simpler to see with the appropriate sub-models. A duality between $\mathrm{QED}_3\,|_{2N=2}$ and easy-plane CP^1 was formulated by including additional external gauge fields B_μ,B'_μ and Chern-Simons terms [53, 87]

$$|D_{b+B}z_1|^2+|D_{b+B'}z_2|^2-|z_1|^4-|z_2|^4-\frac{1}{2\pi}bd\,(B+B')-\frac{1}{2\pi}BdB'-\frac{1}{2\pi}B'dB \quad (3.6.3)$$

$$\Leftrightarrow\quad \overline{\psi}_1 i\not{D}_{a-B}\psi_1+\overline{\psi}_2 i\not{D}_{a+B}\psi_2+\frac{1}{2\pi}adB'+\frac{1}{4\pi}\,(BdB-B'dB')\,, \quad (3.6.4)$$

where b_μ and a_μ are the dynamical gauge fields in bosonic and fermionic models, respectively. By inspecting the charges under the external gauge fields (q_B,$q_{B'}$), we can identify the following bosonic operators

$$(2\mathcal{M}^b_{1/2},2z_1^*z_2)\Leftrightarrow\left((\psi_1^\dagger\widetilde{\mathcal{M}}^f_{1/2})^\dagger,\psi_2^\dagger\widetilde{\mathcal{M}}^f_{1/2}\right). \quad (3.6.5)$$

Here, the first and second component on both sides have charges (1,1) and $(1,-1)$ under B_μ and B'_μ. While an SU(2) doublet structure is manifest in the RHS with the fermion zero modes, it is less clear in the LHS and may be seen as a non-trivial corollary of the duality. This may however be motivated by the self-duality in the easy-plane CP^1 model. The VBS order in the original model $\mathcal{M}^b_{1/2}$ is mapped to the XY order in terms of the dual bosons $w_1^*w_2$. Conversely, monopoles in the dual side are mapped to $z_1^*z_2$ in the original model.

These relations between operators translate back to the QED$_3$-GN $|_{2N=2} \Leftrightarrow$ CP^1 duality. In particular, it is useful to focus on the dual relation between the CP^1 monopole $2\mathcal{M}^f_{1/2}$ and the corresponding dual monopole in QED$_3$-GN $|_{2N=2}$, $\left(\psi_1^\dagger \widetilde{\mathcal{M}}^f_{1/2}\right)^\dagger$. For convenience, we define the following monopole operator $\mathcal{M}^f_{1/2}(x) \equiv 2\left(\psi_1^\dagger \widetilde{\mathcal{M}}^f_{1/2}\right)^\dagger$. Our starting point is then the conjectured dual relation between minimally charged monopoles in QED$_3$-GN $|_{2N=2}$ ($\mathcal{M}^f_{1/2}$) and in CP^1 ($\mathcal{M}^b_{1/2}$) models

$$\mathcal{M}^f_{1/2}(x) \Leftrightarrow \mathcal{M}^b_{1/2}(x). \tag{3.6.6}$$

Using this relation and the operator product expansion (OPE)

$$\mathcal{O}_1(x)\mathcal{O}_2(y) = \sum_n c_n(x-y)\mathcal{O}_n(y), \tag{3.6.7}$$

the scaling dimensions of higher charge monopoles can also be compared. The OPE of two $q = 1/2$ monopole operators yields the expansion over $q = 1$ operators

$$\lim_{y\to x} \mathcal{M}_{1/2}(x)\mathcal{M}_{1/2}(y) = \lim_{y\to x} c(x-y)\mathcal{M}_1(x) + \cdots \tag{3.6.8}$$

where the ellipsis stands for other primary operators with larger scaling dimensions. By definition, $\mathcal{M}_1(x)$ has the smallest scaling dimension in the $q = 1$ topological sector. We can then identify the scaling dimension of $q = 1$ monopole operators on both sides of the duality $\Delta^f_{q=1} = \Delta^b_{q=1}$. This is expected, as these monopoles are conjectured to be components dual SO(5) symmetric traceless **14** multiplet [44, 69]. Using the same logic for higher charge monopoles, we find more generally that

$$\Delta^f_q = \Delta^b_q. \tag{3.6.9}$$

Comparing our results for QED$_3$-GN $|_{2N=2}$ monopoles in Tab. 3.1 to CP^1 monopoles in Ref. [68], we obtain a good agreement for higher charges, as shown in Fig. 3.4. For larger charges, the relative difference tends to 10%. This is a great improvement compared to the results obtained with only the leading-order scaling dimensions : the behaviour is similar and the asymptotic relative difference for large q is 76% instead.

3.7. Transition to a Z_2 spin liquid

The transition out of the U(1) DSL to a Z_2 spin liquid can also be studied with a gauged Gross-Neveu model [30, 49–51]. The Lagrangian describing this transition is written

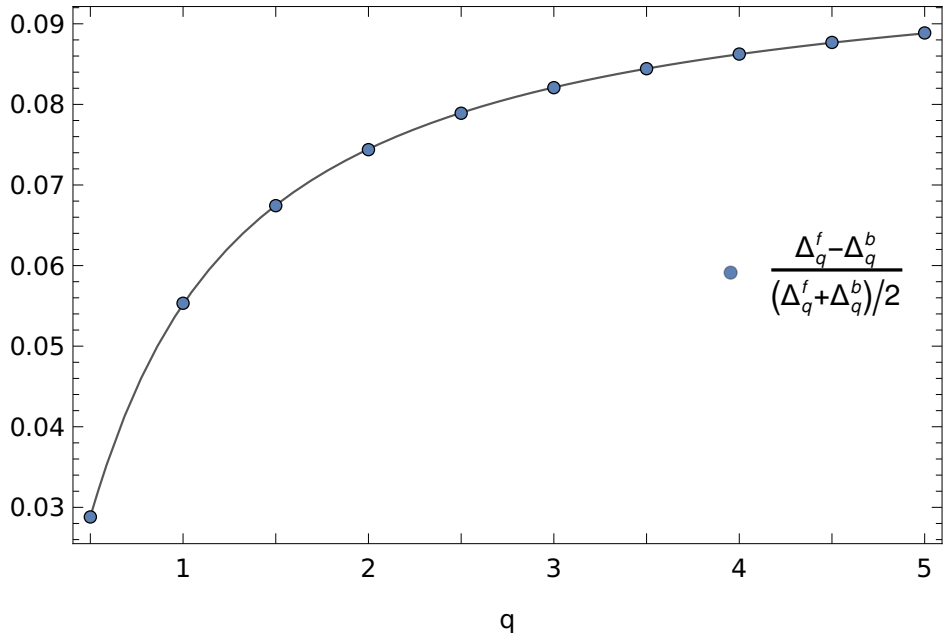

Figure 3.4. Relative difference between the scaling dimensions of monopoles in QED$_3$-GN$|_{2N=2}$ and CP^1 models as a function of the topological charge. The computation is done with next-to-leading-order results in both models. The solid line is a fit $f_0 + f_{-1}q^{-1} + f_{-3/2}q^{-3/2}$, where the asymptote for large charge is approximately a 10% relative difference. The powers used in the fitting function are deduced from Eq. (3.5.1).

in euclidean flat spacetime as

$$\mathcal{L}_\psi = \sum_{i=1}^{2N} -\overline{\psi}_i(\not{\partial} - i\not{\mathcal{A}}_q - i\not{A})\psi_i + \sum_{i=1}^{2N}(\phi^* \psi_i^T i\gamma_2 \psi_i + \text{h.c.}), \tag{3.7.1}$$

where ϕ is a complex scalar that decouples a quartic superconducting pairing term for the fermions. The interaction term included preserves Lorentz invariance. As ϕ describes Cooper pairs, it transforms as $\bar{\psi}_i i\gamma_2 \bar{\psi}_i^T$ under U(1) gauge transformations. The Yukawa interaction term in the above equation is thus gauge invariant. In the Z_2 QSL, ϕ acquires an expectation value, which Higgses the gauge field, leading to a gapped s-wave superconducting state for the Dirac fermions.

We recall that the Dirac conjugate is defined by $\overline{\psi}_a = \psi_a^\dagger \gamma_0$ and $\mathcal{A}_\mu^q$ is the external gauge field that sources the flux of $4\pi q$. The gauge-covariant derivative for the external gauge field $\mathcal{A}_\mu^q$ on a curved spacetime is defined in Eq. (3.2.13). We now introduce the Nambu spinor

defined as

$$\Upsilon_i = \begin{pmatrix} \psi_i \\ i\gamma_2 \overline{\psi}_i^T \end{pmatrix} = \begin{pmatrix} \psi_i \\ C\overline{\psi}_i^T \end{pmatrix}. \tag{3.7.2}$$

In addition, we define $\mathcal{C} = \mathrm{diag}(C,C)$, where $C = i\gamma_2$. The C operator obeys $C^2 = -1$, $C^T = C^{-1} = -C$, and $C\gamma_\mu C = \gamma_\mu^T$. The transpose of the Nambu spinor is given by $\Upsilon_i^T = (\psi_i^T, \overline{\psi}_i C^T) = (\psi_i^T, -\overline{\psi}_i C)$. Thus, the fermionic action can be expressed as

$$S_\Upsilon = \frac{1}{2}\int_{r,r'} \Upsilon_i^T(r)\mathcal{C}\mathcal{G}^{-1}(r,r')\Upsilon_i(r'), \tag{3.7.3}$$

where the (inverse) Nambu Green's function is

$$\mathcal{G}^{-1}(r,r') = \begin{pmatrix} 2\phi^*(r)\delta(r-r') & -\not{D}_{-(A+\mathcal{A}_q)} \\ -\not{D}_{A+\mathcal{A}_q} & 2\phi(r)\delta(r-r') \end{pmatrix}. \tag{3.7.4}$$

As in Sec. 3.4, the fields ϕ and A are expanded about their saddle-point values as $\phi = \langle\phi\rangle + \sigma/\sqrt{2N}$, $A = \langle A\rangle + a/\sqrt{2N}$, where the fluctuations are suppressed by $1/\sqrt{2N}$. At the QCP, the saddle-point values are $\langle\phi\rangle = \langle A\rangle = 0$ [50]. Thus, in terms of the saddle-point and fluctuation fields, the inverse Green's function is

$$\begin{aligned}\mathcal{G}^{-1}(r,r') = \mathcal{G}_0^{-1}(r,r') &+ \frac{1}{\sqrt{2N}}X_\sigma(r)\delta(r-r') \\ &+ \frac{1}{\sqrt{2N}}X_a(r)\delta(r-r').\end{aligned} \tag{3.7.5}$$

Here, $\mathcal{G}_0^{-1}$ is the bare inverse Green's function, determined from the gauge covariant derivative term involving $\mathcal{A}_\mu^q$ in Eq. (3.7.4), and X_σ and X_a are given by

$$X_\sigma = 2\begin{pmatrix} \sigma^* & 0 \\ 0 & \sigma \end{pmatrix}, \quad X_a = \begin{pmatrix} 0 & -\not{a} \\ \not{a} & 0 \end{pmatrix}. \tag{3.7.6}$$

Integrating out the fermions then gives the effective action as $\int \mathcal{D}\Upsilon \exp(-S_\Upsilon) \equiv \exp(-S_{\text{eff}})$, where $S_{\text{eff}} = -\frac{1}{2}(2N)\mathrm{Tr}\log\mathcal{G}^{-1}$. We let Tr denote a "trace" over all relevant degrees of freedom, whereas tr denotes a trace over spinor components. To compute the effective action, we express the fermionic action as a quadratic form in the fluctuation fields and perform a Gaussian functional integral over a and σ. The linear terms in a and σ vanish due to the saddle-point conditions for A and ϕ. Thus, to quadratic order, the effective action becomes

$$S_{\text{eff}} = S_{\text{eff}}|_{\text{s.p.}} + \frac{1}{4}\mathrm{Tr}\,\mathcal{G}_0 X_a \mathcal{G}_0 X_a + \frac{1}{4}\mathrm{Tr}\,\mathcal{G}_0 X_a \mathcal{G}_0 X_\phi + \frac{1}{4}\mathrm{Tr}\,\mathcal{G}_0 X_\phi \mathcal{G}_0 X_a + \frac{1}{4}\mathrm{Tr}\,\mathcal{G}_0 X_\phi \mathcal{G}_0 X_\phi. \tag{3.7.7}$$

The fluctuations are $O(1/(2N))$, thus they cancel the prefactor $2N$. The second and third terms involve both the gauge field and the scalar field. By taking the trace over the Nambu matrix structure, these terms are found to vanish. Indeed, these terms must vanish from gauge invariance. Hence, only the gauge-gauge and scalar-scalar kernels contribute, which is in contrast to the QED$_3$-GN case where mixing between the two sectors exists. After performing the trace over the Nambu indices, the scalar-scalar kernel is

$$\frac{1}{4}\mathrm{Tr}\,\mathcal{G}_0(r',r)X_\sigma(r)\mathcal{G}_0(r,r')X_\sigma(r) = \int_{r,r'} \sigma^*(r)D(r,r')\sigma(r'), \tag{3.7.8}$$

where the scalar kernel is the same as in Eq. (3.4.9). Similarly, the gauge-gauge kernel is the same as in QED$_3$:

$$\frac{1}{4}\mathrm{Tr}\,\mathcal{G}_0(r',r)X_a(r)\mathcal{G}_0(r,r')X_a(r') = \frac{1}{2}\int_{r,r'} a_\mu(r)K_{\mu\nu}(r,r')a_\nu(r'), \tag{3.7.9}$$

where the gauge-gauge kernel is the same as in Eq. (3.4.10). Combining these two results we find that the fluctuation action (obtained after integrating out σ and a) is just the sum of twice the pure GN and the QED$_3$ results. The anomalous dimension for the minimal charge $q = 1/2$ is thus deduced to be

$$\Delta^{(1)}_{\mathrm{QED_3\text{-}Z_2GN}} = \Delta^{(1)}_{\mathrm{QED_3}} + 2\Delta^{(1)}_{\mathrm{GN}} = 0.102846(9). \tag{3.7.10}$$

The value and the error are estimated in the same way as described in Sec. 3.4 and App. 3.I by finding an expression similar to Eq. (3.4.24) for the QED$_3$-Z$_2$GN case. The result is surprisingly close to the QED$_3$-GN case, although the quantum fluctuations possess a different structure at the two transitions. In Table 3.1, we give the answer for higher q. It can be seen that the values of the anomalous dimensions for $q > 1/2$ for the CSL and Z_2 QSL are not as close as in the case of the minimal charge. By using anomalous dimensions up to $q = 13$ shown in App. 3.J, one can again confirm the value of the universal coefficient for CFTs with a U(1) global symmetry as described in Sec. 3.5 : In this case, we find $\gamma_{\mathrm{QED_3\text{-}Z_2GN}} = 0.98(7) \times \gamma_{\mathrm{U}(1)}$.

3.8. Other phase transitions

The QED$_3$-U(N) $\times$ U(N) GN, QED$_3$-chiral XY GN, and QED$_3$-cHGN transitions are also described with GN models, where the fermionic quartic interaction is respectively decoupled

with $N_b = 1,2,3$ real auxiliary bosons

$$S^c = S' = \int d^3x \left[-\overline{\Psi} \left(\not{D}_{A+\mathcal{A}^q} + \phi_I \mu_I \right) \Psi \right] + \ldots , \tag{3.8.1}$$

where the sum over $1 \leq I \leq N_b$ is implicit, and μ_I are Pauli matrices acting on a two-dimensional flavor subspace where

$$\phi_I \mu_I = \begin{cases} \phi_z \mu_z \\ \phi_x \mu_x + \phi_y \mu_y \, . \\ \vec{\phi} \cdot \vec{\mu} \end{cases} \tag{3.8.2}$$

As mentioned previously, the QED$_3$-cHGN model describes the transition from a U(1) DSL to an AFM on the kagome lattice. In this case, the Pauli matrices $\vec{\mu}$ act on magnetic spin subspace. As for the chiral XY interaction, taking μ_x,μ_y to act on a valley subspace, this describes the transition to a VBS order parameter. These transitions were observed for Monte-Carlo simulations on a square lattice where by tuning gauge-field fluctuations, the U(1) DSL is driven to either an AFM or VBS order, depending on the number of fermion flavors [88, 89]. A theoretical study that elucidated the field theory for the transition to an AFM was performed in Ref. [90] (see also Refs. [28, 31] for earlier studies of this model), while the field theory for the transition to the VBS was outlined in Refs. [91–93]. In this work, we used the appellation QED$_3$-GN to designate the model with U($2N$) symmetry, following the convention of Refs. [47, 53], notably. The Pauli matrix in this case acts on valley subspace. However, the label was also used in the literature to refer to the U(N) $\times$ U(N) symmetric model, see Ref. [45] for instance. Both variations of QED$_3$ were considered in Refs. [48, 69].

As shown in Ref. [31], the auxiliary boson in these cases has a non-vanishing expectation value : $\langle |\phi| \rangle \neq 0$ in the monopole background on $S^2 \times \mathbb{R}$. This is also true for other choices of Pauli matrices, not only the specific one prescribed before to describe specific universality classes. For instance, the $\vec{\mu}$ considered for the QED$_3$-cHGN universality class could also act on valley subspace, in which case the order parameter is odd under time reversal. There is still a non-vanishing expectation value of the auxiliary boson. Consequently, the Green's function in Eq. (3.4.45) must be modified to include a non-zero mass for the fermions. Using the addition theorems for spinor monopole harmonics needed to compute the zero-mass Green's function should be sufficient for this adaptation. Real-space kernels like in Eqs. (3.4.9-3.4.11)

would also include Pauli matrices for traces on the magnetic spin subspace, with the number of kernels to compute increasing accordingly with the number of auxiliary bosons N_b.

3.9. Conclusion

We obtained the scaling dimension of monopole operators at the QCP between a U(1) DSL and two topological spin liquids, namely the CSL and the Z_2 QSL, at next-to-leading order in a $1/N$ expansion. The most relevant monopole operator in the CSL case has a minimal charge $q = 1/2$ and a scaling dimension $\Delta_{1/2,\,\mathrm{QED_3\text{-}GN}} = 2N \times 0.26510 + 0.118911(7)$, while the analog scaling dimension in the Z_2 QSL case is $\Delta_{1/2,\,\mathrm{QED_3\text{-}Z_2GN}} = 2N \times 0.26510 + 0.102846(9)$. We also rederived the $\mathrm{QED_3}$ monopole scaling dimensions and found small discrepancies, e.g., the $q = 1/2$ anomalous dimension is $-0.038138(5)$ instead of -0.0383 and so on for other charges up to $q = 5/2$ [16, 61].

With these anomalous dimensions, we obtained a fit in the topological charge q and compared the $O(q^0)$ coefficient with the universal value obtained in a large-charge expansion for operators charged under a global U(1) symmetry [54]. We obtain the expected value $\gamma = -0.0937$ in $\mathrm{QED_3}$, $\mathrm{QED_3}$-GN and $\mathrm{QED_3}$-$\mathrm{Z_2}$GN. We also revisited the conjectured duality between $\mathrm{QED_3}$-GN$\,|_{2N=2}$ and in CP^1 models [53]. Notably, the $q = 1/2$ monopole scaling dimensions in $\mathrm{QED_3}$-GN$\,|_{2N=2}$ agree very well with the scaling dimensions of other operators that are predicted to be equal under the duality. Specifically, the anomalous dimension obtained in this work greatly improves this agreement. We also argued that all monopoles with equal charges should have the same scaling dimensions in the $\mathrm{QED_3}$-GN$\,|_{2N=2}$ and CP^1 models. Using next-to-leading order results for both models, we obtain an agreement that is better for a minimally charged monopole, with a relative difference of 3%. As the topological charge increases, this difference increases and eventually saturates at 10% for $q \to \infty$.

It would be interesting to study monopole operators in the other gauged GN models that we briefly discussed, notably the model describing the transition to an AFM [31–33]. Another interesting aspect to consider that was not included in this work is the case of monopole operators in the pure-GN model. It is a straightforward adaptation to write out the monopole anomalous dimensions in this case and use the results of this work to obtain them. Although there is no $\mathrm{U(1)_{top}}$ due to the absence of a gauge field in this model, these objects still have useful applications. This notably motivated the study of monopoles in

the bosonic O(N) model [61, 94]. A study of the GN global monopoles and some of their applications will appear in a forthcoming work.

Acknowledgements. We thank Silviu Pufu for useful discussions as well as for clarifying key points in his QED$_3$ calculation. We also thank Ofer Aharony, Shai Chester, Joseph Maciejko, and Subir Sachdev for helpful comments. É.D. was funded by an Alexander Graham Bell CGS from NSERC. W.W.-K. and R.B. were funded by a Discovery Grant from NSERC, a Canada Research Chair, a grant from the Fondation Courtois, and a "Établissement de nouveaux chercheurs et de nouvelles chercheuses universitaires" grant from FRQNT.

3.A. Large N non-compact quantum phase transition

An auxiliary boson ϕ can be introduced to decouple the GN term in the action in Eq. (3.2.1) through a Hubbard-Stratonovich transformation

$$S = \int d^3x \left[-\overline{\Psi} \left(\not{\partial} - i\not{A} + \phi \right) \Psi + \frac{N}{h^2}\phi^2 \right], \tag{3.A.1}$$

where the coupling constant h^2 was rescaled with N, the number of valley nodes. The fermion part of the action is now quadratic and can be integrated

$$S_{\text{eff}} = N \left[-\ln\det\left(\not{\partial} - i\not{A} + \phi \right) + \int d^3x \frac{1}{h^2}\phi^2 \right], \tag{3.A.2}$$

where the valley subspace has been traced out. The saddle-point equation for the gauge field is

$$\begin{aligned} 0 = \left.\frac{\delta S_{\text{eff}}}{\delta A_\mu}\right|_{\langle\phi\rangle,\langle A_\mu\rangle} &= iN \int \frac{d^3p}{(2\pi)^3} \text{tr}\left[\frac{\gamma^\mu}{-i\not{p} - i\left\langle \not{A} \right\rangle + \phi} \right] \\ &= iN \int \frac{d^3p}{(2\pi)^3} \text{tr}\left(\frac{\gamma^\mu\gamma^\nu}{\left(p + \langle A\rangle\right)^2 + \langle\phi\rangle^2} \right) \langle A_\nu \rangle \\ &= 2iN \int \frac{d^3p}{(2\pi)^3} \frac{\langle A^\mu\rangle}{\left(p + \langle A\rangle\right)^2 + \langle\phi\rangle^2}, \end{aligned} \tag{3.A.3}$$

which is solved for a vanishing gauge field $\langle a_\mu \rangle = 0$, as required by gauge invariance. Taking a homogeneous ansatz for the pseudo-scalar field, the remaining gap equation is given by

$$0 = \left.\frac{\delta S_{\text{eff}}}{\delta\phi}\right|_{\langle\phi\rangle,\langle A_\mu\rangle=0} = 2N\langle\phi\rangle \left[\frac{1}{h^2} - \int \frac{d^3p}{(2\pi)^3} \frac{1}{p^2 + \langle\phi\rangle^2} \right], \tag{3.A.4}$$

At the QCP, where $\langle\phi\rangle = 0$, the critical coupling is defined through

$$\frac{1}{h_c^2} = \int \frac{d^3p}{(2\pi)^3}\frac{1}{p^2} = 0, \tag{3.A.5}$$

where this result is obtained through zeta-regularization of the integral. In this scheme, only the determinant operator remains in the effective action (3.A.2), i.e., we obtain Eq. (3.2.4).

3.B. Scalar-gauge kernel

We noted earlier that $M_\ell^q(\omega)$ is non-hermitean. Here we elaborate on this point in more detail. First, we note that $H^q_{\mu'}(r,r')$ is imaginary. Conjugating the expression in Eq. (3.4.11), we obtain

$$H^q_{\mu'}(r,r') = i\mathrm{tr}\left[G_q(r,r')\gamma_{\mu'}G_q^\dagger(r,r')\right] \tag{3.B.1}$$

$$\left[H^q_{\mu'}(r,r')\right]^* = -i\mathrm{tr}\left[G_q^*(r,r')\gamma_{\mu'}^*G_q^\intercal(r,r')\right] = -i\mathrm{tr}\left[G_q(r,r')\gamma_{\mu'}^\dagger G_q^\dagger(r,r')\right] \tag{3.B.2}$$

where we used that the trace of a matrix is equal to the trace of the transposed matrix. Here, the gamma matrices are simply the Pauli matrices, thus $\gamma_{\mu'}^\dagger = \gamma_{\mu'}$. As a result, there is an extra sign in the conjugation of $H^q_{\mu'}(r,r')$:

$$\left[H^q_{\mu'}(r,r')\right]^* = -H^q_{\mu'}(r,r'). \tag{3.B.3}$$

Hence, the kernel is imaginary.

Next, we make relevant observation for the kernel Fourier coefficient. The decomposition of $H^q_{\tau'}(r,r')$, by definition (3.4.18, 3.4.19), is

$$H^q_{\tau'}(r,r') = \int_\omega \sum_\ell H_\ell^{q,T}(\omega)e^{-i\omega(\tau-\tau')}P_\ell\left(\hat{n}\cdot\hat{n}'\right), \tag{3.B.4}$$

where we used the addition theorem in Eq. (3.4.33). As for the other scalar-gauge kernel, $H^q_\tau(r',r)$, it can be defined in the same way, but with a different coefficient, say $\widetilde{H}_\ell^{q,T}(\omega)$. This is then related to $H_\ell^{q,T}(\omega)$ by exchanging coordinates in the expression above

$$H^q_{\tau'}(r,r') = \int_\omega \sum_\ell H_\ell^{q,T}(\omega)e^{-i\omega(\tau-\tau')}P_\ell\left(\hat{n}\cdot\hat{n}'\right) = \int_\omega \sum_\ell H_\ell^{q,T}\left(-\omega\right)e^{-i\omega(\tau-\tau')}P_\ell\left(\hat{n}\cdot\hat{n}'\right). \tag{3.B.5}$$

Thus, $\widetilde{H}^{q,T}_{\ell}(\omega) = H^{q,T}_{\ell}(-\omega)$. Since $H^{q}_{\tau'}(r,r')$ is imaginary, we have that $H^{q,T}_{\ell}(-\omega) = -\left[H^{q,T}_{\ell}(\omega)\right]^*$, meaning that

$$\widetilde{H}^{q,T}_{\ell}(\omega) = -\left[H^{q,T}_{\ell}(\omega)\right]^*. \tag{3.B.6}$$

This explains the signs in the first column of Eq. (3.4.19)

3.C. Gauge invariance

Using conservation of the U(1) current $\nabla_\mu J^\mu(r) = 0$ in Eqs. (3.4.6, 3.4.7), one can show the gauge invariance of the kernels

$$\nabla^\mu K_{\mu\mu'}(r,r') = 0, \quad \nabla^{\mu'} K_{\mu\mu'}(r,r') = 0, \quad \nabla^{\mu'} H_{\mu'}(r,r') = 0. \tag{3.C.1}$$

We re-express these conditions in the Fourier transformed space. To do so, we take the divergence of the various eigenvectors of the gauge field

$$\begin{aligned}
\nabla^\mu e^{-i\omega\tau}\mathfrak{a}^T_{\mu,\ell m}(\hat{n}) = \nabla^\mu\left(\frac{1}{-i\omega}Y_{\ell m}(\hat{n})\nabla_\mu e^{-i\omega\tau}\right) &= \frac{1}{-i\omega}Y_{\ell m}(\hat{n})\nabla^\mu\nabla_\mu e^{-i\omega t} \\
&= -i\omega e^{-i\omega\tau}Y_{\ell m}(\hat{n}), \qquad (3.C.2)\\
\nabla^\mu e^{-i\omega\tau}\mathfrak{a}^E_{\mu,\ell m}(\hat{n}) = \nabla^\mu\left(\frac{e^{-i\omega\tau}}{\sqrt{\ell(\ell+1)}}\nabla_\mu Y_{\ell m}(\hat{n})\right) &= \frac{e^{-i\omega\tau}}{\sqrt{\ell(\ell+1)}}\nabla^\mu\nabla_\mu Y_{\ell m}(\hat{n}) \\
&= -\sqrt{\ell(\ell+1)}e^{-i\omega\tau}Y_{\ell m}(\hat{n}), \qquad (3.C.3)\\
\nabla^\mu e^{-i\omega\tau}\mathfrak{a}^B_{\mu,\ell m}(\hat{n}) = \nabla_\mu\left(\frac{e^{-i\omega\tau}}{\sqrt{\ell(\ell+1)}}\frac{\epsilon^{0\mu\nu}}{\sqrt{g(r)}}\nabla_\nu Y_{\ell m}(\hat{n})\right) &= 0e^{-i\omega\tau}Y_{\ell m}(\hat{n}), \qquad (3.C.4)
\end{aligned}$$

which implies the following relation

$$\nabla^\mu\begin{pmatrix}\mathfrak{a}^T_{\mu,\ell m}(\hat{n}) & \mathfrak{a}^E_{\mu,\ell m}(\hat{n}) & \mathfrak{a}^B_{\mu,\ell m}(\hat{n})\end{pmatrix} = \begin{pmatrix}-i\omega & -\sqrt{\ell(\ell+1)} & 0\end{pmatrix}e^{-i\omega\tau}Y_{\ell m}(\hat{n}). \tag{3.C.5}$$

Taking the divergence of the kernels, we obtain

$$\nabla^\mu K_{\mu\mu'}(r,r') = \int_\omega \sum_{\ell=0}^{\infty}\sum_{m=-\ell}^{\ell} e^{-i\omega(\tau-\tau')} Y_{\ell m}(\hat{n}) \begin{pmatrix} -i\omega & -\sqrt{\ell(\ell+1)} & 0 \end{pmatrix} \times \begin{pmatrix} K_\ell^{q,TT}(\omega) & K_\ell^{q,TE}(\omega) & K_\ell^{q,TB}(\omega) \\ K_\ell^{q,TE*}(\omega) & K_\ell^{q,EE}(\omega) & K_\ell^{q,EB}(\omega) \\ K_\ell^{q,TB*}(\omega) & K_\ell^{q,EB*}(\omega) & K_\ell^{q,BB}(\omega) \end{pmatrix} \begin{pmatrix} \mathfrak{a}^{T\dagger}_{\mu,\ell m}(\hat{n}') \\ \mathfrak{a}^{E\dagger}_{\mu,\ell m}(\hat{n}') \\ \mathfrak{a}^{B\dagger}_{\mu,\ell m}(\hat{n}') \end{pmatrix}, \tag{3.C.6}$$

$$\nabla^\mu H_\mu(r,r') = \int_\omega \sum_{\ell=0}^{\infty}\sum_{m=-\ell}^{\ell} e^{-i\omega(\tau-\tau')} Y_{\ell m}(\hat{n}) Y^*_{\ell m}(\hat{n}') \begin{pmatrix} -i\omega & -\sqrt{\ell(\ell+1)} & 0 \end{pmatrix} \begin{pmatrix} -H_\ell^{q,T*}(\omega) \\ -H_\ell^{q,E*}(\omega) \\ -H_\ell^{q,T*}(\omega) \end{pmatrix}, \tag{3.C.7}$$

where $\int_\omega \equiv \int d\omega/(2\pi)$. Requiring gauge invariance and setting these divergences to 0, we obtain the following relations

$$-i\omega K_\ell^{q,TT}(\omega) - \sqrt{\ell(\ell+1)} K_\ell^{q,TE*}(\omega) = 0, \tag{3.C.8}$$

$$-i\omega K_\ell^{q,TE}(\omega) - \sqrt{\ell(\ell+1)} K_\ell^{q,EE}(\omega) = 0, \tag{3.C.9}$$

$$-i\omega K_\ell^{q,TB}(\omega) - \sqrt{\ell(\ell+1)} K_\ell^{q,EB}(\omega) = 0, \tag{3.C.10}$$

$$i\omega H_\ell^{q,T*}(\omega) + \sqrt{\ell(\ell+1)} H_\ell^{q,E*}(\omega) = 0. \tag{3.C.11}$$

Verifications

Let us check one important relation following from gauge invariance :

$$K_\ell^{q,EE}(\omega) = \frac{\omega^2}{\ell(\ell+1)} K_\ell^{q,TT}(\omega). \tag{3.C.12}$$

This is easily verified for $q = 0$ where closed forms of the kernels are easily obtained as discussed in Sec. 3.4.2.1. This is a bit more involved when $q \neq 0$. We have expressions where the dependence on ω is easily isolated, taking the following form

$$K_\ell^{q,ZZ}(\omega) = \int dx \sum_{\ell',\ell''} \frac{E_{q,\ell'} + E_{q,\ell''}}{\omega^2 + \left(E_{q,\ell'} + E_{q,\ell''}\right)^2} \tilde{k}^{q,ZZ}_{\ell,\ell',\ell''}(x), \quad Z \in \{T,E\}. \tag{3.C.13}$$

In the RHS of the gauge invariance condition in Eq. (3.C.12), we may reexpress the ω-dependent function as

$$\frac{\omega^2}{\omega^2 + \left(E_{q,\ell'} + E_{q,\ell''}\right)^2} = 1 - \frac{\left(E_{q,\ell'} + E_{q,\ell''}\right)^2}{\omega^2 + \left(E_{q,\ell'} + E_{q,\ell''}\right)^2}. \tag{3.C.14}$$

Upon integration over ω, the first term is a simple divergence that can be regularized away. In the presence of test function $f(\omega)$, this contribution is $\int d\omega f(\omega) \times 1$ and it again vanishes provided the test function is convergent with no poles. The gauge-invariance condition in Eq. (3.C.12) can then be written by simply comparing the finite parts

$$\begin{aligned}
&\int dx \sum_{\ell',\ell''} \frac{E_{q,\ell'} + E_{q,\ell''}}{\omega^2 + \left(E_{q,\ell'} + E_{q,\ell''}\right)^2} \tilde{k}^{q,EE}_{\ell,\ell',\ell''}(x) \\
&= \int dx \sum_{\ell',\ell''} \left[-\frac{\left(E_{q,\ell'} + E_{q,\ell''}\right)^2}{\ell(\ell+1)} \right] \times \frac{E_{q,\ell'} + E_{q,\ell''}}{\omega^2 + \left(E_{q,\ell'} + E_{q,\ell''}\right)^2} \tilde{k}^{q,TT}_{\ell,\ell',\ell''}(x).
\end{aligned} \tag{3.C.15}$$

This last relation following from gauge invariance was verified for $q = 1/2$. Note that gauge invariance also implies that

$$k^{1/2,TT}_{0,\ell',\ell''}(x) = 0, \tag{3.C.16}$$

which is also verified by direct computation.

3.D. Green's function

3.D.1. Eigenvalues of determinant operator

In a general basis, the gauge covariant derivative acting on a spin-1/2 spinor on spacetime $\mathfrak{M}$ will take the form

$$\not{D}_{\mathcal{A}^q} = e^\mu_b \gamma^b \left[\partial_\mu - \Omega_\mu - i\mathcal{A}^q_\mu \right], \tag{3.D.1}$$

where Ω_μ is the spin connection transporting the fermion fields on spacetime $\mathfrak{M}$. On a flat spacetime $\mathfrak{M} = \mathbb{R}^3$, there are also spin connections in spherical coordinates that can be eliminated with a unitary transformation [95]. In this case, the covariant derivate $\nabla_{\mu=r,\theta,\phi}$ can be traded for a normal derivative $\partial_{\mu=r,\theta,\phi}$

$$\not{D}^{\mathbb{R}^3}_{\mathcal{A}^q} = (e^{\mathbb{R}^3})^\mu_b \gamma^b \left[\partial_\mu - i\mathcal{A}^q_\mu \right]. \tag{3.D.2}$$

Proceeding with the Weyl transformation $\psi \to e^{-\tau}\psi$, $g_{\mu\nu} \to e^{-2\tau}$ discussed in Eq. (3.2.6), the Dirac operator on $S^2 \times \mathbb{R}$ is given by [15]

$$\not{D}^{S^2\times\mathbb{R}}_{\mathcal{A}^q} = \left(e^{S^2\times\mathbb{R}}\right)^\mu_b \gamma^b \left[\partial_\mu - \frac{1}{R}\delta^\tau_\mu - i\mathcal{A}^q_\mu \right]. \tag{3.D.3}$$

To diagonalize this operator, we introduce spinor monopole harmonics

$$S^{\pm}_{q,\ell',m'} = \begin{pmatrix} \pm\alpha_{\pm} Y_{q,\ell',m'} \\ \alpha_{\mp} Y_{q,\ell',m'+1} \end{pmatrix}, \quad \alpha_{\pm} = \sqrt{\frac{\ell' + 1/2 \pm (m' + 1/2)}{2\ell' + 1}}. \tag{3.D.4}$$

These spinors diagonalize the following generalized total spin and angular momentum operators J_q^2, J_q^z, L_q^2. In particular, the spinor monopole harmonics $S^{\pm}_{q,\ell,m}$ have a total spin $j = \ell \pm 1/2$. In the $j = \ell - 1/2$ basis, the Dirac operator mixes the two types of spinors and simply becomes a matrix with c-number entries [15] :

$$\begin{bmatrix} i\not{D}_{\mathcal{A}^q} e^{-i\omega\tau} S^{+}_{q,\ell-1,m} \\ i\not{D}_{\mathcal{A}^q} e^{-i\omega\tau} S^{-}_{q,\ell,m} \end{bmatrix} = \boldsymbol{N}_{q,\ell} \left(\omega + i\boldsymbol{M}_{q,\ell}\right) \begin{bmatrix} e^{-i\omega\tau} S^{+}_{q,\ell-1,m} \\ e^{-i\omega\tau} S^{-}_{q,\ell,m} \end{bmatrix}, \tag{3.D.5}$$

where

$$\boldsymbol{N}_{q,\ell} = -\frac{1}{\ell}\left(q\tau_z + E_{q;\ell}\tau_x\right), \quad \boldsymbol{M}_{q,\ell} = \frac{E_{q;\ell}}{\ell}\left(E_{q;\ell}\tau_z - q\tau_x\right), \quad E_{q;\ell} = \sqrt{\ell^2 - q^2}. \tag{3.D.6}$$

Here, the τ_i are the Pauli matrices acting in the $j = \ell - 1/2$ basis, i.e., they mix the components $S^{+}_{q,\ell-1,m}$ and $S^{-}_{q,\ell,m}$. For $\ell = q$ (we suppose a positive magnetic charge $q > 0$), only $S^{-}_{q,q,m}$ exists and corresponds to a zero mode of the Dirac operator. By diagonalizing this matrix, we retrieve the eigenvalues used in Sec. 3.3.

3.D.2. Green's function

The Green's function can be obtained with the spectral decomposition

$$G_q(r,r') = -\sum_{\lambda} \frac{\psi_\lambda(r)\psi_\lambda^\dagger(r')}{E_\lambda}, \tag{3.D.7}$$

where $\psi_\lambda(r)$ are eigenspinors of the Dirac operator $i\not{D}_{\mathcal{A}^q}\psi_\lambda = E_\lambda\psi_\lambda$ forming a complete basis $\sum_\lambda \psi_\lambda(r)\psi_\lambda^\dagger(r') = \delta(r-r')$. With this formulation, the Green's function respects its defining equation of motion (3.4.32). We can simply keep working in the spinor monopole harmonics basis instead of further diagonalizing. The spectral decomposition of the Green's function in this basis is then

$$G_q(r,r') = -\widetilde{\psi}_\lambda(r)\left(\widetilde{E}^{-1}\right)_{\lambda\lambda'}\widetilde{\psi}^\dagger_{\lambda'}(r'). \tag{3.D.8}$$

The eigenvalue matrix is block diagonal, separating each $j = \ell - 1/2$ sectors. To obtain a Green's function which has two particle-hole indices but which is a scalar with respect to the $+/-$ structure described above, we take the left eigenspinor as a row vector in the

$+/-$ space, $\left[e^{-i\omega\tau}S^{+}_{q,\ell-1,m}(\hat{n}),e^{-i\omega\tau}S^{-}_{q,\ell,m}(\hat{n})\right]$. The action of the Dirac operator on the left eigenspinor is then given by

$$\left[\begin{array}{c} i\not{D}_{\mathcal{A}^q}\left(e^{-i\omega\tau}S^{+}_{q,\ell-1,m}\right) \\ i\not{D}_{\mathcal{A}^q}\left(e^{-i\omega\tau}S^{-}_{q,\ell,m}\right) \end{array}\right]^T = \left(\boldsymbol{N}_{q,\ell}\left(\omega+i\boldsymbol{M}_{q,\ell}\right)\left[\begin{array}{c} e^{-i\omega\tau}S^{+}_{q,\ell-1,m} \\ e^{-i\omega\tau}S^{-}_{q,\ell,m} \end{array}\right]\right)^T \tag{3.D.9}$$

$$= \left[e^{-i\omega\tau}S^{+}_{q,\ell-1,m} \quad e^{-i\omega\tau}S^{-}_{q,\ell,m}\right]\left[\boldsymbol{N}_{q,\ell}\left(\omega-i\boldsymbol{M}_{q,\ell}\right)\right], \tag{3.D.10}$$

where we used that $\boldsymbol{N}^T_{q,\ell}=\boldsymbol{N}_{q,\ell}$, $\boldsymbol{M}^T_{q,\ell}=\boldsymbol{M}_{q,\ell}$ and $\boldsymbol{M}_{q,\ell}\boldsymbol{N}_{q,\ell}=-\boldsymbol{N}_{q,\ell}\boldsymbol{M}_{q,\ell}$. We can read the eigenvalue matrix from this relation and write Green's function[17]

$$G_q(r,r') = -\int\frac{d\omega}{2\pi}\sum_{\ell=q}^{\infty}\sum_{m=-\ell}^{\ell-1}\left[S^{+}_{q,\ell-1,m}(\hat{n}) \quad S^{-}_{q,\ell,m}(\hat{n})\right]\times\frac{e^{-i\omega(\tau-\tau')}}{\boldsymbol{N}_{q,\ell}\left(\omega-i\boldsymbol{M}_{q,\ell}\right)}\left[\begin{array}{c}\left(S^{+}_{q,\ell-1,m}(\hat{n}')\right)^{\dagger}\\ \left(S^{-}_{q,\ell,m}(\hat{n}')\right)^{\dagger}\end{array}\right]. \tag{3.D.11}$$

We can note that $\boldsymbol{N}^{-1}_{q,\ell}=\boldsymbol{N}_{q,\ell}$ as this matrix squares to identity $\boldsymbol{N}^2_{q,\ell}=\ell^{-2}\left(q^2+E^2_{q;\ell}\right)\tau_0=\tau_0$. Also, by noting that $\left|\omega+i\mathbf{M}_{q,\ell}\right|^2=\left(\omega^2+E^2_{q;\ell}\right)\tau_0$, it follows that $\left(\omega-i\mathbf{M}_{q,\ell}\right)^{-1}=\left(\omega^2+E^2_{q;\ell}\right)^{-1}\left(\omega+i\mathbf{M}_{q,\ell}\right)$. Then, the inverse matrix in the spectral decomposition becomes

$$\left(\omega-i\mathbf{M}_{q,\ell}\right)^{-1}\boldsymbol{N}^{-1}_{q,\ell} = \frac{1}{\omega^2+E^2_{q;\ell}}\left(\omega+i\mathbf{M}_{q,\ell}\right)\mathbf{N}_{q,\ell} \tag{3.D.12}$$

$$= \frac{1}{\omega^2+E^2_{q;\ell}}\left(\omega\mathbf{N}_{q,\ell}+E_{q;\ell}\tau_y\right), \tag{3.D.13}$$

where we used that $\mathbf{M}_{q,\ell}\mathbf{N}_{q,\ell}=-iE_{q;\ell}\tau_y$. The spectral decomposition of the Green's function then becomes

$$G_q(r,r') = -\int_{-\infty}^{\infty}\frac{d\omega}{2\pi}\sum_{\ell=q}^{\infty}\sum_{m=-\ell}^{\ell-1}\left[S^{+}_{q,\ell-1,m} \quad S^{-}_{q,\ell,m}\right]\times\frac{e^{-i\omega(\tau-\tau')}}{\omega^2+E^2_{q;\ell}}\left(\omega\mathbf{N}_{q,\ell}+E_{q;\ell}\tau_y\right)\left[\begin{array}{c}\left(S^{+}_{q,\ell-1,m}\right)^{\dagger}\\ \left(S^{-}_{q,\ell,m}\right)^{\dagger}\end{array}\right]. \tag{3.D.14}$$

The contour integral on ω is obtained with the residue theorem

$$\int_{-\infty}^{\infty}\frac{d\omega}{2\pi}\frac{e^{-i\omega(\tau-\tau')}}{\omega^2+E^2_{q;\ell}}\left\{\begin{array}{c}\omega\\1\end{array}\right\} = -i\mathrm{sgn}(\tau-\tau')\frac{e^{-E_{q;\ell}|\tau-\tau'|}}{-2iE_{q;\ell}\mathrm{sgn}(\tau-\tau')}\left\{\begin{array}{c}-iE_{q;\ell}\mathrm{sgn}(\tau-\tau')\\1\end{array}\right\}$$

$$= \frac{1}{2}e^{-E_{q;\ell}|\tau-\tau'|}\left\{\begin{array}{c}-i\mathrm{sgn}(\tau-\tau')\\E^{-1}_{q;\ell}\end{array}\right\}. \tag{3.D.15}$$

[17] The inverse eigenvalue matrix here is $\left[\boldsymbol{N}_{q,\ell}\left(\omega-i\boldsymbol{M}_{q,\ell}\right)\right]^{-1}$ instead of $\left[\boldsymbol{N}_{q,\ell}\left(\omega+i\boldsymbol{M}_{q,\ell}\right)\right]^{-1}$ as described in Ref. [16]. This explains the benign different sign in our Green's function in what follows.

The spectral decomposition after the ω integration becomes

$$G_q(r,r') = \frac{i}{2}\sum_{\ell=q}^{\infty} e^{-E_{q;\ell}|\tau-\tau'|} \sum_{m=-\ell}^{\ell-1} \begin{bmatrix} S^+_{q,\ell-1,m} & S^-_{q,\ell,m} \end{bmatrix} \times \left(\mathrm{sgn}(\tau-\tau')\mathbf{N}_{q,\ell} + \begin{pmatrix} 0 & 1 \\ -1 & 0 \end{pmatrix} \right) \begin{bmatrix} \left(S^+_{q,\ell-1,m}\right)^\dagger \\ \left(S^-_{q,\ell,m}\right)^\dagger \end{bmatrix}. \tag{3.D.16}$$

By inserting Eq. (3.D.4), we obtain a 2×2 matrix whose components are pairs of monopole harmonics

$$G_q(r,r') = (2\times 2 \text{ matrix})_{\tau\tau'} \propto \sum_{\ell'=q}^{\infty} \sum_{m'=-\ell'+1}^{\ell'} Y_{q,\ell'+\delta\ell',m'+\delta m'}(\hat{n}) Y^*_{q,\ell'+\widetilde{\delta}\ell',m'+\widetilde{\delta}m'}(\hat{n}'), \tag{3.D.17}$$

where

$$\begin{cases} \delta\ell',\widetilde{\delta}\ell' & \in \{-1,0\} \\ \delta m',\widetilde{\delta}m' & \in \{0,1\} \end{cases}. \tag{3.D.18}$$

This formulation is used in Sec. 3.4.2.3.

For the minimal charge case, the Green's function can be further simplified by taking the sum on the azimutal quantum number [16], which yields Eq. (3.4.45) in the main text [18]. The phase appearing in Eq. (3.4.45) is given by [16]

$$e^{-i\Theta}\cos\frac{\gamma}{2} = \cos\frac{\theta}{2}\cos\frac{\theta'}{2} + \sin\frac{\theta}{2}\sin\frac{\theta'}{2}e^{-i(\phi-\phi')}. \tag{3.D.19}$$

3.E. Eigenkernels

3.E.1. First basis

We work in spherical normalized coordinates

$$[e^{a=\hat{\theta},\hat{\phi},\hat{\tau}}_{\mu=x,y,z}] = \begin{pmatrix} \cos\theta\cos\phi & -\sin\theta\sin\phi & \sin\theta\cos\phi \\ \cos\theta\sin\phi & \sin\theta\cos\phi & \sin\theta\sin\phi \\ -\sin\theta & 0 & \cos\theta \end{pmatrix}. \tag{3.E.1}$$

[18] The difference that we noted concerning what inverse matrix is used in Eq. (3.D.11) implies an extra sign in the first line of the Green's function.

Using the definitions of the vector spherical harmonics (3.4.14), the eigenkernels in Eqs. (3.4.30, 3.4.31) can be written as

$$\sum_m \mathfrak{a}^{a,E*}_{\ell m}(\hat{n})\mathfrak{a}^{a',E}_{\ell m}(\hat{n}') = \frac{1}{\ell(\ell+1)}\nabla_a\nabla_{a'}\left(\sum_m Y^*_{\ell m}(\hat{n})Y_{\ell m}(\hat{n}')\right), \tag{3.E.2}$$

$$\sum_m \mathfrak{a}^{a,B*}_{\ell m}(\hat{n})\mathfrak{a}^{a',B}_{\ell m}(\hat{n}') = \frac{1}{\ell(\ell+1)}\frac{\epsilon^{ab}\epsilon^{a'b'}}{\sqrt{g(r)g\,(r')}}\nabla_b\nabla_{b'}\left(\sum_m Y^*_{\ell m}(\hat{n})Y_{\ell m}(\hat{n}')\right). \tag{3.E.3}$$

Using the addition formula in Eq. (3.4.33), we obtain the results in Ref. [62].

$$\sum_m \mathfrak{a}^{a,E*}_{\ell m}(\hat{n})\mathfrak{a}^{a',E}_{\ell m}(\hat{z}) = \frac{2\ell+1}{4\pi}\frac{1}{\ell(\ell+1)}\begin{pmatrix} -\left(1-x^2\right)P''_\ell(x) + xP'_\ell(x) & 0 \\ 0 & P'_\ell(x)\end{pmatrix}\begin{pmatrix}\cos\phi & \sin\phi \\ -\sin\phi & \cos\phi\end{pmatrix}, \tag{3.E.4}$$

$$\sum_m \mathfrak{a}^{a,B*}_{\ell m}(\hat{n})\mathfrak{a}^{a',B}_{\ell m}(\hat{z}) = \frac{2\ell+1}{4\pi}\frac{1}{\ell(\ell+1)}\begin{pmatrix} P'_\ell(x) & 0 \\ 0 & -\left(1-x^2\right)P''_\ell(x) + xP'_\ell(x)\end{pmatrix}\begin{pmatrix}\cos\phi & \sin\phi \\ -\sin\phi & \cos\phi\end{pmatrix}. \tag{3.E.5}$$

This may be further simplified by using the differential equation for Legendre polynomials

$$P''_\ell(x) = \frac{1}{1-x^2}\left[2xP'_\ell(x) - \ell(\ell+1)P_\ell(x)\right]. \tag{3.E.6}$$

3.E.2. Second basis

By working in helical coordinates,

$$r^{a=+,z,-} = \frac{1}{\sqrt{2}}\left(-x+iy,\sqrt{2}z,x+iy\right), \tag{3.E.7}$$

the vector spherical harmonics $U^a_{\ell m}(\hat{n})$,$V^a_{\ell m}(\hat{n})$,$W^a_{\ell m}(\hat{n})$ introduced in Sec. 3.4.2.3 take the following form

$$U^a_{\ell m}(\hat{n}) = \begin{pmatrix} \sqrt{\frac{(\ell-m+1)(\ell-m+2)}{(2\ell+2)(2\ell+3)}}Y_{\ell+1,m-1}(\hat{n}) \\ -\sqrt{\frac{(\ell-m+1)(\ell+m+1)}{(\ell+1)(2\ell+3)}}Y_{\ell+1,m}(\hat{n}) \\ \sqrt{\frac{(\ell+m+1)(\ell+m+2)}{(2\ell+2)(2\ell+3)}}Y_{\ell+1,m+1}(\hat{n}) \end{pmatrix}, \tag{3.E.8}$$

$$V^a_{\ell m}(\hat{n}) = \begin{pmatrix} -\sqrt{\frac{(\ell-m+1)(\ell+m)}{2\ell(\ell+1)}}Y_{\ell,m-1}(\hat{n}) \\ \frac{m}{\sqrt{\ell(\ell+1)}}Y_{\ell.m}(\hat{n}) \\ \sqrt{\frac{(\ell-m)(\ell+m+1)}{2\ell(\ell+1)}}Y_{\ell,m+1}(\hat{n}) \end{pmatrix}, \tag{3.E.9}$$

$$W^a_{\ell m}(\hat{n}) = \begin{pmatrix} \sqrt{\frac{(\ell+m-1)(\ell+m)}{2\ell(2\ell-1)}}Y_{\ell-1,m-1}(\hat{n}) \\ \sqrt{\frac{(\ell-m)(\ell+m)}{\ell(2\ell-1)}}Y_{\ell-1,m}(\hat{n}) \\ \sqrt{\frac{(\ell-m-1)(\ell-m)}{2\ell(2\ell-1)}}Y_{\ell-1,m+1}(\hat{n}) \end{pmatrix}, \tag{3.E.10}$$

Using a transformation matrix

$$[e^{\mu=x,y,z}_{a=+,z,-}] = \begin{pmatrix} -1/\sqrt{2} & 0 & 1/\sqrt{2} \\ -i/\sqrt{2} & 0 & -i/\sqrt{2} \\ 0 & 1 & 0 \end{pmatrix}, \tag{3.E.11}$$

these harmonics can be rotated to cartesian coordinates

$$e^\mu_a Z^a_{\ell,m}(\hat{n}), \quad Z = U,V,W, \tag{3.E.12}$$

which corresponds to the harmonics used in the main text.

3.E.3. Kernel coefficients for general q

As we turn to compute kernel coefficients,

$$[K^q_\ell(\omega)]_{XZ} = \frac{1}{2\ell+1}\sum_m \int d^3r d^3r' \sqrt{g(r)}\sqrt{g\,(r')}X^{\mu*}_{\ell,m}(\hat{n})\mathcal{K}^q_{\mu\mu'}(r,r')Z^{\mu'}_{\ell,m}(\hat{n}')e^{i\omega(\tau-\tau')}, \tag{3.E.13}$$

with $X,Z \in \{U,V,W\}$, the real-space kernels can also be worked out in cartesian coordinates

$$K^q_{\mu\mu'}(r,r') = \mathrm{tr}\left[\gamma_\mu G_q(r,r')\gamma_{\mu'}G^\dagger_q(r,r')\right], \quad \gamma_\mu,\gamma_{\mu'} = (\sigma_x,\sigma_y,\sigma_z)\,.$$

In the limit $r' \to 0$, where half of the harmonics can be eliminated (3.4.64), the various functions at play in our computation can be rewritten as (3.4.63)

$$G_q\,(r,0) = (2\times 2 \text{ matrix})_{\tau\tau'} \propto \sum_{\ell'} Y_{q,\ell'+\delta\ell',-q+\delta\mathfrak{m}'}(\hat{n}), \tag{3.E.14}$$

$$K^q_{\mu\mu'}\,(r,0) = (3\times 3 \text{ matrix})_{\mu\mu'} \propto \sum_{\ell',\ell''} Y_{q,\ell'+\delta\ell',-q+\delta\mathfrak{m}'}(\hat{n}) Y_{-q,\ell''+\delta\ell'',q+\delta\mathfrak{m}''}(\hat{n}), \tag{3.E.15}$$

$$Z^{\mu *}_{\ell,m}(\hat{n}) Z^{\mu'}_{\ell,m}\,(\hat{z}) = (3\times 3 \text{ matrix})^{\mu\mu'} \propto Y_{0,\ell+\delta\ell_Z,\delta\mathfrak{m}}(\hat{n}), \tag{3.E.16}$$

where

$$\delta\ell',\ell'' \in \{-1,0\}, \tag{3.E.17}$$

$$\delta\mathfrak{m}',\delta\mathfrak{m}'' \in \{-1,0,1\}, \tag{3.E.18}$$

$$\delta\ell_Z = \{-1,0,1\},\ Z \in \{W,V,U\}, \tag{3.E.19}$$

$$\delta\mathfrak{m} \in \{-2,-1,0,1,-2\}, \tag{3.E.20}$$

As claimed in the main text, the kernel coefficients take the form

$$\begin{aligned} &\int d^3r\sqrt{g(r)} K^q_{\mu\mu'}\,(r,0)\, Z^{\mu *}_{\ell,m}(\hat{n}) Z^{\mu'}_{\ell,m}\,(\hat{z}) \\ &\quad \sim \sum_{\ell',\ell''} \int d\hat{n} Y_{q,\ell'+\delta\ell',-q+\delta\mathfrak{m}'}(\hat{n}) Y_{-q,\ell''+\delta\ell'',q+\delta\mathfrak{m}''}(\hat{n}) Y_{0,\ell+\delta\ell_Z,\delta\mathfrak{m}}(\hat{n}). \end{aligned} \tag{3.E.21}$$

3.F. Results for the $q = 1/2$ computations

We review specific results that concern the $q = 1/2$ computation in Sec. 3.4.2.2. Using the differential equation defining a Legendre Polynomial

$$P''_\ell(x) - \frac{1}{1-x^2}\left[2xP'_\ell(x) - \ell(\ell+1)P_\ell(x)\right] = 0, \tag{3.F.1}$$

and the equivalent relation for $Q''_{q,\ell}(x)$ [16]

$$Q''_{q,\ell}(x) + \frac{1}{1+x}Q'_{q,\ell}(x) + \frac{1}{1-x^2}\left[\ell^2 - \frac{2q^2}{1+x}\right]Q_{q,\ell}(x) = 0, \tag{3.F.2}$$

the integrals appearing in the $q = 1/2$ computation in Sec. 3.4.2.2 can be reformulated in the form

$$\int dx\left[a_{\ell,\ell',\ell''}(x)P_\ell(x) + b_{\ell,\ell',\ell''}(x)P'_\ell(x)\right] Q_{q,\ell'}(x)Q_{q,\ell''}(x). \tag{3.F.3}$$

Specifically, for $q = 1/2$, we obtain

$$\begin{aligned}
\mathcal{I}_1^D &= J_0\left[\ell(\ell+1) - \ell'^2 - \ell''^2 + \frac{1}{2}\right] - J_1 - J_2, \\
\mathcal{I}_2^D &= -J_0, \\
\mathcal{I}_1^T &= -\left(J_1 - J_2\right), \\
\mathcal{I}_1^E &= \left(J_1 - J_2\right)\left[\ell(\ell+1) - \ell'^2 - \ell''^2 + \frac{1}{2}\right], \\
\mathcal{I}_2^E &= -J_1 - J_2, \\
\mathcal{I}_1^B &= \ell(\ell+1)\left[\ell(\ell+1)J_0 - 2J_2\right] - \left[J_1 - J_2 + \ell(\ell+1)J_0\right]\left[\ell'^2 + \ell''^2 - \frac{1}{2}\right], \\
\mathcal{I}_2^B &= J_1 + J_2 - \ell(\ell+1)J_0,
\end{aligned} \tag{3.F.4}$$

where

$$J_0\left(\ell,\ell',\ell''\right) = \int_{-1}^{1} dx \frac{1}{1-x} P_\ell(x) Q_{1/2,\ell'}(x) Q_{1/2,\ell''}(x), \tag{3.F.5}$$

$$J_1\left(\ell,\ell',\ell''\right) = \int_{-1}^{1} dx \frac{1}{1-x} P'_\ell(x) Q_{1/2,\ell'}(x) Q_{1/2,\ell''}(x), \tag{3.F.6}$$

$$J_2\left(\ell,\ell',\ell''\right) = \int_{-1}^{1} dx \frac{x}{1-x} P'_\ell(x) Q_{1/2,\ell'}(x) Q_{1/2,\ell''}(x). \tag{3.F.7}$$

The result for these integrals was obtained in [16] [19]

$$J_0(\ell,\ell_1+1/2,\ell_2+1/2) = -\frac{\left(\ell_1+1/2\right)\left(\ell_2+1/2\right)\begin{pmatrix} \ell & \ell_1 & \ell_2 \\ 0 & 0 & 0 \end{pmatrix}\begin{pmatrix} \ell+1 & \ell_1 & \ell_2 \\ 0 & 1 & -1 \end{pmatrix}}{4\pi^2\sqrt{\ell_1(\ell_1+1)\ell_2(\ell_2+1)}}, \tag{3.F.8}$$

$$\begin{aligned}
J_1(\ell,\ell_1+1/2,\ell_2+1/2) = &\frac{\sqrt{\ell(\ell+1)}\left(\ell_1+1/2\right)\left(\ell_2+1/2\right)\begin{pmatrix} \ell & \ell_1 & \ell_2 \\ 0 & 0 & 0 \end{pmatrix}}{8\pi^2\sqrt{\ell_1(\ell_1+1)\ell_2(\ell_2+1)}} \\
&\times\left[\sqrt{(\ell+2)(\ell+3)}\begin{pmatrix} \ell+1 & \ell_1 & \ell_2 \\ -2 & 1 & 1 \end{pmatrix} - \sqrt{\ell(\ell+1)}\begin{pmatrix} \ell+1 & \ell_1 & \ell_2 \\ 0 & 1 & -1 \end{pmatrix}\right]
\end{aligned} \tag{3.F.9}$$

[19] Our definitions have for the J_i have an extra factor $4\pi/(2\ell+1)$ since we defined them with $P_\ell(x)$ and not $F_\ell(x) = (2\ell+1)P_\ell(x)/(4\pi)$ as in Ref. [16].

$$J_2(\ell,\ell_1+1/2,\ell_2+1/2) = \frac{\sqrt{\ell(\ell+1)}\,(\ell_1+1/2)\,(\ell_2+1/2)\begin{pmatrix}\ell & \ell_1 & \ell_2\\ 0 & 0 & 0\end{pmatrix}}{8\pi^2\sqrt{\ell_1(\ell_1+1)\ell_2(\ell_2+1)}}$$
$$\times\left[\sqrt{(\ell-1)(\ell+2)}\begin{pmatrix}\ell+1 & \ell_1 & \ell_2\\ -2 & 1 & 1\end{pmatrix} - \sqrt{\ell(\ell+1)}\begin{pmatrix}\ell+1 & \ell_1 & \ell_2\\ 0 & 1 & -1\end{pmatrix}\right] \tag{3.F.10}$$

where $\ell' = \ell_1 + 1/2$ and $\ell'' = \ell_2 + 1/2$.

3.G. Remainder coefficients

When computing kernel coefficients in Secs. 3.4.2.2 and 3.4.2.3, we deal with regularized sums as

$$\sum_{\ell'=q+1}^{\infty}\left[-\alpha^Z + \sum_{\ell''=q+1}^{\infty} k^{q,Z}_{\ell,\ell',\ell''}(\omega)\right], \tag{3.G.1}$$

which is the general-q version of the sum in Eq. (3.4.59). As in the main text, $Z \in \{D,T,E,B\}$. Setting a numerical cutoff $\ell'_c = 200 + q$, the remainder of the sum is obtained analytically, as discussed in Sec.3.4.2.2

$$\sum_{\ell'=\ell'_c+1}^{\infty}\left[-\alpha^Z + \sum_{\ell''=q+1}^{\infty} k^{q,Z}_{\ell,\ell',\ell''}(\omega)\right] = \sum_{\ell'=\ell'_c+1}^{\infty}\left[\sum_{p=2}^{k} c^{q,Z}_{\ell,p}(\omega)\,(\ell')^{-p}\right] = \sum_{p=2}^{k} c^{q,Z}_{\ell,p}(\omega)\zeta\,(p,\ell'_c+1)\,. \tag{3.G.2}$$

In our computations, we obtained the remainders down to order $(\ell')^{-18}$. To obtain the coefficients, the expansion in $1/\ell'$ must be carried out, which in turn requires fixing ℓ and q. The resulting expansion then yields the analytic dependence on ω, while the dependence on ℓ and q is found by fitting many coefficients with specific values of ℓ and q. The coefficients we find $c^{q,Z}_{\ell,p}(\omega)$ are polynomials of ω^2, $\ell(\ell+1) \equiv \ell_2$, q^2 (the scalar-gauge kernel $Z = T$ has an extra factor of q)

$$D: \quad \frac{\zeta\left(2,\ell_c'+1\right)}{16\pi}\left(\ell_2-4q^2+2\omega^2\right)+\frac{\zeta\left(4,\ell_c'+1\right)}{256\pi}\Bigg(7\ell_2^2+\ell_2\left(24q^2+8\omega^2-2\right)$$
$$-8\left(-6q^2\omega^2+6q^4+\omega^4\right)\Bigg)+\frac{\zeta\left(6,\ell_c'+1\right)}{1024\pi}\Bigg(13\ell_2^3+2\ell_2^2\left(35q^2-3\left(\omega^2+3\right)\right)$$
$$+4\ell_2\left(5q^2\left(4\omega^2+3\right)+30q^4-9\omega^4-2\omega^2+1\right)+8\left(30q^4\omega^2-10q^2\omega^4-20q^6+\omega^6\right)\Bigg)$$
$$+\ldots \tag{3.G.3}$$

$$T: \quad \frac{\zeta\left(4,\ell_c'+1\right)}{16\pi}q\ell_2+\frac{\zeta\left(6,\ell_c'+1\right)}{128\pi}q\ell_2\left(6\ell_2+20q^2-9\omega^2-8\right)+\ldots \tag{3.G.4}$$

$$E: \quad \frac{\zeta\left(2,\ell_c'+1\right)}{32\pi}\left(\ell_2-4q^2+2\omega^2\right)+\frac{\zeta\left(4,\ell_c'+1\right)}{256\pi}\Bigg(2\ell_2^2+\ell_2\left(12q^2+\omega^2-2\right)+8q^2\left(3\omega^2-4\right)$$
$$-24q^4-2\omega^2\left(2\omega^2+3\right)\Bigg)+\frac{\zeta\left(6,\ell_c'+1\right)}{4096\pi}\Bigg(11\ell_2^3+4\ell_2^2\left(20q^2-3\left(\omega^2+2\right)\right)$$
$$+4\ell_2\left(2q^2\left(5\omega^2-78\right)+60q^4-8\omega^4-6\omega^2+3\right)-16\Big(q^4\left(80-30\omega^2\right)$$
$$+q^2\left(10\omega^4-21\omega^2-88\right)+20q^6-\omega^2\left(\omega^4+5\omega^2+5\right)\Big)\Bigg)+\ldots \tag{3.G.5}$$

$$B: \quad \frac{\zeta\left(2,\ell_c'+1\right)}{32\pi}\left(\ell_2-4q^2+2\omega^2\right)+\frac{\zeta\left(4,\ell_c'+1\right)}{256\pi}\Bigg(5\ell_2^2+\ell_2\left(12q^2+7\omega^2-4\right)+8q^2\left(3\omega^2-4\right)$$
$$-24q^4-2\omega^2\left(2\omega^2+3\right)\Bigg)+\frac{\zeta\left(6,\ell_c'+1\right)}{4096\pi}\Bigg(41\ell_2^3+4\ell_2^2\left(50q^2-3\left(\omega^2+8\right)\right)$$
$$+4\ell_2\left(q^2\left(70\omega^2-208\right)+60q^4-28\omega^4-14\omega^2+17\right)-16\Big(q^4\left(80-30\omega^2\right)$$
$$+q^2\left(10\omega^4-21\omega^2-88\right)+20q^6-\omega^2\left(\omega^4+5\omega^2+5\right)\Big)\Bigg)+\ldots \tag{3.G.6}$$

This dependence on $\omega^2$and $\ell(\ell+1)$ was also observed for global monopoles in the context of the $O(N)$ model [63]

3.H. Only zero modes contribution in the kernels

The contribution of the zero modes in the Green's function (3.D.16) is

$$G_{q;0}(r,r') = \frac{i}{2}\sum_{m=-q}^{q-1}\begin{bmatrix}0 & S^-_{q,q,m}\end{bmatrix}\left(\text{sgn}(\tau-\tau')\begin{pmatrix}-1 & 0\\ 0 & 1\end{pmatrix}\right)\begin{bmatrix}0\\ \left(S^-_{q,q,m}\right)^\dagger\end{bmatrix}. \tag{3.H.1}$$

We focus on the contribution of this function to kernel coefficients. For instance, for the scalar-scalar kernel coefficient (3.4.28), we have

$$D^q_\ell(\omega) = \frac{4\pi}{2\ell+1}\int_r e^{i\omega\tau}\text{tr}\left[G_{q;0}(r,r')G^\dagger_{q;0}(r,r')\right]\sum_m Y^*_{\ell m}(\hat{n})Y_{\ell m}(\hat{n}') + \dots \tag{3.H.2}$$

where the ellipses indicates terms including non-zero modes contributions that have already been incorporated in the main text computations. This "zero-zero mode contribution" has no fermion energy $\sqrt{\ell^2-q^2}\to 0$ and the Green's function can be factorized as

$$G_{q;0}\left(r,0\right) = \text{sgn}\left(\tau\right)\tilde{G}_{q;0}\left(\hat{n},0\right). \tag{3.H.3}$$

The "zero-zero mode contribution " to the kernel coefficient then simplifies to

$$\frac{4\pi}{2\ell+1}\times 2\pi\delta(\omega)\int d\hat{n}\text{tr}\left[\tilde{G}_{q;0}\left(\hat{n},0\right)\tilde{G}^\dagger_{q;0}\left(\hat{n},0\right)\right]\sum_m Y^*_{\ell m}(\hat{n})Y_{\ell m}(\hat{n}'). \tag{3.H.4}$$

Let's then write kernel as

$$D^q_\ell(\omega) = C^q_\ell\delta(\omega) + \text{regular terms} \tag{3.H.5}$$

Hence, looking only at the scalar-scalar kernel, the contribution around $\omega=0$ is [20]

$$\begin{aligned}\frac{1}{2}\int_{-\epsilon}^{\epsilon}\frac{d\omega}{2\pi}\left(\sum_{\ell=0}^{\infty}(2\ell+1)\ln\left[D^q_\ell(\omega)\right]\right) &= \frac{1}{2}\int_{-\epsilon}^{\epsilon}\frac{d\omega}{2\pi}\left(\sum_{\ell=0}^{\infty}(2\ell+1)\ln\left[C^q_\ell\delta(\omega)+\text{“reg.”}\right]\right)\\ &= \frac{1}{2}\int_{-\epsilon}^{\epsilon}\frac{d\omega}{2\pi}\left(\sum_{\ell=0}^{\infty}(2\ell+1)\ln\left[1+\frac{C^q_\ell\delta(\omega)}{\text{“reg.”}}\right]\right)\\ &= \frac{1}{2}\mathcal{J}\int_{-\epsilon}^{\epsilon}\frac{d\omega}{2\pi}\left(\sum_{\ell=0}^{\infty}(2\ell+1)\ln\left[1+\delta(\omega)\right]\right)\end{aligned} \tag{3.H.6}$$

where we changed variable and $\mathcal{J}$ is the resulting Jacobian. We also used $\lim_{\epsilon\to 0}\int_{-\epsilon}^{\epsilon}\frac{d\omega}{2\pi}\ln\text{“reg.”}\to 0$. It turns out that the remaining term also vanishes

$$\int_{-\epsilon}^{\epsilon}\frac{d\omega}{2\pi}\ln\left[1+\delta(\omega)\right] = 0, \tag{3.H.7}$$

as we show in what follows.

[20] The contribution of the $q=0$ kernel in the denominator doesn't matter since it can be isolated and it vanishes $\lim_{\epsilon\to 0}\int_{-\epsilon}^{\epsilon}\frac{d\omega}{2\pi}\ln D^0_\ell(\omega)\to 0$.

The logarithm in Eq. (3.H.7) can be rewritten as an integral

$$\int d\omega \ln\left[1+\delta(\omega)\right] = \int d\omega \int_0^1 dt \frac{\delta(\omega)}{1+t\delta(\omega)}. \tag{3.H.8}$$

We then exchange the order of integration and obtain a vanishing integral

$$\begin{aligned}\int d\omega \ln\left[1+\delta(\omega)\right] = \int_0^1 dt \int d\omega \left[\delta(\omega) \times \frac{1}{1+t\delta(\omega)}\right] &= \int_0^1 dt \frac{1}{1+t\delta(0)} \\ &= \int_0^1 dt \begin{cases} 1 & t=0 \\ 0 & t\neq 0 \end{cases} = 0.\end{aligned} \tag{3.H.9}$$

Generalization

The kernel coefficients, with the "zero-zero mode contribution" explicitly included, can be written as

$$D_\ell^q(\omega) = C_D\delta(\omega) + \mathrm{reg}_D, \tag{3.H.10}$$

$$H_\ell^{q,T}(\omega) = C_{HT}\delta(\omega) + \mathrm{reg}_{FT}, \tag{3.H.11}$$

$$K_\ell^{q,E}(\omega) = C_{KE}\delta(\omega) + \mathrm{reg}_{KE}, \tag{3.H.12}$$

$$K_\ell^{q,B}(\omega) = 0 + \mathrm{reg}_{KB}. \tag{3.H.13}$$

In fact, it turns out that $C_D = -iC_{HT} = -C_{KE}$, but this is not necessary for the argument that follows. Again, let us consider the calculation of the scaling dimension in QED_3-GN near $\omega = 0$. Once again, we can ignore the denominator :

$$\frac{1}{2}\int_{-\epsilon}^{\epsilon}\frac{d\omega}{2\pi}\left\{\left[\ln D_0^q(\omega)\right] + \sum_{\ell=1}^{\infty}(2\ell+1)\ln\left[K_\ell^{q,B}(\omega)\left(D_\ell^q(\omega)K_\ell^{q,E}(\omega) + \left(1+\frac{\omega^2}{\ell(\ell+1)}\right)\left|F_\ell^{q,T}(\omega)\right|^2\right)\right]\right\}. \tag{3.H.14}$$

The $K_\ell^{q,B}(\omega)$ is also regular and can be removed. Also, we already showed that $\int_{-\epsilon}^{\epsilon}\frac{d\omega}{2\pi}\ln D_\ell^q(\omega) = 0$, we can use this to eliminate the $\ell = 0$ contribution. We are left with

$$\frac{1}{2}\int_{-\epsilon}^{\epsilon}\frac{d\omega}{2\pi}\left(\sum_{\ell=1}^{\infty}(2\ell+1)\ln\left[D_\ell^q(\omega)K_\ell^{q,E}(\omega) + \left(1+\frac{\omega^2}{\ell(\ell+1)}\right)\left|F_\ell^{q,T}(\omega)\right|^2\right]\right). \tag{3.H.15}$$

Let us now consider the argument of the logarithm

$$\begin{aligned}
&D_\ell^q(\omega)K_\ell^{q,E}(\omega) + \left(1+\frac{\omega^2}{\ell(\ell+1)}\right)\left|F_\ell^{q,T}(\omega)\right|^2 \\
&\quad = \left[C_D\mathrm{reg}_{KE} + C_D\mathrm{reg}_{KE} + 2\,\mathrm{Re}\left(C_{FT}\mathrm{reg}_{FT}^*\right)\right]\delta(\omega) \\
&\qquad + \left[C_DC_{KE} + |C_{FT}|^2\right]\delta(\omega)^2 + \left[\mathrm{reg}_D\mathrm{reg}_{KE} + \left(1+\frac{\omega^2}{\ell(\ell+1)}\right)|\mathrm{reg}_{FT}|^2\right] \\
&\quad \equiv a\delta(\omega)^2 + b\delta(\omega) + c \\
&\quad = a\left[\delta(\omega)-f_1\right]\left[\delta(\omega)-f_2\right]. \qquad \text{(3.H.16)}
\end{aligned}$$

Then, the scaling dimension correction near $\omega = 0$ can be written as

$$\frac{1}{2}\sum_{\ell=1}^{\infty}(2\ell+1)\int_{-\epsilon}^{\epsilon}\frac{d\omega}{2\pi}\left(\ln\left[\delta(\omega)-f_1\right]+\ln\left[\delta(\omega)-f_2\right]\right) = 0+0. \qquad \text{(3.H.17)}$$

3.I. Fitting procedure for anomalous dimensions

The method used to determine the monopole anomalous dimensions and estimate the errors is described here for QED_3 and QED_3-GN models. To estimate the error, we vary the maximal cutoff $L_{\max}$ (3.4.60) of the dataset used to extrapolate the anomalous dimension to $L \to \infty$.[21]

(1) Compute the anomalous dimension up to the cutoff $L_{\max}$ (for instance, this is $L_{\max} = 65$ for $q = 1/2$)

(2) Extrapolate the behaviour as $L \to \infty$ with a fit $\sum_{i=0}^{k} c_{i;k;L_{\max}} L^{-i}$ with polynomial order $k = 4$ (for $q = 1/2$, we use $L \in [L_{\max} - 10, L_{\max}]$).

(3) Repeat step 2 with smaller values of $L_{\max}$, computing four more times the scaling dimension. For instance, with $q = 1/2$, we repeat with $L_{\max} \in [61, 65]$.

(4) Extrapolate the behaviour as $L_{\max} \to \infty$ with a linear fit in $1/L_{\max}$, $\tilde{c}_0 + \tilde{c}_1/L_{\max}$, using the five anomalous dimensions obtained. The fit and the anomalous dimensions are shown in Fig. 3.5 for the case $q = 1/2$. Additional points down to $L_{\max} = 45$ are also displayed in Fig. 3.5 to discuss the behaviour later on.

(5) Compare the anomalous dimension obtained with the maximal value of $L_{\max}$, that we note in what follows as $L^*_{\max}$ (for $q = 1/2$, $L^*_{\max} = 65$) and the extrapolated value

[21] The cutoff ℓ'_c we use has a negligible contribution to the uncertainty, thanks to the very precise expansion, up to $1/\ell'^{18}$, of the remainder.

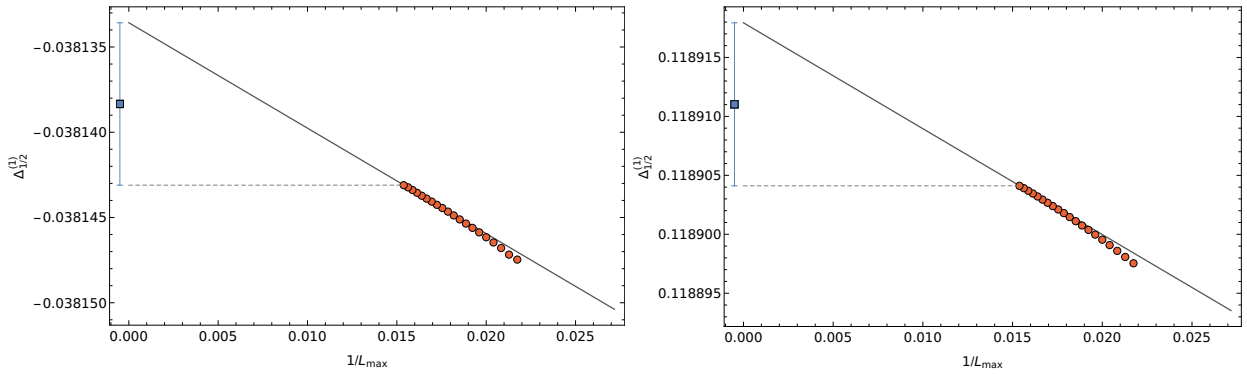

(a) (b)

Figure 3.5. Fitting procedure of anomalous dimensions of the $q = 1/2$ monopole $\Delta^{(1)}_{1/2}$ in (a) QED$_3$; (b) QED$_3$-GN. The points are obtained with fits $\sum_{i=0}^{k} c_{i;k;L_{\max}} L^{-i}$ with $L \in [L_{\max} - 5, L_{\max}]$. The solid line is a linear fit in $1/L_{\max}$ with $L_{\max} \in [61, 65]$. The point with the error bar corresponds to the anomalous dimension computed with Eq.(3.I.1) and shown in Eq. (3.I.2)

at $L_{\max} \to \infty$ and estimate the anomalous dimension as

$$\Delta^{(1)}_q = \frac{1}{2}\left(\Delta^{(1)}_q\Big|_{L_{\max}=L^*_{\max}} + \Delta^{(1)}_q\Big|_{L_{\max}\to\infty}\right) \pm \frac{1}{2}\left(\Delta^{(1)}_q\Big|_{L_{\max}=L^*_{\max}} - \Delta^{(1)}_q\Big|_{L_{\max}\to\infty}\right). \quad (3.I.1)$$

This result with the error bar is shown in Fig. 3.5 for the case $q = 1/2$ and is given by :

$$\Delta^{(1)}_{1/2,\,\mathrm{QED}_3} = -0.038138(5), \quad \Delta^{(1)}_{1/2,\,\mathrm{QED}_3\text{-GN}} = 0.118911(7). \quad (3.I.2)$$

We emphasize that the data used for the extrapolation in step 4 was itself the result of the extrapolation in step 2 (and step 3). The extrapolated value at $L_{\max} \to \infty$ is therefore used as a guiding value. Had we taken a dataset with smaller values of $L_{\max}$, the fitted line would simply overshoot the one currently presented in Fig. 3.5. The anomalous dimension in Eq. 3.I.1 would have more extreme values and thus a greater error.

To further characterize the effect that the size of $L_{\max}$ has on the anomalous dimensions, we also consider the cases $q = 1,3/2$ and $q = 25/2$ where we used a cutoff $L_{\max} = 45 + \lfloor q \rceil$. [22] For those charges obtained with a larger cutoff, we can restrain our dataset and obtain the anomalous dimensions with $L_{\max} = 35 + \lfloor q \rceil$. The results with $L_{\max} = 45 + \lfloor q \rceil$ are slightly

[22] Although we do obtain $q = 25/2$ anomalous dimensions for the largest cutoff, the corresponding values and errors presented in Tab.3.5 are obtained with cutoff $L_{\max} = 35 + \lfloor q \rceil$

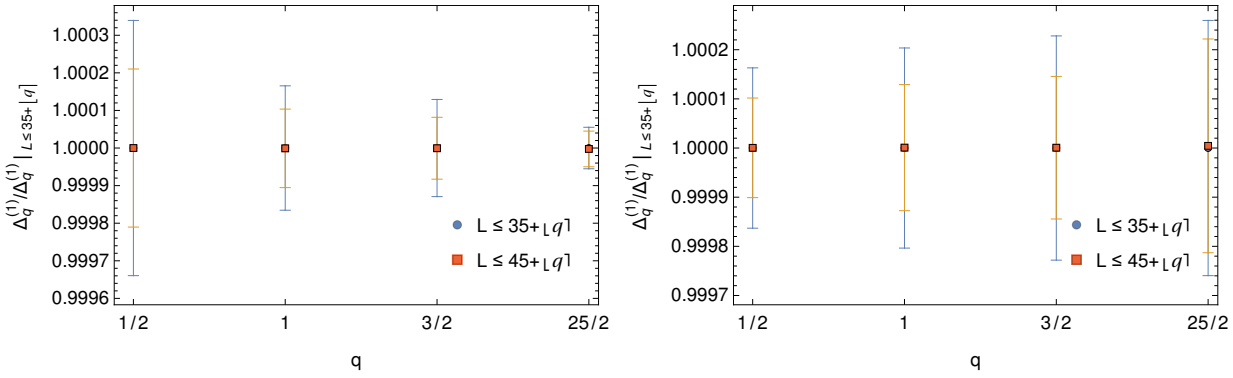

(a) (b)

Figure 3.6. Normalized anomalous dimensions in (a) QED_3 ; (b) QED_3-GN. There are two sets of scaling dimensions obtained for $L_{\max} \in [31 + \lfloor q \rceil, 35 + \lfloor q \rceil]$ $(L \leq 35 + \lfloor q \rceil)$ and $L_{\max} \in [41 + \lfloor q \rceil, 45 + \lfloor q \rceil]$ $(L \leq 45 + \lfloor q \rceil)$. The anomalous dimensions are normalized as $\Delta_q^{(1)}/\Delta_q^{(1)}|_{L \leq 35+\lfloor q \rceil}$.

more precise and very similar to those with $L_{\max} = 35 + \lfloor q \rceil$. As shown in Fig. 3.6, the drift of the anomalous dimension as $L_{\max}$ is increased is very small relatively to the estimated errors, which indicates the stability of our method.

The same procedure was also used for different fitting functions $\sum_{i=0}^{k} c_{i;k;L_{\max}} L^{-i}$ with higher polynomial order $k = 5, 6$, as shown in Fig. 3.7. We find a similar behaviour and more precise results. However, these fits demand a larger dataset. For larger q (and therefore larger maximal cutoff since the cutoff increases with $\lceil q \rceil$), a similar behaviour remains. However, the size of datasets needs to be increased. This was also observed for $q = 1/2$ when comparing relativistic cutoffs $L_{\max}$ of different sizes. It may indicate that errors are overfitted for smaller datasets with higher-order fits, as the effect is less important for $k = 4$. We used the quartic fit for all of the anomalous dimensions quoted in this work.

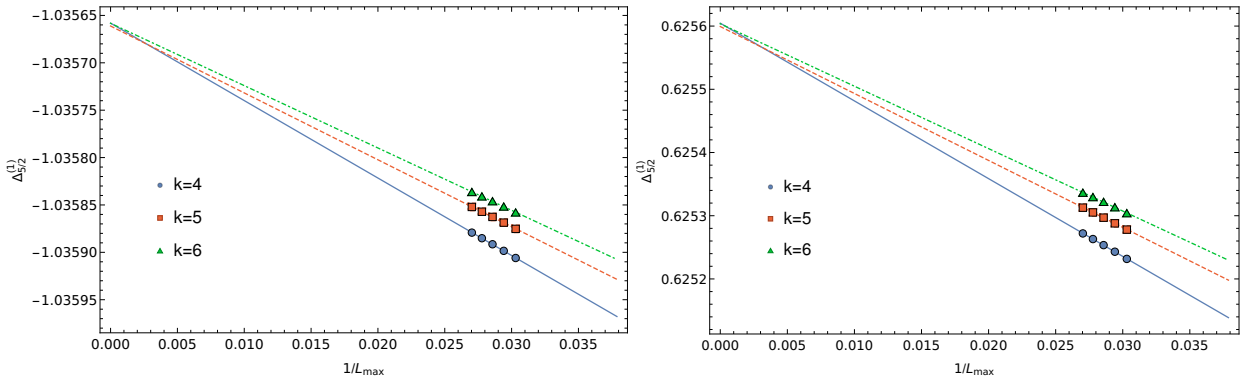

(a) (b)

Figure 3.7. Fitting procedure for anomalous dimensions of the $q = 5/2$ monopole $\Delta^{(1)}_{5/2}$ in (a) QED_3 ; (b) QED_3-GN. The points are obtained with fits $\sum_{i=0}^{k} c_{i;k;L_{\max}} L^{-i}$ with $L \in [L_{\max} - \delta_k, L_{\max}]$ with $\delta_k = \{5,10,14\}$ for $k = \{4,5,6\}$. Each set of five points is obtained by varying $L_{\max} \in [33, 37]$. Solid, dashed, and dot-dashed lines are linear fits in $1/L_{\max}$ of the $k = 4,5,6$ results.

3.J. Monopole scaling dimensions for $1/2 \leq q \leq 13$

Tableau 3.5. Scaling dimension of monopole operators at leading-order and next-to-leading order in $1/N$ in QED_3, QED_3-GN and QED_3-Z_2GN models. The leading-order result is the same in all models. The scaling dimension is $2N\Delta_q^{(0)} + \Delta_q^{(1)}$.

q	$\Delta_q^{(0)}$	$\Delta^{(1)}_{q,\,\mathrm{QED}_3}$	$\Delta^{(1)}_{q,\,\mathrm{QED}_3\text{-GN}}$	$\Delta^{(1)}_{q,\,\mathrm{QED}_3\text{-Z}_2\mathrm{GN}}$
1/2	0.26510	−0.038138(5)	0.118911(7)	0.102846(9)
1	0.67315	−0.19340(3)	0.23561(4)	0.18663(4)
3/2	1.18643	−0.42109(4)	0.35808(6)	0.26528(7)
2	1.78690	−0.70482(9)	0.4879(2)	0.3426(2)
5/2	2.46345	−1.0358(2)	0.6254(2)	0.4202(3)
3	3.20837	−1.4082(2)	0.7705(3)	0.4989(3)
7/2	4.01591	−1.8181(2)	0.9229(3)	0.5789(4)
4	4.88154	−2.2623(3)	1.0824(4)	0.6605(4)
9/2	5.80161	−2.7384(3)	1.2488(4)	0.7439(5)
5	6.77309	−3.2445(3)	1.4218(5)	0.8290(6)
11/2	7.79338	−3.7788(4)	1.6013(5)	0.9160(6)
6	8.86025	−4.3401(4)	1.7869(6)	1.0048(7)
13/2	9.97175	−4.9269(4)	1.9786(7)	1.0955(8)
7	11.12616	−5.5384(5)	2.1762(7)	1.1881(8)
15/2	12.32195	−6.1735(5)	2.3794(7)	1.2825(9)
8	13.55772	−6.8314(5)	2.5882(8)	1.3787(9)
17/2	14.83223	−7.5113(6)	2.8024(9)	1.477(1)
9	16.14432	−8.2125(6)	3.0219(9)	1.577(2)
19/2	17.49296	−8.9345(6)	3.2466(9)	1.678(2)
10	18.87719	−9.6766(7)	3.476(1)	1.781(2)
21/2	20.29609	−10.4383(7)	3.711(2)	1.886(2)
11	21.74886	−11.2191(7)	3.950(2)	1.993(2)
23/2	23.23472	−12.0186(7)	4.195(2)	2.102(2)
12	24.75294	−12.8363(8)	4.444(2)	2.212(2)
25/2	26.30286	−13.6719(8)	4.697(2)	2.323(2)
13	27.88383	−14.5249(8)	4.955(2)	2.437(2)

Bibliographie

[1] A. M. Polyakov, Physics Letters B **59**, 82 (1975), ISSN 0370-2693, URL http://www.sciencedirect.com/science/article/pii/0370269375901628.

[2] A. M. Polyakov, Nuclear Physics B **120**, 429 (1977), ISSN 0550-3213, URL http://www.sciencedirect.com/science/article/pii/0550321377900864.

[3] M. B. Hastings, Phys. Rev. B **63**, 014413 (2000), URL https://link.aps.org/doi/10.1103/PhysRevB.63.014413.

[4] Y. Ran, M. Hermele, P. A. Lee, and X.-G. Wen, Phys. Rev. Lett. **98**, 117205 (2007), URL https://link.aps.org/doi/10.1103/PhysRevLett.98.117205.

[5] Y. Iqbal, F. Becca, and D. Poilblanc, Phys. Rev. B **84**, 020407 (2011), URL https://link.aps.org/doi/10.1103/PhysRevB.84.020407.

[6] Y. Iqbal, F. Becca, S. Sorella, and D. Poilblanc, Phys. Rev. B **87**, 060405 (2013), URL https://link.aps.org/doi/10.1103/PhysRevB.87.060405.

[7] Y.-C. He, M. P. Zaletel, M. Oshikawa, and F. Pollmann, Phys. Rev. X **7**, 031020 (2017), URL https://link.aps.org/doi/10.1103/PhysRevX.7.031020.

[8] H. J. Liao, Z. Y. Xie, J. Chen, Z. Y. Liu, H. D. Xie, R. Z. Huang, B. Normand, and T. Xiang, Phys. Rev. Lett. **118**, 137202 (2017), URL https://link.aps.org/doi/10.1103/PhysRevLett.118.137202.

[9] R. Kaneko, S. Morita, and M. Imada, Journal of the Physical Society of Japan **83**, 093707 (2014), https://doi.org/10.7566/JPSJ.83.093707, URL https://doi.org/10.7566/JPSJ.83.093707.

[10] Y. Iqbal, W.-J. Hu, R. Thomale, D. Poilblanc, and F. Becca, Phys. Rev. B **93**, 144411 (2016), URL https://link.aps.org/doi/10.1103/PhysRevB.93.144411.

[11] S. Hu, W. Zhu, S. Eggert, and Y.-C. He, Phys. Rev. Lett. **123**, 207203 (2019), URL https://link.aps.org/doi/10.1103/PhysRevLett.123.207203.

[12] P. Corboz, M. Lajkó, A. M. Läuchli, K. Penc, and F. Mila, Phys. Rev. X **2**, 041013 (2012), URL https://link.aps.org/doi/10.1103/PhysRevX.2.041013.

[13] V. Calvera and C. Wang, *Theory of Dirac spin-orbital liquids : monopoles, anomalies, and applications to $SU(4)$ honeycomb models* (2021), 2103.13405.

[14] V. Calvera and C. Wang, *Theory of Dirac spin liquids on spin-S triangular lattice : possible application to α-CrOOH(D)* (2020), 2012.09809.

[15] V. Borokhov, A. Kapustin, and X. Wu, Journal of High Energy Physics **2002**, 049 (2002), URL https://doi.org/10.1088/1126-6708/2002/11/049.

[16] S. S. Pufu, Phys. Rev. D **89**, 065016 (2014), URL https://link.aps.org/doi/10.1103/PhysRevD.89.065016.

[17] N. Karthik and R. Narayanan, Phys. Rev. D **100**, 054514 (2019), URL https://link.aps.org/doi/10.1103/PhysRevD.100.054514.

[18] S. M. Chester and S. S. Pufu, Journal of High Energy Physics **2016**, 69 (2016), ISSN 1029-8479, URL https://doi.org/10.1007/JHEP08(2016)069.

[19] S. M. Chester, L. V. Iliesiu, M. Mezei, and S. S. Pufu, Journal of High Energy Physics **2018** (2018), ISSN 1029-8479, URL http://link.springer.com/10.1007/JHEP05(2018)157.

[20] S. Dey, Phys. Rev. B **102**, 235165 (2020), URL https://link.aps.org/doi/10.1103/PhysRevB.102.235165.

[21] N. Read and S. Sachdev, Phys. Rev. Lett. **62**, 1694 (1989), URL https://link.aps.org/doi/10.1103/PhysRevLett.62.1694.

[22] N. Read and S. Sachdev, Phys. Rev. B **42**, 4568 (1990), URL https://link.aps.org/doi/10.1103/PhysRevB.42.4568.

[23] T. Senthil, L. Balents, S. Sachdev, A. Vishwanath, and M. P. A. Fisher, Phys. Rev. B **70**, 144407 (2004), URL https://link.aps.org/doi/10.1103/PhysRevB.70.144407.

[24] T. Senthil, L. Balents, S. Sachdev, A. Vishwanath, and M. P. A. Fisher, Journal of the Physical Society of Japan **74**, 1 (2005), https://doi.org/10.1143/JPSJS.74S.1, URL https://doi.org/10.1143/JPSJS.74S.1.

[25] G. Murthy and S. Sachdev, Nuclear Physics B **344**, 557 (1990).

[26] M. F. Atiyah and I. M. Singer, Bulletin of the American Mathematical Society **69**, 422 (1963), URL https://doi.org/.

[27] X.-Y. Song, C. Wang, A. Vishwanath, and Y.-C. He, Nature Communications **10**, 4254 (2019), ISSN 2041-1723, URL https://doi.org/10.1038/s41467-019-11727-3.

[28] P. Ghaemi and T. Senthil, Phys. Rev. B **73**, 054415 (2006), URL https://link.aps.org/doi/10.1103/PhysRevB.73.054415.

[29] M. Hermele, Y. Ran, P. A. Lee, and X.-G. Wen, Phys. Rev. B **77**, 224413 (2008), URL https://link.aps.org/doi/10.1103/PhysRevB.77.224413.

[30] Y.-M. Lu, G. Y. Cho, and A. Vishwanath, Phys. Rev. B **96**, 205150 (2017), URL https://link.aps.org/doi/10.1103/PhysRevB.96.205150.

[31] É. Dupuis, M. B. Paranjape, and W. Witczak-Krempa, Phys. Rev. B **100**, 094443 (2019), URL https://link.aps.org/doi/10.1103/PhysRevB.100.094443.

[32] É. Dupuis, M. B. Paranjape, and W. Witczak-Krempa, in *Quantum Theory and Symmetries*, edited by M. B. Paranjape, R. MacKenzie, Z. Thomova, P. Winternitz, and W. Witczak-Krempa (Springer International Publishing, Cham, 2021), pp. 327–336, ISBN 978-3-030-55777-5.

[33] É. Dupuis and W. Witczak-Krempa, Annals of Physics p. 168496 (2021), ISSN 0003-4916, URL https://www.sciencedirect.com/science/article/pii/S0003491621001020.

[34] L. Zou, Y.-C. He, and C. Wang, *Stiefel liquids : possible non-lagrangian quantum criticality from intertwined orders* (2021), 2101.07805.

[35] Y.-C. He, Y. Fuji, and S. Bhattacharjee, *Kagome spin liquid : a deconfined critical phase driven by $U(1)$ gauge fluctuation* (2015), arXiv:1512.05381.

[36] L. Janssen and Y.-C. He, Phys. Rev. B **96**, 205113 (2017), URL https://link.aps.org/doi/10.1103/PhysRevB.96.205113.

[37] Y.-C. He, D. N. Sheng, and Y. Chen, Phys. Rev. Lett. **112**, 137202 (2014), URL https://link.aps.org/doi/10.1103/PhysRevLett.112.137202.

[38] S.-S. Gong, W. Zhu, and D. N. Sheng, Scientific Reports **4**, 6317 (2014), ISSN 2045-2322, URL https://doi.org/10.1038/srep06317.

[39] Y.-C. He and Y. Chen, Phys. Rev. Lett. **114**, 037201 (2015), URL https://link.aps.org/doi/10.1103/PhysRevLett.114.037201.

[40] W. Zhu, S. S. Gong, and D. N. Sheng, Phys. Rev. B **92**, 014424 (2015), URL https://link.aps.org/doi/10.1103/PhysRevB.92.014424.

[41] W.-J. Hu, S.-S. Gong, and D. N. Sheng, Phys. Rev. B **94**, 075131 (2016), URL https://link.aps.org/doi/10.1103/PhysRevB.94.075131.

[42] S.-S. Gong, W. Zhu, J.-X. Zhu, D. N. Sheng, and K. Yang, Phys. Rev. B **96**, 075116 (2017), URL https://link.aps.org/doi/10.1103/PhysRevB.96.075116.

[43] A. Wietek and A. M. Läuchli, Phys. Rev. B **95**, 035141 (2017), URL https://link.aps.org/doi/10.1103/PhysRevB.95.035141.

[44] B. Ihrig, L. Janssen, L. N. Mihaila, and M. M. Scherer, Phys. Rev. B **98**, 115163 (2018), URL https://link.aps.org/doi/10.1103/PhysRevB.98.115163.

[45] J. A. Gracey, Phys. Rev. D **98**, 085012 (2018), URL https://link.aps.org/doi/10.1103/PhysRevD.98.085012.

[46] N. Zerf, P. Marquard, R. Boyack, and J. Maciejko, Phys. Rev. B **98**, 165125 (2018), URL https://link.aps.org/doi/10.1103/PhysRevB.98.165125.

[47] R. Boyack, A. Rayyan, and J. Maciejko, Phys. Rev. B **99**, 195135 (2019), URL https://link.aps.org/doi/10.1103/PhysRevB.99.195135.

[48] S. Benvenuti and H. Khachatryan, Journal of High Energy Physics **2019**, 214 (2019), ISSN 1029-8479, URL https://doi.org/10.1007/JHEP05(2019)214.

[49] N. Zerf, C.-H. Lin, and J. Maciejko, Phys. Rev. B **94**, 205106 (2016), URL https://link.aps.org/doi/10.1103/PhysRevB.94.205106.

[50] R. Boyack, C.-H. Lin, N. Zerf, A. Rayyan, and J. Maciejko, Phys. Rev. B **98**, 035137 (2018), URL https://link.aps.org/doi/10.1103/PhysRevB.98.035137.

[51] Y.-M. Lu, Y. Ran, and P. A. Lee, Phys. Rev. B **83**, 224413 (2011), URL https://link.aps.org/doi/10.1103/PhysRevB.83.224413.

[52] B. Roy, V. Juričić, and I. F. Herbut, Phys. Rev. B **87**, 041401 (2013), URL https://link.aps.org/doi/10.1103/PhysRevB.87.041401.

[53] C. Wang, A. Nahum, M. A. Metlitski, C. Xu, and T. Senthil, Phys. Rev. X **7**, 031051 (2017), URL https://link.aps.org/doi/10.1103/PhysRevX.7.031051.

[54] S. Hellerman, D. Orlando, S. Reffert, and M. Watanabe, Journal of High Energy Physics **2015**, 1 (2015), ISSN 1029-8479, arXiv:1505.01537, URL https://doi.org/10.1007/JHEP12(2015)071.

[55] R. Heras, Contemporary Physics **59**, 331 (2018), URL https://doi.org/10.1080/00107514.2018.1527974.

[56] M. A. Metlitski, M. Hermele, T. Senthil, and M. P. A. Fisher, Phys. Rev. B **78**, 214418 (2008), URL https://link.aps.org/doi/10.1103/PhysRevB.78.214418.

[57] W. Rantner and X.-G. Wen, Phys. Rev. B **66**, 144501 (2002), URL https://link.aps.org/doi/10.1103/PhysRevB.66.144501.

[58] M. Hermele, T. Senthil, and M. P. A. Fisher, Phys. Rev. B **72**, 104404 (2005), URL https://link.aps.org/doi/10.1103/PhysRevB.72.104404.

[59] T. T. Wu and C. N. Yang, Nuclear Physics B **107**, 365 (1976), ISSN 0550-3213, URL https://www.sciencedirect.com/science/article/pii/0550321376901437.

[60] T. T. Wu and C. N. Yang, Phys. Rev. D **16**, 1018 (1977), URL https://link.aps.org/doi/10.1103/PhysRevD.16.1018.

[61] S. S. Pufu and S. Sachdev, Journal of High Energy Physics **2013** (2013), ISSN 1029-8479, URL http://link.springer.com/10.1007/JHEP09(2013)127.

[62] E. Dyer, M. Mezei, S. S. Pufu, and S. Sachdev, Journal of High Energy Physics **2015** (2015), ISSN 1029-8479, URL http://link.springer.com/10.1007/JHEP06(2015)037.

[63] E. Dyer, M. Mezei, and S. S. Pufu, *Monopole taxonomy in three-dimensional conformal field theories* (2013), arXiv:1309.1160.

[64] E. Dyer, M. Mezei, S. S. Pufu, and S. Sachdev, Journal of High Energy Physics **2016**, 111 (2016), ISSN 1029-8479, URL https://doi.org/10.1007/JHEP03(2016)111.

[65] O. Aharony and E. Palti, *On convexity of charged operators in cfts and the weak gravity conjecture* (2021), 2108.04594.

[66] G. Cuomo, Physics Letters B **812**, 136014 (2021), ISSN 0370-2693, URL https://www.sciencedirect.com/science/article/pii/S0370269320308170.

[67] A. Monin, Physical Review D **94** (2016), ISSN 2470-0029, URL http://dx.doi.org/10.1103/PhysRevD.94.085013.

[68] A. de la Fuente, Journal of High Energy Physics **2018**, 41 (2018), ISSN 1029-8479, URL https://doi.org/10.1007/JHEP08(2018)041.

[69] S. Benvenuti and H. Khachatryan, *QED's in* 2+1 *dimensions : complex fixed points and dualities* (2019), 1812.01544.

[70] L. Bartosch, Phys. Rev. B **88**, 195140 (2013), URL https://link.aps.org/doi/10.1103/PhysRevB.88.195140.

[71] A. W. Sandvik, Phys. Rev. Lett. **98**, 227202 (2007), URL https://link.aps.org/doi/10.1103/PhysRevLett.98.227202.

[72] R. G. Melko and R. K. Kaul, Phys. Rev. Lett. **100**, 017203 (2008), URL https://link.aps.org/doi/10.1103/PhysRevLett.100.017203.

[73] R. K. Kaul and A. W. Sandvik, Phys. Rev. Lett. **108**, 137201 (2012), URL https://link.aps.org/doi/10.1103/PhysRevLett.108.137201.

[74] S. Pujari, K. Damle, and F. Alet, Phys. Rev. Lett. **111**, 087203 (2013), URL https://link.aps.org/doi/10.1103/PhysRevLett.111.087203.

[75] A. Nahum, J. T. Chalker, P. Serna, M. Ortuño, and A. M. Somoza, Phys. Rev. X **5**, 041048 (2015), URL https://link.aps.org/doi/10.1103/PhysRevX.5.041048.

[76] B. I. Halperin, T. C. Lubensky, and S.-k. Ma, Phys. Rev. Lett. **32**, 292 (1974), URL https://link.aps.org/doi/10.1103/PhysRevLett.32.292.

[77] R. K. Kaul and S. Sachdev, Phys. Rev. B **77**, 155105 (2008), URL https://link.aps.org/doi/10.1103/PhysRevB.77.155105.

[78] F.-J. Jiang, M. Nyfeler, S. Chandrasekharan, and U.-J. Wiese, Journal of Statistical Mechanics : Theory and Experiment **2008**, P02009 (2008), URL https://doi.org/10.1088/1742-5468/2008/02/p02009.

[79] J. Lou, A. W. Sandvik, and N. Kawashima, Phys. Rev. B **80**, 180414 (2009), URL https://link.aps.org/doi/10.1103/PhysRevB.80.180414.

[80] A. W. Sandvik and B. Zhao, Chinese Physics Letters **37**, 057502 (2020), URL https://doi.org/10.1088/0256-307x/37/5/057502.

[81] B. Ihrig, N. Zerf, P. Marquard, I. F. Herbut, and M. M. Scherer, Phys. Rev. B **100**, 134507 (2019), URL https://link.aps.org/doi/10.1103/PhysRevB.100.134507.

[82] S. Pujari, F. Alet, and K. Damle, Phys. Rev. B **91**, 104411 (2015), URL https://link.aps.org/doi/10.1103/PhysRevB.91.104411.

[83] Z. Li, *On conformality and self-duality of* $n_f = 2$ *qed*$_3$ (2021), 2107.09020.

[84] Y. Q. Qin, Y.-Y. He, Y.-Z. You, Z.-Y. Lu, A. Sen, A. W. Sandvik, C. Xu, and Z. Y. Meng, Phys. Rev. X **7**, 031052 (2017), URL https://link.aps.org/doi/10.1103/PhysRevX.7.031052.

[85] R. Ma and C. Wang, Phys. Rev. B **102**, 020407 (2020), URL https://link.aps.org/doi/10.1103/PhysRevB.102.020407.

[86] P. Serna and A. Nahum, Phys. Rev. B **99**, 195110 (2019), URL https://link.aps.org/doi/10.1103/PhysRevB.99.195110.

[87] A. Karch and D. Tong, Phys. Rev. X **6**, 031043 (2016), URL https://link.aps.org/doi/10.1103/PhysRevX.6.031043.

[88] X. Y. Xu, Y. Qi, L. Zhang, F. F. Assaad, C. Xu, and Z. Y. Meng, Phys. Rev. X **9**, 021022 (2019), URL https://link.aps.org/doi/10.1103/PhysRevX.9.021022.

[89] W. Wang, D.-C. Lu, X. Y. Xu, Y.-Z. You, and Z. Y. Meng, Phys. Rev. B **100**, 085123 (2019), URL https://link.aps.org/doi/10.1103/PhysRevB.100.085123.

[90] N. Zerf, R. Boyack, P. Marquard, J. A. Gracey, and J. Maciejko, Phys. Rev. B **100**, 235130 (2019), URL https://link.aps.org/doi/10.1103/PhysRevB.100.235130.

[91] N. Zerf, R. Boyack, P. Marquard, J. A. Gracey, and J. Maciejko, Phys. Rev. D **101**, 094505 (2020), URL https://link.aps.org/doi/10.1103/PhysRevD.101.094505.

[92] L. Janssen, W. Wang, M. M. Scherer, Z. Y. Meng, and X. Y. Xu, Phys. Rev. B **101**, 235118 (2020), URL https://link.aps.org/doi/10.1103/PhysRevB.101.235118.

[93] R. Boyack and J. Maciejko, in *Quantum Theory and Symmetries. CRM Series in Mathematical Physics*, edited by M. B. Paranjape, R. MacKenzie, Z. Thomova, P. Winternitz, and W. Witczak-Krempa (Springer International Publishing, Cham, 2021), pp. 337–345, ISBN 978-3-030-55777-5.

[94] S. Sachdev, Phys. Rev. D **86**, 126003 (2012), URL https://link.aps.org/doi/10.1103/PhysRevD.86.126003.

[95] A. Briggs, H. E. Camblong, and C. R. Ordóñez, International Journal of Modern Physics A **28**, 1350047 (2013), https://doi.org/10.1142/S0217751X13500474, URL https://doi.org/10.1142/S0217751X13500474.

Conclusion

> Le renard connaît beaucoup de choses, mais le hérisson connaît une grande chose.
>
> Archiloque

Les transitions de phase quantiques hors d'un liquide de spin de Dirac (DSL) ont été étudiées. La dimension d'échelle des monopôles a été obtenue aux points critiques quantiques (QCPs) décrits par l'électrodynamique quantique en $2+1$ dimensions avec $2N$ saveurs de fermions sans masse (QED_3) et diverses interactions de type Gross-Neveu (GN). En activant une interaction dépendante du spin, soit le terme de chiral-Heisenberg Gross-Neveu (cHGN), une transition vers un antiferroaimant (AFM) sur réseau kagome est décrite. Dans ce cas, la dimension d'échelle des monopôles est réduite au QCP par rapport à la phase QED_3. Cette réduction, trouvée à l'ordre dominant en $1/N$, augmente avec le spin magnétique des monopôles. La hiérarchie observée parmi les dimensions d'échelle de monopôles a été interprétée en termes d'une brisure de symétrie au QCP avec la théorie des représentations, ce qui a également permis d'extraire la dégénérescence restante pour chaque spin magnétique de monopôle. Des transitions du DSL vers deux liquides de spin quantiques topologiques, soit le liquide de spin chiral (CSL) et le liquide de spin Z_2 (Z_2 QSL) ont également été considérées. La transition vers le CSL est décrite en activant une interaction GN complètement symétrique (QED_3-GN), et celle vers le Z_2 QSL par l'activation d'une interaction GN de type supraconducteur (QED_3-Z_2GN). Les dimensions d'échelle des monopôles obtenues à l'ordre sous-dominant en $1/N$ ont une correction quantique positive pour ces deux QCPs. La comparaison de ces résultats à d'autres résultats analytiques dans la littérature semble compatible avec la dualité $QED_3\text{-GN}\,|_{2N=2} \Leftrightarrow \mathrm{CP}^1$. Des dimensions d'échelles sont obtenues

pour plusieurs charges topologiques q dans QED_3, QED_3-GN et QED_3-Z_2GN. En ajustant le comportement large-q de ces résultats, le coefficient constant $O(q^0)$ trouvé pour chaque modèle concorde avec la valeur universelle prédite pour les théories conformes des champs ayant une symétrie globale U(1).

D'autres avenues intéressantes s'ouvrent suite à cette recherche. Voici quelques idées.

- Calculer les dimensions d'échelle de monopôles pour d'autres modèles. Notamment, le modèle « easy-plane » CP^1 $(\mathrm{ep}-\mathrm{CP}^1)$[1] en 2+1 dimensions serait d'intérêt, puisqu'il permettrait de tester une autre dualité, soit $\mathrm{QED}_3\,|_{2N=2} \Leftrightarrow \mathrm{ep}-\mathrm{CP}^1$ [3]. Des résultats analytiques cohérents avec la dualité mais en tension avec des résultats numériques ont été observés pour cette dualité [4]. À l'aide de l'étude des dimensions d'échelle des monopôles, des remarques semblables ont été pu être faites au Chap. 3 dans le cas de dualité QED_3-GN $|_{2N=2} \Leftrightarrow \mathrm{CP}^1$. De nouveaux résultats pour les dimensions d'échelle des monopôles dans $\mathrm{ep}-\mathrm{CP}^1$ pourraient compléter les observations dans la Réf. [4]. Il serait aussi intéressant d'investiguer l'idée d'une transition faiblement de premier ordre, un scénario évoqué pour les deux dualités [5–7] .

- Obtenir des corrections quantiques pour le modèle étudié aux Chap. 1 et Chap. 2. Les résultats à l'ordre dominant en $1/N$ ne permettent pas de distinguer le résultat avec trois bosons auxiliaires et deux bosons auxiliaires, qui décrivent respectivement les transitions DSL→AFM et DSL→solide de liens de valence. Il serait intéressant de voir comment l'ordre sous-dominant en $1/N$ change la situation.

- Revisiter la méthode présentée au Chap. 2 pour contraindre le spin magnétique des monopôles. Une généralisation pour contraindre le spin de Lorentz pourrait être tentée. Il serait aussi intéressant de reformuler plus formellement la méthode en s'inspirant des récents développements en théorie conforme des champs où les charges

[1] Le modèle CP^1 correspond au modèle abélien de Higgs avec $N = 2$ bosons complexes (ou encore QED_3 scalaire avec une contrainte non linéaire). Le modèle « easy-plane » CP^1 ajoute un terme d'anisotropie brisant la symétrie de saveur $\mathrm{SU}(2) \to \mathrm{U}(1) \times Z_2$, où U(1) est la rotation dans le plan $x-y$ et Z_2 représente l'inversion de spin selon l'axe z [1]. Ce modèle peut être écrit comme deux modèles d'électrodynamique scalaire avec $N = 1$ boson complexe ayant le même champ de jauge [2].

globales d'opérateurs sont utilisées comme paramètre d'expansion. Cette idée remonte à la Réf. [8] où les dimensions d'échelle d'opérateurs chargés sous un groupe de symétrie U(1) ont été développées pour une grande charge. Dans le cas du spin magnétique ou du spin de Lorentz, la charge globale serait de type SU(2).

- Calculer d'autres propriétés des monopôles pour les QCPs déjà considérés (QED_3-cHGN, QED_3-GN, QED_3-Z_2GN). Notamment, il serait intéressant de considérer le « Operator Product Expansion » (OPE) pour les fonctions de corrélations à trois opérateurs monopôles et obtenir les coefficients de l'OPE. Des fonctions 4-points d'opérateurs monopôles ont déjà été considérées dans une étude du modèle QED_3 à l'aide du « conformal bootstrap ».[2] Répéter l'analyse du « conformal bootstrap » en ajoutant les interactions de type GN serait aussi intéressant pour obtenir une comparaison avec nos résultats analytiques pour les dimensions d'échelle de monopôles.

Bibliographie

[1] J. D'Emidio and R. K. Kaul, Phys. Rev. B **93**, 054406 (2016), URL `https://link.aps.org/doi/10.1103/PhysRevB.93.054406`.

[2] S. Benvenuti and H. Khachatryan, Journal of High Energy Physics **2019**, 214 (2019), ISSN 1029-8479, URL `https://doi.org/10.1007/JHEP05(2019)214`.

[3] C. Wang, A. Nahum, M. A. Metlitski, C. Xu, and T. Senthil, Phys. Rev. X **7**, 031051 (2017), URL `https://link.aps.org/doi/10.1103/PhysRevX.7.031051`.

[4] Z. Li, *On conformality and self-duality of $n_f = 2$ qed_3* (2021), `2107.09020`.

[5] S. Benvenuti and H. Khachatryan, *QED's in* 2+1 *dimensions : complex fixed points and dualities* (2019), `1812.01544`.

[6] R. Ma and C. Wang, Phys. Rev. B **102**, 020407 (2020), URL `https://link.aps.org/doi/10.1103/PhysRevB.102.020407`.

[7] P. Serna and A. Nahum, Phys. Rev. B **99**, 195110 (2019), URL `https://link.aps.org/doi/10.1103/PhysRevB.99.195110`.

[2] Des fonctions de corrélation mixtes entre monopôles et bilinéaires fermioniques ont aussi été considérées dans la Réf. [9]

[8] S. Hellerman, D. Orlando, S. Reffert, and M. Watanabe, Journal of High Energy Physics **2015**, 1 (2015), ISSN 1029-8479, arXiv:1505.01537, URL https://doi.org/10.1007/JHEP12(2015)071.

[9] Y.-C. He, J. Rong, and N. Su, *Conformal bootstrap bounds for the* $u(1)$ *dirac spin liquid and* $n = 7$ *stiefel liquid* (2021), 2107.14637.

Contributions de l'auteur

Conformément aux exigences de la FESP, cette annexe vise à détailler ma contribution (ÉD) aux articles compris dans cette thèse. J'ai joué un rôle essentiel dans la réalisation de chaque article. Les nombreuses discussions entre tous les coauteurs pour chaque article témoignent d'un effort collectif et sont sous-entendues dans la description sommaire.

- Chapitre 1 : Idée originale de WWK et discussions préliminaires par ÉD, MBP, WWK. Calculs et rédaction par ÉD. Révision par WWK.

- Chapitre 2 : Idée originale de WWK. Calculs et rédaction par ÉD. Révision par WWK.

- Chapitre 3 : Idée originale de ÉD et WWK. Calculs par ÉD, RB et WWK. Rédaction par ÉD et RB. Révision par RB et WWK.

Chapitre A

Correspondance état-opérateur

La correspondance état-opérateur est utilisée dans tous les chapitres de la thèse pour calculer la dimension d'échelle d'opérateurs monopôles. Elle est décrite plus en détail dans cet annexe. La présentation est inspirée de la Réf. [1] où la correspondance état-opérateur a été utilisée pour étudier les opérateurs monopôles du modèle CP^{N-1}.

A.1. Quantification radiale

La construction de l'espace d'Hilbert dans une théorie quantique des champs repose sur une évolution d'états qui transitent entre des tranches d'espace-temps successives, soit les hypersurfaces de dimensions $d-1$ divisant l'espace-temps d-dimensionnel [2]. Une approche conventionnelle est de choisir un axe temporel et les tranches sont définies pour un temps fixe. Le générateur de translation dans le temps est l'Hamiltonien $\hat{H} = -i\partial/\partial t$. L'exponentiation de l'Hamiltonien $U = \exp\Big(i\hat{H}\Delta t\Big)$ est l'opérateur donnant par son action l'évolution temporelle des états de l'espace d'Hilbert. C'est une approche usuelle pour les théories qui ont la symétrie du renversement de temps, par exemple celles qui ont la symétrie de Poincaré.

Dans les théories conformes des champs (CFT) où des symétries additionnelles sont présentes, notamment celle de dilatation, une autre approche est utile. L'espace-temps est divisé en hypersphères centrées à l'origine. Dans ce cas, c'est la dimension radiale $\hat{r}$, où $r = |x^\mu|$, qui lie les tranches d'espace-temps définies par des rayons d'hypersphère distincts. Le générateur de dilatation $\hat{D}$ faisant partie de l'algèbre du groupe conforme assure la translation radiale. On parle ainsi d'une quantification radiale de l'espace d'Hilbert où l'opérateur d'évolution est donné par $U = \exp\Big(i\hat{D}\hat{r}\Big)$.

La fonction de corrélation deux-points d'un opérateur primaire $\mathcal{O}(x)$ de la CFT est une loi de puissance contrôlée par une dimension d'échelle $\Delta_{\mathcal{O}}$

$$\left\langle \mathcal{O}(x)\mathcal{O}^{\dagger}(y)\right\rangle \sim \frac{1}{|x-y|^{2\Delta_{\mathcal{O}}}}\,. \tag{A.1.1}$$

La dimension d'échelle est un nombre quantique lié à l'opérateur de dilatation. L'action de l'opérateur de dilatation $\hat{D}$ sur un opérateur primaire $\mathcal{O}(x)$ est donné par

$$[\hat{D},\mathcal{O}(x)] = -i\left(\Delta_{\mathcal{O}} + x^{\mu}\partial_{\mu}\right)\mathcal{O}(x)\,. \tag{A.1.2}$$

En particulier, pour un opérateur primaire centré à l'origine, le membre de droite devient simplement l'opérateur primaire multiplié par une constante $[\hat{D},\mathcal{O}(0)] = -i\Delta\mathcal{O}(0)$. Utilisant ce résultat, on peut agir le vide $|0\rangle$ avec l'opérateur primaire $\mathcal{O}(0)$ pour définir un état $|\mathcal{O}\rangle = \mathcal{O}(0)|0\rangle$ ayant une valeur propre $-i\Delta$ sous l'opérateur de dilatation

$$\hat{D}\left(\mathcal{O}(0)|0\rangle\right) = -i\Delta_{\mathcal{O}}\left(\mathcal{O}(0)|0\rangle\right)\,, \tag{A.1.3}$$

où l'invariance du vide sous l'opérateur de dilatation, $\hat{D}|0\rangle = 0|0\rangle$, a été utilisée. Les états propres de dilatation peuvent ainsi être générés par les opérateurs primaires de la théorie. Suivant le même raisonnement, l'opérateur $\mathcal{O}(0)$ et l'état $|\mathcal{O}\rangle$ partagent aussi les mêmes nombres quantiques sous les autres générateurs du groupe de symétrie conforme, d'où l'idée de la correspondance état-opérateur

$$\mathcal{O}(0) \Leftrightarrow |\mathcal{O}\rangle\,. \tag{A.1.4}$$

L'utilité de cette correspondance devient claire suite à une transformation de Weyl qui envoie l'espace-temps euclidien $\mathbb{R}^d$ au cylindre généralisé $S^{d-1}\times\mathbb{R}$, soit $(ds^2)_{\mathbb{R}^d} \to r^{-2}\,(ds^2)_{\mathbb{R}^d} \equiv (ds^2)_{S^{d-1}\times\mathbb{R}}$. En définissant le rayon sur $\mathbb{R}^d$ comme $r = Re^{\tau/R}$, où R est une constante avec des unités de longueur, la nouvelle métrique est donnée par

$$\left(ds^2\right)_{S^{d-1}\times\mathbb{R}} = R^{-2}e^{-2\tau/R}\left(ds^2\right)_{\mathbb{R}^d} = d\tau^2 + d\Omega^2\,. \tag{A.1.5}$$

Ainsi, dans ce nouvel espace, τ définit une direction de « temps » sur $\mathbb{R}$. La dilatation dans le système original devient une translation de « temps »

$$r \to r+\lambda\,, \quad \tau \to \tau + R\log(\lambda/R)\,. \tag{A.1.6}$$

L'opérateur de dilatation est donc envoyé vers un opérateur qui fait une translation dans le « temps », soit l'Hamiltonien. Trouver la dimension d'échelle d'un opérateur $\mathcal{O}$ sur $\mathbb{R}^d$ revient donc à trouver l'énergie Δ/R d'un état $|\mathcal{O}\rangle$ sur $S^{d-1}\times\mathbb{R}$. La correspondance état-opérateur et la définition d'un tel état sont formulées plus en détail dans ce qui suit.

A.2. Fonctionnelle d'onde et correspondance état-opérateur

On commence d'abord par décrire l'évolution temporelle d'une fonction d'onde en mécanique quantique. Soit un espace d'Hilbert en mécanique quantique muni d'états $\{|q\rangle\}$. Cette base est introduite sur chaque tranche de l'espace-temps, séparé dans ce suit selon l'axe du temps. La probabilité de propagation d'une particule dans l'état initial $|q_i\rangle$ à un état final $|q_f\rangle$ en un intervalle de temps T est donnée par

$$\langle q_f,t_f|q_i,t_i\rangle = \langle q_f|e^{-iHT}|q_i\rangle = \int_{q(t_i)=q_i}^{q(t_f)=q_f} \mathcal{D}q(t)e^{iS[q(t)]}\,, \tag{A.2.1}$$

où $|q,t\rangle = e^{-iHt}|q\rangle$. Ce propagateur est utilisé pour définir l'évolution temporelle d'une fonction d'onde comme suit

$$\begin{aligned}\psi(q_f,t_f) = \langle q_f,t_f|\psi\rangle &= \int dq_i \langle q_f,t_f|q_i,t_i\rangle\langle q_i,t_i|\psi\rangle \\ &= \int dq_i \left[\int_{q(t_i)=q_i}^{q(t_f)=q_f} \mathcal{D}q(t)e^{iS[q(t)]}\right]\psi(q_i,t_i)\,.\end{aligned} \tag{A.2.2}$$

De la même manière, on peut travailler en théorie des champs avec une fonctionnelle d'onde. Le point de vue de Heisenberg où la fonctionnelle d'onde $|\Psi\rangle$ est indépendante du rayon r (on utilise maintenant la quantification radiale), mais pas les opérateurs, est utilisé. On introduit un ensemble de champs classiques Φ_0 définis à un rayon donné comme $\Phi|_r \equiv \Phi(|x|=r,\sigma)$, où σ désigne les coordonnées d'espace sur l'hypersphère de rayon r_0. Ces champs peuvent être associés à un état propre de l'opérateur de champ $\hat{\Phi}|_r\Big|\Phi|_r\Big\rangle = \Phi|_r\Big|\Phi|_r\Big\rangle$. La propagation entre deux tels états peut encore être écrite avec une intégrale de chemin dont la mesure est restreinte aux champs dans l'intervalle $r_i < r < r_f$ où les bords sont contraints, c'est-à-dire

$$\begin{aligned}\left\langle \Phi_f|_{r_f}\middle|\Phi_i|_{r_i}\right\rangle &= \int_{\Phi|_{r_i}=\Phi_i|_{r_i}}^{\Phi|_{r_f}=\Phi_f|_{r_f}} \mathcal{D}\Phi e^{iS[\Phi]} \\ &\equiv \prod_{r_i<r<r_f}\int \mathcal{D}\Phi|_r \delta(\Phi|_{r_i}-\Phi_i|_{r_i})\delta(\Phi|_{r_f}-\Phi_f|_{r_f})e^{iS[\Phi]}\,.\end{aligned} \tag{A.2.3}$$

Ce propagateur est utilisé pour généraliser la relation à l'Éq. (A.2.2) dans la théorie quantique des champs (QFT)

$$\Psi[\Phi_f|_{r_f},r_f] = \int \mathcal{D}\Phi_i|_{r_i} \left[\int_{\Phi|_{r_i}=\Phi_i|_{r_i}}^{\Phi|_{r_f}=\Phi_f|_{r_f}} \mathcal{D}\Phi e^{iS[\Phi]}\right] \Psi[\Phi_i|_{r_i},r_i]\,, \tag{A.2.4}$$

où la fonctionnelle d'onde projetée est définie comme $\Psi[\Phi|_r,r] = \left\langle \Phi|_r \middle| \Psi \right\rangle$. En écrivant plus explicitement l'intégrale de chemin, il est possible d'isoler la contribution de la condition initiale comme un facteur pondérant l'intégrale de chemin

$$\begin{aligned}\Psi[\Phi_f|_{r_f},r_f] = &\prod_{r_i<r<r_f} \int \mathcal{D}\Phi|_r \delta(\Phi|_{r_f} - \Phi_f|_{r_f}) e^{iS[\Phi]} \\ &\times \int \mathcal{D}\Phi_i|_{r_i} \delta(\Phi|_{r_i} - \Phi_i|_{r_i}) \Psi[\Phi_i|_{r_i},r_i]\,.\end{aligned} \tag{A.2.5}$$

En particulier, lorsque la fonctionnelle d'onde initiale est définie pour $r_i = 0$, l'information encodée dans la condition initiale est définie en un seul point de l'espace-temps. Autrement dit, l'intégrale de chemin maintenant définie dans le disque $r < r_f$ est modifiée en un seul point $r = 0$. Ainsi, cette condition $\Psi[\Phi_i|_{r_i=0},r_i = 0]$ peut être remplacée par l'insertion d'un opérateur local $\mathcal{O}_\Psi(0)$

$$\begin{aligned}\Psi[\Phi_f|_{r_f},r_f] &= \prod_{0<r<r_f} \int \mathcal{D}\Phi|_r \delta(\Phi|_{r_f} - \Phi_f|_{r_f}) e^{iS[\Phi]} \mathcal{O}_\Psi(0) \\ &\equiv \int^{\Phi|_{r_f}=\Phi_f|_{r_f}} \mathcal{D}\Phi e^{iS[\Phi]} \mathcal{O}_\Psi(0)\,.\end{aligned} \tag{A.2.6}$$

Avant de poursuivre, la notation est modifiée légèrement. D'abord, on remplace maintenant $r_f \to R$. Ensuite, on introduit l'opérateur $\mathcal{O}_i(0)$ qui est associé à une fonction d'onde Ψ_i tel que

$$\Psi_i[\Phi_0|_R,R] = \int^{\Phi|_R=\Phi_0|_R} \mathcal{D}\Phi e^{iS[\Phi]} \mathcal{O}_i(0)\,. \tag{A.2.7}$$

A.3. Effet de l'Hamiltonien

Sur chaque tranche radiale d'espace-temps, on peut définir un champ bâti à l'aide du courant de dilatation

$$H_S(R) = \int d^d x \delta(|x| - R) n^\mu j^D_\mu\,, \tag{A.3.1}$$

où $n^\mu(x)$ est la normale qui pointe vers l'extérieur de l'hypersphère en $|x| = R$. L'action de cette fonction sur l'opérateur primaire résulte en sa variation sous l'action de l'opérateur de dilatation $H_S(R)\mathcal{O}(x) \sim \delta_D \mathcal{O}(x)$ [3], à condition que l'insertion de l'opérateur soit à

l'intérieur de l'hypersphère $|x| < R$. Plus précisément, en utilisant l'Éq. (A.1.2), on obtient [1]

$$H_S(R)\mathcal{O}(x) = \frac{1}{R}\left(\Delta_{\mathcal{O}} + x^\mu \partial_\mu\right)\mathcal{O}(x)\,, \quad |x| < R\,. \tag{A.3.2}$$

On peut aussi définir un Hamiltonien quantique $\hat{H}_S(R)$ dont l'action sur une fonctionnelle d'onde est [1]

$$\left(\hat{H}_S(R)\Psi_i\right)[\Phi_0|_R,R] = \lim_{\epsilon\to 0^+}\int \prod_{R-\epsilon\leq r<R+\epsilon} \mathcal{D}\Phi|_r \delta(\Phi_0|_R - \Phi|_r) H(R)\Psi_i[\Phi|_r,R-\epsilon]\,. \tag{A.3.3}$$

En particulier, si la fonctionnelle d'onde $\Psi_i[\Phi_0|_R,R]$ est bâtie avec un opérateur primaire $[\hat{D},\mathcal{O}_i(0)] = -i\Delta_{\mathcal{O}_i}\mathcal{O}_i(0)$ dans l'Éq. (A.2.7), une équation aux valeurs propres est obtenue

$$\begin{aligned}\left(\hat{H}_S(R)\Psi_i\right)[\Phi_0|_R,R] &= \lim_{\epsilon\to 0^+}\int \prod_{R-\epsilon\leq r<R+\epsilon} \mathcal{D}\Phi|_r \delta(\Phi_0|_R - \Phi|_r) \\ &\quad\times \int^{\Phi'|_{R-\epsilon}=\Phi|_r} \mathcal{D}\Phi' e^{iS[\Phi']} H(R)\mathcal{O}_i(0) \\ &= \frac{\Delta_{\mathcal{O}_i}}{R}\Psi_i[\Phi_0|_R,R]\,.\end{aligned} \tag{A.3.4}$$

Ainsi, Ψ_i est un état propre de l'Hamiltonien $\hat{H}_S(R)$ avec une énergie $\Delta_{\mathcal{O}_i}/R$. À l'inverse, on peut montrer que les états propres de l'Hamiltonien $\hat{H}_S(R)$ peuvent être écrits en termes d'opérateurs, ce qui assure une correspondance un à un entre états et opérateurs [1].

A.4. Utilisation de la correspondance

Le calcul de $\Delta_{\mathcal{O}}$ devient un problème assez standard en théorie des champs lorsqu'on laisse tendre $R \to \infty$. L'intégrale de chemin se fait alors sur tous les degrés de liberté du champ Φ, et la fonctionnelle d'onde devient une fonction de partition

$$Z_{\mathcal{O}} = \int \prod_{0<r<\infty} \mathcal{D}\Phi|_r e^{iS[\Phi]}\mathcal{O}(0)\,. \tag{A.4.1}$$

L'énergie totale du système est alors donnée par

$$E = -\lim_{\beta\to\infty}\frac{1}{\beta}\ln Z_{\mathcal{O}}\,, \tag{A.4.2}$$

où β est le rayon du cercle « thermique » obtenu par la compactification de $\mathbb{R}$ dans l'espace-temps $S^{d-1}\times\mathbb{R}$ obtenu suite à la transformation conforme. Le calcul de cette quantité à l'aide d'un développement en $1/N$, où $2N$ est le nombre de saveurs fermioniques, est réalisé dans le texte principal. Dans ce cas, il s'agit d'un opérateur monopôle qui est inséré à l'origine. Tel

qu'argumenté dans la Réf. [4], l'opérateur monopôle modifie la condition frontière du champ de jauge de telle sorte qu'un flux $4\pi q$ perce la sphère entourant le point d'insertion. Pour représenter cet effet, il suffit d'inclure dans l'action un champ de jauge externe implémentant le champ d'un monopôle de Dirac avec une charge q

$$\mathcal{A}^q = q\,(1-\cos\theta)\,\mathrm{d}\phi, \tag{A.4.3}$$

ou $\mathcal{A}^q_\mu = \delta^\phi_\mu\,(1-\cos\theta)\,/\sin\theta$ en notation composantes. Une corde de Dirac vient contrebalancer la singularité en $\theta = \pi$.

Bibliographie

[1] M. A. Metlitski, M. Hermele, T. Senthil, and M. P. A. Fisher, Phys. Rev. B **78**, 214418 (2008), URL `https://link.aps.org/doi/10.1103/PhysRevB.78.214418`.

[2] S. Rychkov, *EPFL Lectures on Conformal Field Theory in D ≥ 3 Dimensions*, SpringerBriefs in Physics (Springer International Publishing, Cham, 2017), ISBN 978-3-319-43625-8, URL `//www.springer.com/gp/book/9783319436258`.

[3] J. Polchinski, *String theory. Vol. 1 : An introduction to the bosonic string*, Cambridge Monographs on Mathematical Physics (Cambridge University Press, 2007), ISBN 978-0-511-25227-3, 978-0-521-67227-6, 978-0-521-63303-1.

[4] V. Borokhov, A. Kapustin, and X. Wu, Journal of High Energy Physics **2002**, 044 (2002), URL `https://doi.org/10.1088/1126-6708/2002/12/044`.